

Winter 2006

Modeling of a soft sensitive marine silty clay deposit for a landfill expansion study

John Roche

University of New Hampshire, Durham

Follow this and additional works at: <https://scholars.unh.edu/thesis>

Recommended Citation

Roche, John, "Modeling of a soft sensitive marine silty clay deposit for a landfill expansion study" (2006). *Master's Theses and Capstones*. 243.

<https://scholars.unh.edu/thesis/243>

This Thesis is brought to you for free and open access by the Student Scholarship at University of New Hampshire Scholars' Repository. It has been accepted for inclusion in Master's Theses and Capstones by an authorized administrator of University of New Hampshire Scholars' Repository. For more information, please contact nicole.hentz@unh.edu.

MODELING OF A SOFT SENSITIVE MARINE SILTY
CLAY DEPOSIT FOR A LANDFILL EXPANSION STUDY

BY

JOHN ROCHE
B.S. Civil Engineering, University of New Hampshire, 2004

THESIS

Submitted to the University of New Hampshire
in Partial Fulfillment of
the Requirements for the Degree of

Master of Science
in
Civil Engineering

December, 2006

UMI Number: 1439288

INFORMATION TO USERS

The quality of this reproduction is dependent upon the quality of the copy submitted. Broken or indistinct print, colored or poor quality illustrations and photographs, print bleed-through, substandard margins, and improper alignment can adversely affect reproduction.

In the unlikely event that the author did not send a complete manuscript and there are missing pages, these will be noted. Also, if unauthorized copyright material had to be removed, a note will indicate the deletion.

UMI[®]

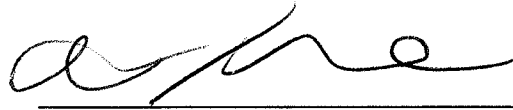
UMI Microform 1439288

Copyright 2007 by ProQuest Information and Learning Company.

All rights reserved. This microform edition is protected against unauthorized copying under Title 17, United States Code.

ProQuest Information and Learning Company
300 North Zeeb Road
P.O. Box 1346
Ann Arbor, MI 48106-1346

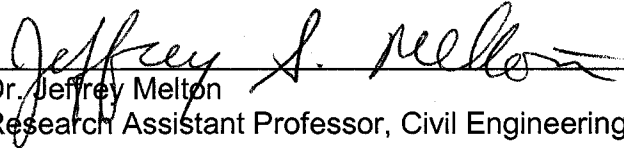
This thesis has been examined and approved.



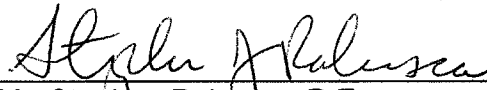
Thesis Director, Dr. Jean Benoît
Professor and Chair, Civil Engineering



Dr. Pedro de Alba
Professor, Civil Engineering



Dr. Jeffrey Melton
Research Assistant Professor, Civil Engineering



Mr. Stephen Rabasca, P.E.
Geotechnical Engineer, Soil Metrics, LLC.

12/15/06
Date

DEDICATION

To my parents, Dave and Carol Roche, who have provided never-ending support and encouragement to all of their children.

ACKNOWLEDGEMENTS

Many thanks to all of my family and friends who have provided incredible support during this research.

For his unending support and guidance, my sincere thanks to my advisor, Professor Jean Benoit.

Many thanks for Stephen Rabasca of Soil Metrics, LLC. for providing the opportunity to perform this research, and for providing a wealth of data from the RWS site.

For their assistance during the research program, and service on my thesis committee, I thank Professors Pedro de Alba and Jeffrey Melton.

Thanks to the employees of ARA/Vertek for their assistance in preparation of the piezocone system.

For their patience and assistance providing drilling support, thanks to Great Works Test Borings, Inc.

Thanks to my fellow graduate students Steve Hall and Marc Grenier for their assistance in the field, and to the many undergraduates who assisted during laboratory testing.

TABLE OF CONTENTS

DEDICATION	iii
ACKNOWLEDGEMENTS	iv
LIST OF TABLES	x
LIST OF FIGURES	xi
ABSTRACT	xx

CHAPTER	PAGE
INTRODUCTION	1
I. IN SITU TESTING	3
1.1 Introduction	3
1.2 Field Shear Vane Testing	3
1.2.1 Field Vane History	3
1.2.2 The Geonor H-10 Vane Borer	4
1.2.3 General Mechanics of the Field Vane	6
1.2.4 Factors Influencing the Field Vane	8
1.3 Cone Penetration Testing	12
1.3.1 Piezocone History	12
1.3.2 Piezocone Mechanics	20
1.3.2.1 Tip and Friction Sleeve Load Measurement	20
1.3.2.2 Pore Pressure Measurement Location	21
1.3.2.3 Filter Element Considerations	26
1.3.3 Piezocone Testing System	27
1.3.3.1 The Hogentogler 10 Ton Cone	27

1.3.3.2	Depth/Velocity Transducer	30
1.3.3.3	Data Acquisition System.....	31
1.3.4	Filter Element Saturation.....	34
1.4	Dilatometer Testing.....	36
1.4.1	Dilatometer History.....	36
1.4.2	Operating Principle of the Dilatometer	38
II.	SITE CHARACTERISTICS.....	42
2.1	Site History.....	42
2.2	Subsurface Conditions.....	46
2.2.1	Stratigraphy	46
2.2.2	The Presumpscot Formation	49
2.2.3	Groundwater Conditions.....	50
2.2.4	Soil Properties	51
2.3	Geotechnical Monitoring	56
2.4	Geotechnical Monitoring Assessment	58
III.	IN SITU TESTING PROGRAM.....	61
3.1	Purpose of the Site Investigation	61
3.2	Testing Locations.....	62
3.3	Field Shear Vane Testing Procedure.....	64
3.4	Piezocone Testing Procedure.....	65
3.4.1	Introduction.....	65
3.4.2	Summary of the CPTu Procedure	66
3.5	Dilatometer Testing Procedure	68
3.6	Laboratory Testing Procedures	68

IV. INTERPRETATION OF IN SITU TEST DATA.....	72
4.1 Field Shear Vane Data	72
4.1.1 Data Reduction.....	72
4.1.2 Undrained Shear Strength Correction.....	74
4.1.2.1 Corrections Used.....	74
4.1.2.2 Index Properties of the Soil	75
4.2 Piezocone and Dilatometer Data.....	76
4.2.1 Introduction.....	76
4.2.2 Corrections to Piezocone Point and Friction Resistance	77
4.2.3 Preparation of the Dilatometer Data.....	82
4.2.4 Stratigraphy	82
4.2.4.1 Introduction.....	82
4.2.4.2 Interpretation Using the Piezocone	83
4.2.4.3 Interpretation Using the Dilatometer.....	97
4.2.5 Undrained Shear Strength (S_u)	100
4.2.5.1 Introduction.....	100
4.2.5.2 Interpretation Using the Piezocone	100
4.2.5.3 Interpretation Using the Dilatometer.....	112
4.2.6 Stress History (OCR).....	116
4.2.6.1 Introduction.....	116
4.2.6.2 Interpretation Using the Piezocone	116
4.2.6.3 Interpretation Using the Dilatometer.....	124
4.2.7 Preconsolidation Pressure (σ'_p).....	127
4.2.7.1 Introduction.....	127
4.2.7.2 Interpretation Using the Piezocone	127

4.2.7.3 Interpretation Using the Dilatometer.....	135
4.2.8 Coefficient of Lateral Earth Pressure At-Rest (K_0).....	138
4.2.8.1 Introduction.....	138
4.2.8.2 Interpretation Using the Piezocone	138
4.2.8.3 Interpretation Using the Dilatometer.....	140
4.2.9 Coefficient of Horizontal Consolidation (c_h).....	142
V. FINITE ELEMENT MODELING	148
5.1 Introduction	148
5.2 Plaxis Finite Element Software	149
5.2.1 Introduction.....	149
5.2.2 Plaxis Soil Models	150
5.2.2.1 Introduction.....	150
5.2.2.2 The Soft Soil Model (SSM)	151
5.2.2.3 The Mohr-Coulomb Model (MC Model)	157
5.3 Finite Element Model.....	160
5.3.1 Introduction.....	160
5.3.2 Model Geometry.....	161
5.3.3 Material Properties	165
5.3.4 Initial Conditions.....	170
5.3.5 Model Calculation Phases.....	171
5.4 Finite Element Model Validation	175
5.5 Prediction of Future Soil Strengths	187
VI. SUMMARY AND CONCLUSIONS	196
6.1 Summary.....	196

6.2 Conclusions	197
6.3 Future Work	199
LIST OF REFERENCES	201
APPENDICES	213
APPENDIX A FIELD SHEAR VANE TEST DATA	214
APPENDIX B CALIBRATION OF THE VANE APPARATUS.....	226
APPENDIX C CALIBRATION OF THE PIEZOCONE	229
APPENDIX D PLAXIS MATERIAL PROPERTIES.....	238
APPENDIX E PLAXIS MODEL VALIDATION FIGURES.....	240
APPENDIX F UNDRAINED SHEAR STRENGTH GAIN FIGURES	258
APPENDIX G LABORATORY CONSOLIDATION CURVES.....	274

LIST OF TABLES

		Page
Table 2.1	Results of 2006 Atterberg Limits Tests	51
Table 2.2	Results of 2006 One-Dimensional Consolidation Tests	54
Table 2.3	Consolidation Properties of the Soft Gray Silty Clay Layer	55
Table 3.1	Summary of In Situ Tests Performed	64
Table 3.2	One-dimensional Consolidation Test Load Increments	71
Table 4.1	Borehole B-11 Field Shear Vane Results	72
Table 4.2	Index Properties for Correction of Undrained Shear Strength From the Field Shear Vane	76
Table 4.3	Proposed Soil Classification Based on DMT I_D Values (After Marchetti, 1980)	98
Table 4.4	Modified Time Factors (T^*) from Houlsby and Teh (1988)	144
Table 4.5	Results of CPTu Dissipation Tests; c_h estimated using method of Teh and Houlsby (1991)	144
Table 5.1	Compacted Ash Unit Weight by Cell	170
Table 5.2	East/West Profile Calculation Phases	173
Table 5.3	North/South Profile Calculation Phases	174
Table D.1	Plaxis Material Cluster Properties	239

LIST OF FIGURES

		Page
Figure 1.1	Geonor H-10 Vane Borer and Torque Measuring Head (Geonor, Inc.)	5
Figure 1.2	Shear Stress Distribution on Cylindrical Surface of Field Vane (Chandler 1988).....	8
Figure 1.3	Disturbance of Soft Soils Due to Vane Borer Advancement (Top) and Vane Blade Insertion (Bottom) (Ahnberg et al., 2004)	9
Figure 1.4	Influence of Consolidation on Undrained Shear Strength (Roy and Leblanc, 1988).....	10
Figure 1.5	Vane Shear Correction Factor (After Aas et al., 1986).....	12
Figure 1.6	Dutch Cone with Conical Mantle (Sanglerat, 1972).....	14
Figure 1.7	Begemann Type Cone with Friction Sleeve (Sanglerat, 1972)	15
Figure 1.8	Electric Friction Cone (Lankelma Cone Penetration Testing, Ltd.)	16
Figure 1.9	Standard Designs and Filter Locations of Piezoprobes (1-2) and Piezocones (3-11) (Campanella et al. 1988)	18
Figure 1.10	Typical Filter Element Location Nomenclature (After Mayne and Chen, 1994)	22
Figure 1.11	Effect of Filter Element Location on Measured Pore Pressures in Normal to Moderately Overconsolidated Clay (After Powell and Quaterman, 1991)	23
Figure 1.12	Effect of Filter Element Location on Measured Pore Pressures in Heavily Overconsolidated Clay (After Lunne et al., 1997)	24
Figure 1.13	Unequal End Areas of the Piezocone (Jamiolkowski et al., 1985)	25
Figure 1.14	60 Degree Cone Tip and Filter Element	28
Figure 1.15	Photograph of 10 Ton Hogentogler Cone	30
Figure 1.16	Schematic of the Data Acquisition System for Piezocone	32

Figure 1.17	Screen Capture of the Aligent BenchLink Software.....	34
Figure 1.18	Flat Dilatometer Blade with Flexible Steel Membrane	36
Figure 1.19	Effect of Geometry on Distortions in Clay (after Baligh, 1975)	38
Figure 1.20	Schematic of Membrane Displacement Mechanism (Marchetti et al., 2001)	39
Figure 1.21	Disassembled View of Dilatometer Blade Membrane (Marchetti, 2001)	40
Figure 1.22	Dilatometer Control Unit.....	41
Figure 2.1	Location Map, RWS Ashfill/Balefill Facility.....	42
Figure 2.2	RWS Landfill Schematic	44
Figure 2.3	Undrained Shear Strength of Virgin (unloaded) Soil at the RWS Ashfill/Balefill	48
Figure 2.4	Summary of the Natural Moisture Content, Preconsolidation Pressure, Overconsolidation Ratio and In Situ Void Ratio from Laboratory Tests	53
Figure 2.5	Example Results of CK_0 UDSS Test Indicating Strain Softening Past 2% Shear Strain	60
Figure 3.1	Exploration Location Plan for Current Research	62
Figure 3.2	Method for Assembly of the Piezocone Filter Element in the Field (After Larsson, 1992).....	67
Figure 3.3	Floating-ring Consolidation Apparatus.....	70
Figure 4.1	Uncorrected, Corrected and Remolded Undrained Shear Strength with Sensitivity Profile from Field Shear Vane Profile at B-11	73
Figure 4.2	Vane Shear Correction Factor (After Aas et al., 1986)	75
Figure 4.3	Piezocone Output at CPTu B-11, Corrected Tip Resistance (q_t), Friction Sleeve Resistance (f_s), Pore Pressure (u_2).....	79
Figure 4.4	Piezocone Output at CPTu P-3, Corrected Tip Resistance (q_t), Friction Sleeve Resistance (f_s), Pore Pressure (u_2).....	80

Figure 4.5	Piezocene Output at CPTu I-3/I-4, Corrected Tip Resistance (q_t), Friction Sleeve Resistance (f_s), Pore Pressure (u_2).....	81
Figure 4.6	Normalized CPTu Data for Soil Classification; Pore Pressure Ratio (B_q), Normalized Friction Ratio (F_r), Normalized Cone Resistance (Q_t) (After Wroth, 1984, 1988).....	85
Figure 4.7	Proposed Soil Behavior Classification Chart from CPTu Data (After Roberston et al., 1986).....	86
Figure 4.8	Soil Behavior Classification Chart Based on Normalized CPTu Data (After Robertson, 1990).....	87
Figure 4.9	Soil Behavior Classification at CPTu B-11, Using Method of Robertson (1990).....	89
Figure 4.10	Soil Behavior Classification at CPTu P-3, Using Method of Robertson (1990).....	90
Figure 4.11	Soil Behavior Classification at CPTu I-3/I-4, Using Method of Robertson (1990).....	91
Figure 4.12	Proposed Soil Behavior Classification Chart for Fine-Grained Soils (After Larsson and Mulabdic, 1991).....	92
Figure 4.13	Soil Behavior Classification at CPTu B-11, Using Method of Larsson and Mulabdic (1991).....	94
Figure 4.14	Soil Behavior Classification at CPTu P-3, Using Method of Larsson and Mulabdic (1991).....	95
Figure 4.15	Soil Behavior Classification at CPTu I-3/I-4, Using Method of Larsson and Mulabdic (1991).....	96
Figure 4.16	Soil Behavior Classification at DMT B-11, Based on DMT I_D Values (After Marchetti, 1980).....	99
Figure 4.17	Results of Undrained Shear Strength from Direct Shear Tests Against Excess Pore Pressure Generated at the Face of the Cone Tip in Swedish and Norwegian Clays Indicating a Linear Relationship (After Larsson and Mulabdic, 1991).....	107
Figure 4.18	Undrained Shear Strength Profile at CPTu B-11 Based on Methods of Excess Pore Pressure and Total Cone Resistance.....	109

Figure 4.19	Undrained Shear Strength Profile at CPTu P-3 Based on Methods of Excess Pore Pressure and Total Cone Resistance	110
Figure 4.20	Undrained Shear Strength Profile at CPTu I-3/I-4 Based on Methods of Excess Pore Pressure and Total Cone Resistance	111
Figure 4.21	Comparison Between Undrained Shear Strength Measures by DMT and by other Methods at the National Research Site of Bothkennar, UK (After Nash et al., 1992)	113
Figure 4.22	Undrained Shear Strength Profile at DMT B-11 Based on K_D ..	115
Figure 4.23	Relationship between Overconsolidation Ratio and the Ratio of Excess Pore Pressure (u_1) to Effective Vertical Stress in Swedish and Norwegian Clays (After Larsson and Mulabdic, 1991).....	117
Figure 4.24	Relationship between Effective Tip Resistance and Overconsolidation Ratio with Pore Pressure Recorded behind The Cone Tip (u_2) (After Larsson and Mulabdic, 1991)	119
Figure 4.25	Relationship between Effective Tip Resistance, Normalized for the Effects of Plasticity and Overconsolidation Ratio with Pore Pressure Recorded behind the Cone Tip (u_2) (After Larsson and Mulabdic, 1991).....	119
Figure 4.26	Piezocone OCR Profile at CPTu B-11 based on methods of Larsson and Mulabdic (1991), Houlsby (1988) and Chen and Mayne (1994)	121
Figure 4.27	Piezocone OCR Profile at CPTu P-3 based on methods of Larsson and Mulabdic (1991), Houlsby (1988) and Chen and Mayne (1994)	122
Figure 4.28	Piezocone OCR Profile at CPTu I-3/I-4 based on methods of Larsson and Mulabdic (1991), Houlsby (1988) and Chen and Mayne (1994)	123
Figure 4.29	Correlation between K_D and OCR for Cohesive Soils at Various Geographical Locations (After Kamei and Iwasaki, 1995).....	125
Figure 4.30	Overconsolidation Ratio Profile at DMT B-11	126
Figure 4.31	Relationship between Net Tip Resistance and the Preconsolidation Pressure in Swedish and Norwegian Clays (After Larsson and Mulabdic, 1991).....	129

Figure 4.32	Linear Relationship between Net Tip Resistance, Normalized For the Effects of Soil Plasticity and Preconsolidation Pressure (After Tavenas and Leroueil, 1987)	130
Figure 4.33	Estimation of the Preconsolidation Pressure Profile at CPTU B-11 Based on Methods of Kulhawy and Mayne (1990), Larsson and Mulabdic (1991), and Tavenas and Leroueil (1987)	132
Figure 4.34	Estimation of the Preconsolidation Pressure Profile at CPTU P-3 Based on Methods of Kulhawy and Mayne (1990), Larsson and Mulabdic (1991), and Tavenas and Leroueil (1987)	133
Figure 4.35	Estimation of the Preconsolidation Pressure Profile at CPTU I-3/I-4 Based on Methods of Kulhawy and Mayne (1990), Larsson and Mulabdic (1991), and Tavenas and Leroueil (1987)	134
Figure 4.36	Profile of the Preconsolidation Pressure at DMT B-11 Calculated from Site Specific OCR by Dilatometer.....	136
Figure 4.37	Comparison of Preconsolidation Pressure determined by CPTU B-11, DMT B-11 and Laboratory Data	137
Figure 4.38	Estimates of K_0 based on CPTu and DMT Data at CPTu B-11 And DMT B-11 Respectively.....	141
Figure 4.39	Dissipation of Excess Pore Pressure at 3.68 m (12.07 ft) Depth.....	146
Figure 4.40	Dissipation of Excess Pore Pressure at 7.96 m (26.11 ft) Depth.....	147
Figure 5.1	Logarithmic Relationship between Volumetric Strain and Mean Effective Stress (Plaxis Material Models Manual).....	154
Figure 5.2	Schematic of Soft Soil Model Yield Function (Plaxis, 2002)	156
Figure 5.3	Soft Soil Model Yield Contour in Principal Effective Stress Space (Plaxis, 2002)	157
Figure 5.4	Elastic Perfectly Plastic Behavior.....	158
Figure 5.5	Mohr-Coulomb Failure Envelope	159
Figure 5.6	Mohr-Coulomb Yield Envelope	159
Figure 5.7	RWS Landfill Schematic	160
Figure 5.8	15-Node Triangular Element.....	161

Figure 5.9	East/West Plaxis Profile	163
Figure 5.10	East/West Profile – Plaxis Mesh	Attached CD
Figure 5.11	North/South Profile – Plaxis Mesh	Attached CD
Figure 5.12	Undrained Shear Strength Profiles for Modeling, East/West Profile.....	166
Figure 5.13	Undrained Shear Strength Profiles for Modeling, North/South Profile.....	167
Figure 5.14	Overconsolidation Ratio Profile for Modeling, East/West Profile.....	168
Figure 5.15	Overconsolidation Ratio Profile for Modeling, North/South Profile.....	169
Figure 5.16	East/West Profile with Historic Monitoring Installations	176
Figure 5.17	North/South Profile with Historic Monitoring Installations	177
Figure 5.18	SPL-1 (Cell 1b) – Plaxis Predicted vs. Measured Settlements	180
Figure 5.19	Piezometer P-2 (Cell 1b) – Plaxis Predicted vs. Measured Pore Pressures	181
Figure 5.20	Piezometer P-5 (Cell 5b) – Plaxis Predicted vs. Measured Pore Pressures	182
Figure 5.21	Inclinometer I-3a Cumulative Displacement – Plaxis Predicted Vs. Measured Displacement.....	184
Figure 5.22	SPL-4 (Cell 2) - Plaxis Predicted vs. Measure Settlements.....	185
Figure 5.23	Piezometer P-1 (Cell 1b) - Plaxis Predicted vs. Measure Pore Pressures	186
Figure 5.24	Locations of Strength Change Analysis.....	188
Figure 5.25	Plaxis Predicted Change in Effective Overburden Pressure with Time (B-4 Location)	190
Figure 5.26	Change in Undrained Shear Strength at B-1 (1994-2002)	191
Figure 5.27	Change in Undrained Shear Strength at B-1 (2002-2030)	193
Figure 5.28	Change in Undrained Shear Strength at I-3/I-4 (2002-2030)....	194

Figure B.1	Geonor H-10 Calibration Equipment (Geonor, Inc.)	227
Figure C.1	Geotest S5710 Load Frame with Piezocone	230
Figure C.2	Cone Tip Support for Laboratory Loading	231
Figure C.3	Friction Sleeve Support for Laboratory Loading	232
Figure C.4	Point Load Cell Calibration	234
Figure C.5	Friction Sleeve Load Cell Calibration.....	235
Figure C.6	Effect of Tip Resistance on Friction Sleeve Load Cell.....	236
Figure C.7	Pore Pressure Transducer Calibration.....	237
Figure D.1	East/West Plaxis Profile.....	Attached CD
Figure D.2	North/South Plaxis Profile	Attached CD
Figure E.1	Piezometer P-4 (Cell 2) Plaxis Predicted vs. Measured Pore Pressures North/South Model.....	241
Figure E.2	SPL-1 (Cell 1b) Plaxis Predicted vs. Measured Settlement North/South Model	242
Figure E.3	SPL-11 (Cell 4) Plaxis Predicted vs. Measured Settlement North/South Model	243
Figure E.4	SPL-12 (Cell 4) Plaxis Predicted vs. Measured Settlement North/South Model	244
Figure E.5	SPL-15 (Cell 5a) Plaxis Predicted vs. Measured Settlement North/South Model	245
Figure E.6	SPL-16 (Cell 5a) Plaxis Predicted vs. Measured Settlement North/South Model	246
Figure E.7	Piezometer P-1 (Cell 1b) Plaxis Predicted vs. Measured Pore Pressures East/West Model.....	247
Figure E.8	Piezometer P-3 (Cell 3b) Plaxis Predicted vs. Measured Pore Pressures East/West Model.....	248
Figure E.9	Piezometer P-I3a (Cell 3b) Plaxis Predicted vs. Measured Pore Pressures East/West Model.....	249
Figure E.10	Piezometer P-I5a (Cell 5b) Plaxis Predicted vs. Measured Pore Pressures East/West Model.....	250

Figure E.11	SPL-2 (Cell 1b) Plaxis Predicted vs. Measured Settlement North/South Model	251
Figure E.12	SPL-7 (Cell 3b) Plaxis Predicted vs. Measured Settlement North/South Model	252
Figure E.13	SPL-8 (Cell 3b) Plaxis Predicted vs. Measured Settlement North/South Model	253
Figure E.14	SPL-9 (Cell 5b) Plaxis Predicted vs. Measured Settlement North/South Model	254
Figure E.15	SPL-10 (Cell 5b) Plaxis Predicted vs. Measured Settlement North/South Model	255
Figure E.16	Inclinometer I-5a Plaxis Predicted vs. Measured Displacement North/South Model	256
Figure E.17	Inclinometer I-6a Plaxis Predicted vs. Measured Displacement North/South Model	257
Figure F.1	Change in Undrained Shear Strength at I-3/I-4 (2002-2006)	259
Figure F.2	Change in Undrained Shear Strength at B-4 (2002-2030)	260
Figure F.3	Change in Undrained Shear Strength at B-11 (2006-2030)	261
Figure F.4	Change in Undrained Shear Strength at P-3 (1994-2002)	262
Figure F.5	Change in Undrained Shear Strength at P-3 (2002-2030)	263
Figure F.6	Change in Undrained Shear Strength at P-5 (1994-2002)	264
Figure F.7	Change in Undrained Shear Strength at P-5 (2002-2030)	265
Figure F.8	Plaxis Predicted Change in Effective Overburden Pressure with Time (B-1 Location)	266
Figure F.9	Plaxis Predicted Change in Effective Overburden Pressure with Time (B-11 Location)	267

Figure F.10	Plaxis Predicted Change in Effective Overburden Pressure with Time (I-3/I-4 Location)	268
Figure F.11	Plaxis Predicted Change in Effective Overburden Pressure with Time (P-3 Location)	269
Figure F.12	Plaxis Predicted Change in Effective Overburden Pressure with Time (P-5 Location)	270
Figure F.13	Plaxis Predicted Change in Pore Pressure with Time (B-11 Location).....	271
Figure F.14	Plaxis Predicted Change in Pore Pressure with Time (I-3/I-4 Location).....	272
Figure F.15	Plaxis Predicted Change in Pore Pressure with Time (P-3 Location).....	273
Figure G.1	Results of One-dimensional Consolidation Test (B-11 Location, El. 17.1 m)	275
Figure G.2	Results of One-dimensional Consolidation Test (B-11 Location, El. 15.1 m)	276
Figure G.3	Results of One-dimensional Consolidation Test (B-11 Location, El. 13.6 m)	277
Figure G.4	Results of One-dimensional Consolidation Test (B-11 Location, El. 10.5 m)	278

ABSTRACT

MODELING OF A SOFT SENSITIVE MARINE SILTY CLAY DEPOSIT FOR A LANDFILL EXPANSION STUDY

by

John Roche

University of New Hampshire, December, 2006

An in situ testing program and finite element modeling of Presumpscot Formation glaciomarine clays in South Portland, Maine was undertaken as part of a landfill expansion feasibility study. The very soft sensitive silty clay foundation soils have been monitored during the 20 year lifespan of the landfill facility by an array of settlement platforms, inclinometers, piezometer clusters and periodic field shear vane tests. During this time large horizontal displacements have been observed at a discrete elevation corresponding to a zone of reduced undrained shear strength. Proposals call for a vertical expansion at the site above existing landfill cells. While this proposal will require field corroboration that sufficient strength gain of the foundation soils has occurred to maintain minimum safety factors, a preliminary estimate of future strength conditions will aid the planning and design processes.

An in situ testing program consisting of piezocone, field shear vane and dilatometer profiles was performed along with laboratory testing of undisturbed samples to determine the geotechnical properties of the landfill foundation soils. These properties were then used with historical data to create two-dimensional finite element models of the landfill, and to simulate waste loading rates over the lifespan of the facility. The models were then used to project the strength properties and behavior of the soil as additional waste is placed in the proposed vertical expansion.

XX

A comparison between historical data from the site and the modeling results demonstrated that the finite element models provide a good indication of the current behavior of the foundation soils with regards to the changes in pore pressure and magnitude of settlement due to loading. While the finite element soil behavior model did not work well in the zones of large displacement; results demonstrated that the calculated increase in undrained shear strength based on the dissipation of excess pore pressure closely matches the changes observed in field shear vane tests during the past ten years throughout the remainder of the profile. The conclusions drawn in this research program is hoped to provide useful information for the site engineer, as well as a strong basis for continuing research.

INTRODUCTION

The Regional Waste Systems, Inc. (RWS) Ashfill/Balefill landfill facility accepts for storage nearly half of the 500,000 tons of incinerator ash produced annually at the RWS "waste-to-energy" plant. The soils underlying the RWS site consist primarily of soft sensitive marine silty clays. In order to maintain adequate factors of safety with regards to global stability at the site, a comprehensive knowledge of the foundation soil properties is required to ascertain their response under continued loading.

Throughout the 20 year life of the RWS facility laboratory and in situ testing programs have been completed in order to determine acceptable waste loading rates and slope geometry in newly constructed cells. In addition, long-term monitoring of an extensive instrumentation array in conjunction with periodic assessments of in situ undrained shear strength have been conducted to evaluate the performance of the foundation soils.

Monitoring of the site conditions has revealed a zone, 1.8 to 2.4 meters (six to eight feet) thick, of large horizontal displacement has developed in the last 13 years within the soft gray silty clay layer. The shear strains within this zone are approaching or are within the range where peak shear stress is expected. Additional strain levels within this layer may result in a reduction of the undrained shear strength of the soil, a condition known as strain softening. Field shear vane profiles completed in 2002 adjacent to profiles completed in 1994 indicate that less strength gain has occurred than expected, and in some cases strength loss has been observed in these zones.

These observations have led to concern with regards to the reliable evaluation of the changing properties of the foundation soils as well as the safety factor of the landfill slopes.

A fourth phase of construction and filling at the facility has been proposed, which would place a layer of waste over the existing landfill. While this phase is not proposed to begin for 20 to 25 years, the underlying clay stratum will require strength gain to make this proposal feasible from a stability standpoint.

The objectives of this research project were to determine the increase of undrained shear strength in the future of the foundation soils for preliminary design of the fourth phase of ash filling, and to investigate the potential causes of the zone of large horizontal displacement. To that end a finite element model of the landfill was constructed to forecast the subsurface conditions in the future. Three in situ test devices were used to profile the subsurface at the RWS site and develop a set of soil properties for use in modeling. Piezocone profiles were completed at the site, with additional dilatometer and field shear vane tests carried out in a virgin area of the site in a K_0 environment. With a complete set of virgin soil properties, the model was constructed to match the loading of the landfill, with the model performance assessed through comparison to the records from site instrumentation data.

CHAPTER I

IN SITU TESTING

1.1 - Introduction

Three in situ test methods were used at the RWS landfill during the course of this research. The field shear vane, which has been used at the site in the past, was used to provide a baseline profile of the undrained shear strength. The piezocone and the dilatometer were used across the site to create profiles of multiple geotechnical parameters in a near-continuous manner. This chapter describes the development of these devices, factors influencing the quality of their data, and the general testing procedures.

1.2 - Field Shear Vane Testing

1.2.1 - Field Vane History

The field shear vane test was developed to determine the undrained shear strength and sensitivity to disturbance of saturated fine grained soils comprised primarily of clay sized particles. The field shear vane test, commonly referred to as the field vane, is a relatively simple test to perform and the data reduction to develop the undrained shear strength is minimal. The test consists of the slow rotation to failure of a vane blade connected with rods to a torque measuring device at the surface of a

MODELING OF A SOFT SENSITIVE MARINE SILTY
CLAY DEPOSIT FOR A LANDFILL EXPANSION STUDY

BY

JOHN ROCHE
B.S. Civil Engineering, University of New Hampshire, 2004

THESIS

Submitted to the University of New Hampshire
in Partial Fulfillment of
the Requirements for the Degree of

Master of Science
in
Civil Engineering

December, 2006

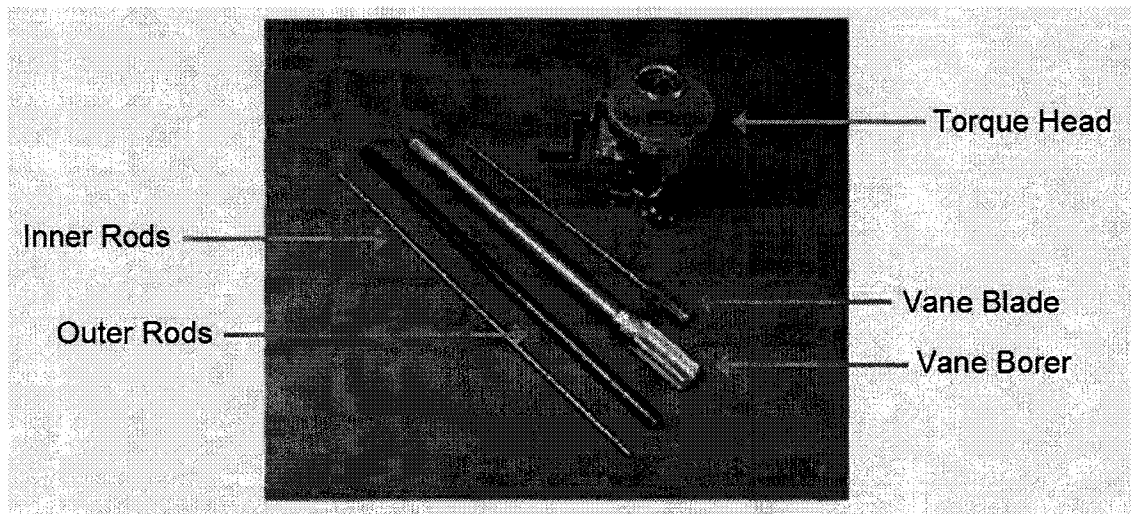


Figure 1.1 - Geonor H-10 Vane Borer and Torque Measuring Head (Geonor, Inc.)

The vane borer houses the vane blades, and can be directly advanced through soft fine-grained materials and some stiff clays or hard sand layers. The vane borer protects the vane blades, which are sized 55 mm x 110 mm or 65 mm x 130 mm, during advance, and cleans the blades as they are retracted into the vane borer housing following the completion of a test.

The vane borer system adheres to the recommendations for equipment design originally recommended by Calding and Odenstad (1950) with the vane blade having four wings and a height to diameter ratio of 2:1. The system also follows recommendations calling for the vane to be advanced a minimum of 5 vane diameters from the protective housing during testing to decrease the effects of disturbance.

A set of inner and outer drill rods are used in the system to eliminate measurement errors due to rod-soil friction. This provides a better indication of the undrained

shear strength of fine-grained cohesive soils than methods using thicker unprotected vane blades with hand held torque wrenches for measurement.

The system is advanced to the desired test depth and the vane blades are extended from the vane borer. A crank handle is then inserted into the torque head and rotations begin with a rate of 0.1 degrees per second, although variation within a range of 0.05 to 2.0 degrees per second is permissible. The torque measuring head displays the torque applied to the vane blades on a dial gauge. A calibration of the torque head, as described in Appendix B, is performed prior to testing allowing the user to directly correlate the instrument reading to undrained shear strength values.

1.2.3 - General Mechanics of the Field Vane

The undrained shear strength is measured from the maximum observed torque applied to the vane blades at the time of failure. This torque can then be manipulated to determine the undrained shear strength of the soil, using certain assumptions. When the failure surface of the soil is assumed to be cylindrical and equal to the vane diameter, the shearing forces are assumed to be uniform across the blade surfaces on both the vertical and horizontal axis. This assumption provides a rectangular stress distribution. In addition the assumption is made that an isotropic stress distribution exists along the edges of the vane blade, which implies that the strength developed is equal on the vertical and horizontal sides of the vane despite different failure mechanisms. An important assumption which is made is that no drainage occurs during the shearing of the soil. Finally the interpretation of field vane test data assumes that there is no progressive failure, but

instead rapid failure of the soil. Following these assumptions, a vane with an H/D ratio of 2 would use the following equation to determine undrained shear strength:

$$S_u = (6M) / (7\pi D^3) \quad [1-1]$$

Where S_u represents the undrained shear strength, M represents the maximum applied torque and D is the vane blade diameter. Further analysis of the validity of these assumptions was performed by Donald et al. (1977) using a three dimensional finite element analysis. The distributions of stresses along the horizontal and vertical sides of the vane were examined, and while it was determined that the vertical distribution is nearly rectangular, the stress distribution along the horizontal surfaces is not, as shown in Figure 1.2. The stress distribution here was found to vary with distance from the center of the vane. Further analysis has revealed however that the strength mobilized during shearing is primarily from the vertical shearing. A standard vane with H/D equal to 2 would have approximately 86% of the shearing resistance along the vertical surfaces. While the non-rectangular stress distribution along the top of the vane is not ideal, the large percentage of the total shear resistance provided by the vertical edges of the blades reduces the impact of the incorrect initial assumptions on the calculated undrained shear strength.

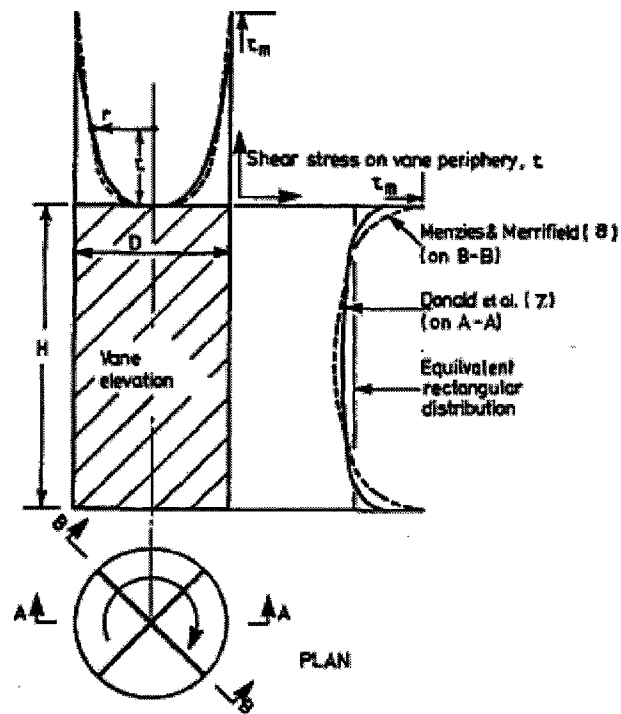


Figure 1.2 - Shear Stress Distribution on Cylindrical Surface of Field Vane (Chandler 1988)

1.2.4 - Factors Influencing the Field Vane

The soft soils that are tested using the field shear vane are by nature sensitive to disturbance caused by the insertion of the vane blades, as shown in Figure 1.3. While factors such as these are likely to have an effect on the peak undrained shear strength determined at each test interval, the assumption that no disturbance occurs typically governs the interpretation approach. Further assumptions, such as the shape of the failure surface, the size and thickness of the vane, the stress distribution along the edges of the vane, a constant rate of strain and that failure occurs before significant drainage also may over simplify the interpretation of field vane test data.

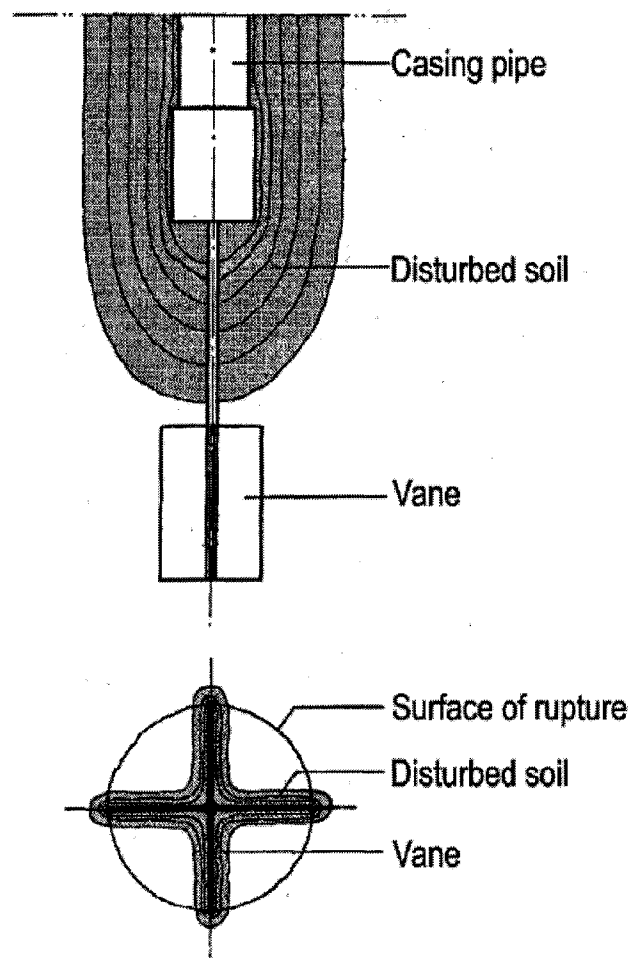


Figure 1.3 - Disturbance of Soft Soils Due to Vane Borer Advancement (Top) and Vane Blade Insertion (Bottom) (Ahnberg et al., 2004)

Methods to correct the raw field vane strength profile to account for some of these effects were used in this report. Other effects are accounted for in the construction and use of the field vane, which has been standardized based on the results of extensive laboratory tests and simulations. For example the disturbance of the soil is minimized by the standardized thickness of the vane blade and the distance the blade is extended from the vane borer. Corrections were applied to the field vane profile at boring B-11 to account for the time to failure (Chandler, 1988) and for the

plasticity and overconsolidation ratio (Aas et al., 1986). This section will report the theory supporting the correction factors while the specific numerical process used to calculate the correction factor is reported in Section 4.1.2.1.

At the standard vane rotation rate of 6 degrees per minute failure should typically occur within 5 minutes from the start of the test, as noted in ASTM D-2573 "Standard Test Method for Field Vane Shear Test in Cohesive Soil" and by Chandler (1988). If failure of the soil at the test depth is not observed within this time, the clay may begin to consolidate as it is being sheared which will affect the strength of the soil. Tests conducted on low plasticity Canadian clays by Roy and Leblanc (1988), which allowed consolidation over periods ranging from 15 to 10,000 minutes before rotation of the vane reveal a significant increase in strength when the time prior to shearing is increased, as shown in Figure 1.4. Additionally, the time to failure was increased in these tests by altering the vane rotation rate at test locations incrementally from 1 to 6 degrees per minute.

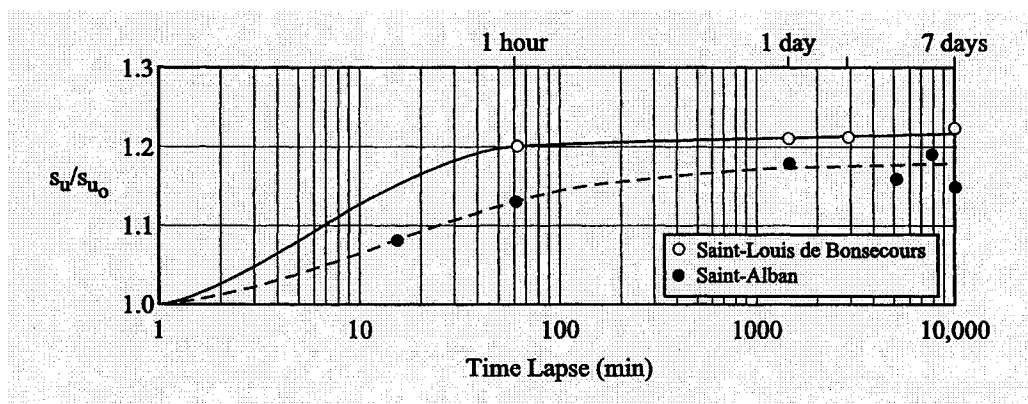


Figure 1.4 - Influence of Consolidation on Undrained Shear Strength (Roy and Leblanc, 1988)

Similar work has been performed by Torstensson (1977) and Wiesel (1973) on high plasticity Swedish clays. The findings from these researchers helped to develop a

relationship that closely matches Bjerrums (1972) curve which corrects the strength based on the plasticity index of the soil. It is important to note however that these correction factors for time to failure are only applicable to soils with a plasticity index greater than or equal to 5.

Further studies (Aas et al., 1986) have been performed that were based upon the work initially performed by Bjerrum (1972). The foundation of this work was the relationship between the void ratio and the overburden stress with time. As consolidation occurs locally around the vane blade following insertion, the material can gain strength above the true in situ value. The work by Aas et al. (1986) hypothesized that the overconsolidation ratio might be a better indicator to correct the vane strength rather than the method described in the original work by Bjerrum (1972). Aas et al. (1986) used the ratio of undrained shear strength to vertical overburden stress as a factor to correct the vane strength, as it was found to fit closely with the trend of the overconsolidation ratio. The factor of safety of embankment failures was then back calculated and plotted against this ratio, revealing a linear trend. Clays with different plasticity indexes however plotted along different lines. Therefore the correction factor μ proposed by Aas et al., (1986), and shown in Figure 1.5 relates both the plasticity index and the undrained shear strength to vertical overburden stress ratios.

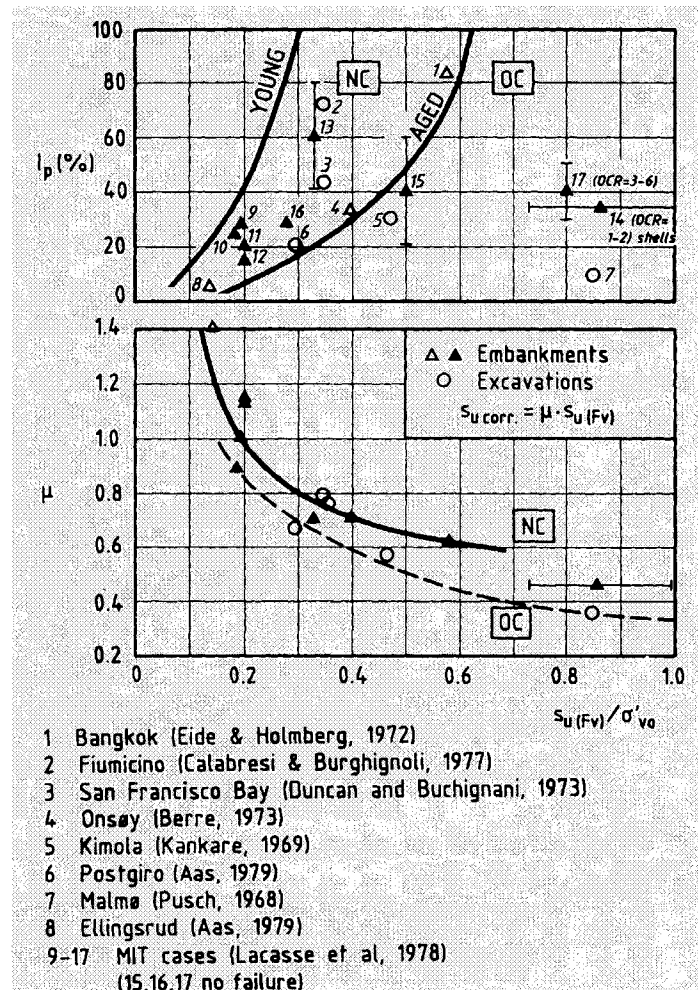


Figure 1.5 - Vane Shear Correction Factor (After Aas et al., 1986)

1.3 - Cone Penetration Testing

1.3.1 - Piezocone History

The cone penetration test (CPT) consists of a cylindrical probe with a conical tip that is attached to drill rods and pushed into the ground at a constant rate of 2 cm/sec while taking either continuous or intermittent measurements of the resistance to penetration. Often times the probe is advanced using a conventional drilling rig or a specialized cone penetration truck, though lightweight anchored trailer or frame

mounted hydraulic pistons are used in practice as well. The advancements in CPT technology from simple mechanical cones to advanced electronic cones are briefly described in this section.

The first cone penetration tests were conducted in Holland during the early 1930's by a Rijkwaterstaat (Dept. of Public Works) engineer P. Barentsen (Barentsen, 1936). These early tests consisted of a system of inner and outer rods, with a cone tip attached to the inner rods in an attempt to eliminate the frictional resistance of the soil acting against the drill rods and impacting the overall resistance values. The penetration resistance was measured using a manometer at the ground surface, and corrected by subtracting the weight of the rods to give a true indication of tip resistance. Successful implementation of the penetration resistance data in evaluating pile capacity by engineers and researchers including Buisman (1935), Huizinga (1942) and others encouraged the further development of the mechanical cone penetrometer.

Shortly after the Second World War an improvement on the original Dutch cone design was proposed and subsequently implemented by Vermeiden (1948). As in earlier iterations this design only provided a measure of the tip penetration resistance; however it employed a significant change in the penetrometer geometry. This change added a conical section just above the cone, with the intent of preventing soft or loose soils from entering the gap between the inner and outer rods. In such conditions earlier designs were susceptible to this infiltration, thus contributing to erroneous measurements or inability to continue advancing the cone. This design, as seen in Figure 1.6, became known as the Dutch Mantle Cone.

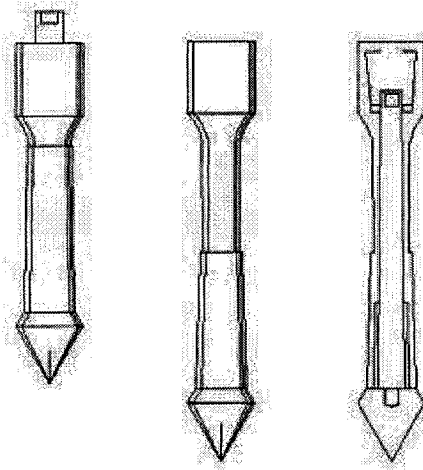


Figure 1.6 - Dutch Cone with Conical Mantle (Sanglerat, 1972)

Along with the Dutch Mantle Cone, a second type of mechanical penetrometer remains in use. The Begemann Friction-Cone was first used in 1953 and improved upon the Dutch Mantle cone by adding the ability to measure the local frictional resistance along the shaft of the cone, commonly referred to as the sleeve or skin resistance. The probe, as shown in Figure 1.7 is advanced by pushing both the inner and outer rods to a new measurement depth, and then pushing the inner rods and tip ahead of the system and measuring the point resistance. After 35.5 mm of movement the friction sleeve is engaged and both the point and friction sleeve advance in unison. The force required to advance the combined system is measured, and the difference between the initial point resistance and the combined resistance is recorded as the sleeve resistance. The advantage of measuring the sleeve resistance as well as the tip resistance is evidenced in the greater analytical power of CPT data, as discussed in the later sections of this report.

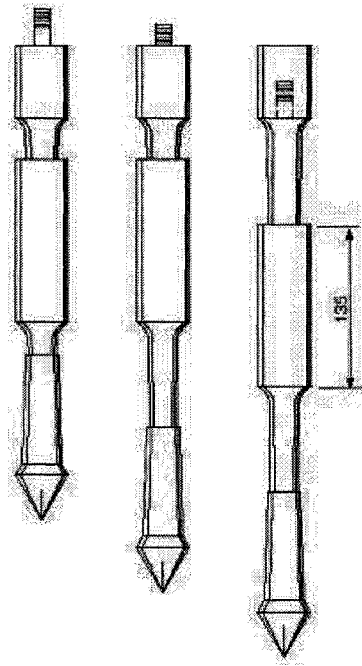


Figure 1.7 - Begemann Type Cone with Friction Sleeve (Sanglerat, 1972)

Mechanical cone penetrometers have remained in use since their development, especially in developing countries because they are relatively rugged, inexpensive and simpler devices. The use of mechanical cones is limited though, as they do not perform well in very soft soils or soils with large variations in penetration resistance, especially highly stratified deposits.

Development of electric cone penetrometers, as seen in Figure 1.8, is believed to have begun in Berlin, Germany during the Second World War (Broms and Flodin, 1988). This cone used a cable to transmit electric signals to the surface. De Ruitter (1971) is generally credited however with introducing the first true electric cone penetrometer capable of continuous measurement of both the point and friction resistance. The electric cone uses load cells or strain gauges to measure the tip and sleeve resistance, and transmit information to a user at ground surface using cables

strung through the center of the drill rods. This design is advantageous as it allows for continuous measurements and electronic recording of resistance, and eliminates the need for two sets of rods. Electric cone penetrometers also allow for a continuous push of the drill string, whereas mechanical cones required the operator to advance the inner and outer sections of the cone separately. Advancement in the design of load cells and electronics also allowed for accurate measurements in very soft soils.

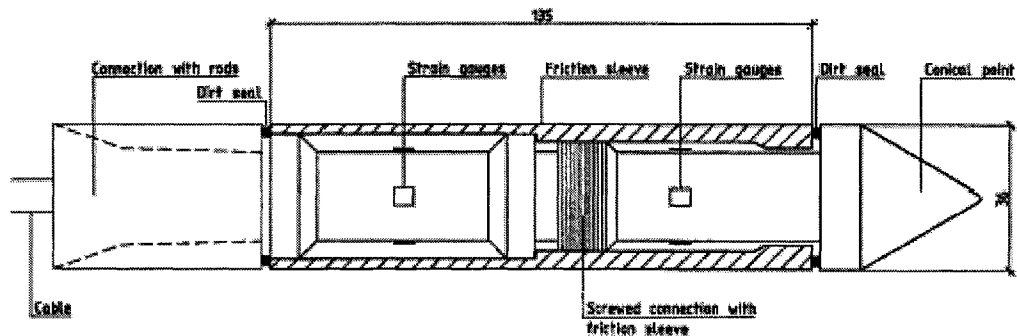


Figure 1.8 - Electric Friction Cone (Lankelma Cone Penetration Testing, Ltd.)

The many advantages of electric cone penetrometers lead to the rapid advancement in research and design of these devices. A significant amount of studies were conducted by the Delft Soil Mechanics Laboratory, as well as manufacturers and individual researchers in order to compare the performance of the electric cones with mechanical cones, and to optimize the geometry of the electric cone. As a result of this development most cone penetrometers currently in use conform to standardized dimensions and tolerances such as those outlined in ASTM D 5778, "Standard Test Method for Performing Electronic Friction Cone and Piezocone Penetration Testing of Soils". This standard describes the cone penetrometer as a cylindrical probe 35.7 mm in diameter having a conical tip with a 60 degree apex angle. Standard cones

have a 10 ton tip capacity with a projected tip area of 10 cm^2 and immediately behind the tip is a 13 cm long friction sleeve with a surface area of 150 cm^2 . In certain cases the projected area of the tip can vary from 5 to 15 cm^2 . A smaller projected area is advantageous in soft soils, as the tip capacity is reduced, allowing an increase in the sensitivity of the tip load cells. Larger cones are more rugged in design, and have the ability to house additional sensors. ASTM recommends that the friction sleeve dimensions for non-standard cones retain the proportions of friction sleeve of the 10 cm^2 cone.

Following the development of the electric cone penetrometer the next major advancement in cone penetration testing came from the first European Conference on Penetration Testing (ESOPT-1) in 1974. At this conference a pair of papers were presented (Janbu and Senneset, 1974; Schmertmann, 1974) and in the years immediately following subsequent work was presented (Wissa et al., 1975; Torstensson, 1975) detailing the use of piezometer cones. These cones, while shaped and operated in a similar manner as electric cones, measured pore water pressure as they are advanced. These piezometer cones were used in combination with tip and friction resistance provided by electric cones by using the probes in adjacent boreholes. Baligh et al. (1980) suggested that the combination of these parameters could provide relatively good indications of the stratigraphy and overconsolidation ratio in fine grained deposits.

The successful use of these two probes led to the development of an electric cone capable of measuring the pore pressure as well (Roy et al., 1980; de Ruiter, 1981; Baligh et al., 1981; Campanella and Robertson, 1981). This combination of the two

probe types is known as the piezocone, with the piezocone test referred to using the acronym CPTu. Piezocones use filters to allow the soil pore water pressure to be transmitted through a hydraulic circuit to a pressure transducer. Early piezocones had this filter element installed at various locations on the probe. Typical installation locations were at the tip of the cone, midway along the face of the cone, immediately after the shoulder of the cone, and along the shaft of the probe following the friction sleeve as shown on Figure 1.9.

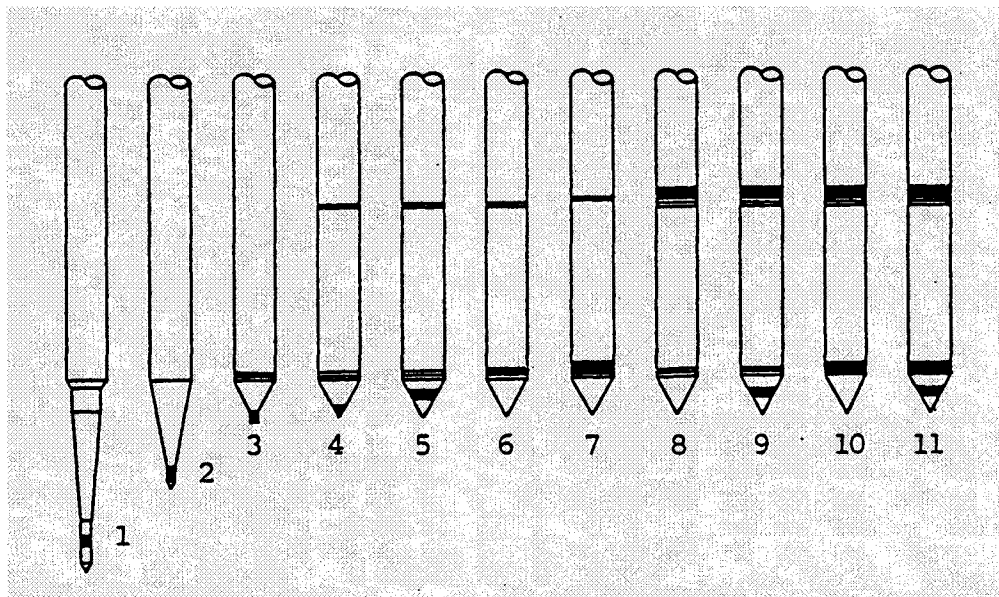


Figure 1.9 - Standard Designs and Filter Locations of Piezoprobes (1-2) and Piezocones (3-11) (Campanella et al. 1988)

Each location of the filter element has various advantages and disadvantages. For instance, a filter located at the tip of the cone is very sensitive to the changes in pore pressure as the cone is advanced, though this location also poses a significant threat of damage to the filter should a coarse layer be encountered.

It is important to note that the measured pore pressure, u_i , during penetration is a combination of two pressures. The first pressure which contributes to u_i is the

hydrostatic pore pressure, a function of the groundwater conditions at the test location. The hydrostatic pore pressure is commonly referred to as the u_0 condition. The second component of the pore pressure measured by the cone is the excess pore pressure (Δu) generated in the soil during penetration of the probe. The excess pore water pressure is described in greater detail in Section 1.3.2.2.

A unanimous agreement on an optimal location for the filter element has yet to be reached, though the general trend in practice has shifted from the mid-face (u_1) filter placement to the location immediately behind the cone (u_2) as the preferred filter configuration. For research and special projects certain cones are available with elements at two or three locations, allowing the user to determine the effect of pore pressure on the measured tip and sleeve resistances.

Further development of the piezocone has focused on the optimization of geometry and operational functionality of the probe. Piezocone manufacturers and researchers have successfully implemented additional sensors into the piezocone for specialty testing purposes. Of these sensors, temperature and inclination sensors are often used to ensure that the standard piezocone is operating normally. For geotechnical applications these specialty cones include the seismic cone, lateral stress cone, acoustic cone, dynamic cone, miniature cone and the vibratory cone. As cones are able to continuously log data, specialty cones have been developed for geo-environmental site characterization as well. These cones are able to measure the electrical resistivity, pH, redox potential (Ollie et al., 1992) and the presence of hydrocarbons through laser-induced fluorescence (Hirshfield et al., 1984).

Manufacturers have developed video cones as well, allowing the operator to see the material that the cone is advancing through.

1.3.2 - Piezocone Mechanics

1.3.2.1 - Tip and Friction Sleeve Load Measurement

The point load and friction sleeve load measurements are determined by changes in the resistance of strain gauges attached to the cylindrical strain element within the cone. This change in resistance causes a change in the voltage output from the load sensors and is interpreted into units of force and pressure using calibration factors.

There are two general configurations for load cells found in commonly available piezocones. The independent load cell configuration features load cells that measure the effects from one specific source, either the point load or the friction sleeve load. Subtraction type cones are available as well; in such cones the load cells work in series on the same strain element. The point load cell is measured from the load cell at the base of the strain element. A step in the strain element then transfers the load from the friction sleeve to the upper portion of the strain element, which records the combined effect of point and friction loads. The sleeve resistance is then electronically evaluated by subtracting the measurement of the point load cell.

Schapp and Zuidberg (1982) indicate that the subtraction type cone is a more rugged design, as the strain element can be much larger than that of an independent type. However it must be noted that because of the larger forces the combined load

cell must measure, there is a potential for the reduction of the accuracy of this friction sleeve measurement.

1.3.2.2 - Pore Pressure Measurement Location

As mentioned in Section 1.3.1 of this report, piezocones have been developed with filters at various locations on the probe, as no consensus for a standardized location has been reached. It is however important to take into account the location of the pore pressure filter element when selecting a particular cone for use at a site, and for interpretation of the data.

For ease of communication, a standard nomenclature has been developed to describe the location of the filter element on the piezocone. As illustrated in Figure 1.10, these locations have been denoted u_1 , u_2 and u_3 , and likewise cones are referred to by their respective filter locations as Type 1, Type 2 or Type 3. The u_1 location is used however to refer to a filter located at the tip of the cone or at the mid-face of the cone. Additionally some literature refers to the tip location as u_t , the mid-face location as u_{face} , and the u_2 location as u_{bt} .

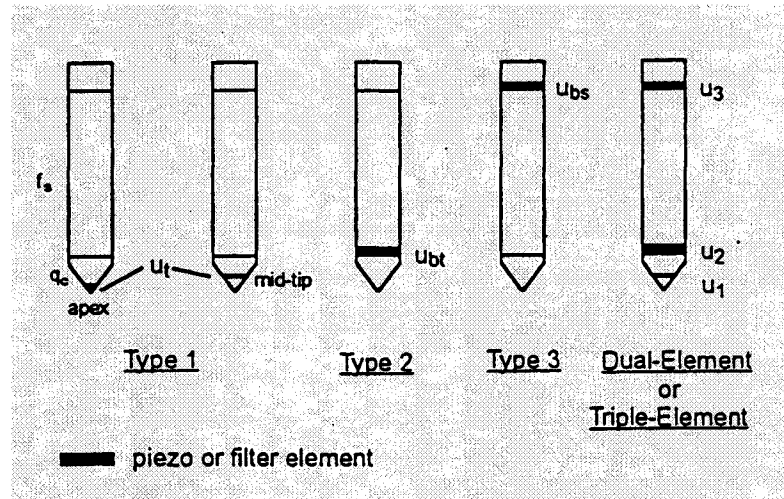


Figure 1.10 - Typical Filter Element Location Nomenclature
(After Mayne and Chen, 1994)

While the hydrostatic pore pressure (u_0) is generally known, the filter location is known to affect the pore pressures measured, and therefore cause a misinterpretation of the excess pore pressures that are generated during advance. During advance in free draining materials, the excess pore pressure generated is typically negligible. When advancing the cone in low permeability soils high excess pore pressures can be generated at the tip. Shear stresses (deviatoric stresses) are exerted as well as the soil fails around the cone tip, and these stresses can yield an increase or decrease in pore pressure. Lunne et al. (1986a) have reported findings that indicate the pore pressures measured at the tip of the cone are very similar to those measured along the face of the cone. For cones measuring the pore pressure in the u_2 or u_3 locations the pore pressures measurements can vary greatly from the pressure at the tip or face of the cone.

In soft normally to moderately over consolidated soils this shear stress will yield a positive pore pressure as the soils contract, while decreases in pore pressure have

been noted in heavily overconsolidated soils due to their dilative nature. In either case, the pore pressures will generally decrease past the shoulder of the cone as the normal stress is reduced. For the case of the contractive soils the excess pore pressures gradually dissipate with distance from the tip. This behavior is noted in Figure 1.11, which compares the pore pressures measured at various locations along the piezocone in lightly overconsolidated Bothkennar clay (Powell and Quarterman, 1991) as the pore water pressure recorded at the tip is greater than that measured at the u_2 location, which in turn is greater than that measured at the u_3 location.

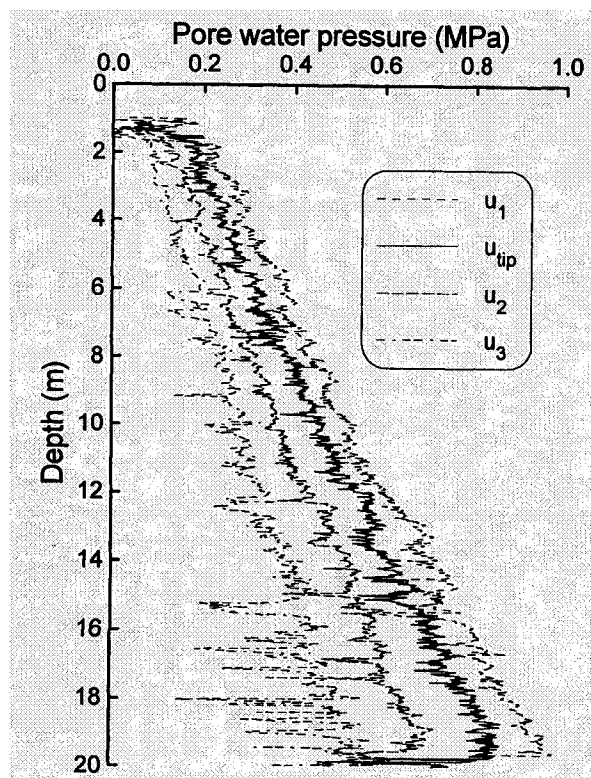


Figure 1.11 - Effect of Filter Element Location on Measured Pore Pressures in Normal to Moderately Overconsolidated Clay (After Powell and Quaterman, 1991)

In dilative soils this behavior is especially pronounced, and can lead to difficulty in interpretation and further computation. In some cases a negative pore pressure has

been recorded due to this behavior (Campanella et al., 1982; Torstensson, 1982). Figure 1.12 presents a comparison of the pore pressures recorded at various locations on the piezocone in a heavily overconsolidated Gault clay as an example of the extreme pore pressure gradient which can occur (after Lunne et al, 1997). The pore pressure measured at the u_2 location is significantly less than that measured in the u_1 position, while the pressure measured at the u_3 location is near zero.

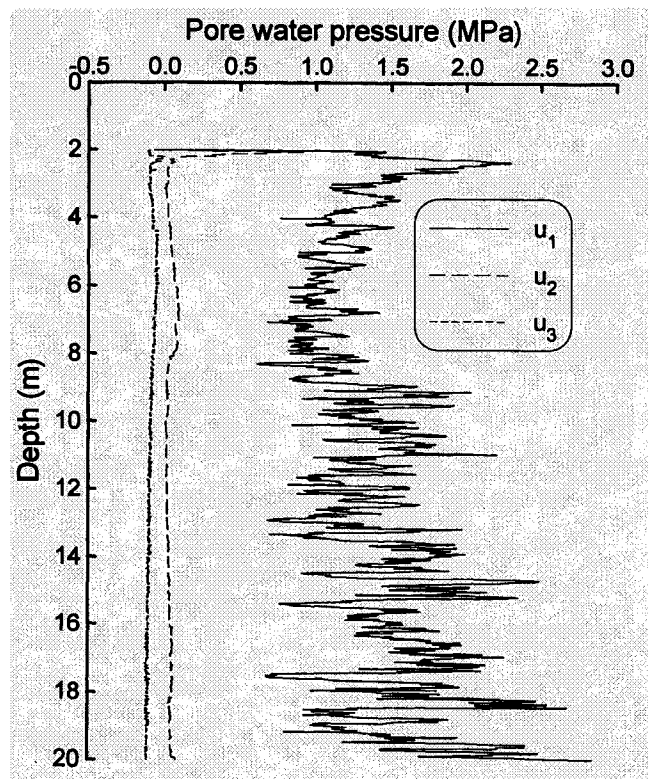


Figure 1.12 - Effect of Filter Element Location on Measured Pore Pressures in Heavily Overconsolidated Clay (After Lunne et al., 1997)

The choice of filter location for a particular piezocone also has an effect on the pore pressure dissipation characteristics, the effectiveness in defining stratigraphy and the end area corrections to the tip and sleeve resistance measurements. End area corrections account for the water pressure acting on the different projected areas of

the tip and friction sleeve that can impact the true penetration resistance. Figure 1.13 schematically presents the unequal areas which impact the piezocone tip.

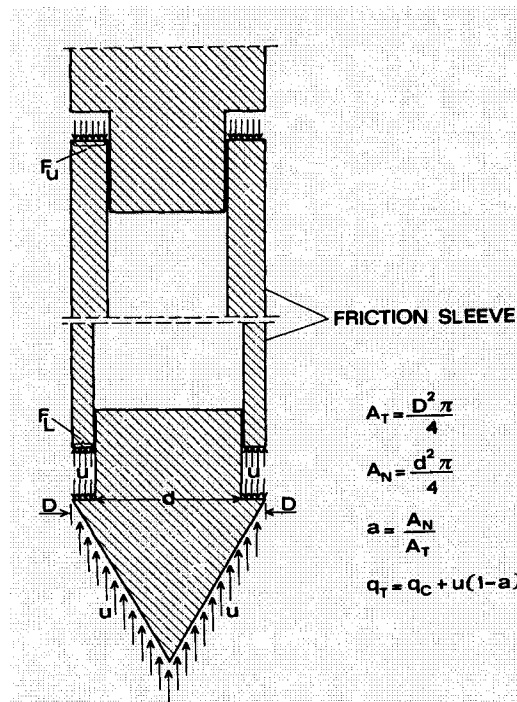


Figure 1.13 - Unequal End Areas of the Piezocone (Jamiolkowski et al., 1985)

When conducting a dissipation test with the piezocone, by halting the penetration and allowing for the decay of excess pore pressures, a pressure gradient such as that observed in heavily overconsolidated soils can result in an initial rise in pore pressure when measured in the u_2 location. In normally consolidated fine grained soils, such as those found at the research site, the pressure gradient is not as drastic, and it has been reported that dissipation data behind the tip is in good agreement with data measured at the tip.

When a detailed stratigraphic profile is required, it is suggested that the pore pressure be measured on the face or tip of the cone, especially in heavily overconsolidated soils (Baligh and Levadoux, 1980). Filters in this location will

provide sharp definitions of changes in pore pressure, which can be beneficial in determining changes in stratigraphy. Some authors suggest that because the pore pressures are only reduced by between 10% and 30% at the shoulder in normally consolidated clays, as reported by Mayne et al. (1990), that the advantages of this filter location for reasons such as a reduced possibility for damage to the filter element justifies the use of a Type 2 cone for stratigraphic definition (Campanella and Robertson, 1988).

While the selection of the filter element location may be a compromise depending on the available equipment and the purpose of the investigation, it is important to note that the filter location can affect the data and therefore the interpretation of soil properties. It is therefore critical that the end users of data from piezocone profiles are aware of the filter location and its potential effect on measured pore pressures.

1.3.2.3 - Filter Element Considerations

The filter element also plays an important role in the quality of data produced during the advancement of the piezocone. A fast response time to changes in pore pressure is important, and research has suggested that this is a function of the compressibility and viscosity of the saturation fluid, the permeability of the porous element, the area to wall thickness ratio of the element, the rigidity of the element and finally the air entry resistance of the filter element (Smits, 1982).

No significant difference in pore pressure response has been found between water and glycerin, or water and silicone oil (Bruzzi and Battaglio, 1989; Larsson and Mulabdic, 1991), therefore an optimization of the filter material must be considered. A high permeability of the filter element material is desirable as this can allow the

pressures to be transmitted quickly; as is a high air entry resistance, to maintain element saturation. These two properties are conflicting though, as most filters cannot exhibit high values for both.

An element with a high rigidity is crucial as well, especially for piezocones with the filter element at the tip. In such cases, when advancing the probe through stiff soils the filter can compress, leading to artificially high pore pressures. A 30 percent increase in pore pressure has been reported in such cases (Battaglio et al., 1986). Both steel and rigid ceramic filters are available for use when these conditions are encountered, however if penetrating through coarse grained materials, low ductility steel filters are subject to abrasion and reduction in permeability.

Piezocones with filters located at the u_2 or u_3 locations can take advantage of filter elements manufactured with polypropylene, a low rigidity porous plastic material, with less concern for the compressibility affecting pore pressure measurements. Polypropylene filters saturated with a high viscosity fluid have the advantage of high permeability and high air entry resistance.

It has been suggested by Campanella and Robertson (1988) that filter elements be changed following each completed profile, as clogging or a reduction in permeability may occur due to abrasion.

1.3.3 - Piezocone Testing System

1.3.3.1 - The Hogentogler 10 Ton Cone

The piezocone used for this investigation was an electric 10 ton subtraction cone purchased from Hogentogler & Co., Inc. Since the purchase of the piezocone the

CPT division of Hogentogler & Co., Inc. has been acquired by Applied Research Associates (ARA)/Vertek. All references to the manufacturer imply ARA/Vertek unless otherwise noted.

During the work performed at the RWS site, the piezocone was equipped with four sensors, enabling the measurement of tip resistance, sleeve resistance, pore water pressure and probe inclination. This cone has is also equipped with a geophone for seismic use; however this feature was not used during the testing program. The piezocone uses a standard 60 degree tip with a 10 cm² projected area, and a 13 cm long friction sleeve with a total surface area of 150 cm². The pore water pressures are measured behind the tip, in the u₂ position.

The cone tip is machined to allow the saturation fluid to transmit soil pore water pressures through the filter to the pore pressure transducer, which is housed within the strain element. The pore pressure transducer has a capacity of 3450 kPa (500 psi) through a range of 7.5 volts. The probe uses a polypropylene filter element available from the probe manufacturer which is 5 mm thick (Figure 1.14).

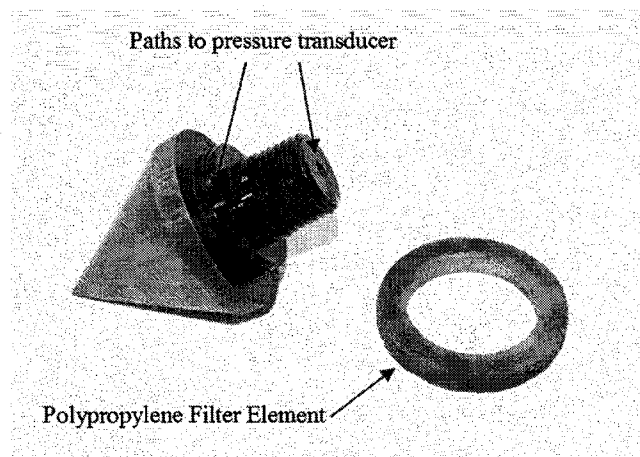


Figure 1.14 - 60 Degree Cone Tip and Filter Element

The cone tip threads through an equal end area adaptor into the strain element. The lower portion of the strain element is fitted with strain gauges that capture only the tip resistance. The friction sleeve is fitted over the strain element prior to the installation of the cone tip and has a stepped inner diameter such that it can apply a load to the upper portion of the strain element. Strain gauges are fitted to this upper portion as well and record the combined tip and sleeve resistance. The friction sleeve is secured to the probe with the cone tip (Figure 1.15).

Wires from the strain gauges and pore pressure transducer run through the center of the strain element as well as through a collar above the friction sleeve and into the electronics housing. The electronics housing contains the inclinometer, which has a range of +/- 15 degrees. The cone tip has a capacity of 100 MPa while the friction sleeve capacity is 1000 kPa, each over a span of 7.5 volts. This housing can be disassembled by the user to inspect or repair the strain gauge wiring, however the manufacturer recommends against this as disassembly and reassembly could easily damage the electronics. Above the electronics housing is the coupler housing to which an electronic cable is connected to transmit data to the ground surface.

At the ground surface the cable is connected to a junction box which is equipped with a 15 volt DC linear power supply powering all sensors in the cone. Rather than having a ground for each sensor output (channel) the junction piezocone has a common ground for all channels. The power supply is a low-noise unit to help prevent interference between channels.

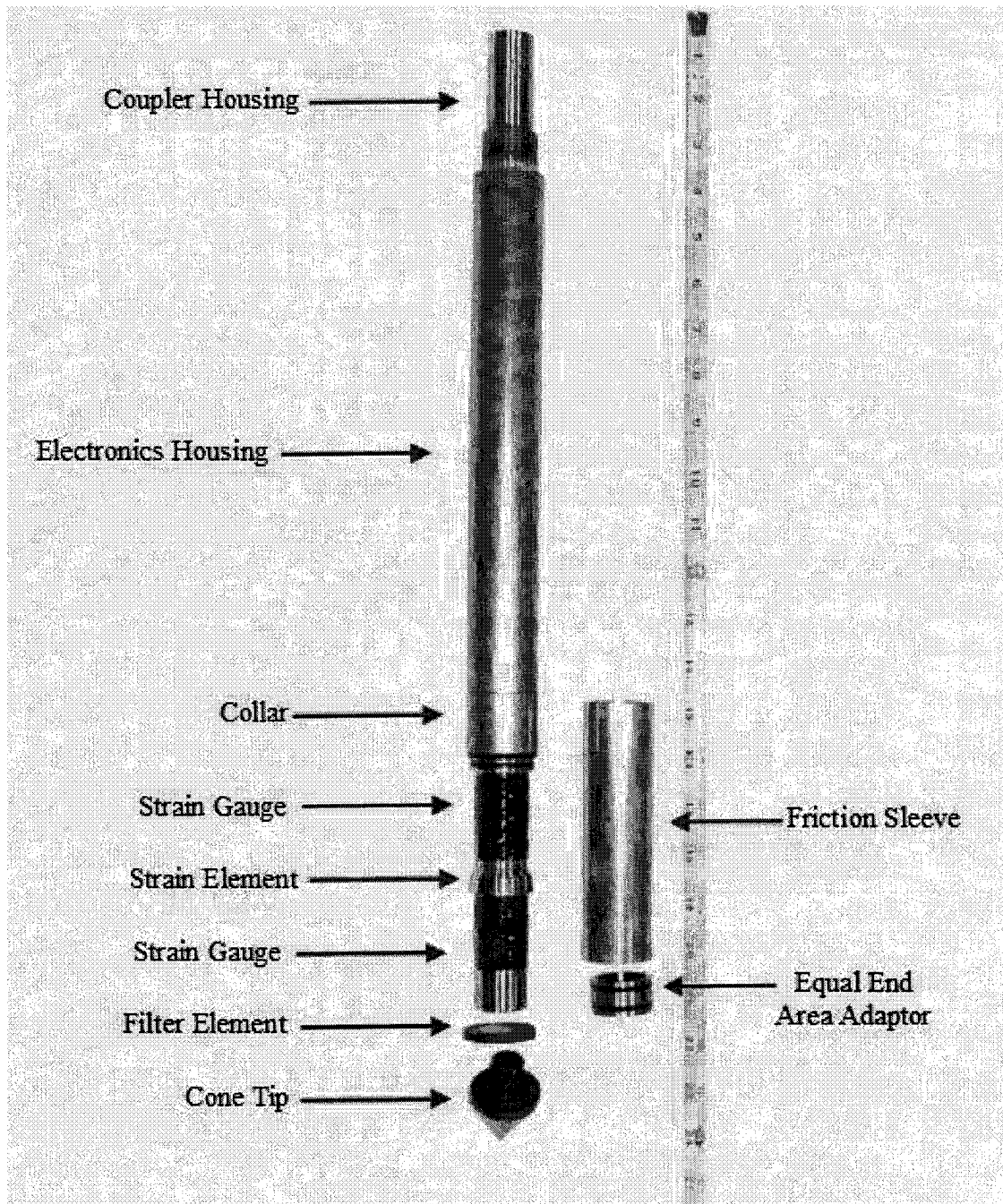


Figure 1.15 - Photograph of 10 Ton Hogentogler Cone
(Scale in inches)

1.3.3.2 - Depth/Velocity Transducer

To allow the operator to correlate piezocone output to the depth of the probe, and monitor the advance rate of the drill string, a combination position and velocity

transducer is installed within the data acquisition chain. At the RWS site a model DV301 Cable Extension Transducer, manufactured by Celesco Transducer Products, Inc. was used for this purpose. This transducer uses a precision potentiometer to measure position, and a self generating DC tachometer to provide the velocity of a thin stainless steel cable.

The transducer is mounted at the drill head of a drilling rig, and the cable is attached to a stationary point on the drill rig. As the drill rods are advanced via pushing by the drill head the stainless steel cable is retracted into the transducer. The potentiometer outputs a voltage correlating to the cable extension distance, while the tachometer outputs a separate voltage correlating to the angular velocity of the spool of stainless steel cable.

1.3.3.3 - Data Acquisition System

A data acquisition system is required to receive, process and store the outputs from the sensors in the piezocone and from the position/velocity transducer. The data acquisition system consists of three major devices; a junction box; a data switch / analog to digital converter; and a portable computer. A schematic of the data acquisition system is presented in Figure 1.16.

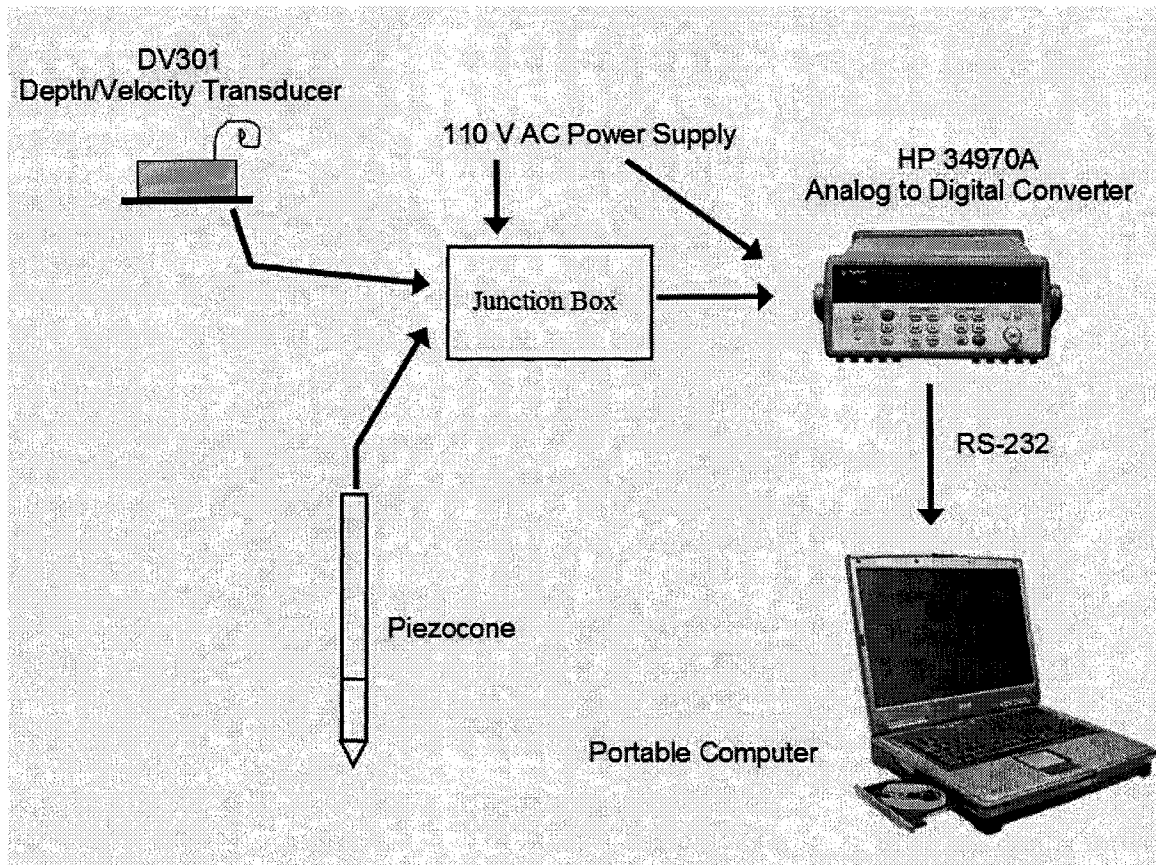


Figure 1.16 - Schematic of the Data Acquisition System for Piezocone

The junction box is externally powered and directly receives the voltage output of sensors from both the piezocone and the position/velocity transducer. Each output voltage is treated as a separate channel in the junction box and is sent via a single cable to the data acquisition unit.

The data switch unit is a model HP 34970A, manufactured by Hewlett Packard. This unit uses a high-precision 16-Channel Reed Multiplexer module to accept and process each channel, and is capable of high speed scanning of active channels. The data switch unit captures six analog data outputs from the junction box; sleeve resistance, tip resistance, pore pressure, inclination, depth and penetration rate. The individual output voltages of these six channels are then scaled according to the

calibration factor of each sensor and digitized for further processing by the computer. While the data switch is capable of handling 600 readings per second on an individual channel, the RS-232 interface from the HP 34970A to the computer has a limited data transfer rate. It was determined that a scanning interval of 0.2 seconds per channel would provide sufficient accuracy without overloading the buffer of the RS-232 interface.

A portable computer was used to accept and store incoming data from the HP 34970A unit. Data collection was handled by the Agilent BenchLink Data Logger v1.5 software. This software allows the operator to interface with and adjust scanning properties of the data switch. In addition to storing the incoming data the software displays the measurements from each data channel in real time as shown in Figure 1.17. At the conclusion of a piezocone profile the data is then saved in a spreadsheet format for further manipulation.



Figure 1.17 - Screen Capture of the Agilent BenchLink Software

1.3.4 - Filter Element Saturation

Accurate pore pressure response during a piezocone test is recognized to be dependent on the complete saturation of the hydraulic circuit leading to the pore pressure transducer (Campanella et al., 1981; Battaglio et al., 1981; Lacasse and Lunne, 1982). Proper saturation of the filter element and the hydraulic circuit is critical for accurate measurement of pore pressures. A loss of complete saturation allows air to mix with the saturation fluid. Air is approximately 10,000 times more compressible than water, as well as silicone oil. As a result the piezocone will not accurately measure the pore pressure as the pressure at the transducer cannot reach equilibrium with the external pressure due to the volume change from the compression of air and the continuous advance of the probe. Incomplete saturation of the filter element or entrapped air within the circuit will lead to a delay in the

response of the sensor to both increases and decreases in the soil pore water pressure.

Common saturation fluids are de-aired water, glycerin and silicone oil. Each fluid has been used with success, however the low viscosity of de-aired water can cause the filter element to become unsaturated in coarse grained materials, in unsaturated clays, or prior to insertion in the borehole. For work performed in soft, low permeability clays, as are found at the test site, the piezocone manufacturer recommended the use of silicone oil with polypropylene filter elements. This combination combines a high permeability filter element, allowing faster response to pore pressure changes, with a low viscosity saturation fluid, which provides a high air entry resistance.

Silicone oil is not miscible with water, and generally requires a more complex saturation process when compared to the use of de-aired water. The laboratory filter saturation process consisted of a sealed vacuum chamber, connected to a high-vacuum pump with a dessicator and vacuum gauge inline. New unsaturated elements were placed in the vacuum chamber alongside a container of silicone oil. The silicone oil used for saturation was Methyl Silicone 10,000CS, manufactured by Nye Lubricants. After a period of 18-24 hours the vacuum chamber was jarred, causing the elements to fall into the silicone oil, where they remained for upwards of 48 hours under continued vacuum. A set of pre-saturated filters was purchased from the manufacturer as well to provide an additional supply for field use.

1.4 - Dilatometer Testing

1.4.1 - Dilatometer History

The Flat Dilatometer Test (DMT) was developed in Italy in 1980 by Silvano Marchetti and is currently used in more than 40 countries, both for research and in practice. The dilatometer is a thin blade with a flexible circular steel membrane on one face which is advanced into the ground for testing at 15 to 20 cm intervals (Figure 1.18). The dimensions of the blade have been standardized (ASTM D 6635) to be 15 mm thick and 96 mm wide. The taper of the blade is 50 mm with an apex angle of 24 to 32 degrees. The thin steel membrane is mounted flush to the surface of the blade, and held in place with a retaining ring and small machine screws. The membrane is 60 mm in diameter and is typically 0.20 mm thick, though 0.25 mm thick membranes are available.

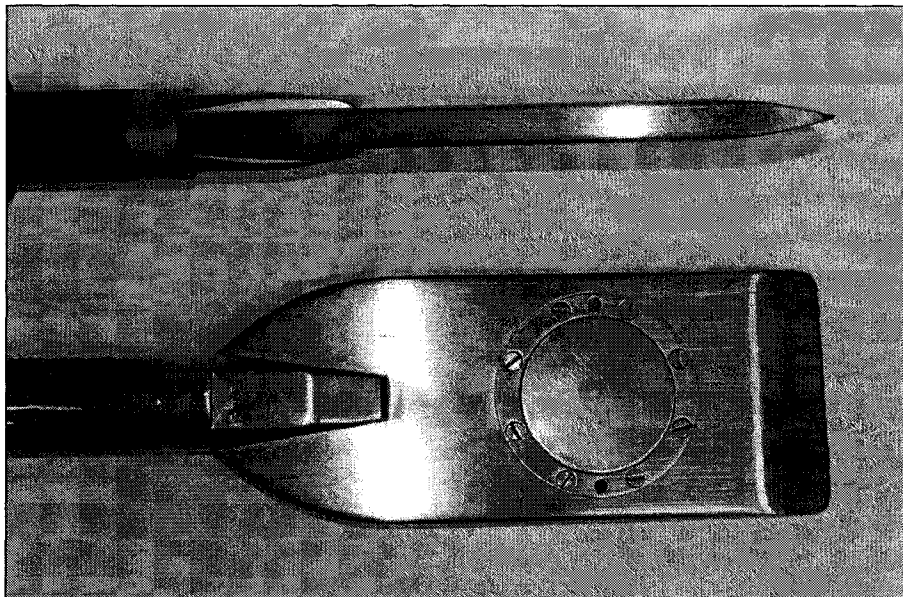


Figure 1.18 - Flat Dilatometer Blade with Flexible Steel Membrane

The dilatometer has proven successful in determining basic geotechnical soil properties, and performs especially well in settlement analyses. The test is defined as a penetration test rather than a pressuremeter test by Marchetti (1980), as the test distorts the in situ stress and strain conditions by displacement during advance of the probe. This test advances a thin steel blade through the soil, and at test depths expands a thin steel membrane using pressurized gas. The pressures required to expand the membrane to specific displacements can then be used to estimate soil properties. The expansion of the membrane during the flat dilatometer test does not bring soil to a failure state, but instead records pressures at specific displacements.

An advantage to using the DMT is that the shallow angle of the blade (20 degrees) reduces disturbance during penetration relative to the CPT, therefore there is less disturbance of the in situ stress-strain state the soil adjacent to the membrane. This effect is presented in Figure 1.19, created by Baligh (1975) to display the amount of disturbance caused during penetration of a cone shaped object, and a wedge shaped object.

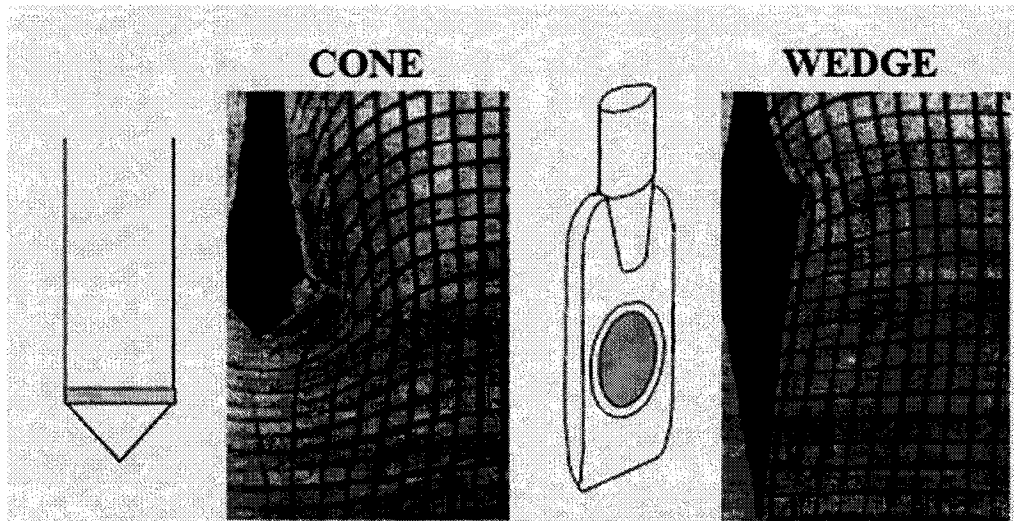


Figure 1.19 - Effect of Geometry on Distortions in Clay (after Baligh, 1975)

Few changes have been made to the overall design or operation of the device since its introduction, with the exception of special research probes equipped with pore water pressure transducers and/or sensors to monitor the continuous displacement of the membrane. The devices which have been instrumented with these components allow for a better understanding of the response of the soil during the expansion of the membrane.

1.4.2 - Operating Principle of the Dilatometer

The Flat Dilatometer test equipment consists of two major systems, the control unit at surface level and the dilatometer blade below ground. These two systems are joined using a pneumatic-electrical cable that is strung through the drill rods. The drill rods used are generally those used for CPT soundings, and the dilatometer blade may be advanced using conventional drilling rigs, cone penetrometer rigs, or a portable frame with hydraulic ram. In some cases the equipment may be driven through especially hard or cemented strata, though this must be done with caution to not damage the equipment.

Within the dilatometer blade, housed behind the membrane are components of the buzzing alarm system that indicates the position of the membrane at specific displacements (Figures 1.20 and 1.21). The pneumatic-electrical cable is used to provide pressure to the membrane, and the electrical signal for the buzzer. The test begins as pressure is applied and the membrane lifts off of the sensing disk (typically 0.05 mm displacement) this displacement the A reading is made. With increased pressure the membrane expands further and at 1.1 mm displacement, the B reading is recorded. As the pressure is released after the B reading the membrane returns to the lift off displacement of 0.05 mm. At this point the C reading is recorded from the pressure gauges.

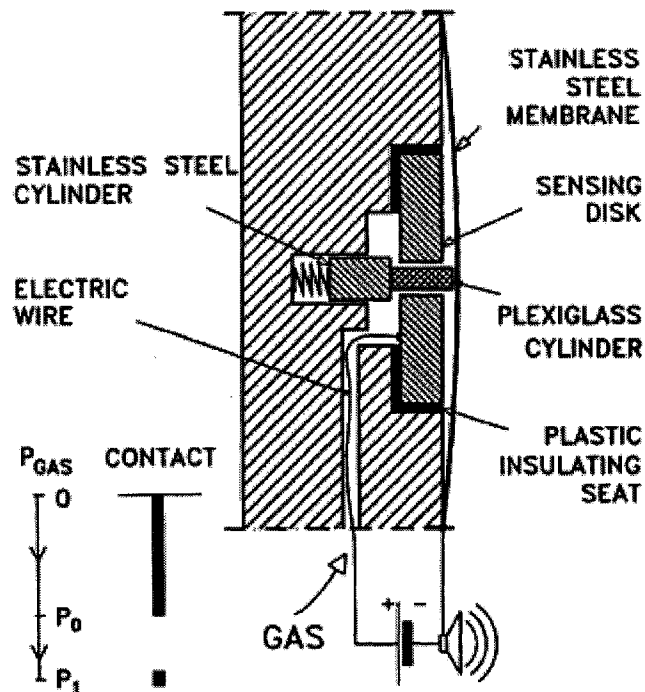


Figure 1.20 - Schematic of Membrane Displacement Mechanism (Marchetti et al., 2001)

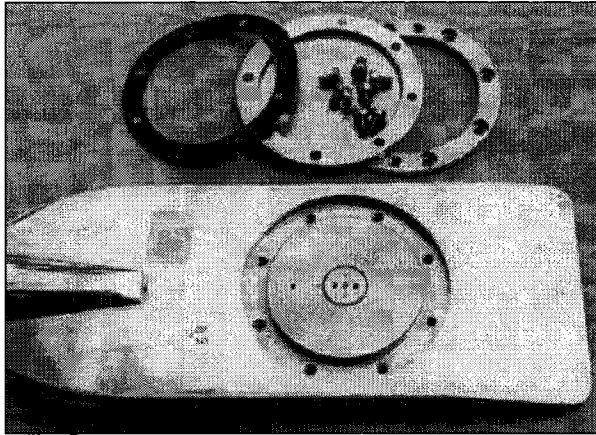


Figure 1.21 - Disassembled View of Dilatometer Blade Membrane (Marchetti, 2001)

The control unit consists of both low-range (0 to 10 bar) and high-range (0 to 60 bar) dial gauges that are used to record the A, B and C pressures (Figure 1.22). Two ranges are used to allow for better accuracy when measuring very soft materials. The two gauges are connected in parallel, enabling the user to monitor both gauges where needed. Should the low-range gauge reach its maximum measurable pressure the system will automatically exclude the gauge to prevent damage. Valves are housed within the unit to control gas flow to the dilatometer blade, and to vent the system to deflate the membrane. A main valve is used to isolate the control unit from the gas source, while secondary valves are used to control the rate of flow in small increments. The pressure source to inflate the dilatometer membrane is connected to the control unit with pneumatic tubing. The gas pressure tank is fitted with a regulator as a safeguard against over inflation and dry nitrogen is the recommended gas (ASTM D 6635). A buzzing signal alarm is mounted in the control unit housing, which also contains the connections for the pneumatic-electrical cable, an electrical ground cable, and calibration equipment.

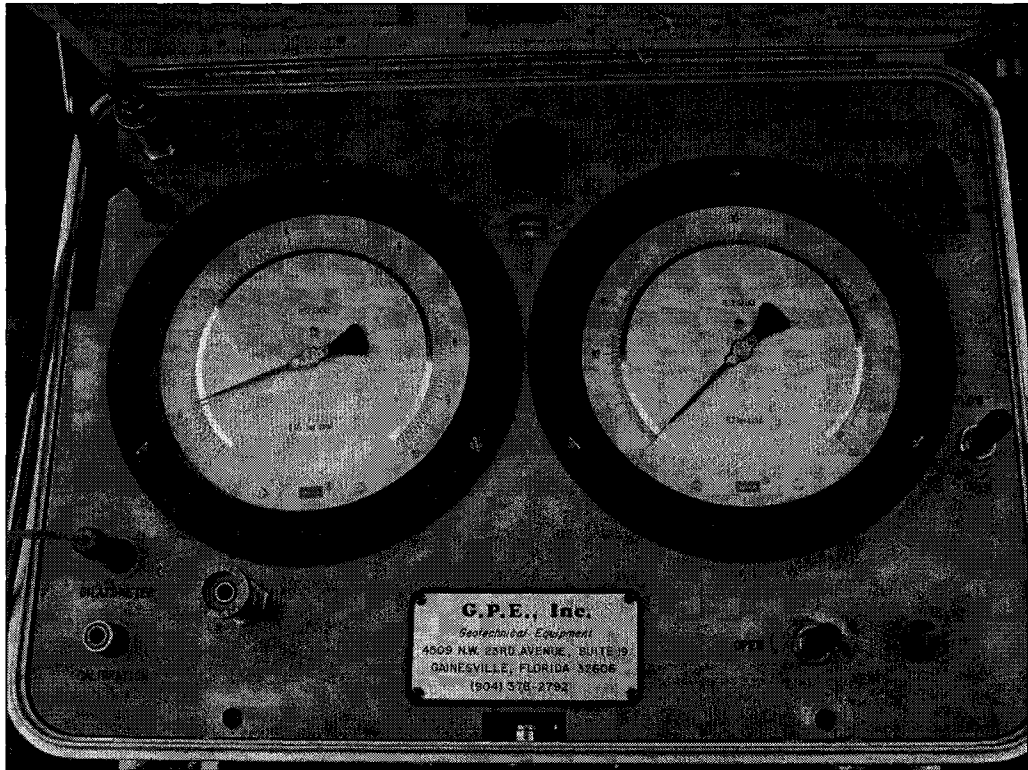


Figure 1.22 - Dilatometer Control Unit

CHAPTER II

SITE CHARACTERISTICS

2.1 - Site History

The Regional Waste Systems, Inc. (RWS) Ashfill/Balefill Facility in South Portland, Maine as shown in Figure 2.1 is located approximately 3.2 kilometers (2 miles) west of the Portland International Jetport, and 3.2 kilometers to the north and west of the I-95/I-295 interchange.

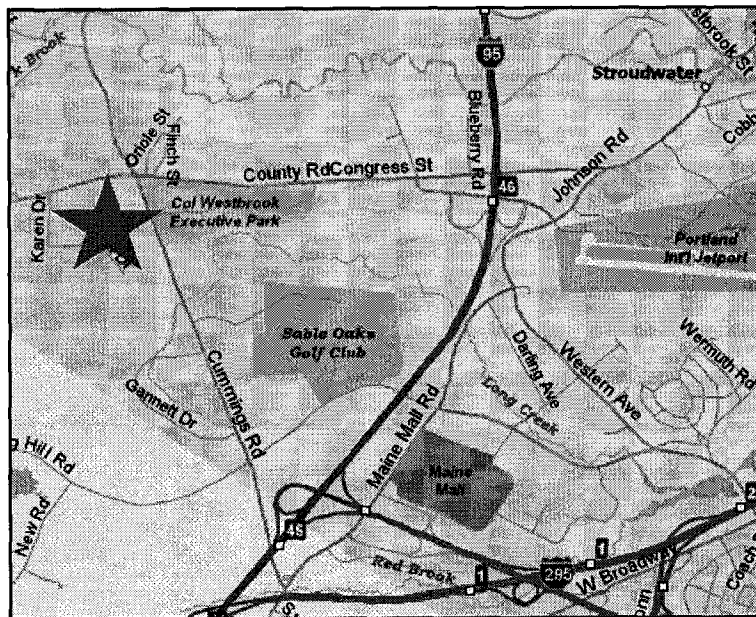


Figure 2.1 - Location Map, RWS Ashfill/Balefill Facility

The site has used phased design and filling operations throughout its lifespan to account for changes in the strength of the underlying soft silty clays and to maintain

adequate factors of safety against failure. In addition to the phased operation of the facility, the site has been well instrumented to monitor the behavior of the clay stratum with time. The site wide monitoring installations are discussed in greater detail in later sections of this report.

The original design and permitting process for the RWS facility was completed in 1985 by E.C. Jordan, Co. This design planned for a 20 year operating life span at the facility, with three distinct filling phases. The Maine Department of Environmental Protection (MeDEP) approved the multi-stage design and granted permits for the construction and filling of the Phase I cells in 1988. The Phase I cells consisted of Cells 1a, 1b and 2, which are located in the central portion of the site, as seen in Figure 2.2. During Phase I a stability berm was constructed along the east and west sides of cell 1b to counteract the driving forces of the ash fill, thus maintaining a minimum factor of safety against a deep rotational slope failure.

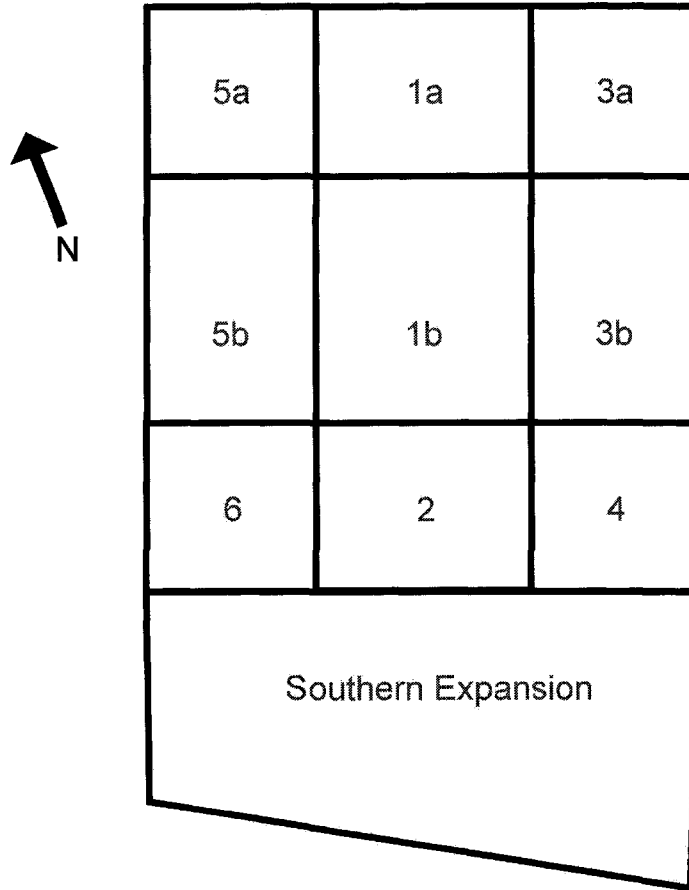


Figure 2.2 - RWS Landfill Schematic

Phase II consists of two separate filling operations, referred to as Phase IIa and IIb. Slope stability analysis and design for Phase II began in 1993, and in the spring of that year MeDEP approved the construction of the Phase II cells. Approval for the placement of waste in these cells was granted between June of 1994 and January of 1995.

Phase IIa consisted of the filling of cells 3a, 3b, 4, 5a, 5b, and 6. In addition stability berms varying between 2.75 and 3.1 meters high were constructed north of cell 1a and across the entire southern side of the landfill to resist the driving forces additional ash fill would create and maintain adequate factors of safety. Material required to construct these new berms was largely taken from the berms to the east

and west of cell 1b. While the cell 1b berms were necessary during the initial filling phase of the landfill, the placement of ash in cells adjacent to cell 1b allowed for the safe removal of these berms. Phase IIb consisted of placing a layer of waste over the entire landfill, with a peak thickness of approximately 9.75 meters (el. 31.3 m) in the center of cell 1b. Stability berms were once again required at the site to increase the factor of safety for side slopes and in hopes of reducing the rate of shear strain in the soft clay stratum. These berms were constructed on both the north and east sides of the facility during Phase IIb filling. This phase was completed during the winter of 2005.

Phase III is another vertical expansion similar to Phase IIb. In Phase III the slopes were once again designed to meet or exceed a minimum factor of safety against global failure of 1.3. The final maximum elevation proposed in this phase is 36.2 meters, in the center of cell 1b.

An application for a 20-acre Southern Expansion was completed and approved by the MeDEP in 2000. This proposed expansion will be required for the continued operation of the RWS facility in the upcoming years, as the end of the 20 year projected life span is nearing. Construction activity began at this location in the fall of 2005 with a stability berm placed along the southern side of the existing landfill. A fourth phase of construction and filling at the facility has been proposed. This final phase would place a layer of waste over the southern portion of the existing landfill. While Phase IV is not proposed to begin for 20 to 25 years, the underlying clay stratum will require strength gain to make this proposal feasible from a stability standpoint.

2.2 - Subsurface Conditions

2.2.1 - Stratigraphy

Geotechnical investigations conducted by E.C. Jordan, Co. (1985) for the initial design and a subsequent supplemental investigation prior to the Phase IIa stability analyses, performed by Peterson-Rabasca Geoengineers (1994) have characterized the subsurface conditions at the site in a series of boreholes. This data has been supplemented with various in situ tests and laboratory testing of undisturbed samples. The overburden soils generally consist of glacio-marine silty clays with interbedded fine sand layers at depth. These overburden soils overlie glacial tills and bedrock.

The silty clays present at the site consist of a weathered stiff olive-brown crust over a near normally consolidated soft gray clay layer. Both of these layers are of the Presumpscot Formation. The weathered crust typically extends to a depth of 3.05 meters across the site, while the soft gray silty clay varies between 9.15 and 21.3 meters thick within the footprint of the landfill. The soft clay is generally 9.15 to 12.2 meters thick in the northern portion of the site, increasing in thickness towards the center of the landfill. Field shear vane profiles have classified this gray clay as sensitive to very quick. The soft layer gradually tapers to the south of the site, and is not present in the Southern Expansion area.

Towards the lower extent of the soft gray silty clay layer sand lenses of gradually increasing thickness are observed. The granular material and glacial till is generally 1.5 to 9.15 meters thick across the site and consists of dense moderately stratified fine sands with varying amounts of gravel and silt. Boring logs from the 1994

exploration program note bedrock surface elevations varying between +6.1 meters to -1.2 meters with an average ground surface elevation of 21.3 meters.

The weathered olive-brown crust is generally stiffer than the soft gray clay, with undrained shear strengths ranging from 143.6 kPa (3000 psf) at the surface to approximately 23.9 kPa (500 psf) at the interface with the soft gray clay. Previous investigations have shown that the soft gray clay has an undrained shear strength varying between 12 and approximately 33.5 kPa (250 and 700 psf). An uncorrected field shear vane strength profile from tests performed at locations which have not been influenced by the loading at the RWS Facility is shown in Figure 2.3. Laboratory testing has indicated that the soft gray clay generally has a moisture content on the order of 10 to 15 percent greater than the weathered crust. The lower measured undrained shear strengths within the clay control the global stability at the site.

Undrained Shear Strength Profile (Virgin Conditions)

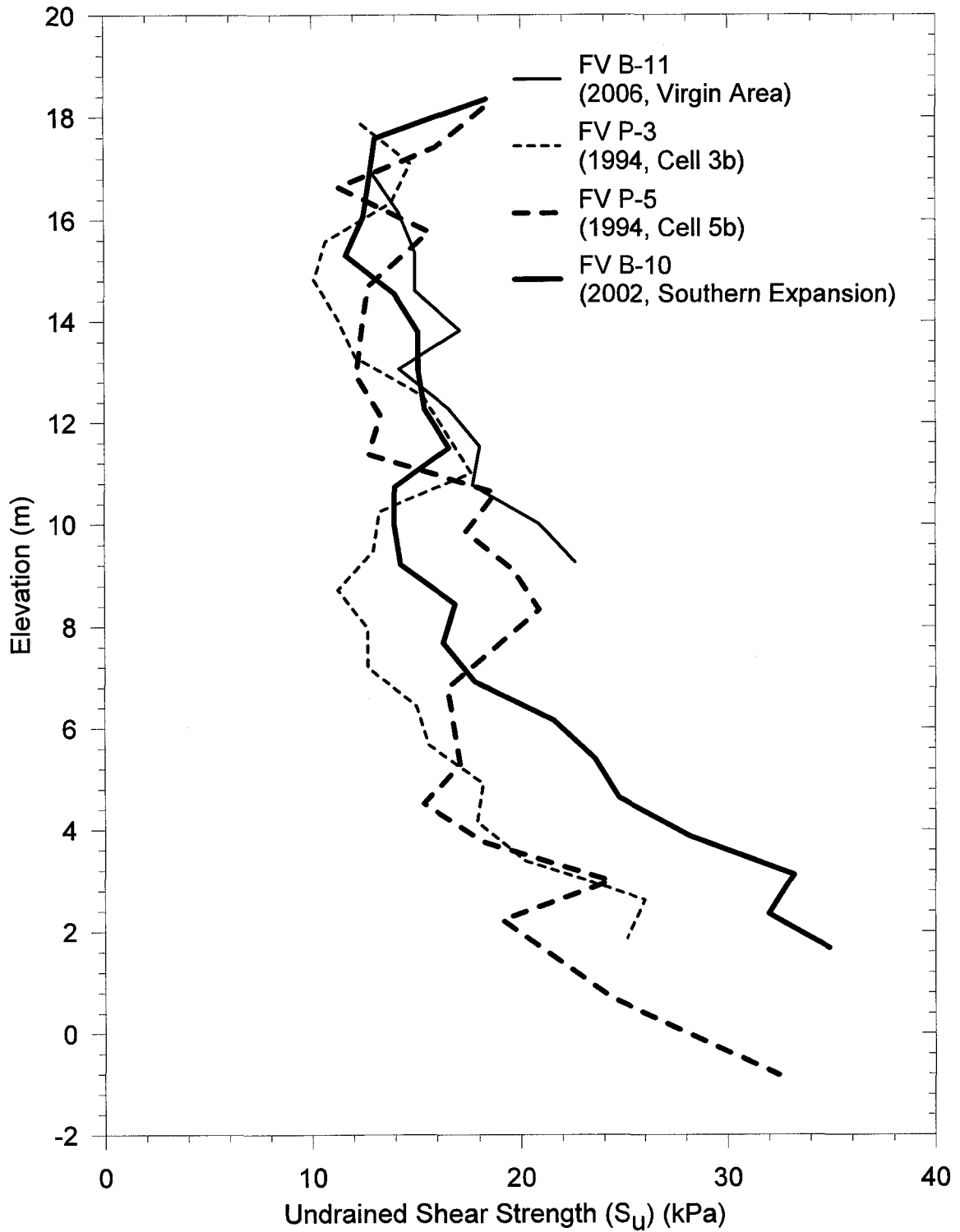


Figure 2.3 - Undrained Shear Strength of Virgin (unloaded) Soil at the RWS Ashfill/Balefill

2.2.2 - The Presumpscot Formation

The Presumpscot Formation clays found at the site were deposited in the Pleistocene era, towards the end of the last great ice age. As the glaciers which covered much of New England formed, the immense weight of the ice caused a depression in the earth's crust. With the increase in global temperatures the glaciers retreated and the depressed crust did not immediately rebound. This allowed the low lying areas to be flooded with seawater forming a large relatively shallow sea. Melt water from the retreating ice sheets carried sediment into this sea, where it deposited over time forming the Presumpscot Formation.

The formation is characterized by its soft clays overlying relatively thin layers of glacial till over bedrock. Silt size particles, rather than clay sized particles are the dominant material in this formation. These particles fall into the category of rock flour, as they originate from the bedrock of the region which was finely ground by glacial action. Minerals present in the fine grained portions of the formation include quartz, feldspars, muscovite, biotite and orthoclase (Beem, 2004). Presumpscot Formation clays have been noted to include higher amounts of quartz and feldspar in relation to the silt size particles, which tend to include higher amounts of micas.

While the formation may appear to be one massive unit throughout its depth, at shallower depths it has been observed to be comprised of alternating thin layers of very fine sands, silts and clays. Deeper in the formation this layering has not been observed and it appears to be a relatively uniform clay deposit. At the RWS facility there have been no observations of layering, though this does not entirely rule out the presence of alternating thin layers. Typically the layering within the shallower

depths is directly observed in the exposed faces of roadway cuts. Large cuts have not been made at the RWS site exposing the clay, and in situ testing methods used at the site were not able to detect the boundaries of these very thin layers. At the RWS facility a discontinuity has been observed in shear strength profiles for areas where clay thickness is greater than 15.25 meters. This anomalous zone is generally 1.8 to 2.4 meters thick and occurs between 7.6 and 12.2 meters elevation. This zone may be an occurrence of a large variation within the stratum or be indicative of the change to the deeper unit of the Presumpscot Formation.

2.2.3 - Groundwater Conditions

Initial design investigations performed by E.C. Jordan, Co. in 1985 noted two groundwater units that exist at the landfill site. An upper unit exists in the clay stratum and is generally near the original ground surface. Groundwater observations at the location of the field shear vane testing (Boring B-11) noted a depth to groundwater of 0.15 meters (el. 21.03 m). The lower unit exists in the granular material and is confined by the overlying clay stratum and the underlying glacial till and bedrock. Across the landfill site the piezometric head measured at the interface of the clay stratum and the granular material has been observed to vary between 2.1 and 3.05 meters above the ground surface.

The general trend of groundwater flow across the site is in an east-northeast direction, while the two groundwater units at the site contribute to an overall vertical upward flow.

2.2.4 - Soil Properties

The results of laboratory testing performed on undisturbed piston samples have been provided by Soil Metrics, LLC for the RWS site. This testing was performed in 1985 and 1994 by Haley & Aldrich, Inc. and MIT. Testing included the determination of Atterberg limits, natural moisture content, consolidated undrained triaxial tests, direct simple shear tests and one-dimensional consolidation tests. Additional testing has been performed in 2006 at the University of New Hampshire (UNH) from samples recovered at the B-11 test location. This work included several determinations of Atterberg limits and natural moisture content. In addition one-dimensional consolidation and unconfined unconsolidated triaxial tests were performed. The laboratory testing procedures are discussed in Section 3.6.

Samples from the B-11 test location were found to have liquid limit (w_L) ranging between 39.6 and 48% with an average value of 43.7%, and a plastic limit (w_P) varying between 20.0 and 29.4% with an average of 24.2%. Table 2.1 presents the results of the Atterberg limits tests performed specifically for this research.

Table 2.1 - Results of 2006 Atterberg Limits Tests

El. (m)	Liquid Limit (w_L)	Plastic Limit (w_P)	Plasticity Index (PI)
18.4	48.0%	25.1%	22.9%
17.5	47.0%	28.6%	18.4%
16.6	42.8%	20.0%	22.8%
14.8	43.8%	20.1%	23.7%
13.6	44.4%	29.4%	15.0%
12.0	39.6%	23.9%	15.7%
10.5	40.3%	22.2%	18.1%

The natural moisture (w_N) content is typically well above the liquid limit indicating a sensitive clay, and varies from 41 to 56.2%. These properties generally agree with the results of the previous testing conducted at the site, with the exception of the liquid limit. The UNH samples were found to be within the range of liquid limits previously reported, though the average value of 43.7% is approximately 8.5% greater than the earlier work. The results of the index tests are provided in Figure 2.4, with data from the 2006 laboratory testing highlighted in red.

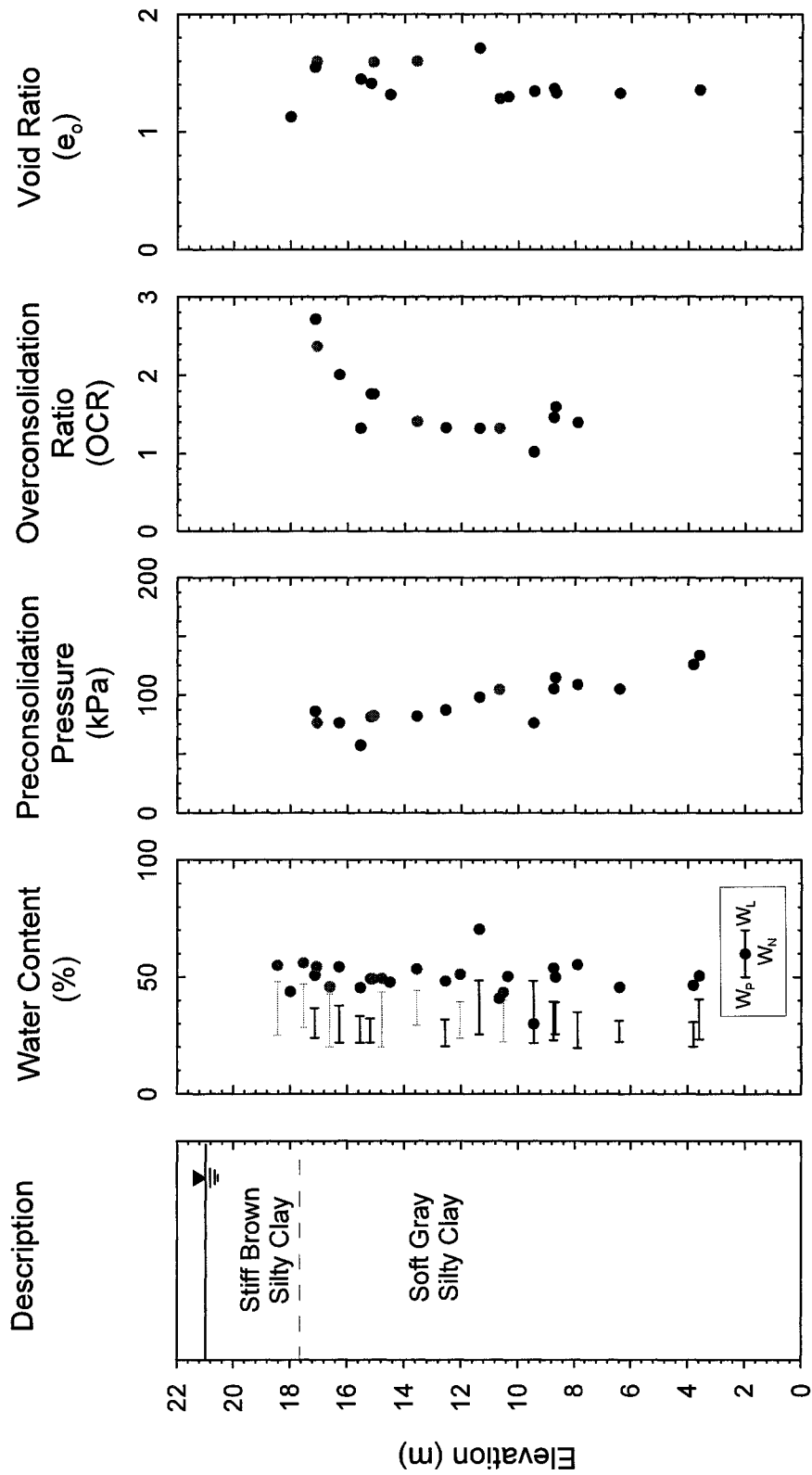


Figure 2.4 - Summary of the Natural Moisture Content, Preconsolidation Pressure, Overconsolidation Ratio and In Situ Void Ratio from Laboratory Tests

The stress history, as determined by one-dimensional consolidation tests are also shown in Figure 2.4. The maximum past pressure, σ'_p , decreases in magnitude from the stiff brown silty clay to a minimum of 57.5 kPa at approximately 15.5 meters elevation where it then increases in a near linear fashion. The range of maximum past pressures in the soft gray silty clay observed in laboratory testing is 57.5 kPa to 134.1 kPa. From the maximum past pressure the overconsolidation ratio (OCR) is determined, as shown in Figure 2.4. In situ tests indicate the OCR is above 10 in the stiff brown silty clay crust. The OCR decreases in the soft gray silty clay to an elevation of approximately 12.2 meters, below which the OCR remains steady at an average value of 1.35.

Consolidation properties, as determined by the one-dimensional consolidation tests performed in 2006 are shown in Table 2.2, while an overall summary of consolidation tests is presented in Table 2.3. Also included in this table are the input parameters presented in the 2002 In-Situ Vane Shear Testing Report prepared by Soil Metrics, LLC for a settlement analysis performed at the site using the TCON software developed by TAGAssoft, LTD. Consolidation curves from the 2006 laboratory tests are presented in Appendix G.

Table 2.2 - Results of 2006 One-Dimensional Consolidation Tests

El. (m)	Compression Index (C_c)	Recompression Index (C_r)	Overconsolidation Ratio (OCR)	Preconsolidation Pressure (σ'_p) [kPa]
17.1	0.586	0.012	2.75	86.2
15.1	0.529	0.014	1.50	79.5
13.6	0.118	0.002	1.35	91.0
10.5	0.565	0.018	1.55	106.8

Table 2.3 - Consolidation Properties of the Soft Gray Silty Clay Layer

Summary of 1-Dimensional Consolidation Tests		
	Range	Average
Modified Compression Index (C_{ce})		
UNH (2006)	0.366 to 0.439	0.392
Haley & Aldrich (1994)	0.320 to 0.460	0.375
Haley & Aldrich (1985)	0.356 to 0.562	0.433
TCON Analysis (2002)	0.350 to 0.400	0.372
Modified Recompression Index (C_{re})		
UNH (2006)	0.008 to 0.014	0.010
Haley & Aldrich (1994)	0.002 to 0.014	0.009
Haley & Aldrich (1985)	0.015 to 0.027	0.022
TCON Analysis (2002)	0.010 to 0.015	0.014
Modified Creep Index ($C_{\alpha e}$)		
UNH (2006)	0.0030 to 0.0046	0.0036
Horizontal Permeability (k_h) (ft/day)		
EC Jordan (1985)	-	2.27×10^{-3}
Vertical Permeability (k_v) (ft/day)		
UNH (2006)	3.7×10^{-5} to 3.5×10^{-4}	1.81×10^{-4}
EC Jordan (1985)	2.83×10^{-3} to 2.55×10^{-4}	-
Coeff. Of Consolidation (c_v) (ft²/day)		
UNH (2006)	0.048 to 0.155	0.096
TCON Analysis (2002)	-	0.060

Where the modified compression indices are expressed as:

$$C_{ce} = \frac{C_c}{1+e} \quad [2-1]$$

$$C_{re} = \frac{C_r}{1+e} \quad [2-2]$$

$$C_{\alpha e} = \frac{C_\alpha}{1+e} \quad [2-3]$$

2.3 - Geotechnical Monitoring

Monitoring of the RWS site has been performed for over 10 years to aid in the design of each construction and filling stage, as well as providing an early indicator of potential failure. There are three types of installations monitored at the site; inclinometers, piezometers and settlement platforms. Waste placement locations and waste loading rates have been recorded as well. Data collected at each installation can then be reduced to determine the stability of the landfill and to verify that maximum rates of displacement are not surpassed. Each installation is recorded at regular intervals, and when data recovered is outside of the expected range of results a system is in place to increase the frequency of monitoring. Though instrumentation locations have changed to accommodate construction activity, current instrumentation consists of six inclinometers, 30 vibrating wire piezometers, and 14 settlement platforms.

With regards to stability at the site, the inclinometer, piezometer and settlement platform information is critical. Of these three monitored parameters the inclinometer data is perhaps most important as it can provide magnitudes and rates of displacement continuously with depth. Inclinometers therefore can identify the general location of a failure surface as it develops. As waste is placed at the landfill the values recorded from these three installations is expected to change, and as waste loading slows or ends, a reduction in the rate of change is expected to occur.

Inclinometers have been installed around the perimeter of the landfill, and record the amount of horizontal displacement with time across the entire clay stratum. With the

measurement of horizontal displacement a shear strain can be calculated and compared to the strength of clay measured in laboratory tests. Laboratory testing of clay samples recovered from the RWS facility exhibit strain softening. As the laboratory sample is loaded it will exhibit a peak strength, after which the material does not catastrophically fail, but it begins to lose strength. Multiple laboratory tests have indicated that the range of maximum shear strains above which the specimen will begin to lose strength is 2 to 4 percent. If an unexpected rate change is observed, or the cumulative amount of shear strain has surpassed the 2 to 4 percent maximum within the clay stratum, failure may be imminent. Settlement platforms measure the vertical deformation in the clay layer as a result of settlement due to waste loading. The reactions to loading measured at settlement platforms and piezometers, which measure the pore pressure increase and rate of dissipation, can be predicted to a relative degree. These values are monitored as a sudden and unexpected change in the rate of settlement or pore pressure dissipation after loading has stopped may also be indicative of progressive failure.

Stability at the site will be heavily dependent on the unit weight of the material being placed into cells, as well as the geometry of these cells. If unit weights or slopes exceed the maximum values used in design, failure may occur. It is therefore vital that these values be measured and construction activity be monitored on a periodic basis. The geometry of each cell is checked periodically by a survey of the landfill site. The unit weight of the ash and baled waste that is being placed is quite variable. Two methods are in use at the RWS facility to monitor the unit weight of the material being placed. The first method is a direct calculation based on the surveyed geometry of the landfill and the weight recorded as being placed. The

weight of material placed in each cell is determined by recording the loaded and unloaded weights of vehicles transporting ash to the landfill. Cell volumes can be calculated from this information, and the general unit weight of a cell can be calculated. In conjunction with this method, the pore pressure response, as measured with the piezometers is observed as a cell is loaded. While the pore pressures may not respond fully to the weight of the material due to stress dissipation and the locations of piezometers, this second method is generally useful for comparison to other calculated information.

While the strength gain in the clay stratum is not monitored through the five means described previously, this data is important for future design considerations. Field Shear Vane testing programs have been conducted in 1994 and 2002 at the site to determine the change in strength over time. An additional analysis of the change in strength at the site will be possible using the undrained shear strength calculated through CPTu profiles conducted during this study.

2.4 - Geotechnical Monitoring Assessment

The geotechnical monitoring installations have thus far performed well in indicating areas of concern in the clay stratum at the site. Periods during which rates of displacement, or pore pressure dissipation have exceeded guidance criterion set by the design engineers have accompanied periods of activity in specific cells. When such events occur the concerning data has been shown to return to expected values at the conclusion of filling activities. This is important to note as an example of successful monitoring of the stability of the landfill. These installations have served

as early warning systems and if the response in the clay stratum had continued to increase at unacceptable rates, corrective action could be taken before failure. Had the installations not been present the potential for failure may not be known until after failure had occurred.

During the lifespan of the landfill stability berms have been constructed to control the rate of shear strain in the clay. These berms have been constructed prior to additional filling in adjacent cells in response to large strains observed from the inclinometer measurements. Large shear strains have been observed at the RWS facility since the monitoring began in 1993. The cumulative shear strain observed in certain layers of the clay stratum is approaching the maximum shear strain before failure occurs, as denoted by substantial strength loss. Inclinometer data has observed this behavior, and has found that it occurs within discrete 1.8 to 2.45 meter (6 to 8 feet) thick zones between 7.6 and 12.2 meters (25 and 40 feet) elevation. Current cumulative shear strains across the site are approaching, or have exceeded the peak range of 2% to 4%, ranging from 2.1% in the North to 3.4% in the East. An example of the results from a direct simple shear laboratory test displaying the strain softening behavior is presented in Figure 2.5.

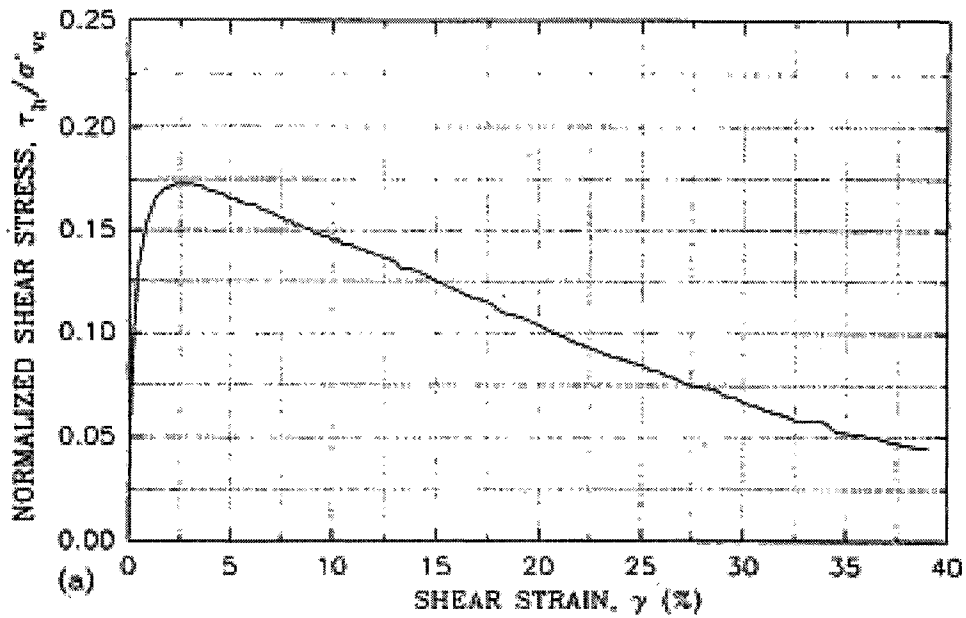


Figure 2.5 - Example Results of CK₀UDSS Test Indicating Strain Softening Past 2% Shear Strain

Shear vane strength profiles have observed a lower than expected strength in these zones of large horizontal displacement. Comparisons between the 1994 and 2002 investigations show a 1.2 to 3.6 kPa (approximately 8% to 18%) strength loss in these zones. This information may indicate that the clay stratum is experiencing strain softening, which is important to account for in stability analyses. At the current time the rate of shear strain has decreased, as a result of a change in filling operations. The typical range of incremental shear strain varies from 0.01 to 0.03% per month, with the exception of the northern side of the landfill which experiences much less than 0.01% per month. Settlement of the clay stratum across the site varies from 30.5 to 96.5 centimeters (12 to 38 inches).

CHAPTER III

IN SITU TESTING PROGRAM

3.1 - Purpose of the Site Investigation

The overall goal of the investigation is to determine the change in undrained shear strength with time at select locations at the site. To complete this task a computer model was required and the development of a set of soil properties for use in the computer model was therefore necessary. The computer model will enable all of the conditions at this large and complex site to be accounted for, allowing the site owners to forecast future soil conditions at the site, and to adjust the time scale and size of proposed construction and filling accordingly.

To help characterize the properties of the foundation soils at the RWS site, piezocone profiles were completed at three locations within the RWS facility, in conjunction with one Field Shear Vane (FV) profile and one Flat Dilatometer (DMT) profile. The piezocone profiles were performed at the B-11, P-3 and I-3/I-4 locations, along with two dissipation tests, performed using the piezocone, at the B-11 location. Several undisturbed thin-walled tube samples were recovered adjacent to the Field Shear Vane and Flat Dilatometer profiles at the B-11 area for laboratory testing. Figure 3.1 displays these test locations on a schematic diagram of the RWS landfill.

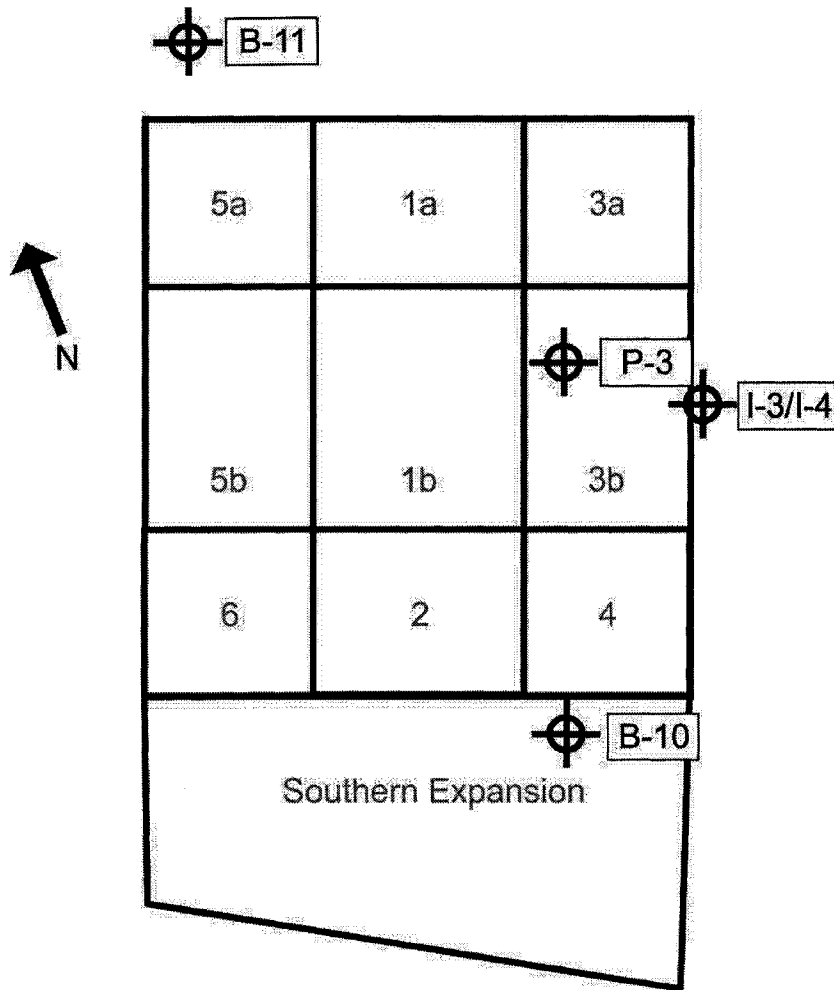


Figure 3.1 - Exploration Location Plan for Current Research

3.2 - Testing Locations

The location of Borehole B-11 was chosen with the intent that this unloaded area would provide strength results comparable to initial unloaded K_0 conditions. The location is over 60 meters from the toe of the northern slope of the landfill, and 15 to 18 meters from a stability berm that is approximately 2 meters in height. The finite element analyses performed at the RWS site, as discussed in Chapter 5 have confirmed that the location of Borehole B-11 is not influenced by the existing landfill.

The field vane and dilatometer profiles at the B-11 location were used to assess the most suitable empirical relationships correlating CPTu measurements to the undrained shear strength, the stress history and the at-rest lateral earth pressure coefficient. The chosen empirical relationships were then adjusted to closely match the FV for undrained shear strength and DMT profiles for stress history and lateral earth pressure, creating site specific relationships that were then used at other piezocone test locations within the landfill to assess the current properties of the soft clay stratum. These properties were also used to develop parameters for the finite element models of the site. The change in undrained shear strength prior to 2006 at Borehole B-11 cannot be measured, as previous testing programs have not included field vane profiles at or near this location. A prediction of the future conditions will however be possible through finite element analysis.

The remaining two piezocone profiles, at Boreholes P-3 and I-3/I-4 were chosen as field vane testing had been completed at each location in the past. An initial field vane strength profile was completed at Borehole P-3 in 1994 prior to loading in the immediate area. This profile was considered to be representative of "initial conditions" at the site (Rabasca, 2003). A second field vane profile was conducted in 2002 to assess strength changes in the soft clay stratum after a loading of up to 23 feet of ash. During the 2002 field shear vane testing program a profile was completed at the I-3/I-4 location at the toe of Cell 3b. The piezocone profiles at these locations will be compared to the field shear vane profiles from 2002 and used to assess the strength change with time in the clay stratum.

Table 3.1 provides a summary of the tests performed at each location during the course of this research.

Table 3.1 - Summary of In Situ Tests Performed

Profile Designation	General Location	In Situ Test Performed	Date Completed	Total Depth (m)	Elevation at Bottom (m)
CPTu B-11	Virgin Area	Piezocone	1/17/2006	14.21	6.97
CPTu B-11	Virgin Area	Dissipation	1/20/2006	7.96	13.22
FV B-11	Virgin Area	Field Vane	1/18/2006	11.84	9.34
DMT B-11	Virgin Area	Dilatometer	4/7/2006	12.60	8.58
CPTu P-3	Cell 3b	Piezocone	1/16/2006	27.30	-0.94
CPTu I-3/I-4	Toe of Cell 3b	Piezocone	1/17/2006	20.10	3.82

3.3 - Field Shear Vane Testing Procedure

Field vane testing of the soft clay stratum at the RWS facility was conducted at location B-11. In situ testing was performed using the Geonor H-10 Vane Borer with drilling support provided by Great Works Test Borings, Inc of Rollinsford, NH. Summary plots of the peak and remolded strengths, along with sensitivity versus elevation are presented in Section 4.1.1. The results from individual tests are provided in Appendix A.

Boring B-11 was advanced to 3.7 meter depth using standard wash boring techniques and a 10.2 cm (4 inch) (ID) casing. This depth was chosen as this is the approximate interface between the weathered stiff silty clay crust and the gray soft silty clay.

The vane borer apparatus was advanced to the bottom of the cased borehole and pushed into the clay, where the vane blade was extended 50 cm (19.7 in.) out of the

vane borer for the first test. The vane blade used in this profile had dimensions of 65mm by 130mm.

The torque measuring head was then installed at the surface and torque was applied to the frictionless rod system at a constant rate of rotation. Standard test methods specify a rotation rate of 0.1 deg/second; this was applied by maintaining one rotation of the handle every two seconds. The test was conducted for two to three minutes past failure, with torque measurements recorded at intervals varying between 15 and 30 seconds. At the completion of the test the vane was rotated ten times and the test procedure restarted to measure the remolded strength. After the remolded strength was found the torque head was removed and the vane was then retracted into vane borer. The borer was then advanced to the next test depth and this procedure was repeated. A total of eleven tests were performed at this location generally at 0.76 meter (2.5 ft) intervals.

3.4 - Piezocone Testing Procedure

3.4.1 - Introduction

The standard cone penetration testing method is described in ASTM standard D-5778. The test procedure used at the RWS facility is described herein, with the addition of alternative test procedures when necessary. A rubber-tracked drilling rig, CME model 850, was used at the RWS site and subsequent references to the means of piezocone advance will reference this equipment. The use of a specialty CPTu vehicle or lightweight, portable rig will require minor variations in procedure, though test methodologies should be similar.

3.4.2 - Summary of the CPTu Procedure

Preparation of the borehole is a critical step to ensure that the piezocone remains saturated prior to the start of advancement. A pre-drilled and water-filled borehole is adequate in locations with a shallow depth to groundwater. In cases where the groundwater table is at a significant depth, the probe can be encased in a water filled rubber sheath and lowered into a pre-drilled borehole. Penetration of probe into soil would then puncture the sheath and allow it to tear away from the equipment. In certain circumstances the pre-drilling may be required to prevent damaging or overloading the equipment, as in the case of a fill material with cobbles or other obstructions.

At the RWS facility the boreholes at the P-3 and I-3/I-4 locations were situated over ash fill, and therefore were required to be cased and cleaned to a depth penetrating into the clay stratum. At the B-11 location the borehole was cased and cleaned to a depth of approximately 2 meters in order to penetrate part of the stiff overconsolidated crust. At the remaining locations the borehole was cased and cleaned through the ash and into the crust material. All boreholes at the test site were filled with water to the height of the casing above ground.

While the borehole was being prepared, the complete data acquisition system, including the piezocone was assembled and powered for 30 to 45 minutes prior to recording zero load measurements. During this time the saturated filter element was installed on the piezocone. To assemble and saturate the hydraulic circuit the cone was turned upside down and a funnel with a tight fitting rubber gasket was placed over the cone and slowly filled with de-aired water, as seen in Figure 3.2. The cone

tip was then removed and a plastic syringe was used to remove air from the channels machined within the tip. The filter was then removed from a sealed container and inserted onto the tip while underwater. The silicone oil was found to have the tendency to trap air bubbles on surfaces such as the threads of the cone tip, and therefore the plastic syringe was used to force the air bubbles from all such surfaces. Additionally it was found that assembling the apparatus completely following insertion of the saturated filter element, could create additional entrapped air bubbles. Removing the tip and again using the syringe to remove any remaining air bubbles a second time appeared to provide a saturated hydraulic circuit.

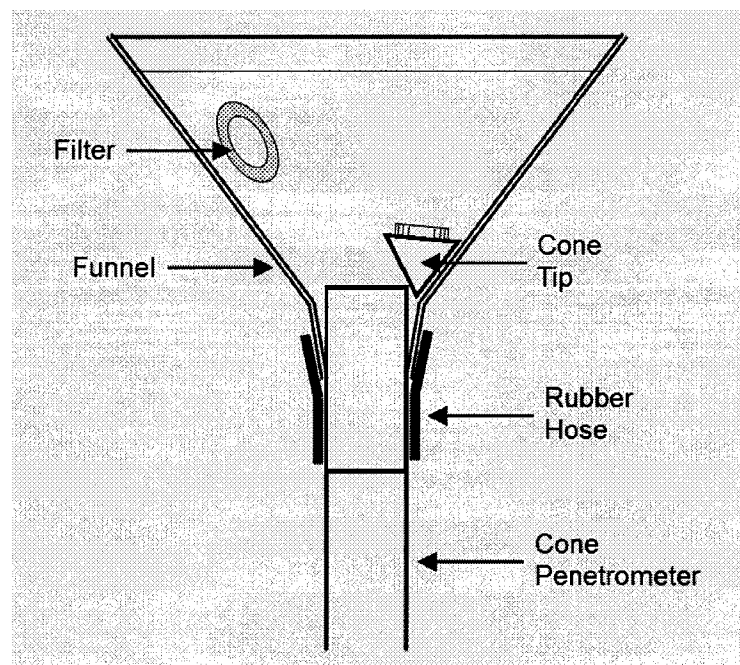


Figure 3.2 - Method for Assembly of the Piezocone Filter Element in the Field
(After Larsson, 1992)

Following the preparation of the cone and the borehole, the cone is inserted into the borehole and initial zero-load readings are recorded for all data channels. The piezocone was then advanced through the clay stratum at a rate of 2 ± 0.5 cm/sec,

with additional drill rods added at 1 m (3.28 feet) intervals. Advance of the piezocone was terminated after the probe penetrated into the stratified fine sand layers underlying the clay deposit. The probe was then retracted to the ground surface and final zero-load readings were recorded.

3.5 - Dilatometer Testing Procedure

A single dilatometer profile of the soft gray silty clay stratum was completed adjacent to the piezocone profile in the virgin testing area. This sounding started at a depth of 2.6 meters, in a pre-bored, uncased hole. The test equipment was advanced using a hydraulic ram with a 1.22 meter stroke mounted to a portable steel load frame. Sand bags were used to stabilize the frame and resist the uplift forces caused by blade advancement. The sounding was terminated within the transition zone between the soft gray silty clay and the underlying glacial sands, with a refusal depth of 12.6 meters.

Individual tests were conducted at 20 cm intervals, and the test equipment was advanced to the next test depth at a rate of approximately 2 cm/sec. Data was recorded using the procedure outlined in Section 1.4.2 of this report.

3.6 - Laboratory Testing Procedures

Laboratory testing was performed on the soft gray silty clay to complement existing geotechnical information and to help in the analysis of piezocone and dilatometer data, and for use in the finite element modeling. Testing consisted of four one-dimensional consolidation tests, and seven Atterberg limits tests. Due to the very

sensitive nature of the soft gray silty clay, care was taken to minimize disturbance during sampling, as well as during sample preparation and testing. When compared to data from previously conducted laboratory tests on the soft gray silty clay in Figure 2.4, the data from this research is generally in agreement. This indicates that the quality of the 2006 data is at a minimum equivalent to the previously reported data.

A total of seven thin wall tube samples of the soft gray silty clay were recovered using a piston sampler at the B-11 location. To minimize disturbance and allow for a dissipation of excess pore pressures generated during the advance of the piston sampler, a period of 15 minutes was allowed to pass before the samples were extracted from the borehole. These samples were transported to the University of New Hampshire and stored in a temperature and humidity controlled environment until testing was to be performed.

The one-dimensional consolidation tests were performed using a floating-ring consolidation apparatus (Figure 3.3), following the methods outlined in ASTM D2435 "Standard Test Methods for One-Dimensional Consolidation Properties of Soils Using Incremental Loading".

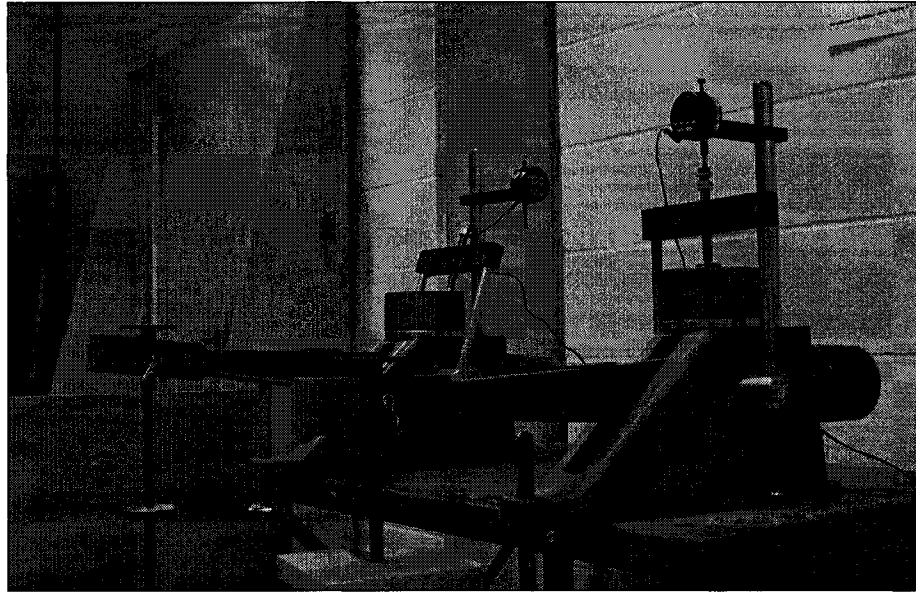


Figure 3.3 - Floating-ring Consolidation Apparatus

The samples from elevation 17.1, 15.1 and 10.5 meters were loaded at 24 hour increments according to the schedule presented in Table 3.2. The load increments for the sample recovered at 13.6 meters elevation were selected based upon the increments from previously reported testing, and are presented in Table 3.2 as well. During each 24 hour loading increment, the deformation of the sample was recorded at elapsed times of 0, 6, 15, 30 and 60 seconds; 2, 4, 8, 15, 30 minutes; and 1, 2, 4, 8, and 24 hours.

Table 3.2 - One-dimensional Consolidation Test Load Increments

Samples recovered at El. 17.1, 15.1, 10.5 m		Sample recovered at El. 13.6 m	
Load (kg)	Equivalent pressure (kPa)	Load (kg)	Equivalent pressure (kPa)
1	31	0.24	7.51
2	61.9	0.53	16.55
3	92.9	1	31
6	185.8	2	61.9
12	371.6	4	123.8
24	743.2	8	247.6
6	185.8	16	495.2
24	743.2	4	123.8
48	1486.4	16	495.2
12	371.6	32	990.4
		8	247.6

The Atterberg Limits of seven samples were determined using the test methods for determining both the liquid limit and plastic limit and were performed in accordance with ASTM D4318-00 "Standard Test Method for Liquid Limit, Plastic Limit, and Plasticity Index of Soils". The results of these tests are presented in Table 2.1.

CHAPTER IV

INTERPRETATION OF IN SITU TEST DATA

4.1 - Field Shear Vane Data

4.1.1 - Data Reduction

The raw data from each of the eleven tests conducted at boring B-11 were reduced to plots of shear stress versus rotation of the vane blades in degrees. The maximum values from each of these tests correspond to the undrained shear strength. Table 4.1 displays the undrained shear strength, remolded strength, sensitivity and elevation information for each test, this data is presented graphically in Figure 4.1. The reduced data from each of the eleven individual tests can be found in Appendix A.

Table 4.1 - Borehole B-11 Field Shear Vane Results

B-11 Geonor Vane Shear Test Data - 2006					
Test No.	Depth (m)	Elevation (m)	Su (peak) (kPa)	Su (remolded) (kPa)	Sensitivity (peak/remolded)
B-11.1	4.3	16.9	13.44	1.21	11
B-11.2	5.0	16.2	14.77	1.36	11
B-11.3	5.8	15.4	15.55	1.81	9
B-11.4	6.5	14.6	15.55	1.69	9
B-11.5	7.3	13.9	17.78	1.51	12
B-11.6	8.1	13.1	14.77	1.66	9
B-11.7	8.8	12.3	17.18	1.21	14
B-11.8	9.6	11.6	18.75	1.87	10
B-11.9	10.3	10.8	18.39	1.51	12
B-11.10	11.1	10.1	21.70	2.86	8
B-11.11	11.8	9.3	23.51	2.56	9

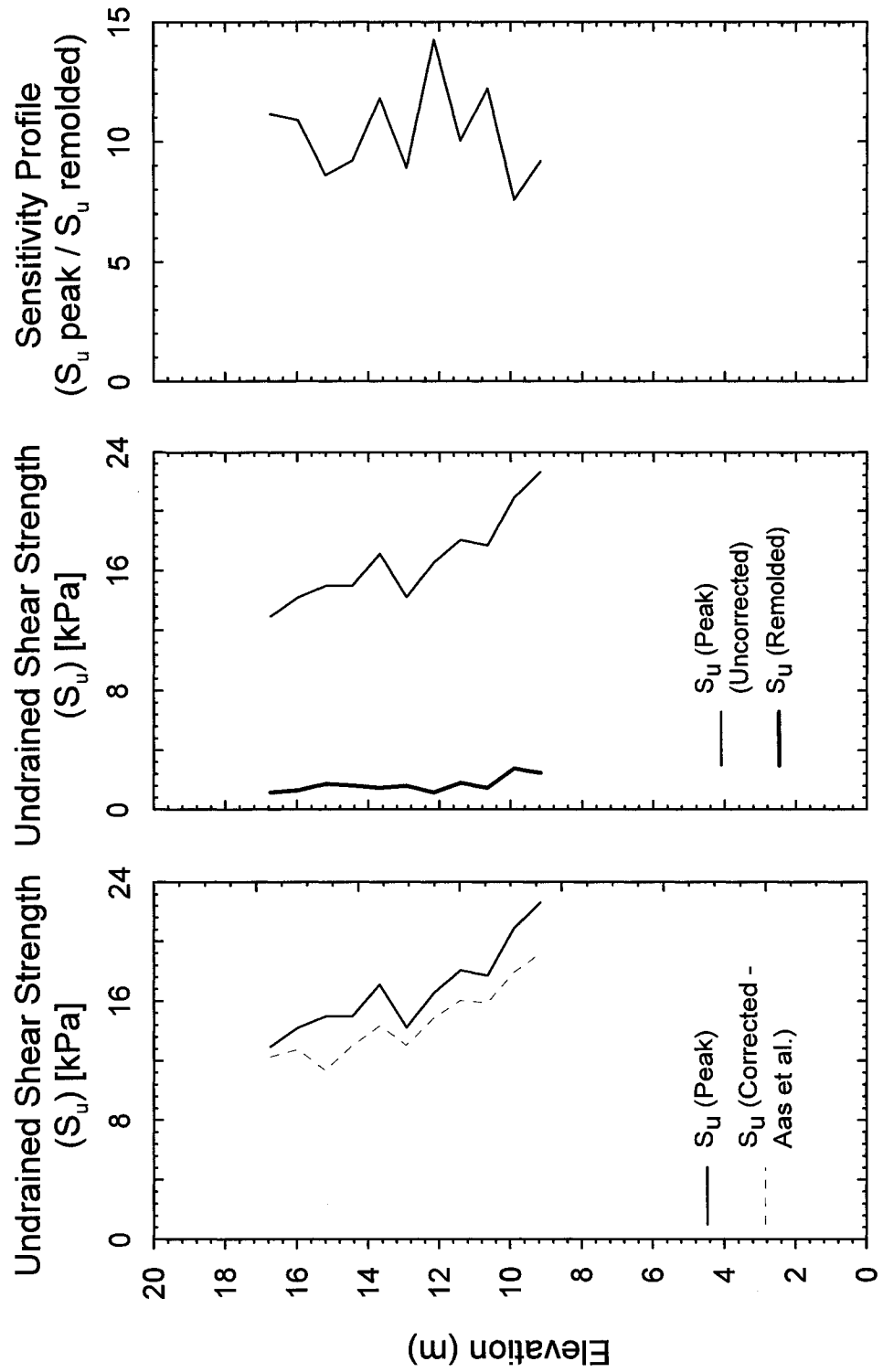


Figure 4.1 - Uncorrected, Corrected and Remolded Undrained Shear Strength with Sensitivity Profile from Field Shear Vane Profile at B-11

4.1.2 - Undrained Shear Strength Correction

4.1.2.1 - Corrections Used

Correction factors have been examined for application to the undrained shear strength values found in boring B-11. A relationship for correcting each data point has been developed for the time to failure (t_f), as well as the effect of aging and OCR. A detailed discussion of these corrections can be found in Section 1.2.4. To preserve continuity with previous work conducted at the site, further use of the field vane data in this research will reference uncorrected strengths.

The correction for time to failure, as described by Chandler (1988) is required for those tests where failure was reached after 10 minutes time had elapsed from the beginning of rotation of the vane blade. In such cases, the correction proposed by Chandler to reduce the strength has been used, as the measured strength is expected to rise with increasing time to failure. It should be noted that the correction as reported by Chandler (1988) appears to have an incorrect sign associated with the factor "b" based on further examples used in the literature. The correction factor used in this report is shown below:

For clays with a Plasticity Index (I_p) > 5%

$$\mu_R = 1.05 - b(I_p)^{0.5} \quad [4-1]$$

Where b is equal to:

$$b = 0.015 + 0.0075(\log t_f) \quad [4-2]$$

The effects of aging and OCR on the clay were corrected using the Aas et al. (1986) reinterpretation of the charts created by Bjerrum (1972), as seen in Figure 4.2.

Correction values from these figures were interpolated as closely as possible. Each point along the strength profile at boring B-11 was corrected using this manner.

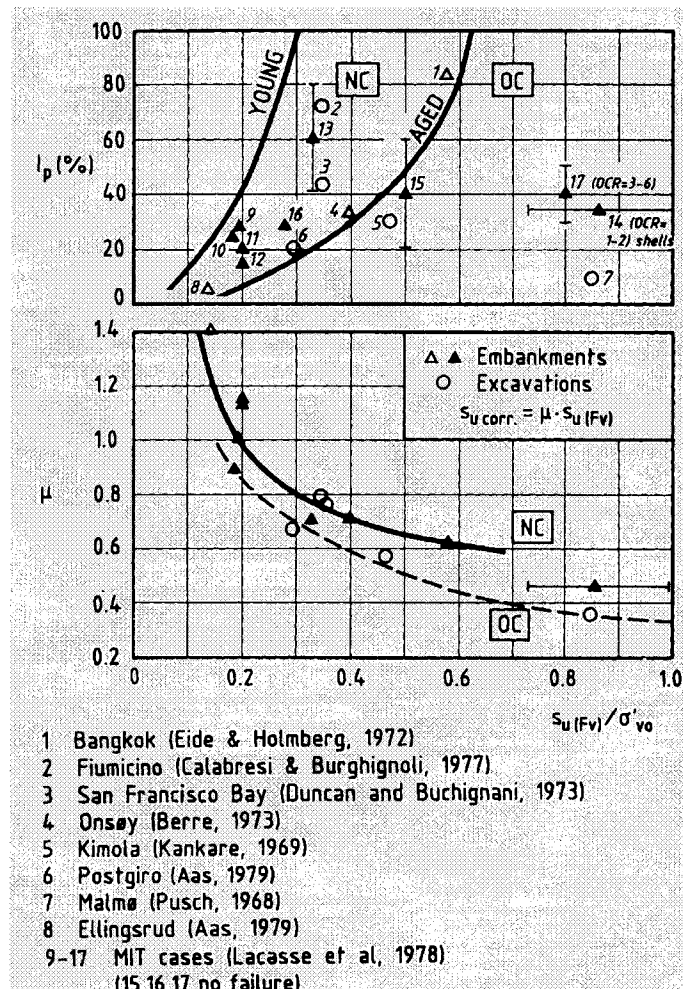


Figure 4.2 - Vane Shear Correction Factor (After Aas et al., 1986)

4.1.2.2 - Index Properties of the Soil

The corrections described in Section 4.1.2.1 were performed by dividing the entire profile into discrete 0.75 meter thick layers and using the average soil properties for each layer to compute the correction. The results of laboratory and field tests during the 1994 field exploration program at the site were used to determine the required index properties. These properties, as well as both the uncorrected and corrected

values for undrained shear strength are presented in Table 4.2. The corrected undrained shear strength profile is presented in Figure 4.1 alongside the uncorrected profile.

Table 4.2 - Index Properties for Correction of Undrained Shear Strength From the Field Shear Vane

B-11 Geonor Vane Shear Test Data - 2006							
Test No.	Depth (m)	Elevation (m)	Su (peak) (kPa)	I _p	σ' _p (kPa)	λ (Aas et al. 1986)	Su _{CORR} (kPa)
B-11.1	4.3	16.7	12.93	13.6	83.8	0.95	12.29
B-11.2	5.0	16.0	14.21	16.0	74.7	0.90	12.79
B-11.3	5.8	15.2	14.96	11.0	62.2	0.76	11.37
B-11.4	6.5	14.5	14.96	10.5	83.4	0.87	13.02
B-11.5	7.3	13.7	17.11	10.8	86.2	0.84	14.37
B-11.6	8.1	12.9	14.21	11.2	89.0	0.92	13.07
B-11.7	8.8	12.2	16.53	13.5	92.3	0.90	14.88
B-11.8	9.6	11.4	18.04	21.1	96.9	0.89	16.05
B-11.9	10.3	10.7	17.69	21.9	99.6	0.90	15.92
B-11.10	11.1	9.9	20.88	20.0	101.7	0.86	17.96
B-11.11	11.8	9.2	22.62	18.1	103.7	0.85	19.23

Where S_{UCORR} is equal to:

$$S_{UCORR} = S_u(\text{peak}) \cdot \mu_R \cdot \lambda \quad [4-3]$$

And where T_f is equal to the time to failure from insertion of the vane blades.

4.2 - Piezocone and Dilatometer Data

4.2.1 - Introduction

For each soil property there exist multiple theoretical and empirical relationships to interpret the CPTu data. The relationships for both CPTu and DMT analysis have been developed from a large data set, often from multiple sites around the world, and can have a significant amount of scatter in the results. Therefore when possible, it is advisable to adjust the empirical relationship to suit a specific location

using an agreed upon baseline data set. The goal of this section is to introduce the reader to the methods of data reduction, the empirical relationships used at the RWS test site and to present the data from the B-11 location.

4.2.2 - Corrections to Piezocone Point and Friction Resistance

In addition to the application of calibration factors to translate the output voltages to usable values and where applicable corrections for inclination and temperature effects, the piezocone data must also be corrected for the effect of pore pressure on the probe. Pore pressures generated during advance of the cone can impact the loads recorded by the friction and point resistance load cells. This phenomena, known as the “unequal area effect” is due to both the geometry of the probe, and the pore pressure differential along the shaft of the piezocone.

The point resistance (q_c) is corrected using the cone area ratio (a). The ratio is equal to the ratio of the cross-sectional area of the piezocone shaft to the projected area of the cone tip and typically ranges from 0.9 to 0.55. The manufacturer of the piezocone used in this work has reported the cone area ratio to be 0.8. The corrected tip resistance value (q_t) is found as follows.

$$q_t = q_c + u_2(1 - a) \quad [4-4]$$

The friction sleeve resistance (f_s) is similarly impacted due to the unequal end areas at either end of the sleeve. The pore pressure differential between the u_3 and u_2 positions can falsely increase the sleeve resistance value. For this research no pore pressure measurements are available at the u_3 location, therefore the uncorrected friction sleeve resistance (f_s) value was used rather than the corrected value (f_t) as it

is not recommended to correct the resistance without those pore pressures (Lunne et al., 1997)

At the CPTu B-11 sounding (el. 21.18 m) a hole was pre-drilled to a depth of approximately 2 meters. The piezocone was advanced through the soft gray silty clay into the glacial sands to a refusal depth of 14.21 meters. The piezocone outputs of corrected tip resistance, sleeve resistance, pore pressure and a profile of estimated stratigraphy from these results is displayed in Figure 4.3. The same outputs are presented for the CPTu P-3 and CPTu I-3/I-4 soundings in Figures 4.4 and 4.5 respectively.

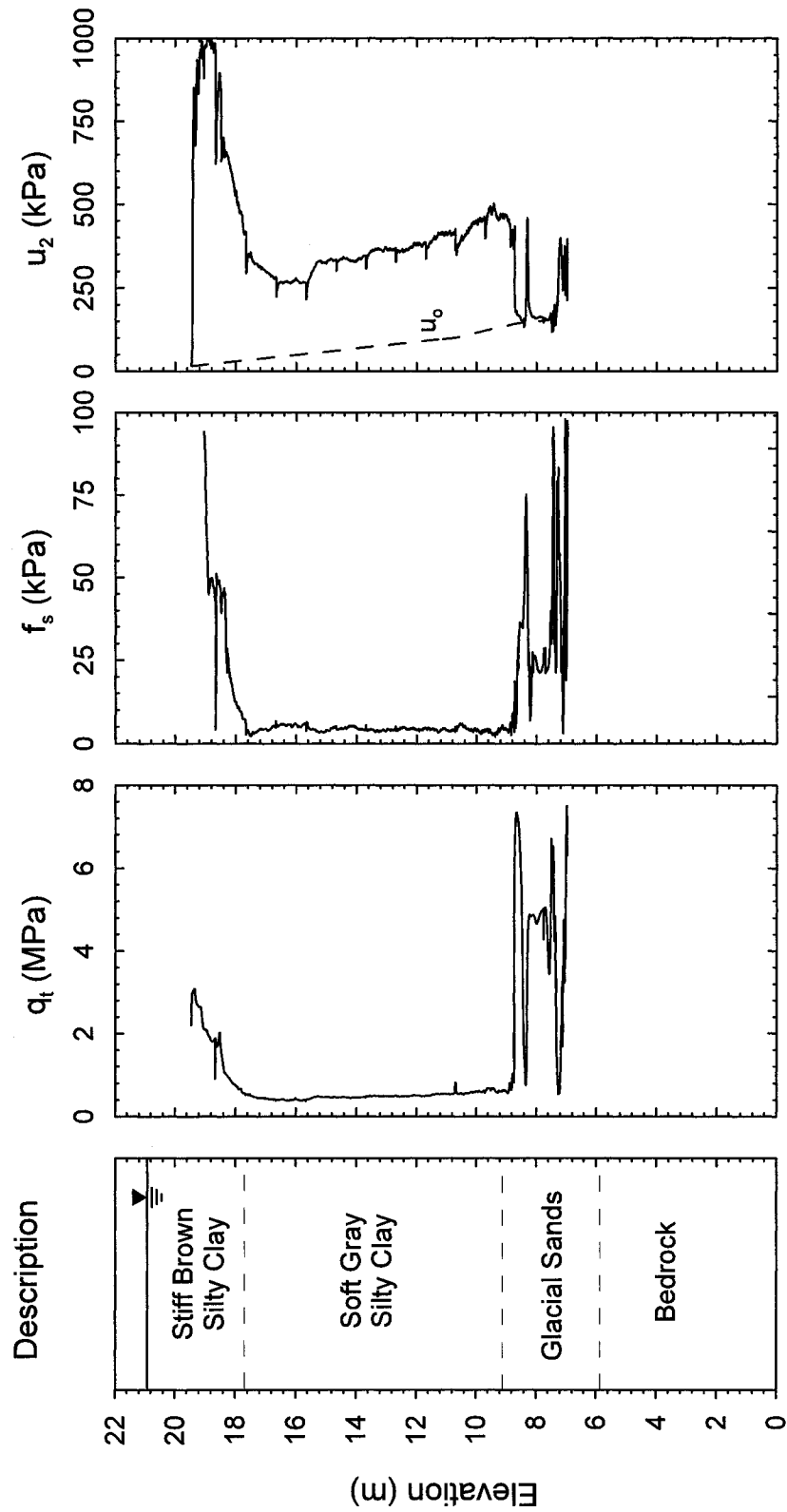


Figure 4.3 - Piezocone Output at CPTu B-11, Corrected Tip Resistance (q_t), Friction Sleeve Resistance (f_s), Pore Pressure (u_2)

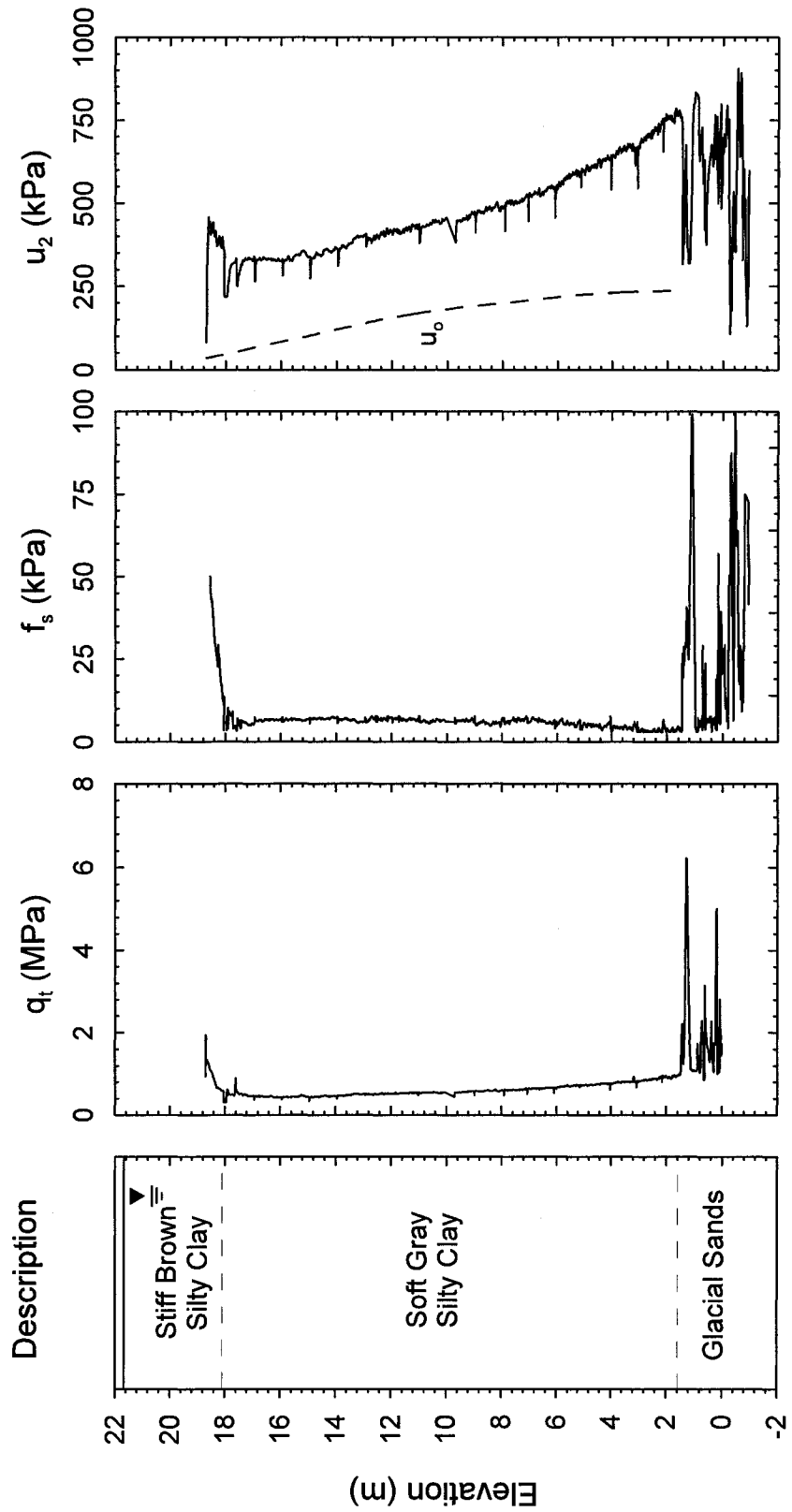


Figure 4.4 - Piezocone Output at CPTu P-3, Corrected Tip Resistance (q_t), Friction Sleeve Resistance (f_s), Pore Pressure (u_2)

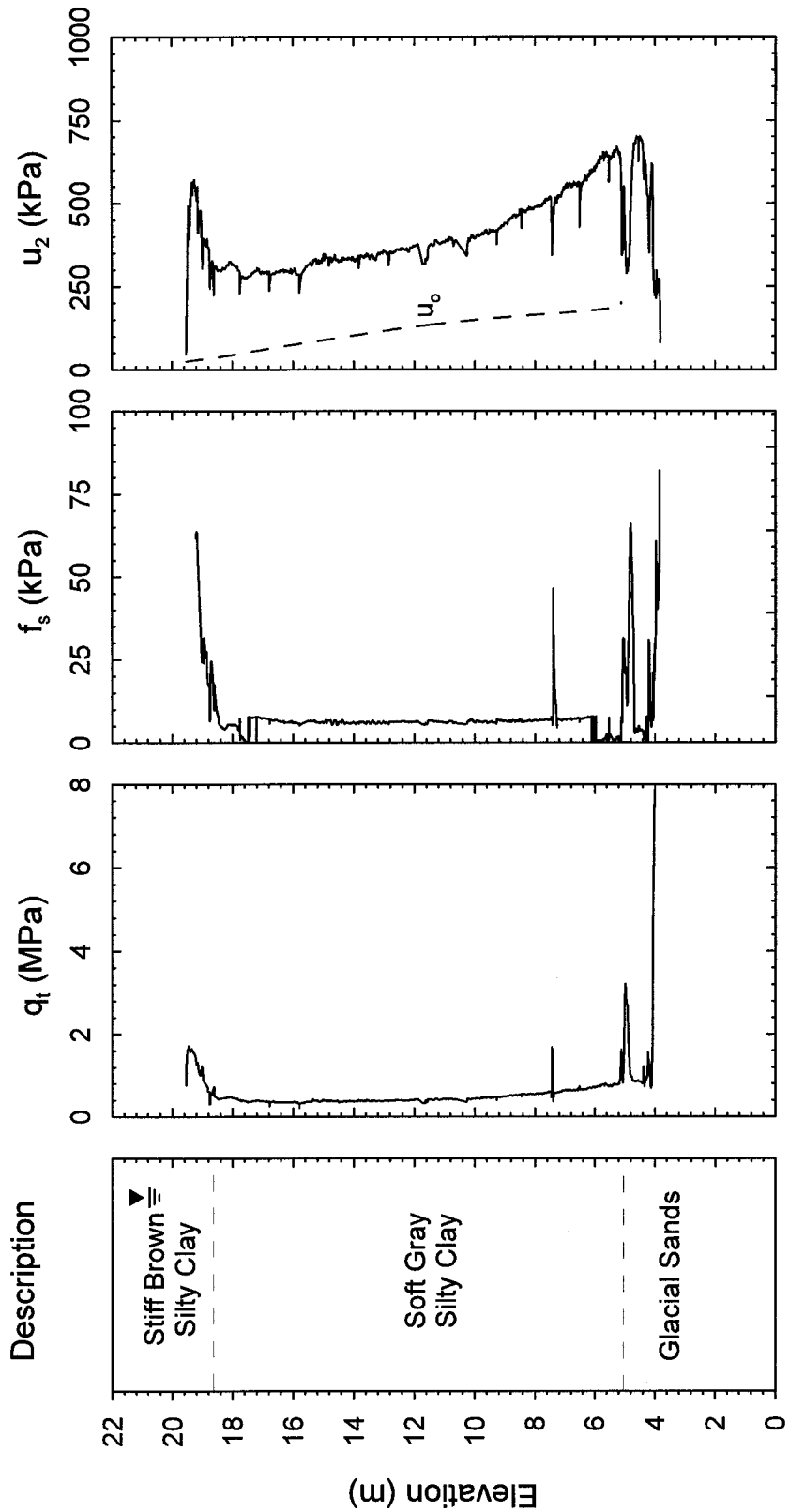


Figure 4.5 - Piezocone Output at CPTu I-3/I-4, Corrected Tip Resistance (q_t), Friction Sleeve Resistance (f_s), Pore Pressure (u_2)

4.2.3 - Preparation of the Dilatometer Data

In order to manipulate the DMT data into usable soil properties, the raw field data of A, B and C pressure measurements must first be corrected for the membrane stiffness (ΔA and ΔB), gage zero offset (Z_M), and feeler pin elevation. These corrected values, p_0 , p_1 and p_2 , are referred to as objective parameters (Marchetti, 2001) and can then be used to calculate the DMT indices which are then used to determine soil properties. The formulas to perform this correction are expressed as:

$$p_0 = 1.05 \cdot (A - Z_M + \Delta A) - 0.05 \cdot (B - Z_M - \Delta B) \quad [4-5]$$

$$p_1 = B - Z_M - \Delta B \quad [4-6]$$

$$p_2 = C - Z_M + \Delta A \quad [4-7]$$

4.2.4 - Stratigraphy

4.2.4.1 - Introduction

Though the piezocone and dilatometer do not recover samples for later examination and classification, each tool can be used to create a stratigraphic profile. General observations of the soil type can be made by observing the instrument outputs even when little processing has been performed. For example Figure 4.3 displays low tip resistance and high pore pressure values, indicative of soft clays. Additional processing of the data can successfully yield further information about the soil at a specific depth. The continuous profile provided by the piezocone, or near continuous profile from the dilatometer can be useful tools to quickly and effectively characterize the stratigraphy at a test site.

It is important to note however that the classifications provided by these tools is indicative of soil behavior, as opposed to an actual classification based upon grain sizes and distributions.

4.2.4.2 - Interpretation Using the Piezocone

The behavior of soil can generally be interpreted using a combination of the corrected tip resistance, sleeve resistance and pore pressures measured by the piezocone. Studies have shown that the sleeve resistance is often a less accurate indicator of soil behavior type (Lunne et al., 1986; Gillespie, 1990). This is especially true for soft soils, where the friction sleeve resistance is very small, and the load cell resolution is not capable of detecting small changes accurately. While the friction sleeve resistance is typically not solely used for classification, it is used in conjunction with the tip resistance and the pore pressure in compound parameters. These compound parameters typically relate the tip resistance (q_t) and the friction resistance (f_s), or relate the tip resistance (q_t), pore pressure (u) and overburden stress (σ_{vo}). Three such parameters, proposed by Wroth (1984, 1988) are often used in soil classification charts. The parameters, a pore pressure ratio (B_q), normalized friction ratio (F_r) and normalized cone resistance (Q_t) are shown in Figure 4.6 and are expressed as:

$$B_q = \frac{u_2 - u_o}{q_t - \sigma_{vo}} \quad [4-8]$$

$$F_r = \frac{f_s}{q_t - \sigma_{vo}} \quad [4-9]$$

$$Q_t = \frac{q_t - \sigma_{vo}}{\sigma'_{vo}} \quad [4-10]$$

This figure displays the close agreement between the parameters, indicating relatively little difference in the material behavior across the site.

Robertson et al. (1986) proposed a three-dimensional classification chart, shown in Figure 4.7. The classification system uses the friction ratio (f_s/q_t) and the pore pressure ratio (B_q) both plotted against the corrected tip resistance (q_t). Each chart has a series of numbered cells which correspond to soil behavior. The charts also offer an insight to the stress history (OCR), sensitivity (S_t) and void ratio, expressed in terms of the relative density (D_r). In the event that a soil layer falls within different, unrelated zones between the two charts, the interpretation must be made based on other observation of behavior.

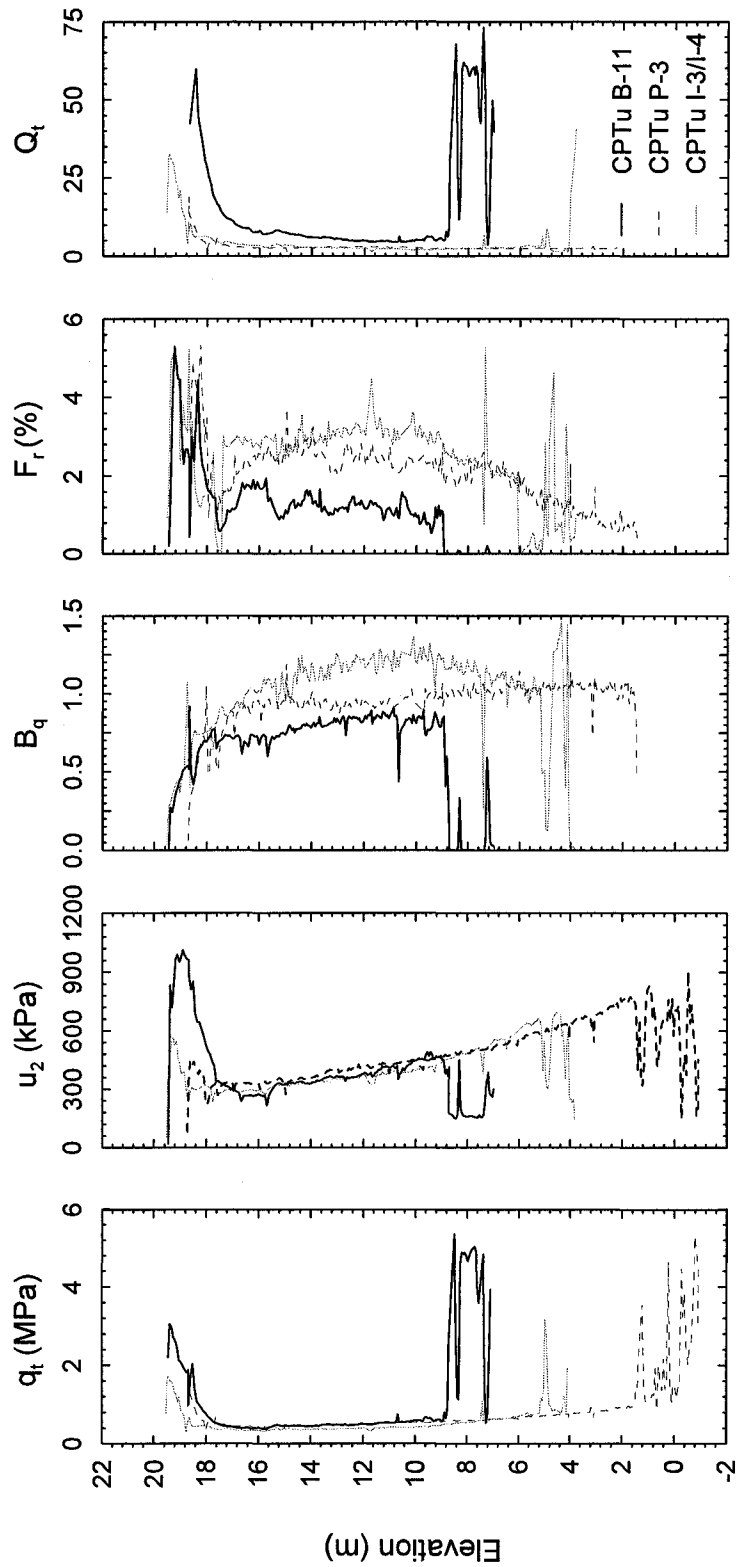


Figure 4.6 - Normalized CPTu Data for Soil Classification; Pore Pressure Ratio (B_q), Normalized Friction Ratio (F_r), Normalized Cone Resistance (Q_t) (After Wroth, 1984, 1988)

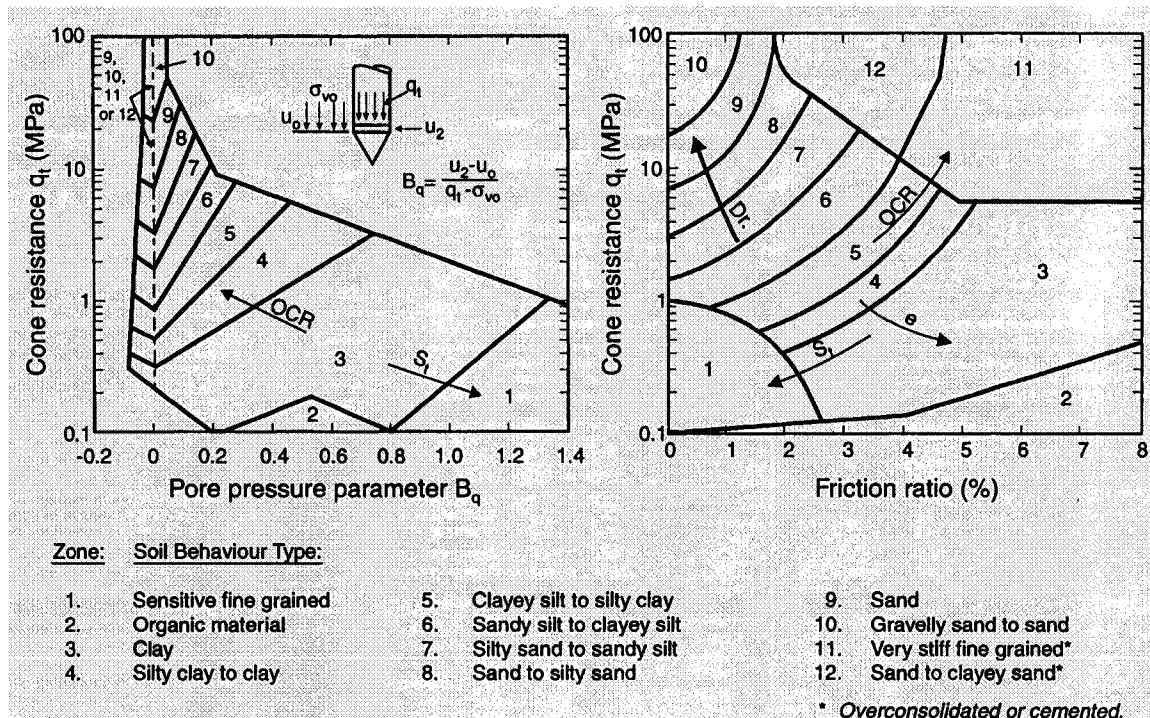


Figure 4.7 - Proposed Soil Behavior Classification Chart from CPTu Data (After Robertson et al., 1986)

The classification method of Robertson et al. (1986) works well, provided the piezocone sounding does not extend past 30 meters (98.4 ft) depth. As the overburden pressure increases, so do the tip resistance (q_t), friction sleeve resistance (f_s) and the pore pressure (u). The increase of these values could change the zone within which a soil falls, despite the fact that the material is uniform with depth.

To remedy this, a revision of this system was proposed by Robertson (1990) that normalizes the values of q_t and the friction ratio with the overburden stress at the measurement depth. The classification system is once again three dimensional, plotting both the normalized friction ratio (F_r) and pore pressure ratio (B_q) against the normalized friction ratio (Q_t). The modified classification system by Robertson

(1990), presented in Figure 4.8 is used in the same manner as the system by Robertson et al. (1986).

The piezocone profiles at the RWS site are less than 30 meters deep, and therefore either classification system could be used. The method by Robertson (1990) was selected for use to avoid any minor variations in classification due to a change in the overburden stress. Figures 4.9, 4.10 and 4.11 present the classification results from the RWS site as separate data points for the stiff brown weathered silty clay crust, the soft gray silty clay and the glacial sands at the B-11, P-3 and I-3/I-4 locations respectively.

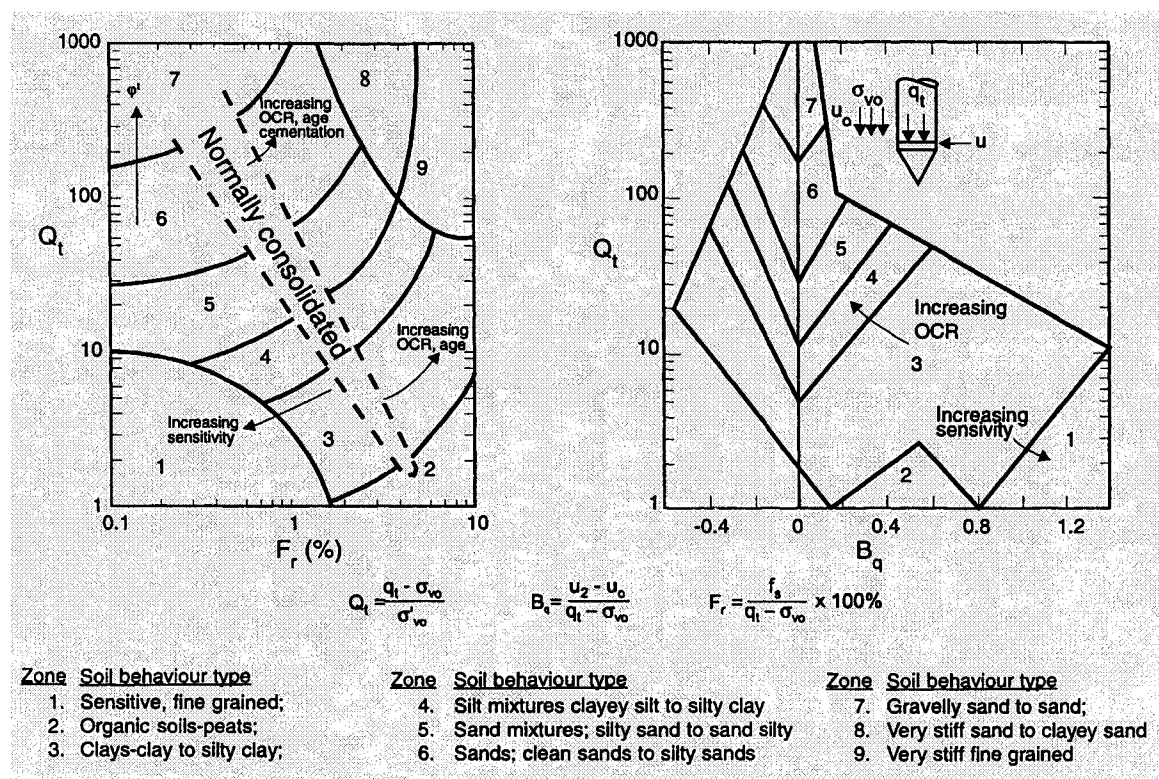
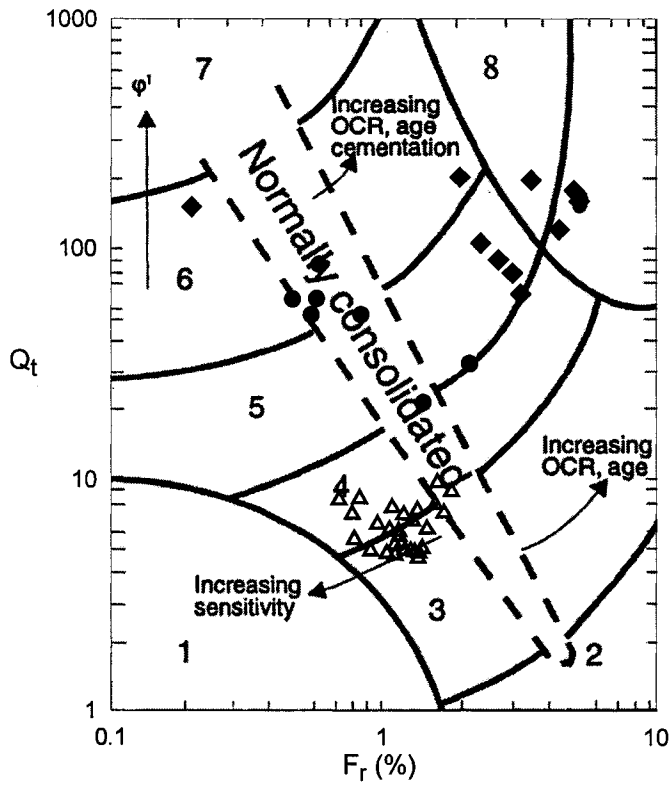


Figure 4.8 - Soil Behavior Classification Chart Based on Normalized CPTu Data (After Robertson, 1990)

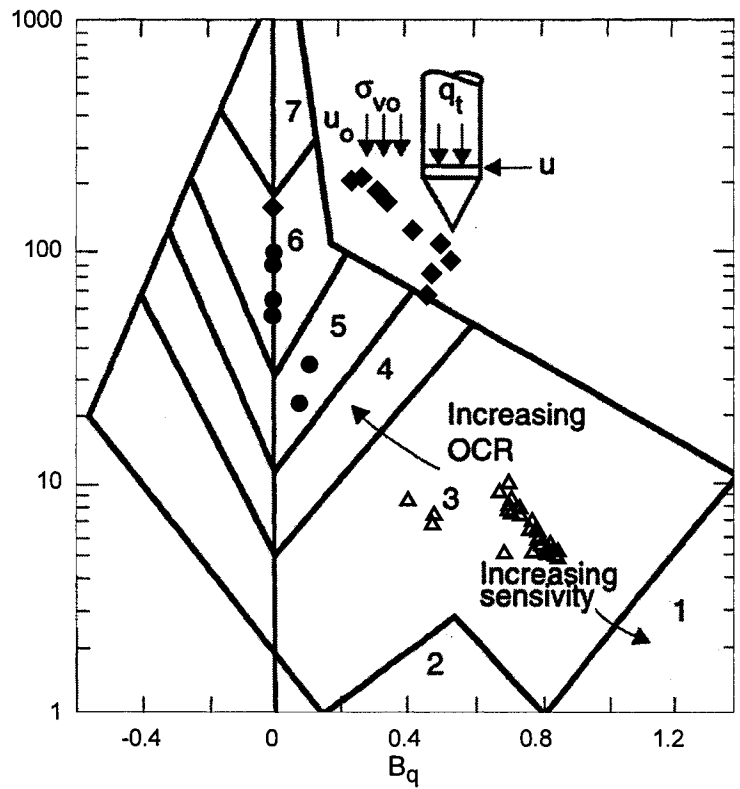
The chart to the left (Q_t vs. F_r) in these figures classifies the soft gray silty clay as having behavior of a sensitive, near normally consolidated clay/silt mixture. The charts to the right (Q_t vs. B_q) verify this behavior as the material falls within Zones 1 (Sensitive, fine grained) and 3 (Clays-clay to silty clay). The glacial sands, which have been observed to be medium to fine sand with varying amounts of silt and clay fall within Zones 5 and 6 on both charts at CPTu B-11. These zones indicate the material generally behaves as sand with varying amounts of silt, from clean sand to sandy silt. At CPTu P-3 and I-3/I-4 the glacial sands are classified as behaving as a fine grained silt/clay mixture.

The data points from the brown silty clay crust fall within multiple zones on the chart. Data points from this material exhibit behavior of material in Zones 3 and 4, indicating a overconsolidated silt/clay mixture and Zones 5 and 6, indicating a sandy material. Zones 3 and 4 accurately describe the composition stiff brown silty clay crust. To refine the behavior classification of the material, the interpretation of must be supported by other factors, such as the stress history. The high OCR of the crust material supports the Zone 4 (Clayey Silt to Silty Clay) and Zone 9 (Very stiff fine grained) classification of the soil behavior type.

Figure 4.9 - Soil Behavior Classification at CPTu B-11, Using Method of Robertson (1990)



Zone	Soil Behavior Type
1	Sensitive, Fine Grained
2	Organic Soils - Peats
3	Clays - Clay to Silty Clay
4	Silt Mixtures, Clayey Silt to Silty Clay
5	Sand Mixtures; Silty Sands to Sandy Silt



Zone	Soil Behavior Type
6	Sands; Clean Sands to Silty Sands
7	Gravelly Sand to Sand
8	Very Stiff Sand to Clayey Sand
9	Very Stiff Fine Grained

- ◆ Weathered Brown Clay
- ▲ Soft Gray Clay
- Glacial Sands

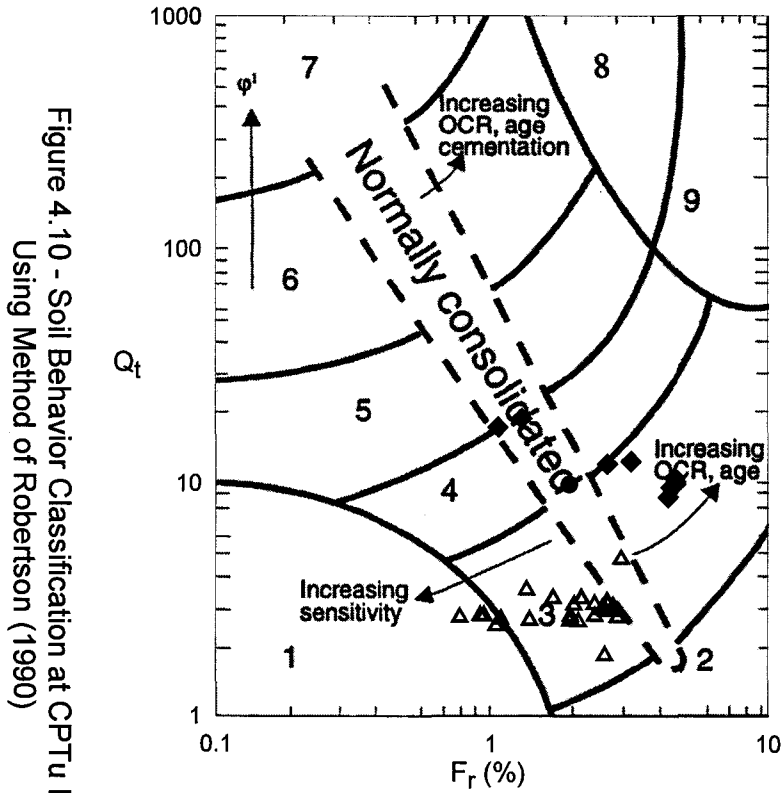
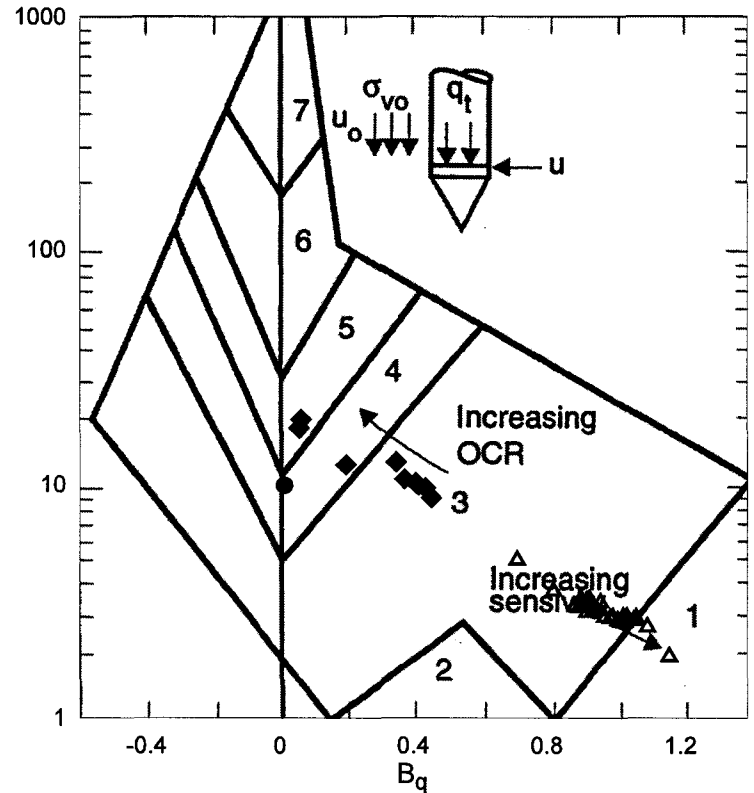


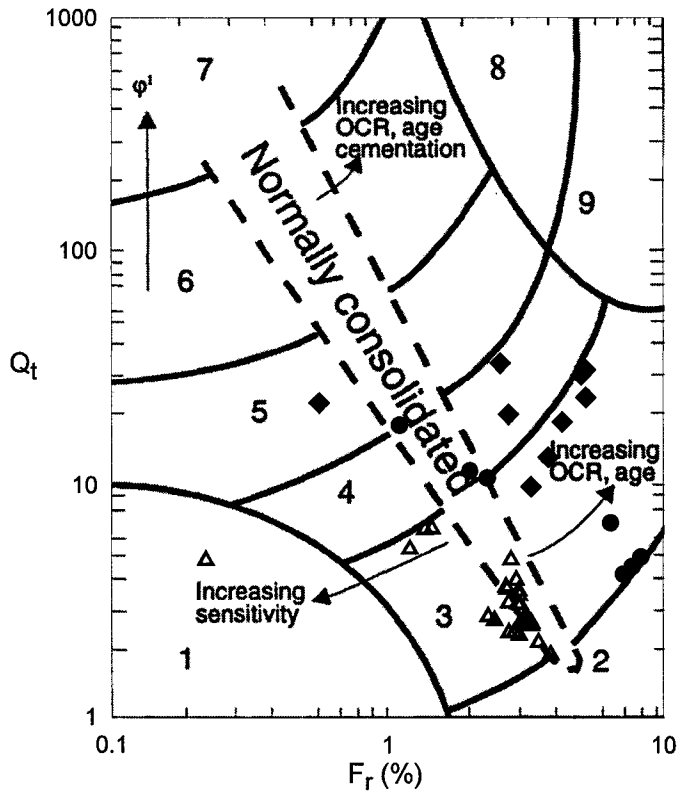
Figure 4.10 - Soil Behavior Classification at CPTu P-3, Using Method of Robertson (1990)

Zone	Soil Behavior Type
1	Sensitive, Fine Grained
2	Organic Soils - Peats
3	Clays - Clay to Silty Clay
4	Silt Mixtures, Clayey Silt to Silty Clay
5	Sand Mixtures; Silty Sands to Sandy Silt

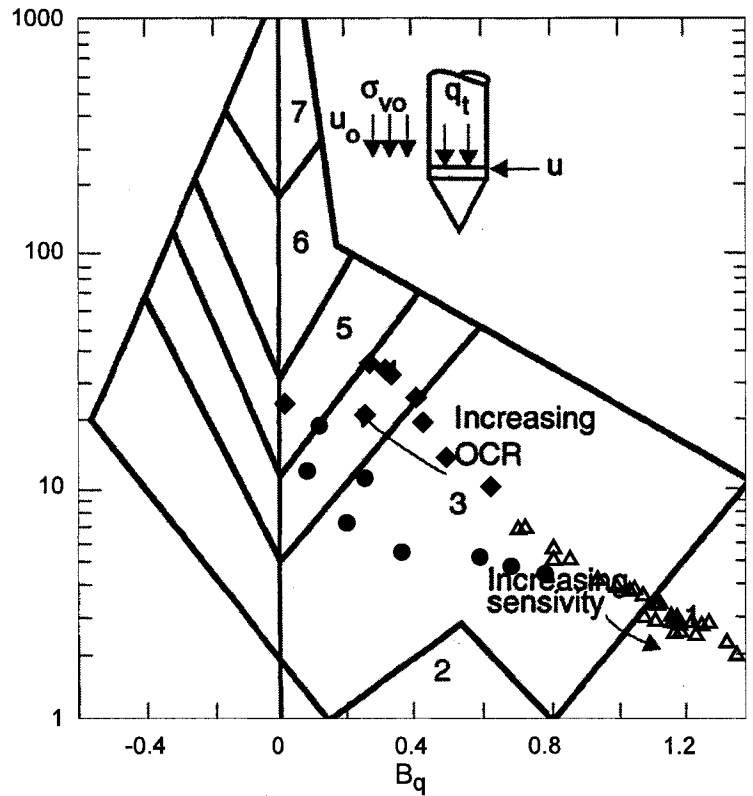


Zone	Soil Behavior Type	Symbol
6	Sands; Clean Sands to Silty Sands	◆ Weathered Brown Clay
7	Gravelly Sand to Sand	▲ Soft Gray Clay
8	Very Stiff Sand to Clayey Sand	● Glacial Sands
9	Very Stiff Fine Grained	

Figure 4.11 - Soil Behavior Classification at CPTu I-3/I-4,
Using Method of Robertson (1990)



Zone	Soil Behavior Type
1	Sensitive, Fine Grained
2	Organic Soils - Peats
3	Clays - Clay to Silty Clay
4	Silt Mixtures, Clayey Silt to Silty Clay
5	Sand Mixtures; Silty Sands to Sandy Silt



Zone	Soil Behavior Type
6	Sands; Clean Sands to Silty Sands
7	Gravelly Sand to Sand
8	Very Stiff Sand to Clayey Sand
9	Very Stiff Fine Grained

- ◆ Weathered Brown Clay
- △ Soft Gray Clay
- Glacial Sands

A second classification system has been proposed by Larsson and Mulabdic (1991) for clays and gyttjas based on a large database of piezocone soundings from test sites in Sweden and Norway. Gyttjas are highly organic muds deposited in lakes, and are commonly encountered in Sweden. The classification method is based on the pore pressure parameter (B_q) and the net cone resistance ($q_r - \sigma_{v0}$), and is depicted in Figure 4.12.

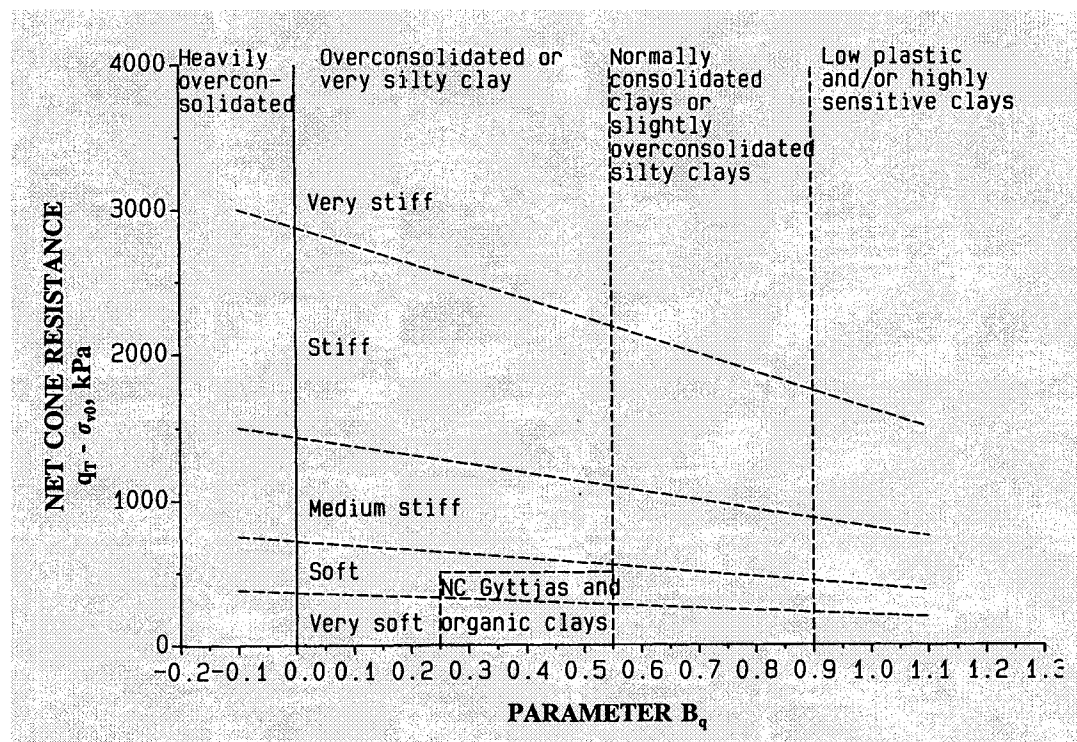
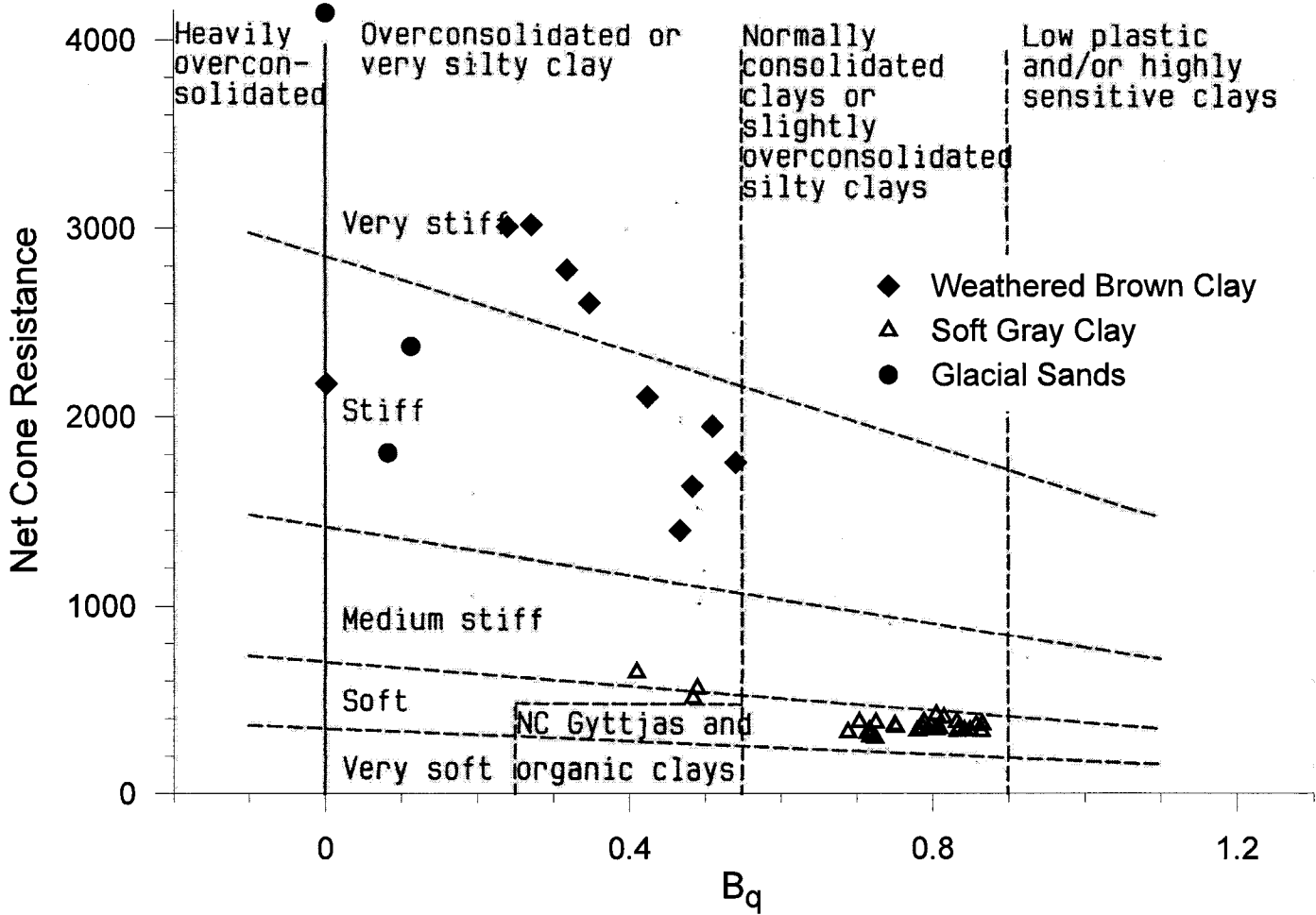


Figure 4.12 - Proposed Soil Behavior Classification Chart for Fine-Grained Soils (After Larsson and Mulabdic, 1991)

Figure 4.12 distinguishes the overconsolidation ratio, the stiffness, the sensitivity and the type of clay. The same data points presented in Figures 4.9, 4.10 and 4.11 and classified using the method of Robertson (1990) are classified using the method of Larsson and Mulabdic (1991) in Figures 4.13, 4.14 and 4.15.

The brown silty clay crust is classified as medium stiff to very stiff overconsolidated or very silty clay using this method. The soft gray silty clay material is generally classified as very soft to soft clay which is near normally consolidated and highly sensitive. Three points within the soft gray silty clay stratum in the CPTu B-11 profile are classified as soft to medium stiff overconsolidated or very silty clay. Further examination of the data reveals that at these test depths a sharp increase in tip resistance occurs, which may indicate lenses of coarse grained material. Many of the data points from the glacial sands fall outside of the boundaries of this classification chart, indicating that most of the material is likely sand or a sand mixture with silt. Some data points from the glacial sands do plot within the classification system of Larsson and Mulabdic (1991). These data points likely represent thin layers of silt or clay within the sand.

Figure 4.13 - Soil Behavior Classification at CPTu B-11, Using Method of Larsson and Mulabdic (1991)



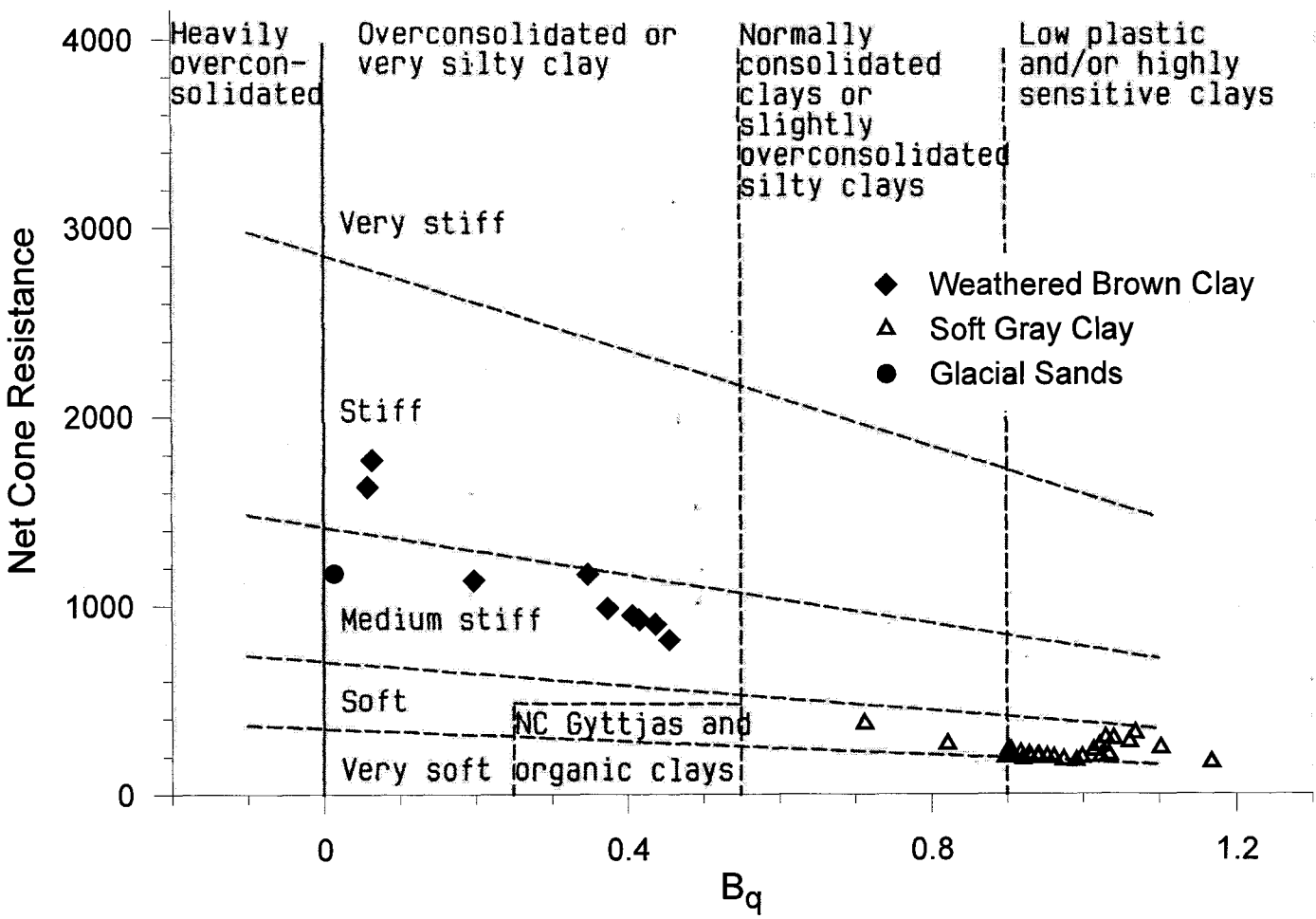


Figure 4.14 - Soil Behavior Classification at CPTu P-3, Using Method of Larsson and Mulabdic (1991)

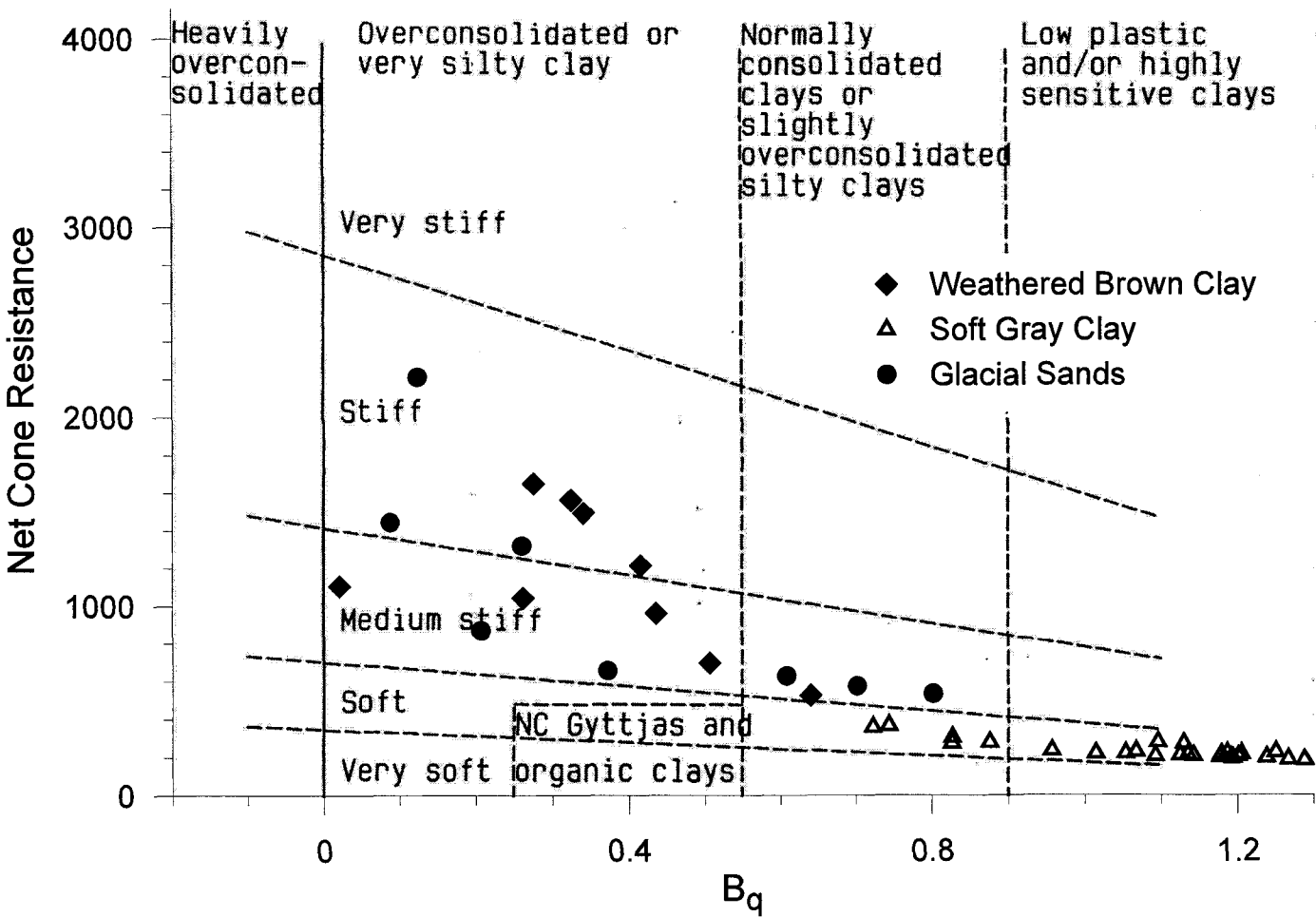


Figure 4.15 - Soil Behavior Classification at CPTu 1-3/1-4, Using Method of Larsson and Mulabdic (1991)

It appears that the soil classification system proposed by Robertson (1990) performs very well for a wide range of soils. Despite the multiple soil behavior types indicated for the crust material, a successful interpretation of the soil behavior is possible throughout the profile. The effect of the high overconsolidation ratio on pore pressures measured in the u_2 position and the large tip resistance recorded within the crust understandably contribute to the uncertainty between the behavior of heavily overconsolidated clay and a coarse grained material which contains some fines. Therefore the method of Larsson and Mulabdic (1991) may be better suited when classifying such material.

The method of Larsson and Mulabdic (1991) performs well when classifying the behavior of the fine grained material within each of the three piezocone profiles as well. The ability to reveal a change in material behavior even in very thin layers indicates that the method of Larsson and Mulabdic (1991) may play an important role in determining the cause of the anomalous zone in deeper profiles, as a thin layer of coarse grained material may affect the behavior of the soil.

4.2.4.3 - Interpretation Using the Dilatometer

Marchetti observed that in initial profiles completed using the dilatometer, the material index (I_D) is closely related to the prevailing grain size fraction. The parameter I_D provides a relationship between the spacing of p_0 and p_1 , which describes the soil stiffness. The expression for I_D is presented in Equation 4.11:

$$I_D = \frac{p_1 - p_0}{p_0 - u_0} \quad [4-11]$$

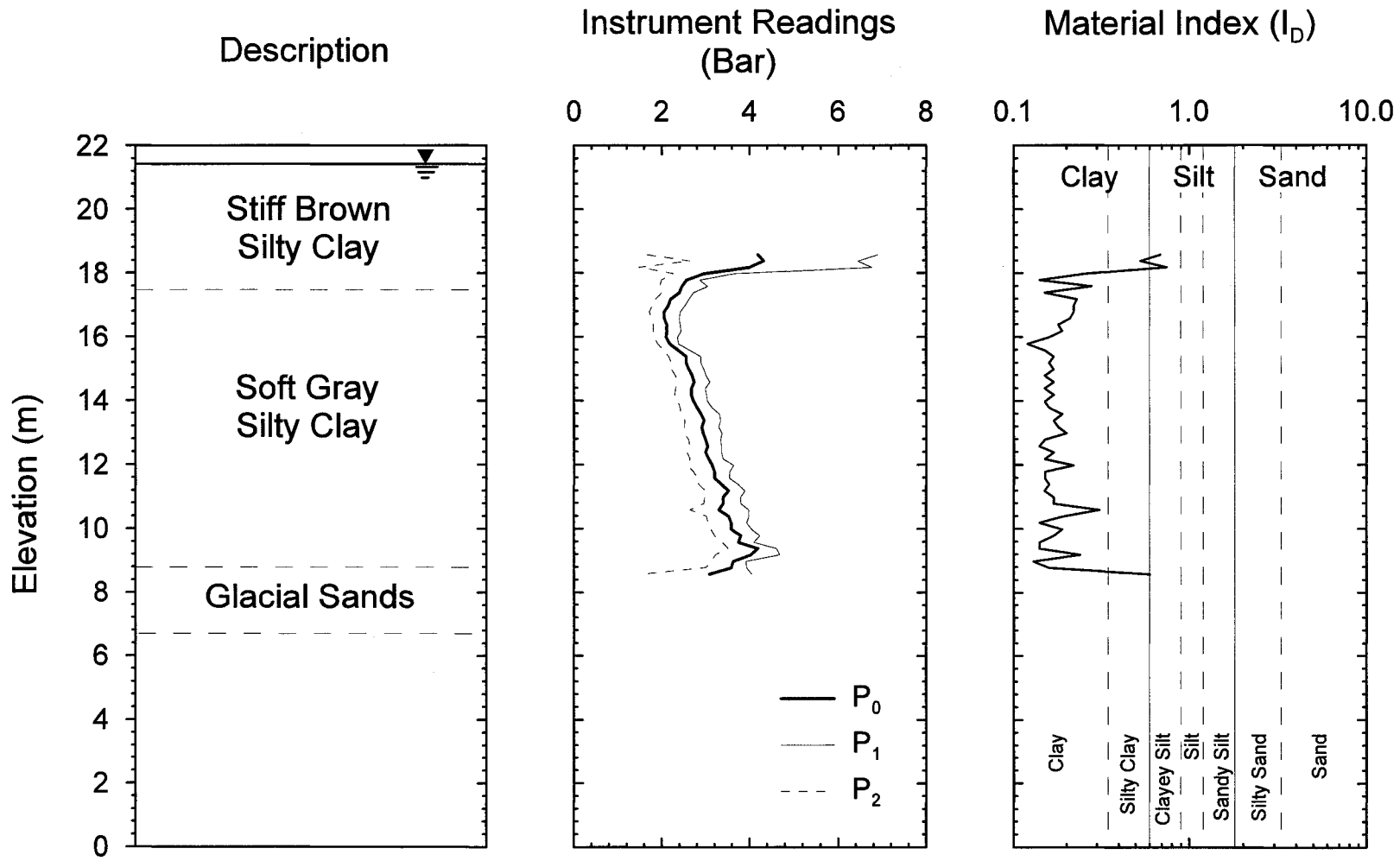
The material index does not indicate the soil type based on a grain size analysis; however like the piezocone, it provides an indication of the behavior of the soil. Marchetti (1980) noted that the value I_D increases rapidly as the percentage of fines decreases, and does not appear to be influenced by the overconsolidation ratio. Table 4.3 summarizes the ranges of I_D which correspond to various soil types proposed by Marchetti (1980).

Table 4.3 - Proposed Soil Classification Based on DMT I_D Values
(After Marchetti, 1980)

	Clays		Silts			Sands	
	<i>Clay</i>	<i>Silty Clay</i>	<i>Clayey Silt</i>	<i>Silt</i>	<i>Sandy Silt</i>	<i>Silty Sand</i>	<i>Sand</i>
Values of I_D	0.10 to 0.35	0.35 to 0.60	0.60 to 0.90	0.90 to 1.20	1.20 to 1.80	1.80 to 3.30	3.30+

Following the ranges defined in Table 4.3, the dilatometer profile at B-11 of I_D is presented in Figure 4.16. Throughout the soft gray silty clay layer the material is classified as behaving as clay with little to no silt. Within the interface zone of the stiff brown silty clay crust and the soft gray silty clay the material varies classification from silty clay to clayey silt. At the interface between the soft gray silty clay and the glacial sands the classification indicates that the material behaves as silty clay. While the dilatometer does provide a good indication of the soil behavior, it does have limitations. Detection of thin layers, which may be critical for design, is not possible as the test is not conducted continuously. In addition the dilatometer is known to incorrectly classify clays as silts or clays with sand fractions as silt (Marchetti et al., 2001).

Figure 4.16 - Soil Behavior Classification at DMT B-11, Based on DMT I_p Values
(After Marchetti, 1980)



4.2.5 - Undrained Shear Strength (S_u)

4.2.5.1 - Introduction

The undrained shear strength (S_u) of a soil can depend on many factors, and therefore there is no single method appropriate for determining the in situ strength of a soil. The rate of strain, the stress path, stress history, plasticity and mode of failure are some of the characteristics that will contribute to how the soil will respond to an imposed stress (Campanella et al., 1988).

In order to develop site specific relationships to aid in the interpretation of the undrained shear strength, a set of baseline strengths must be developed for this site. While no general consensus exists on what method is best suited for developing this baseline, recommendations for a unified test method for correlation do exist, such as using the undrained triaxial compression test (Wroth, 1988). Commonly used methods include the field vane, triaxial compression tests (CAUC), direct simple shear (DSS) and the average of triaxial compression, triaxial extension and DSS tests. At the RWS site the uncorrected undrained shear strength profiles from field shear vane tests have been used as baselines for both the piezocone and dilatometer profiles.

4.2.5.2 - Interpretation Using the Piezocone

A wide variety of theoretical and empirical relationships have been developed in order to estimate the undrained shear strength using the piezocone. Of the theoretical relationships, Lunne et al. (1997) have grouped the available methods into five classes:

- Classical bearing capacity theory
- Cavity expansion theory (Vesic, 1975; Konrad and Law, 1987)
- Conservation of energy combined with cavity expansion theory (Baligh, 1975)
- Linear and non-linear stress-strain relationships (Ladanyi, 1963)
- Strain path theory (Baligh, 1985; Teh and Houlsby, 1991)

While each method uses different theory, each adapts a single relationship to express the undrained shear strength in terms of piezocone data. The relationship in Equation 4.12 is developed from the bearing capacity relationship for deep foundations and is expressed as:

$$S_u = \frac{q_t - \sigma}{N_c} \quad [4-12]$$

Where N_c is a theoretical cone factor and σ may be the in situ total stress (σ_o), the vertical total stress (σ_{vo}), the horizontal total stress (σ_{ho}) or the octahedral total stress (σ_i). Using a relationship such as this would indicate that for a certain soil, knowing the correct value of N_c would help determine the S_u . Typical values for N_c range between 15 and 20, however values as low as 10 in soft normally consolidated clays, and as high as 30 in stiff overconsolidated clay have been reported. The solutions which are based directly upon the classical bearing capacity theory assume failure of a rigid plastic material (Lunne et al., 1997).

Vesic (1975) expanded on the theoretical manner in which N_c is determined by relating the bearing capacity of the soil to the pressure required to expand a

spherical cavity in an infinite elasto-plastic material. This cavity would represent the failure surface ahead of the cone tip. This theoretical representation results in the following expression, where I_r is the rigidity index (G/S_u) of the soil:

$$N_c = \frac{4}{3} \cdot (1 + \ln I_r) + 2.57 \quad [4-13]$$

Konrad and Law (1987) employ the cavity expansion theory as well to determine the undrained shear strength, however a hemispherical failure zone is assumed at the tip of the cone.

Baligh (1975) approached the problem in a similar manner by using cavity expansion theory, however the theoretical value N_c accounts for conservation of energy. This theory assumes that the work required to advance the cone a unit distance is equal to the work required to expand a cylindrical cavity and to advance the cone at a constant rate over a unit distance.

Estimating the theoretical cone factor using strain path theory provides a good example of the many factors which can influence the undrained shear strength, while also illustrating the cumbersome nature of many theoretical relationships. The strain path method, first proposed by Baligh (1985) and further expanded upon by Teh and Housby (1991) develops a set of stress and strain paths representative of soil advancing past a stationary cone. The theoretical cone factor developed by Teh and Housby (1991) using this approach accounts for several factors, many of which may not be commonly available:

$$N_{kt} = N_s \cdot \left(1.25 + \frac{l_r}{2000}\right) + 2.4\alpha_f - 0.2\alpha_s - 1.8\Delta \quad [4-14]$$

Where: $N_s = 4/3 \cdot [1 + \ln(l_r)]$

$$\alpha_f = \text{cone roughness factor} = \left(\sqrt{3\tau_f}\right) / (2S_u)$$

Where $0 < \alpha_f < 1$ and τ_f is the shear stress on the cone face boundary

α_s = shaft roughness factor

$$\Delta = (\sigma_{vo} - \sigma_{ho}) / 2S_u$$

It should be noted that N_{kt} is normally used when the cone factor is derived empirically (Konrad and Law, 1987).

As can be observed, the method for computing N_{kt} using the relationship developed by Teh and Houlsby (1991) can become very intensive. Using empirical relationships to determine S_u or N_{kt} can provide a good correlation with the baseline data set. These empirical relationships are often based on total point resistance (q_t), effective point resistance (q_t and u) or based on excess pore pressure (Δu).

The value of N_{kt} can be directly calculated from the classical bearing capacity relationship by using the corrected point resistance and the overburden stress at the depth of a known undrained shear strength. The bearing capacity relationship is rearranged to give this relationship:

$$N_{kt} = \frac{q_t - \sigma_{vo}}{S_u} \quad [4-15]$$

Using the undrained shear strength from field vane data at borehole B-11 the average value for N_{kt} was determined to be 21.34. This method was not examined further as the field vane data would influence the interpretation of the zone of reduced strength using the piezocone. The piezocone and field vane undrained shear strength profiles must remain independent when assessing whether the zone of reduced strength is real or an artifact from testing.

Estimation of the undrained shear strength using the total cone resistance has been studied by many researchers using the relationship expressed in Equation 4.15. The value of N_{kt} will be specific to each test site; however typical ranges have been reported for certain material types. In non-fissured overconsolidated clays Kjekstad et al. (1978) reports an average value of 17 when using triaxial compression tests for reference values. In normally consolidated marine clays, such as those found at the RWS site, Lunne and Kleven (1981) report N_{kt} as having a range of 11 to 19 with an average of 15 when using the field vane for reference strengths. Research by Aas et al. (1986) indicates that the cone factor can be influenced by the plasticity index of the soil. A similar trend observed by Powell and Quarterman (1988) confirms this influence. A relationship developed by Larsson and Mulabdic (1991) accounts for the plasticity of the soil using the liquid limit, and has been examined for this research. This relationship expresses N_{kt} as:

$$N_{kt} = 13.4 + 6.65 \cdot w_L \quad [4-16]$$

Where w_L is the liquid limit expressed in decimal form.

Estimation of the undrained shear strength using effective cone resistance has been suggested using Senneset (1982), and further examined by Campanella et al. (1982). The relationship from Campanella et al. (1982) is expressed as:

$$S_u = \frac{q_t - u_2}{N_{ke}} \quad [4-17]$$

Although this method has been observed to correlate well with the pore pressure parameter B_q , Lunne et al. (1997) recommends that it generally not be used in soft normally consolidated clays. In such circumstances the pore water pressure measured in the u_2 position can be close to 90% of the tip resistance. In this case the value in the numerator of the relationship can become very small, and thus increasingly subject to errors in the tip resistance of pore pressure measurements.

Estimating the undrained shear strength using the excess pore pressure ($\Delta u = u_2 - u_0$) can produce good correlations with the baseline values due to the generation of large pore pressures in clays. In this scenario the pore pressure transducer is typically operating in its higher range, where the accuracy of the transducer is typically greater. Many relationships using excess pore pressure to determine the undrained shear strength are semi-theoretical; however the most basic relationship is described as:

$$S_u = \frac{\Delta u}{N_{\Delta u}} \quad [4-18]$$

The semi-theoretical relationships using both theory and the excess pore pressure are based upon cavity expansion theory. Results from this work have been reported

by Vesic (1972), Massarch and Broms (1981), Campanella et al. (1985), Mayne and Holtz (1988), and Kulhawy and Mayne (1990) and others.

In a fully empirical approach, using results from Swedish and Norwegian clays, Larsson and Mulabdic (1991) determined that the relationship is dependent on the plasticity of the material. This dependency appears to be quite small however, as a clear trend is observed in the data presented in Figure 4.17 despite the fact that the plasticity has not been accounted for.

Based on this observation from the data presented by Larsson and Mulabdic (1991) the undrained shear strength was examined at the RWS site using a value of $N_{\Delta u}$ that was not corrected for effects of plasticity.

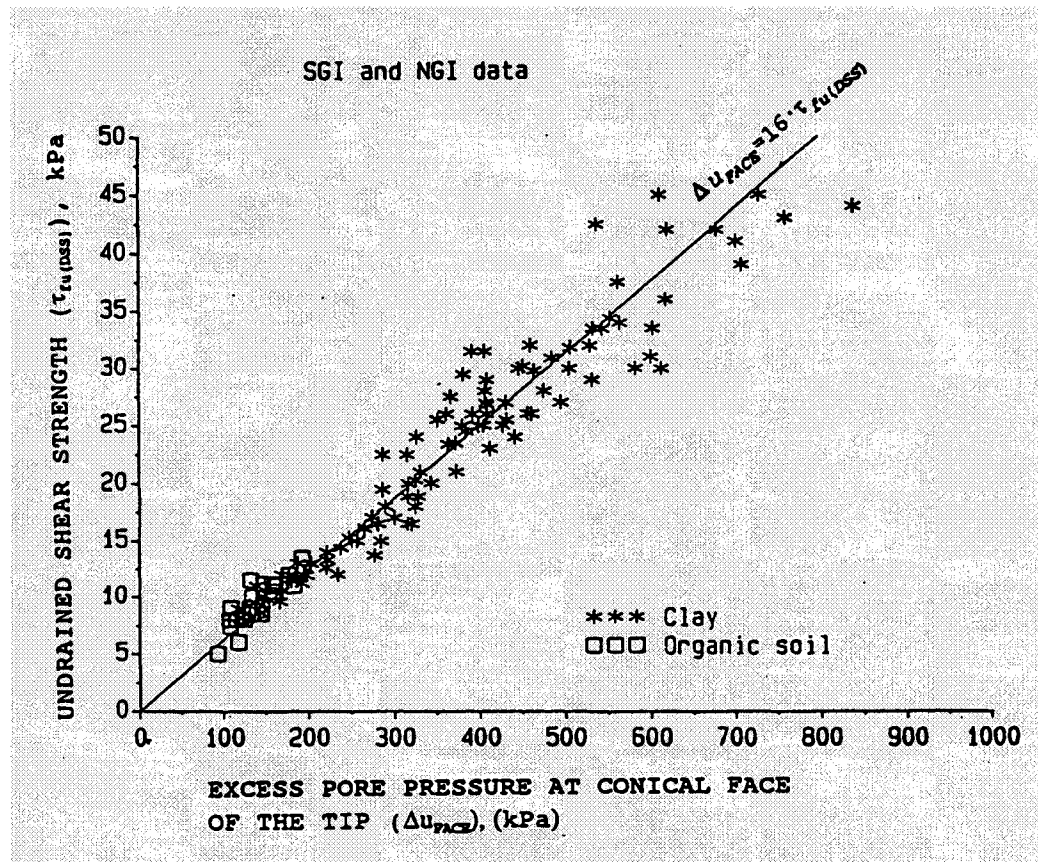


Figure 4.17 - Results of Undrained Shear Strength from Direct Shear Tests against Excess Pore Pressure Generated at the Face of the Cone Tip in Swedish and Norwegian Clays Indicating a Linear Relationship (After Larsson and Mulabdic, 1991)

The undrained shear strength at the three piezocone profiles was determined using the total cone resistance method from Equation 4.16 (Larsson and Mulabdic, 1991) and using the excess pore pressure method presented in Equation 4.18. These profiles are presented in Figures 4.18, 4.19 and 4.20 for the CPTu B-11, P-3 and I-3/I-4 locations respectively. As the relationship developed by Larsson and Mulabdic (1991) is based upon data from European clays and is not specific to this test location, a relationship was developed for soils at this site using the same format. The constants in Equation 4.16 were adjusted to fit the piezocone data to the field vane strength profile. This relationship expresses N_{kt} as:

$$N_{kt} = 15.4 + 11.48 \cdot w_L \quad [4-19]$$

The excess pore pressure relationship closely matches the reference field vane strength data; while the site specific relationship based on total tip resistance, developed from the B-11 data, tends to slightly under predict the strength in the P-3 and I-4/I-4 profiles. One disadvantage of the total tip resistance method is that sandy lenses and layers will produce a high tip resistance, and therefore high undrained shear strength. While the strength of the soil may increase in these layers, displaying this as a higher undrained shear strength, rather than the appropriate friction angle term may lead to improper interpretation when interpreting the data for design.

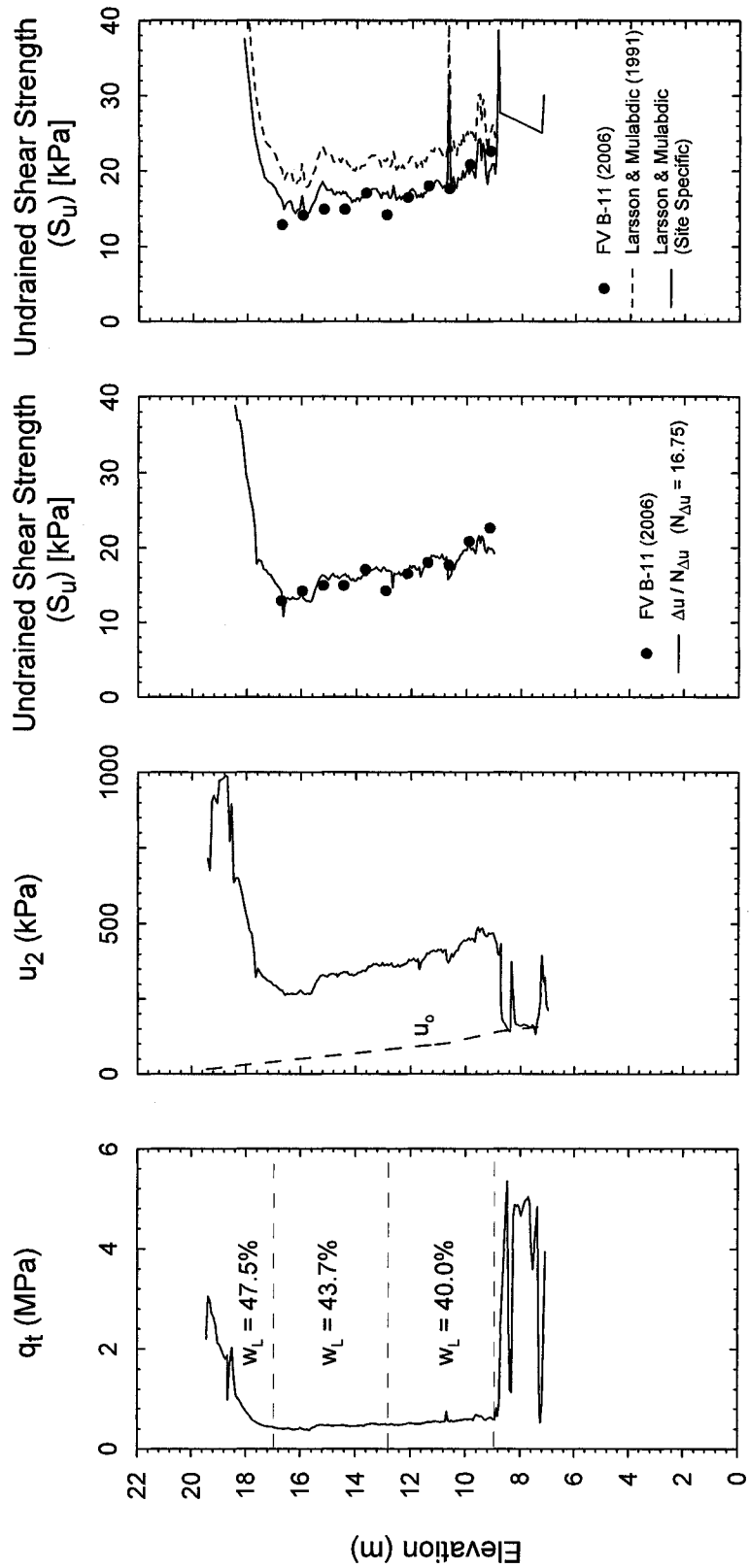


Figure 4.18 - Undrained Shear Strength Profile at CPTu B-11 Based on Methods of Excess Pore Pressure and Total Cone Resistance

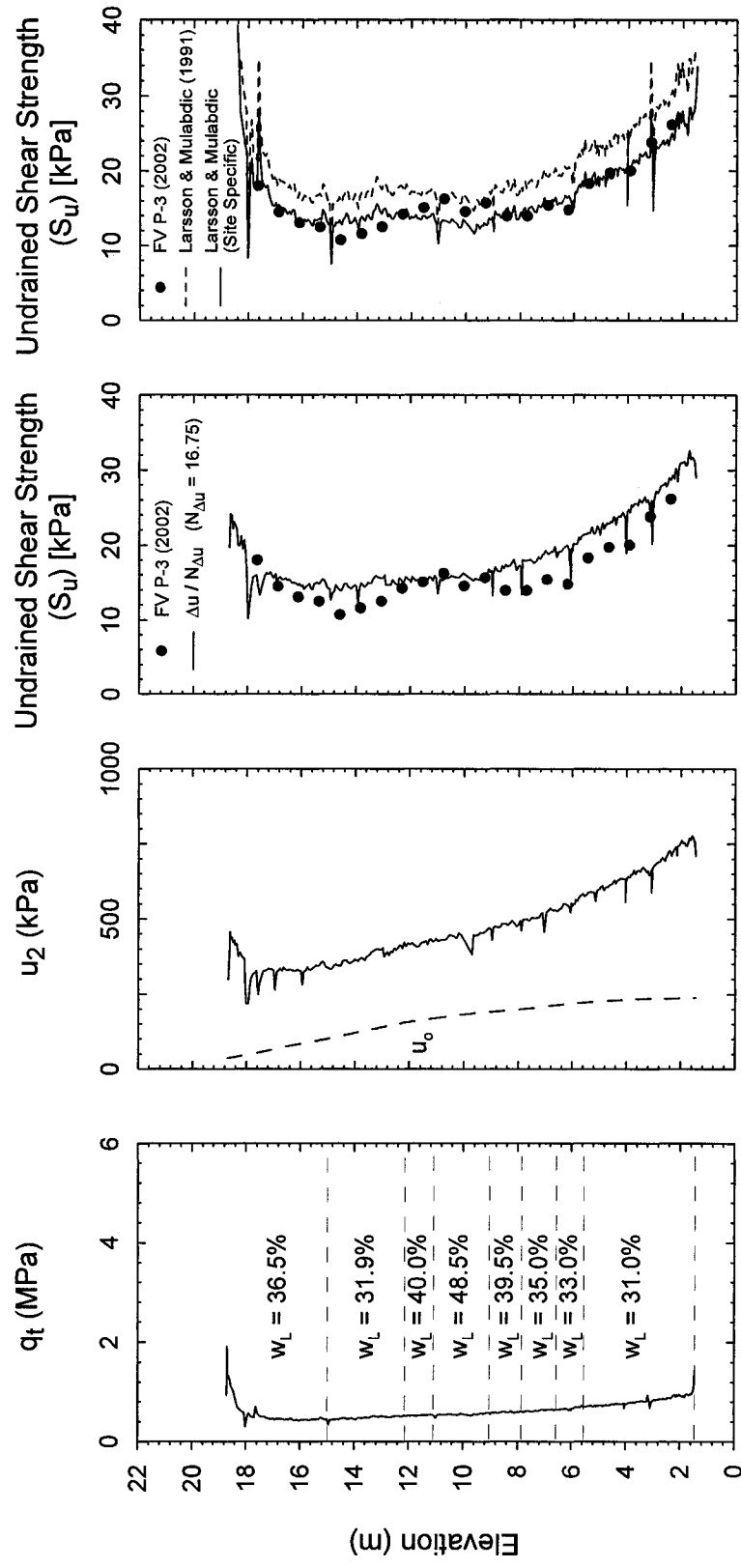


Figure 4.19 - Undrained Shear Strength Profile at CPTu P-3 Based on Methods of Excess Pore Pressure and Total Cone Resistance

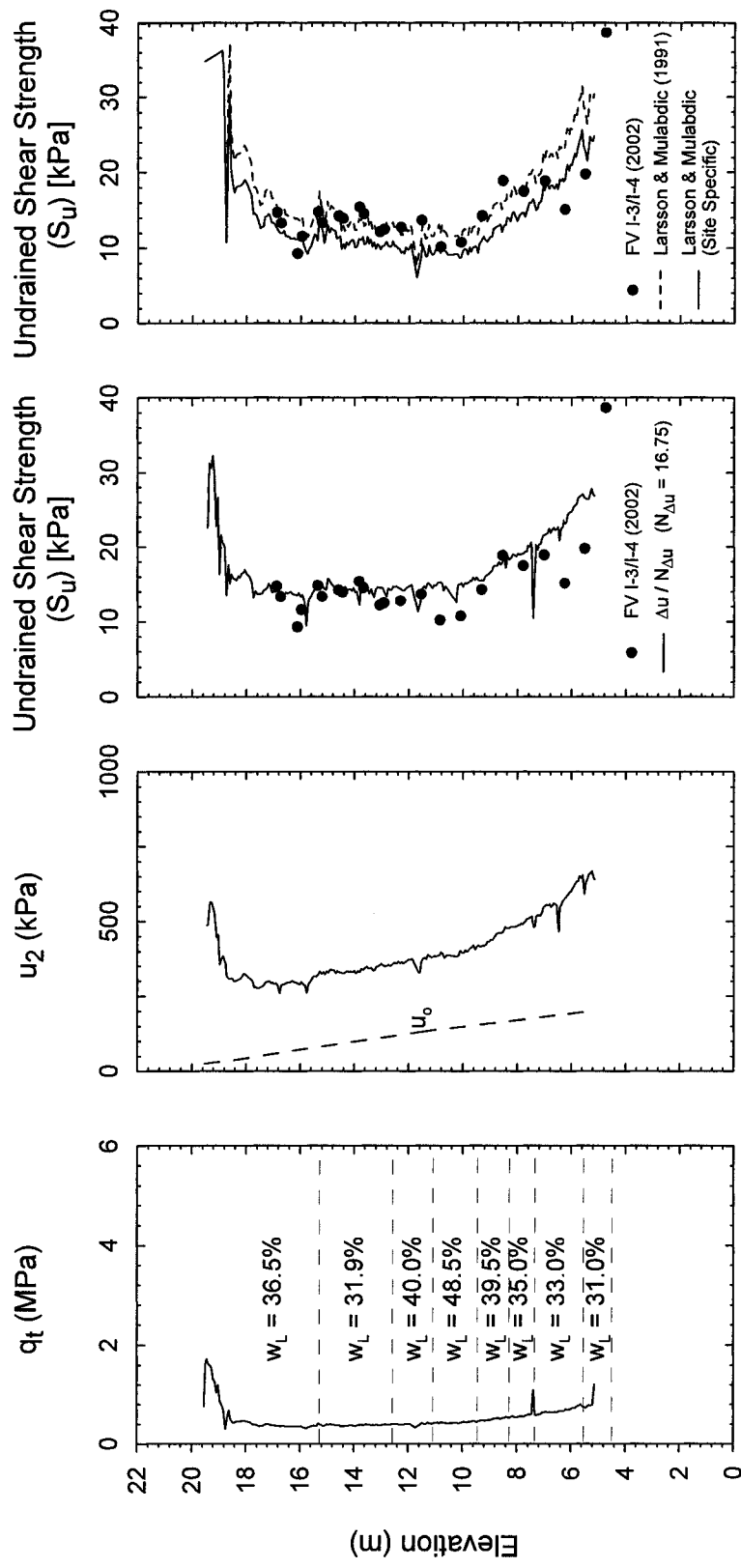


Figure 4.20 - Undrained Shear Strength Profile at CPTu I-3/I-4 Based on Methods of Excess Pore Pressure and Total Cone Resistance

4.2.5.3 - Interpretation Using the Dilatometer

Interpretation of the undrained shear strength from the dilatometer arose from the known correlation between the stress ratio (S_u/σ'_{vo}) and the OCR of a soil. Marchetti (1980) observed that the dilatometer intermediate parameter K_D , the horizontal stress index, was closely related to the OCR as well. This prompted an investigation by Marchetti into a possible relationship between the ratio of undrained shear strength and effective vertical stress to the value of K_D . Based upon observations at multiple test sites, Marchetti (1980) derived a relationship relating the value of K_D to the undrained shear strength:

$$S_u = 0.22\sigma'_{vo} \cdot (0.5K_D)^{1.25} \quad [4-20]$$

Where K_D is:

$$K_D = \frac{p_0 - u_0}{\sigma'_{vo}} \quad [4-21]$$

In this relationship the 0.22 value is taken from the ratio of S_u to σ'_{vo} observed at these sites. Further investigations performed by Nash et al. (1992) and Burghignoli et al. (1991) have reported that the initial relationship performs well when compared to reference strength values, as seen in Figure 4.21.

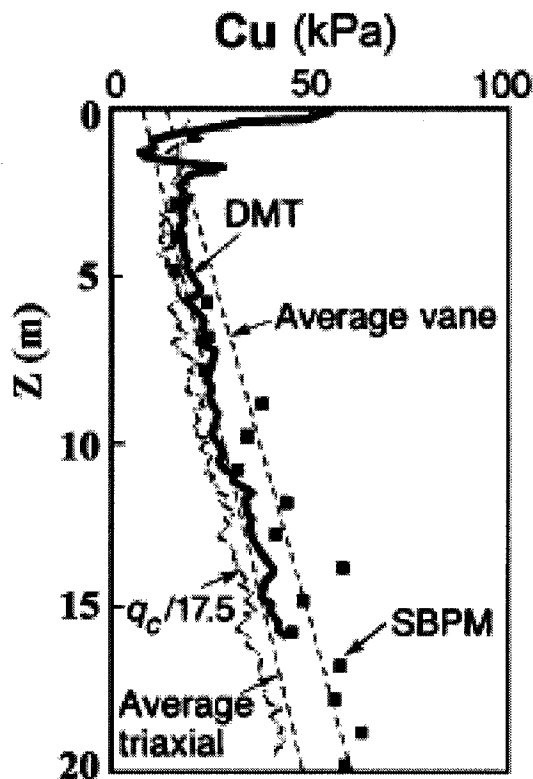


Figure 4.21 - Comparison Between Undrained Shear Strength Measured by DMT and by other Methods at the National Research Site of Bothkennar, UK (After Nash et al., 1992)

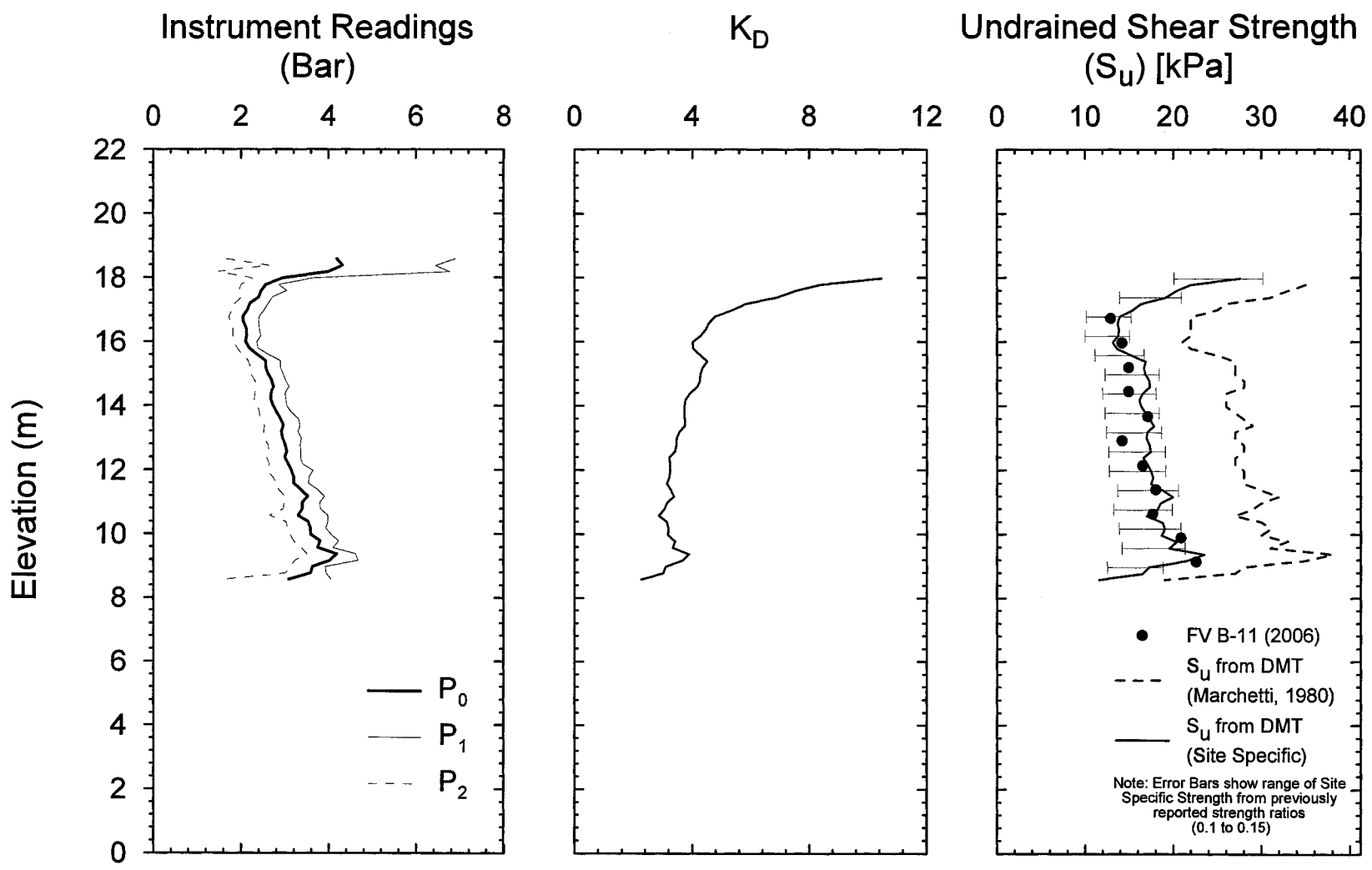
Marchetti (1980) notes that the estimated undrained shear strength is typically underestimated by up to 30% when using this approach.

A profile of undrained shear strength at the B-11 location using the original relationship by Marchetti (1980) is presented in Figure 4.22 alongside the reference uncorrected field vane strength data. The original equation clearly overestimates the undrained shear strength; however it does fit the general trend of the reference data well. Models of the RWS site have incorporated a stress ratio (S_u/σ'_{vo}) between 0.1 and 0.15 (Rabasca, 2002). Using this data a site specific relationship was developed to best fit the reference data. The site specific relationship was determined to be:

$$S_u = 0.137\sigma'_{vo} \cdot (0.5K_D)^{1.25} \quad [4-22]$$

This relationship is plotted in Figure 4.22 as well, with error bars showing the stress ratio range of 0.1 to 0.15, and a solid line indicating the value of 0.137. The undrained shear strength very closely matches the reference strength values, indicating that the dilatometer is a very useful tool for determining the strength of fine grained soils.

Figure 4.22 - Undrained Shear Strength Profile at DMT B-11 Based on K_D



4.2.6 - Stress History (OCR)

4.2.6.1 - Introduction

The stress history plays a critical role in the finite element modeling at the RWS site. It is important to note that the OCR of a soil can be affected due to aging and environmental effects, and this can be observed in the stiff weathered brown crust material at the site. In cases such as this, the OCR best describes the ratio of the yield stress to the current effective overburden pressure (Lunne et al., 1997).

4.2.6.2 - Interpretation Using the Piezocone

In saturated clay, the magnitude of pore water pressures generated during the advance of the piezocone is influenced by the overconsolidation ratio. Heavily overconsolidated clays will exhibit dilative behavior, which can result in negative pore water pressures. For a specific clay and conditions, as the OCR decreases the excess pore pressure generated will increase. Because of this observed behavior, most research has focused on pore pressures and tip resistance for describing the trend of the OCR throughout a profile. Many of these relationships are based on the following parameters:

- u/q_t
- B_q
- $\Delta u/\sigma'_{vo}$
- $\Delta u/q_t$

These relationships often account for the plasticity of the material, as this factor influences the OCR. Of the many relationships developed for the estimation of the

OCR from piezocone data, three empirical relationships were examined and compared to the baseline values available from oedometer tests.

Larsson and Mulabdic (1991) have presented a relationship based upon data collected from well documented test sites in Sweden, Norway and Scotland. Analysis of this data suggested a relationship between OCR and $\Delta u/\sigma'_{vo}$, and in addition, the ratio of excess pore pressure to the effective overburden pressure was found to correlate with the plasticity of the soil. Figure 4.23 presents the data set normalized for the effects of soil plasticity, from which the empirical relationship is developed:

$$\log OCR = 0.24 \left[\frac{\Delta u/\sigma'_{vo}}{2.8 + 2.65 \cdot w_L} \right] - 0.14 \quad [4-23]$$

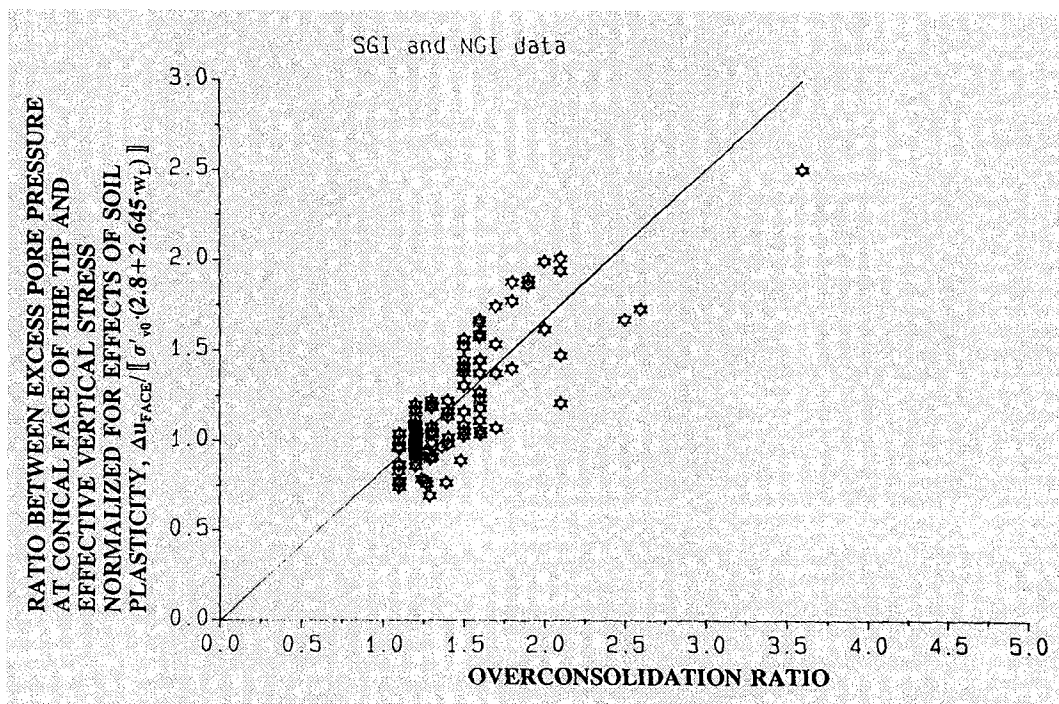


Figure 4.23 - Relationship between Overconsolidation Ratio and the Ratio of Excess Pore Pressure (u_1) to Effective Vertical Stress in Swedish and Norwegian Clays (After Larsson and Mulabdic, 1991)

The second method of interpretation uses both the tip resistance and the pore pressure measured by the cone. This method, suggested by Houlsby (1988), incorporates a relationship between $(q_{t-u}) / \sigma'_{vo}$ and the OCR. As discussed in Section 4.2.7 of this report, the $q_{EFFECTIVE}$ parameter (q_{t-u}) is an effective method for estimation of the preconsolidation pressure. Like the method of Larsson and Mulabdic (1991), this method also accounts for the soil plasticity. Figure 4.24 shows a considerable scatter in the data set when plotted against the OCR. However, a better correlation is observed in Figure 4.25 when the pore pressure is recorded at the u_2 position, and the data set is normalized for the plasticity of the soil. It is important to note the scale of the vertical axes in Figures 4.24 and 4.25 to observe the effect of the normalization for the soil plasticity. The relationship from Houlsby (1988) is presented numerically as:

$$\log OCR = 0.167 \left[\frac{q_T - u_2}{\sigma'_{vo} \cdot (5.0 \cdot w_L - 0.6)} \right] - 0.05 \quad [4-24]$$

Chen and Mayne (1994) examined a number of empirical relationships to correlate CPTu data with the OCR, and report that the parameter $(q_{t-u}) / \sigma'_{vo}$ shows a strong statistical trend. From the data set analyzed, Chen and Mayne (1994) recommend that a good first order estimate of the overconsolidation ratio is provided by:

$$OCR = 0.53 \left[\frac{q_T - u_2}{\sigma'_{vo}} \right] \quad [4-25]$$

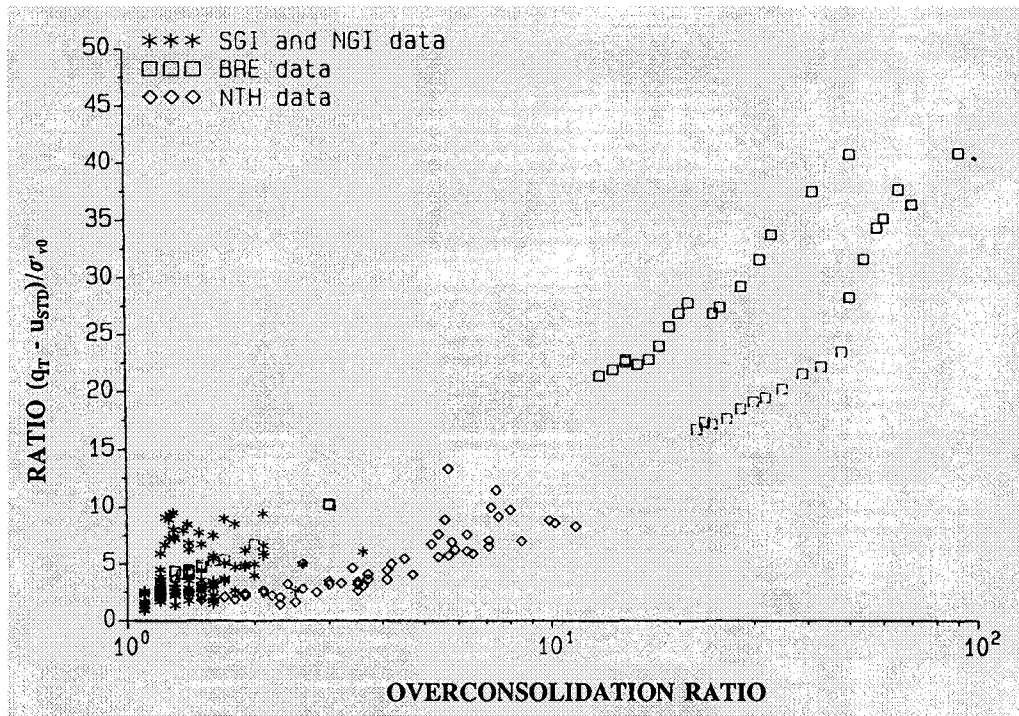


Figure 4.24 - Relationship between Effective Tip Resistance and Overconsolidation Ratio with Pore Pressure Recorded behind the Cone Tip (u_2) (After Larsson and Mulabdic, 1991)

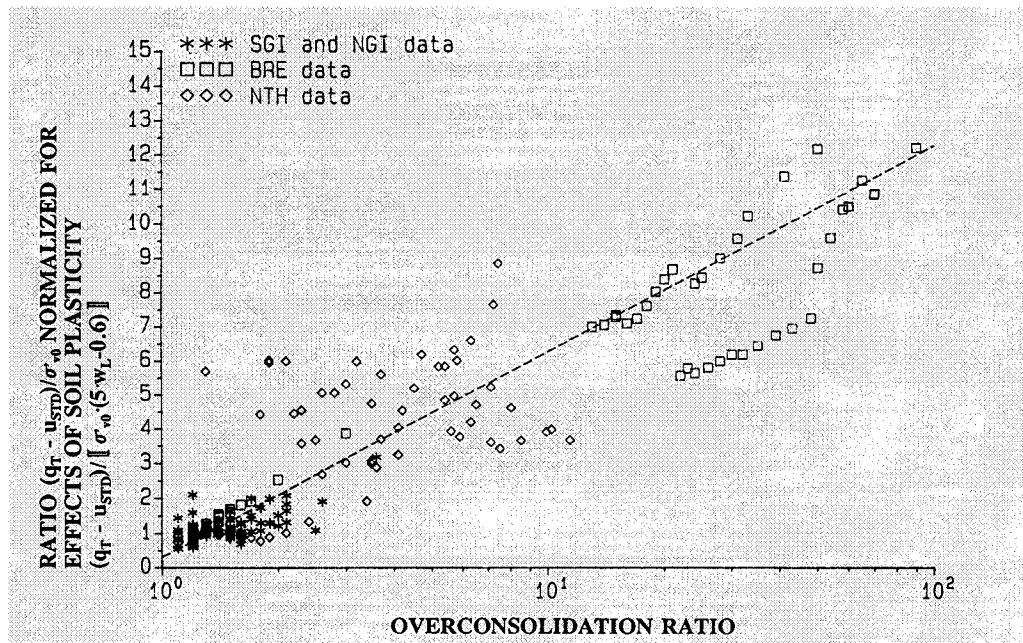


Figure 4.25 - Relationship between Effective Tip Resistance, Normalized for the Effects of Plasticity and Overconsolidation Ratio with Pore Pressure Recorded behind the Cone Tip (u_2) (After Larsson and Mulabdic, 1991)

The OCR profiles at each piezocone test location as determined by the methods of Larsson and Mulabdic (1991), Houlsby (1988) and Chen and Mayne (1994) are presented in Figures 4.26, 4.27 and 4.28 alongside baseline oedometer values. At the B-11 location each method appears to provide a good prediction of the stress history throughout the profile. At the remaining locations the overconsolidation ratio is expected to be less than the baseline values, and closer to the value of 1 in the upper portion of the soft gray clay, as waste loading has occurred between the time the laboratory and in situ tests were performed. At these locations the method of Houlsby (1988) performs very well. The method of Larsson and Mulabdic (1991) generally provides a good indication of the overconsolidation ratio above 15.5 meters elevation in the P-3 and I-3/I-4 profiles. The overconsolidation ratio is greatly underestimated at the I-3/I-4 location by the method of Chen and Mayne (1994). It is important to note that none of the three methods have been modified into site specific relationships, as they each closely match the reference OCR values from laboratory oedometer tests in the B-11 location. While the methods of Houlsby (1988) and Larsson and Mulabdic (1991) both account for the liquid limit, as well as the effective vertical overburden stress and the u_2 pore pressure, the method of Houlsby (1988) is perhaps the most suitable of the three methods for interpretation of the overconsolidation ratio this site. Based upon the trends observed in Figures 4.26, 4.27 and 4.28 it appears that the incorporation of the tip resistance by Houlsby is especially important when the u_2 pore pressure is low.

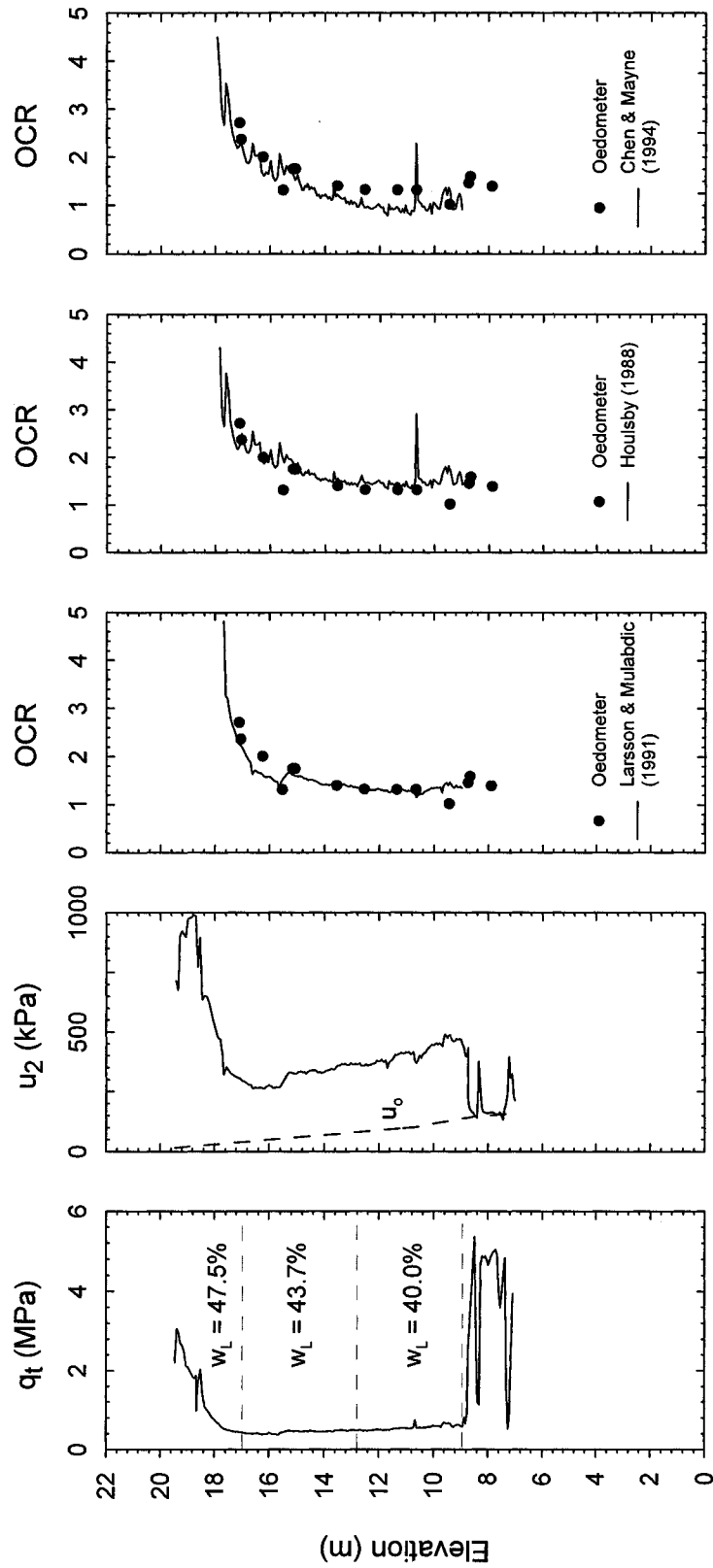


Figure 4.26 - Piezocone OCR Profile at CPTu B-11 based on methods of Larsson and Mulabdic (1991), Houlby (1988) and Chen and Mayne (1994)

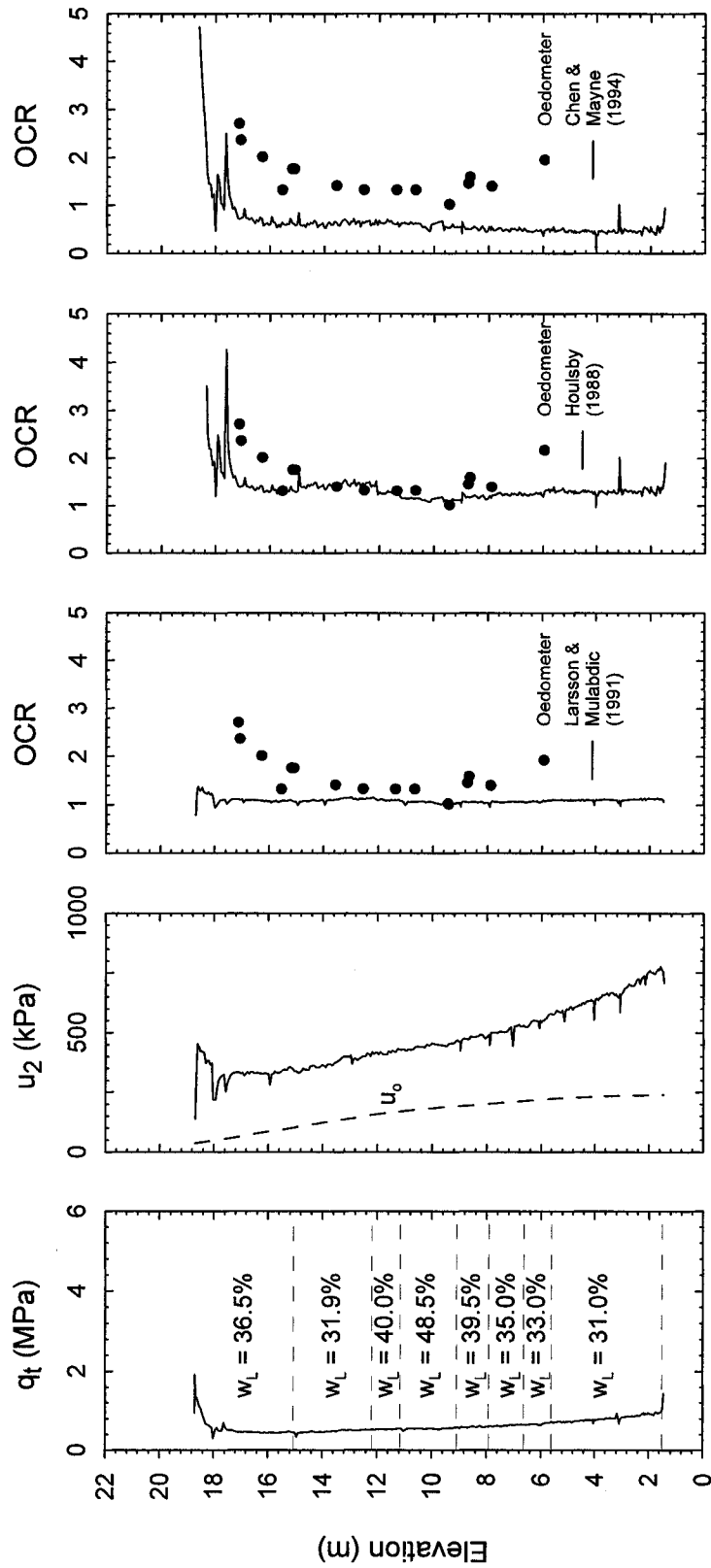


Figure 4.27 - Piezocone OCR Profile at CPTu P-3 based on methods of Larsson and Mulabdic (1991), Housby (1988) and Chen and Mayne (1994)

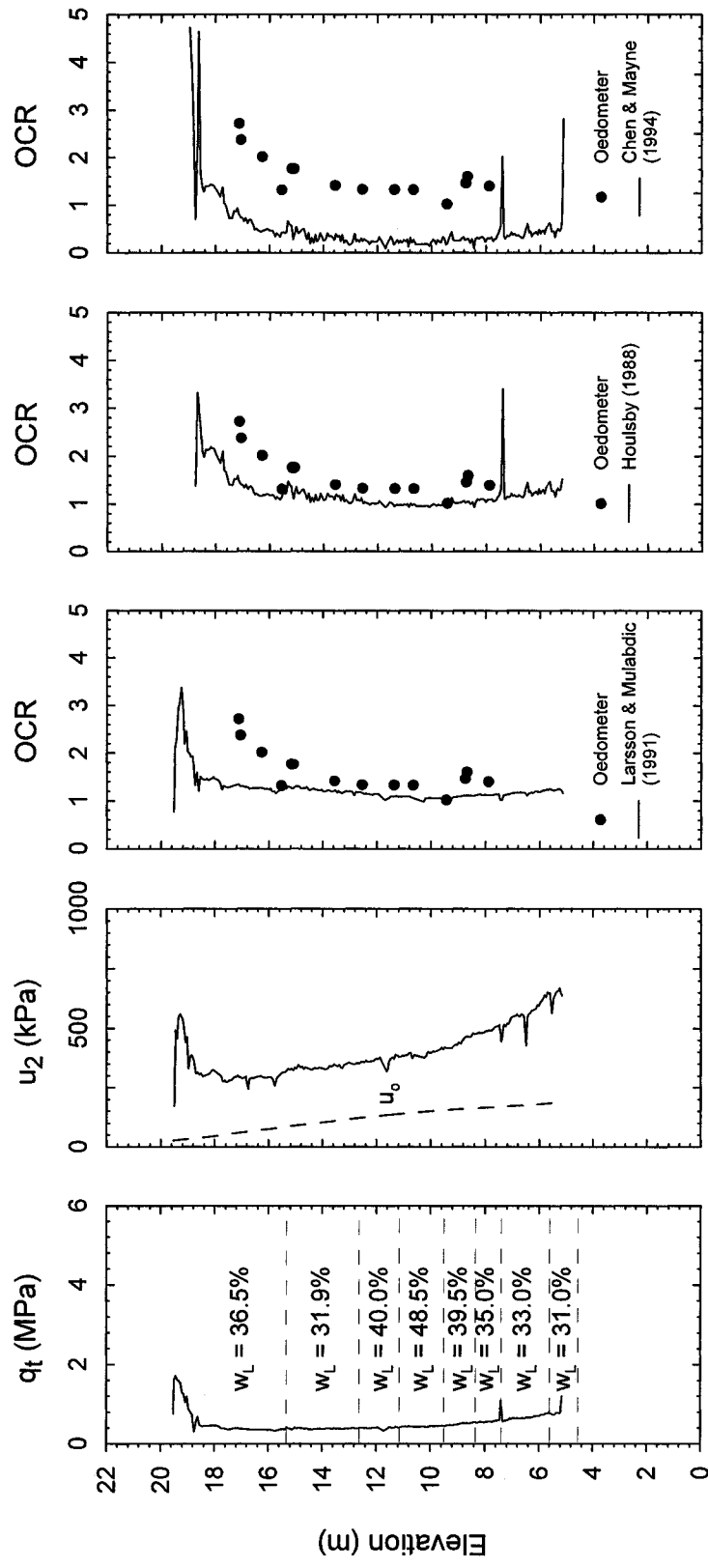


Figure 4.28 - Piezocone OCR Profile at CPTu I-3/I-4 based on methods of Larsson and Mulabdic (1991), Houlby (1988) and Chen and Mayne (1994)

4.2.6.3 - Interpretation Using the Dilatometer

The horizontal stress index (K_D) parameter of the dilatometer can be used to compute the overconsolidation ratio when the value of I_D is less than 1.2, indicating a cohesive material. A direct correlation between the value of K_D and the OCR has been observed by Marchetti (1980), where a K_D value of 2 indicates normally consolidated clay. This understanding may be useful in another manner at the RWS site as well, as Totani et al. (1997) notes that a sudden change in the value of K_D equal 2 would indicate a slip surface. This behavior may be evident within the anomalous zone, where large shear strains have been noted. The relationship used to initially estimate the OCR at the RWS test site is the original correlation proposed by Marchetti (1980)

$$OCR = (0.5 \cdot K_D)^{1.56} \quad [4-26]$$

This correlation has been examined by various researchers (Jamiolkowski et al., 1988; Kamei and Iwasaki, 1995), and has been confirmed with minor variations to account for variations from site to site, one example of which is observed in Figure 4.29.

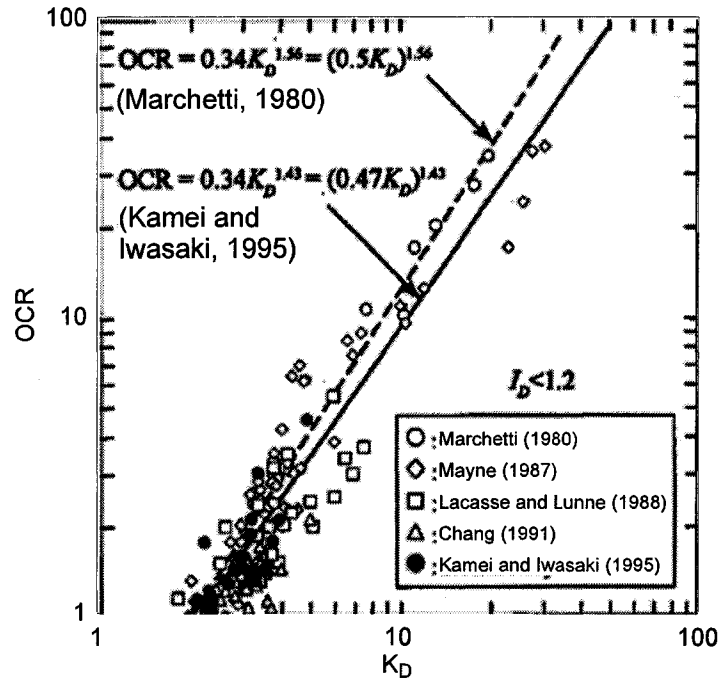


Figure 4.29 - Correlation between K_D and OCR for Cohesive Soils at Various Geographical Locations (After Kamei and Iwasaki, 1995)

The original relationship from Marchetti (1980) appears to overestimate the OCR by 60 to 80% at the RWS site, as observed in Figure 4.30. As a result, a site specific relationship was developed to estimate the OCR by modifying the relationship originally presented by Marchetti. The site specific relationship for estimating the OCR is expressed as:

$$OCR = (0.375 \cdot K_D)^{1.25} \quad [4-27]$$

The site specific relationship is based upon the baseline values from multiple oedometer tests across the test site, and appears to provide a good indication of the OCR.

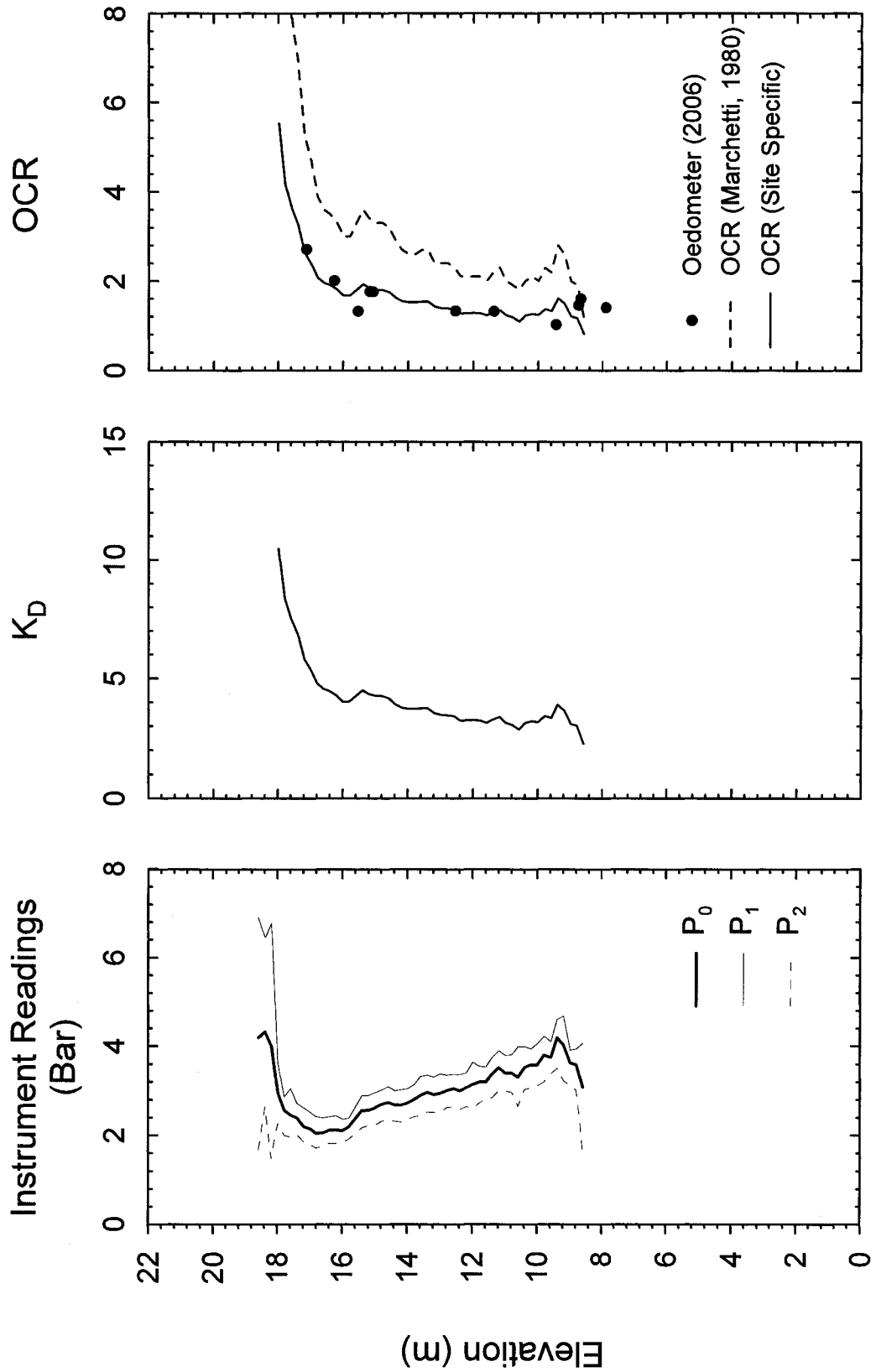


Figure 4.30 - Overconsolidation Ratio Profile at DMT B-11

4.2.7 - Preconsolidation Pressure (σ'_p)

4.2.7.1 - Introduction

Though there exist relationships to directly estimate the OCR, which relates the preconsolidation pressure (σ'_p) and the current effective vertical stress, an estimation of σ'_p remains useful for the analysis of the RWS test site. The change in strength in the anomalous zone, as observed in the FV P-3 and FV P-5 profiles in Figure 2.3, may be linked with a change in the OCR. The effective stresses within the stratum appear to be one cause for this change; it is possible that a change in the preconsolidation pressure may be a contributing factor as well. An examination of the preconsolidation pressure with depth may indicate the cause of this zone is due to changes in geologic conditions.

4.2.7.2 - Interpretation Using the Piezocone

Typical relationships directly relate the tip resistance and the excess pore pressure generated during advance of the piezocone to the preconsolidation pressure. Larsson and Mulabdic (1991) indicate that the estimation of the preconsolidation pressure using excess pore pressure produces better results than relationships using the tip resistance. These relationships are based upon theory describing the generation of pore pressures with loading, which has been related to forces generated by the piezocone by Konrad and Law (1987). The general theory relates the preconsolidation pressure to an effective tip resistance, $q_{\text{EFFECTIVE}}$. For clays with an OCR of less than 15-20 this relationship becomes:

$$\sigma'_p \approx q_{\text{EFFECTIVE}} = q_t - u_{\text{FACE}} \quad [4-28]$$

In this research the pore pressures were not recorded at the face of the cone tip, therefore the net tip resistance ($q_t - \sigma_{vo}$), as suggested by Larsson and Mulabdic (1991), was instead used to determine the preconsolidation pressure.

Larsson and Mulabdic (1991) describe the logic behind using the net tip resistance in the following manner. The preconsolidation pressure and the soil plasticity are contributing factors when interpreting the undrained shear strength of a soil. Likewise, relationships correlating the net tip resistance and the excess pore pressure generated during advance of the piezocone are successful in estimating the undrained shear strength. Therefore it is likely that there exists a relationship between these factors and the preconsolidation pressure. Three relationships based upon the net tip resistance have been examined and compared to the baseline values from oedometer tests conducted by Haley & Aldrich, Inc. and at the University of New Hampshire.

The relationships by Larsson and Mulabdic (1991) and Kulhawy and Mayne (1990) are quite similar and do not directly account for the soil plasticity. The relationship by Larsson and Mulabdic (1991) was developed from tests conducted on Swedish and Norwegian clays, and provides a good fit as seen in Figure 4.31. This relationship is displayed numerically as

$$\sigma'_p = 0.292 \cdot (q_t - \sigma_{vo}) \quad [4-29]$$

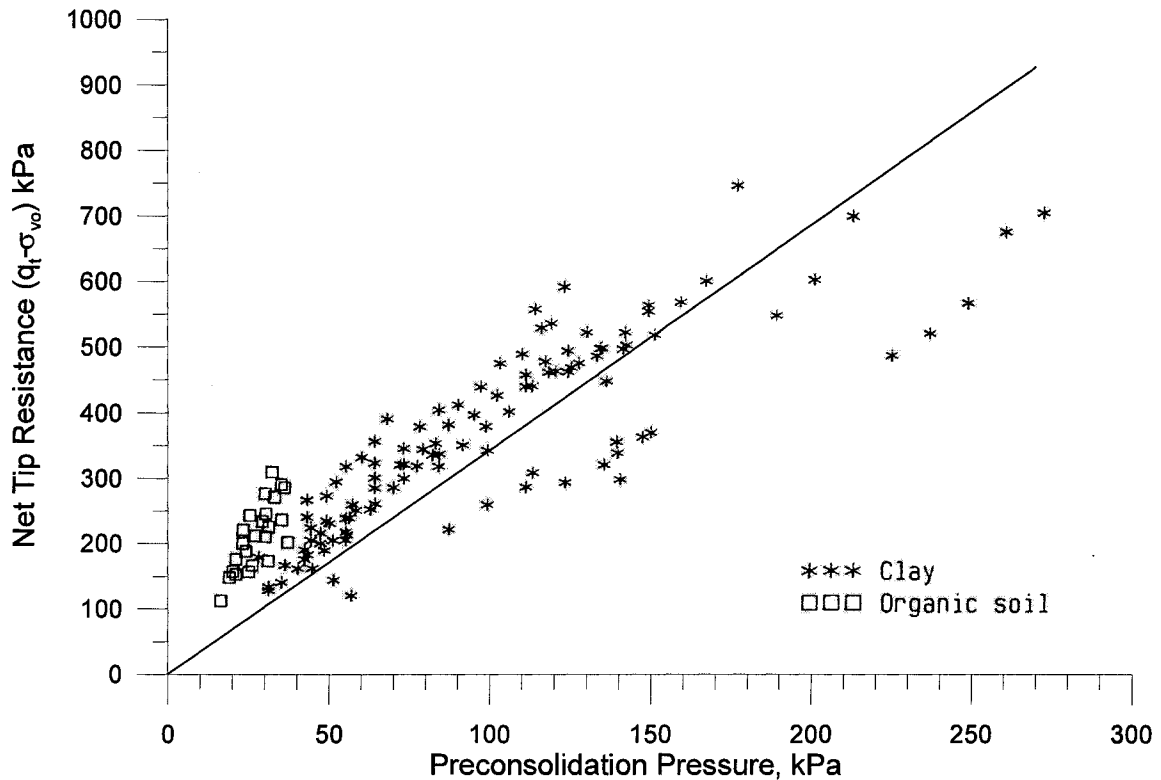


Figure 4.31 – Relationship between Net Tip Resistance and the Preconsolidation Pressure in Swedish and Norwegian Clays (After Larsson and Mulabdic, 1991)

The relationship from Kulhawy and Mayne (1990) is very similar, and is displayed numerically as

$$\sigma'_p = 0.33 \cdot (q_t - \sigma_{vo}) \quad [4-30]$$

Tavenas and Leroueil (1987) compiled data from tests performed in clays in eastern Canada. The data from Figure 4.32 is from soft clays with overconsolidation ratios less than two, and displays a good fit. In this figure the net tip resistance is normalized by the liquid limit by the following equation

$$\sigma'_p = \frac{(q_t - \sigma_{vo})}{1.21 + 4.4 \cdot w_L} \quad [4-31]$$

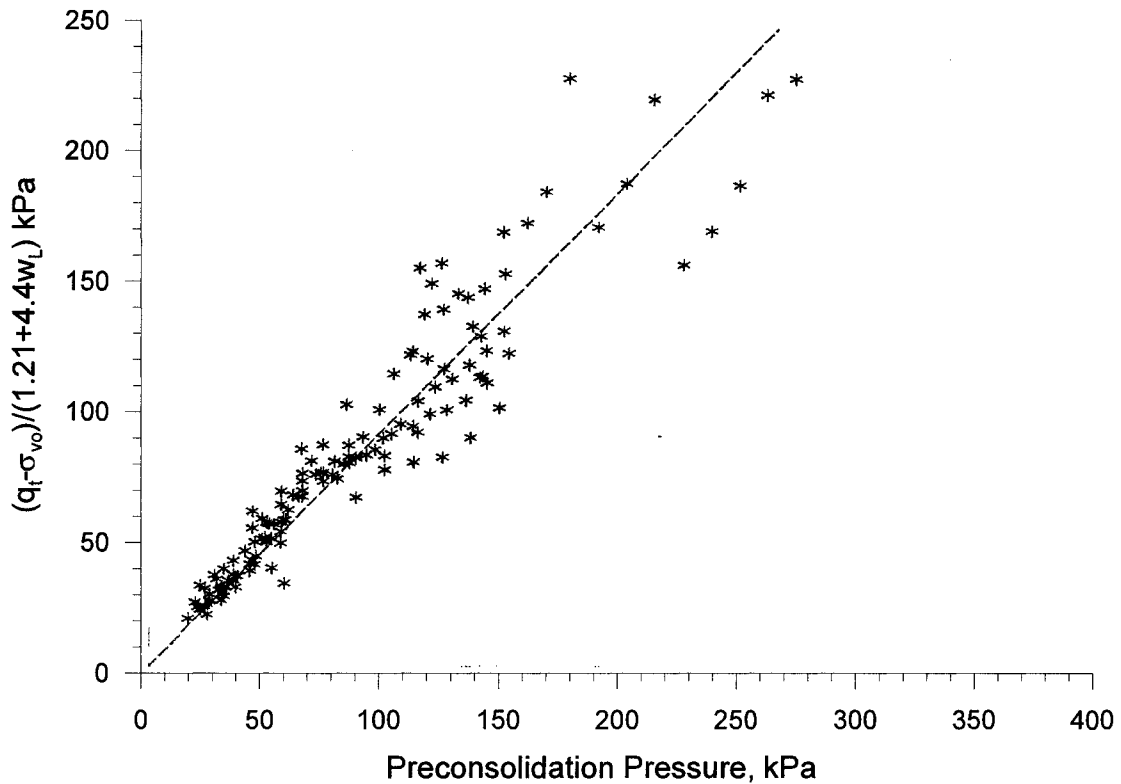


Figure 4.32 - Linear Relationship between Net Tip Resistance, Normalized for the Effects of Soil Plasticity and Preconsolidation Pressure (After Tavenas and Leroueil, 1987)

The preconsolidation pressure estimated by each of these three relationships is presented in Figures 4.33, 4.34 and 4.35 plotted alongside the baseline values from the oedometer, the tip resistance (q_t) and the pore pressure recorded by the piezocone (u_2). The preconsolidation pressure at the P-3 and I-3/I-4 locations is expected to be greater than the baseline values, as up to 7 meters of waste loading has occurred at these locations after the laboratory testing was performed. At the B-11 location the methods of Kulhawy and Mayne (1990) and Larsson and Mulabdic (1991) overestimate the value, though the Larsson and Mulabdic data does show a

close match below 10.7 meters (35 feet) elevation. The method of Tavenas and Leroueil (1987) overestimates the preconsolidation pressure as well; however it appears to match the trend of the baseline values closer. All three methods for determining the preconsolidation pressure at the P-3 location match the oedometer values closely, indicating the value is under predicted. The preconsolidation pressure is underestimated by all three methods in the I-3/I-4 profile as well. A modified version of the method of Tavenas and Leroueil (1997) specific to the RWS site and optimized for the B-11 profile is also presented in those Figures using the following equation:

$$\sigma'_p = \frac{(q_t - \sigma_{vo})}{1.65 + 5.35 \cdot w_L} \quad [4-32]$$

Of the three methods used to determine the preconsolidation pressure from the piezocone data at the RWS site, no single method appears to perform better than the others.

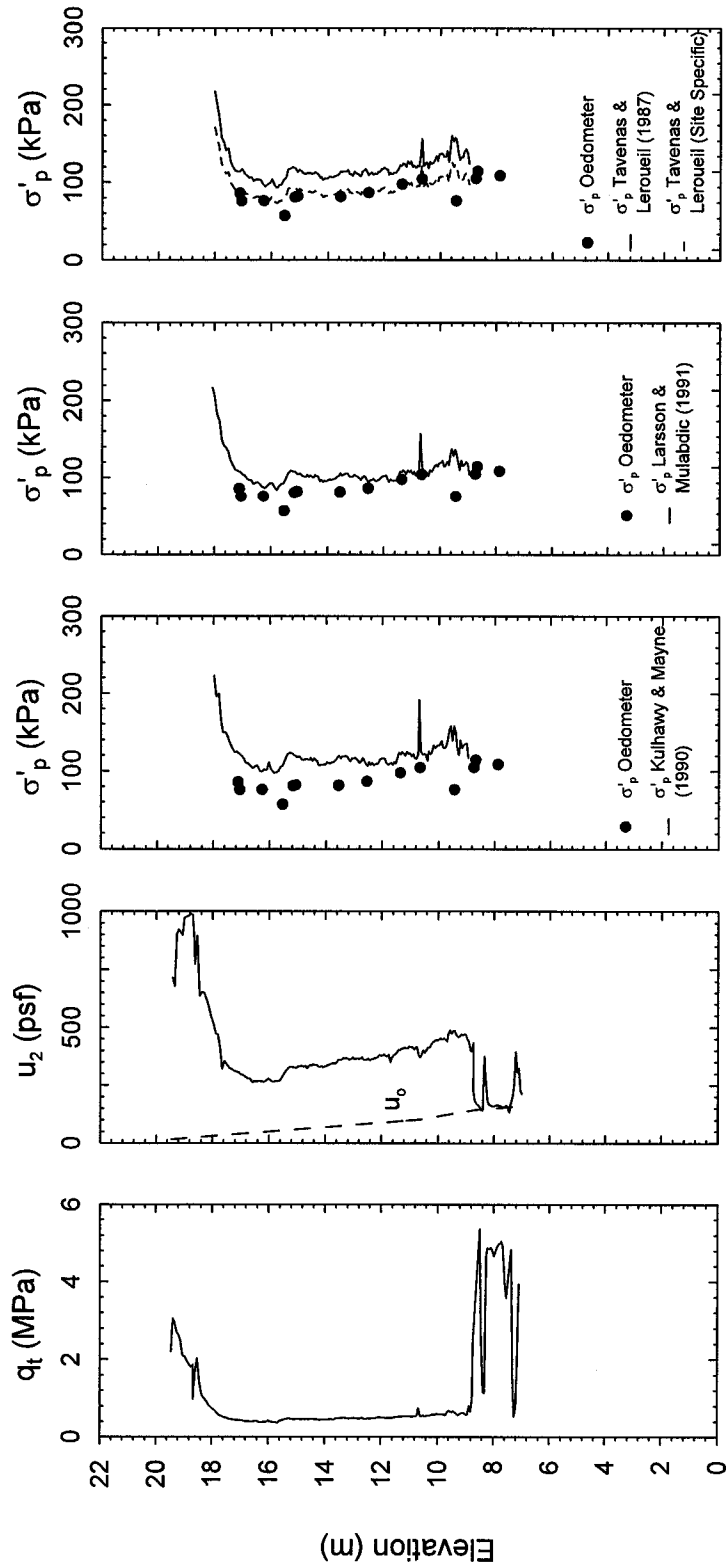


Figure 4.33 - Estimation of the Preconsolidation Pressure Profile at CPTu B-11 Based on Methods of Kulhawy and Mayne (1990), Larsson and Mulabdic (1991), and Tavenas and Leroueil (1987)

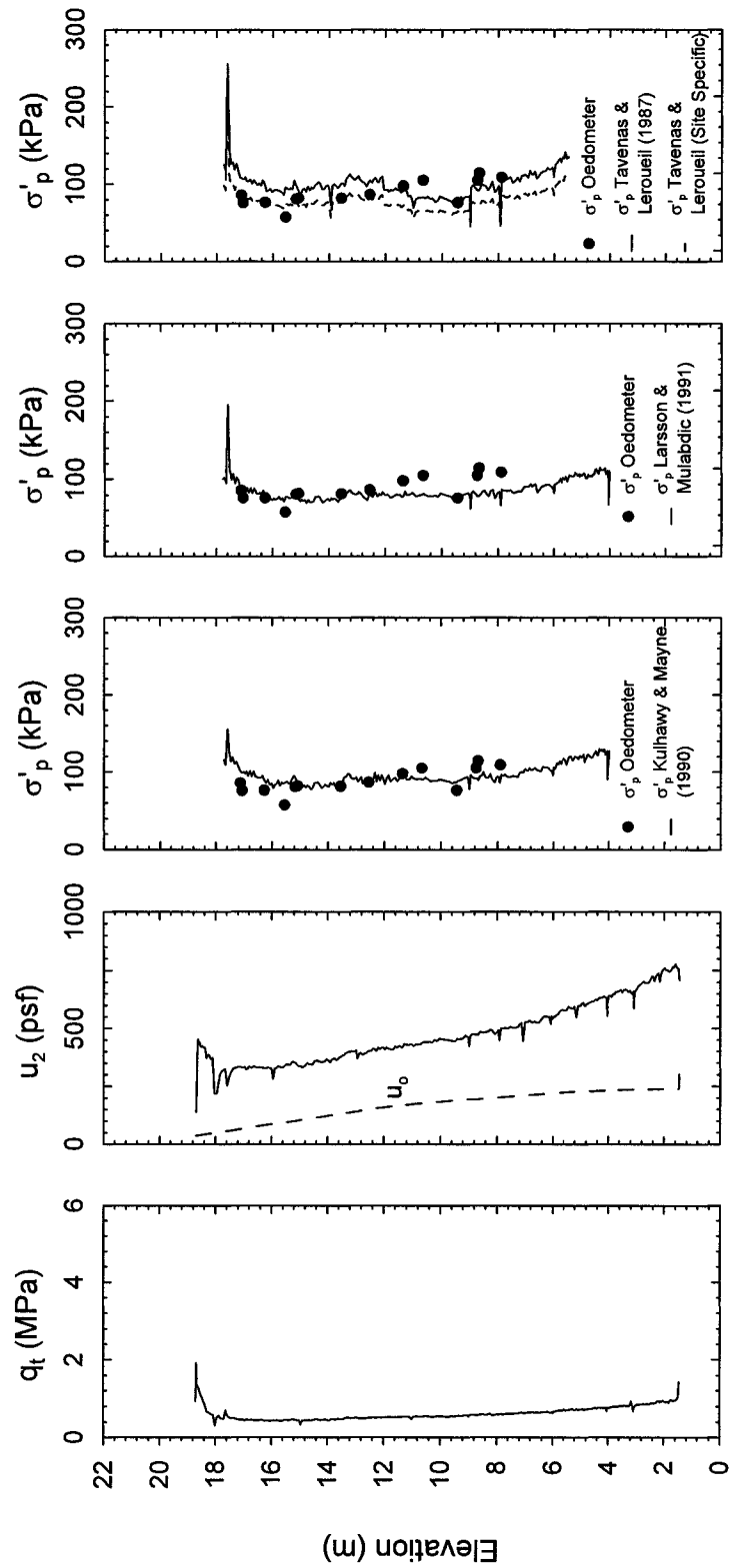


Figure 4.34 - Estimation of the Preconsolidation Pressure Profile at CPTu P-3 Based on Methods of Kulhawy and Mayne (1990), Larsson and Mulabdic (1991), and Tavenas and Leroueil (1987)

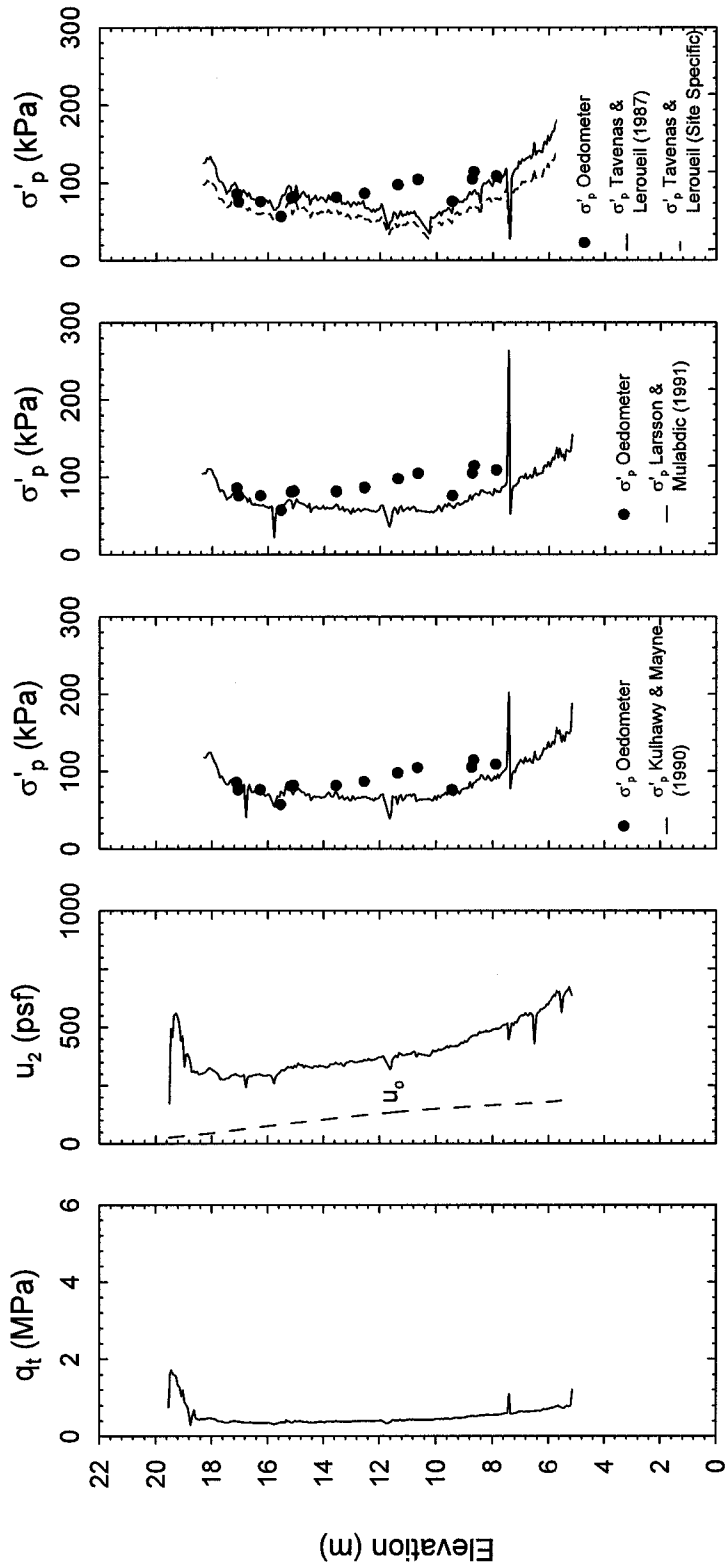


Figure 4.35 - Estimation of the Preconsolidation Pressure Profile at CPTu I-3/I-4 Based on Methods of Kulhawy and Mayne (1990), Larsson and Mulabdic (1991), and Tavenas and Leroueil (1987)

4.2.7.3 - Interpretation Using the Dilatometer

There are no existing relationships between dilatometer output and the preconsolidation pressure. The preconsolidation pressure can be determined at the B-11 dilatometer test location however by using the OCR determined in Section 4.2.6.3 of this report and the vertical effective overburden pressures. Figure 4.36 presents a plot of the preconsolidation pressures determined using the site specific OCR relationship. It is therefore logical that the preconsolidation pressure closely matches the oedometer data in Figure 4.36. For comparison purposes Figure 4.37 presents the site specific relationship for determining the preconsolidation pressure from CPTu data, the values calculated based on OCR from DMT data and preconsolidation pressure determined by laboratory oedometer tests. With the exception of two oedometer data points at 15.8 and 9.2 meters elevation, the preconsolidation pressure from the piezocone at CPTu B-11 and the dilatometer closely match the laboratory data.

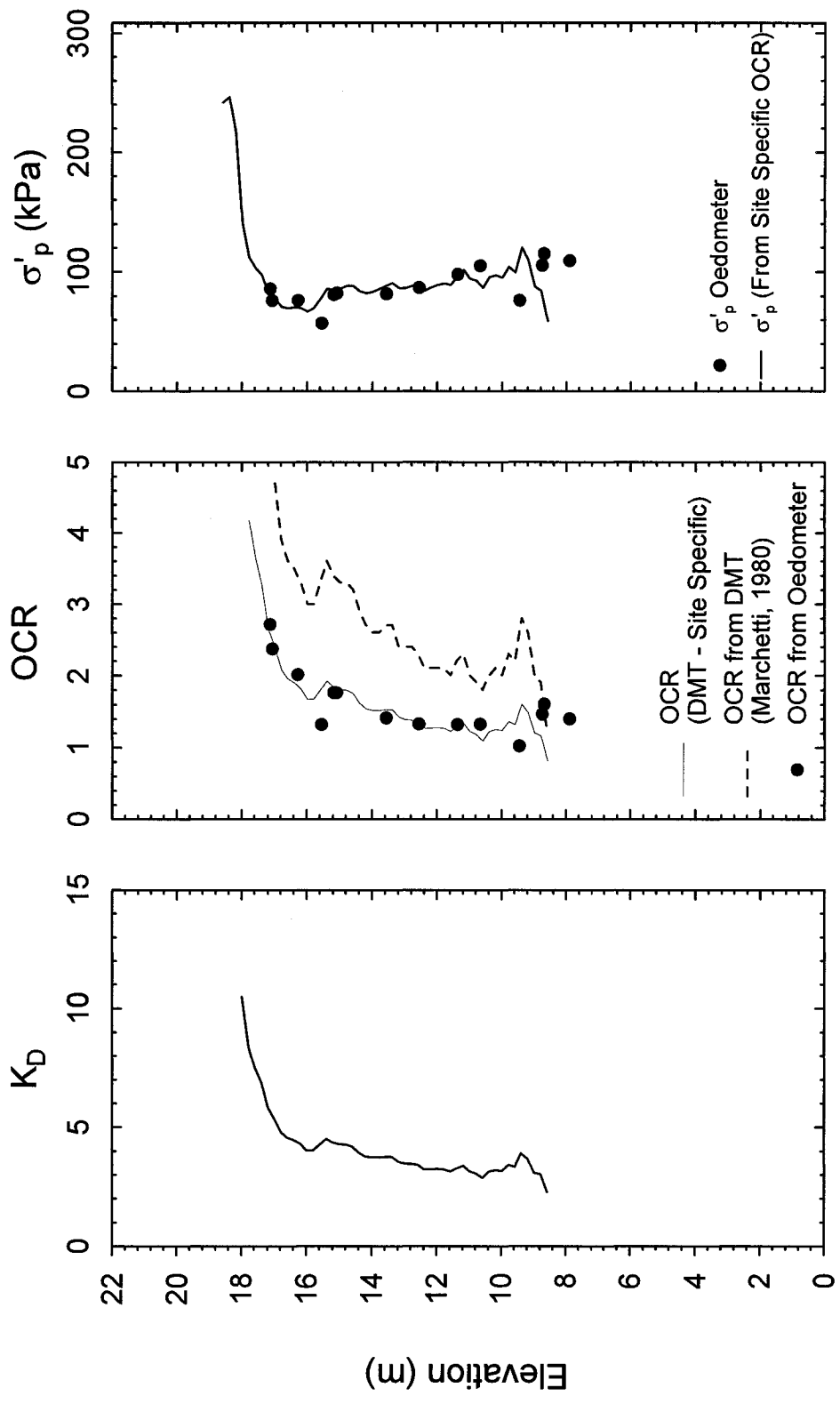


Figure 4.36 - Profile of the Preconsolidation Pressure at DMT B-11 Calculated from Site Specific OCR by Dilatometer

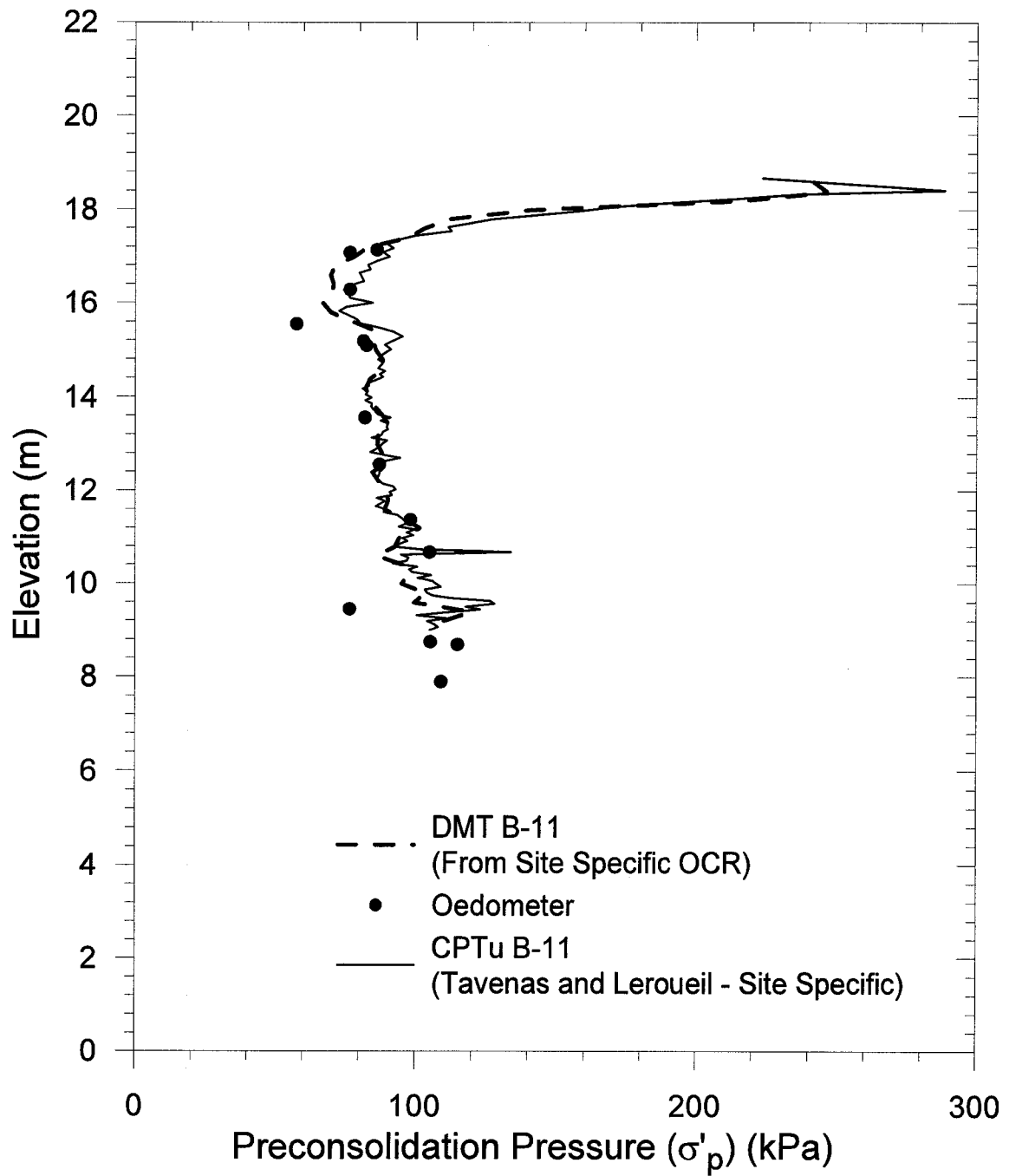


Figure 4.37 - Comparison of Preconsolidation Pressure determined by CPTu B-11, DMT B-11 and Laboratory Data

4.2.8 - Coefficient of Lateral Earth Pressure At-Rest (K_0)

4.2.8.1 - Introduction

The coefficient of lateral earth pressure at-rest (K_0) is the ratio of the effective horizontal stress to the vertical effective stress at a given depth. The estimate of K_0 values within the soft gray silty clay at the RWS test site is also an important factor in modeling the subsurface conditions in the finite element software. Both the dilatometer and the piezocone are capable of providing estimations of K_0 ; however obtaining accurate values is a difficult task. The dilatometer does have an advantage over the piezocone though, as it directly measures the horizontal resistance to load; where the piezometer measures the vertical resistance to load, which is influenced by σ_h (Kulhawy and Mayne, 1990).

Where other soil properties analyzed in this research using both the CPTu and DMT data have readily available baseline values to develop site specific equations, no such baseline exists for K_0 values. Relationships for determining the at-rest lateral earth pressure coefficients of normally consolidated soils using the drained peak friction angle of the soil are available from Jaky (1944) and Brooker and Ireland (1965) among others. Using these relationships a reasonable value for K_0 in normally consolidated clay would be in the range of 0.5 to 0.6.

4.2.8.2 - Interpretation Using the Piezocone

Three ideologies have developed for interpreting K_0 using piezocone data, based either upon measured pore pressure differentials, friction sleeve measurements or tip resistance.

The few relationships for estimating K_o using piezocone pore pressure data are typically suited for piezocones with filter elements in either the u_1 , or both the u_1 and u_2 locations.

Estimates of K_o have been provided based on the difference between the pore pressure at the u_1 and u_2 locations by Sully and Campanella (1991). The difference of these two values, normalized by the effective overburden stress plotted against K_o from other means of testing shows promising results, however it does have a high degree of scatter. Kulhawy and Mayne (1990) have estimated K_o using the normalized excess pore pressure from the u_1 position as well. Neither of these methods however is suitable for this research, as pore pressures were measured at the u_2 location.

Correlations measuring the lateral stress on the friction sleeve have been unsuccessful in correlating this value to the horizontal stress, and no reliable relationships have been created (Jefferies et al., 1987; Campanella et al., 1990; Masood et al., 1990). The friction sleeve measurements are typically quite low, especially in soft clays, and therefore using this value to determine K_o is not as reliable as the tip resistance or pore pressure.

Kulhawy and Mayne (1990) developed a relationship relating the normalized net tip resistance to the K_o as determined from self-boring pressuremeter tests in adjacent boreholes. This formula, as follows, will be used for interpreting K_o from piezocone data at the RWS test site:

$$K_o = 0.1 \cdot \left(\frac{q_t - \sigma_{vo}}{\sigma'_{vo}} \right) \quad [4-33]$$

4.2.8.3 - Interpretation Using the Dilatometer

Marchetti (1980) presented a correlation for K_o in uncemented clays using the DMT which provides a generally satisfactory estimate of the coefficient (Marchetti et al., 2001).

$$K_o = \left(\frac{K_D}{1.5} \right)^{0.47} - 0.6 \quad [4-34]$$

Other researchers (Lacasse and Lunne, 1988; Kulhawy and Mayne, 1990) have reported using slightly modified forms of this equation. The estimate of K_o from DMT data was based on the original equation by Marchetti (1980). The estimates of K_o from both the DMT and CPTu data are presented in Figure 4.38. The piezocone data appears to slightly underestimate K_o between 32 and 40 feet elevation, while the DMT data appears to slightly overestimate the value throughout the entire profile. Because no baseline values are available for this site, no site specific correlations were developed for the CPTu and DMT data.

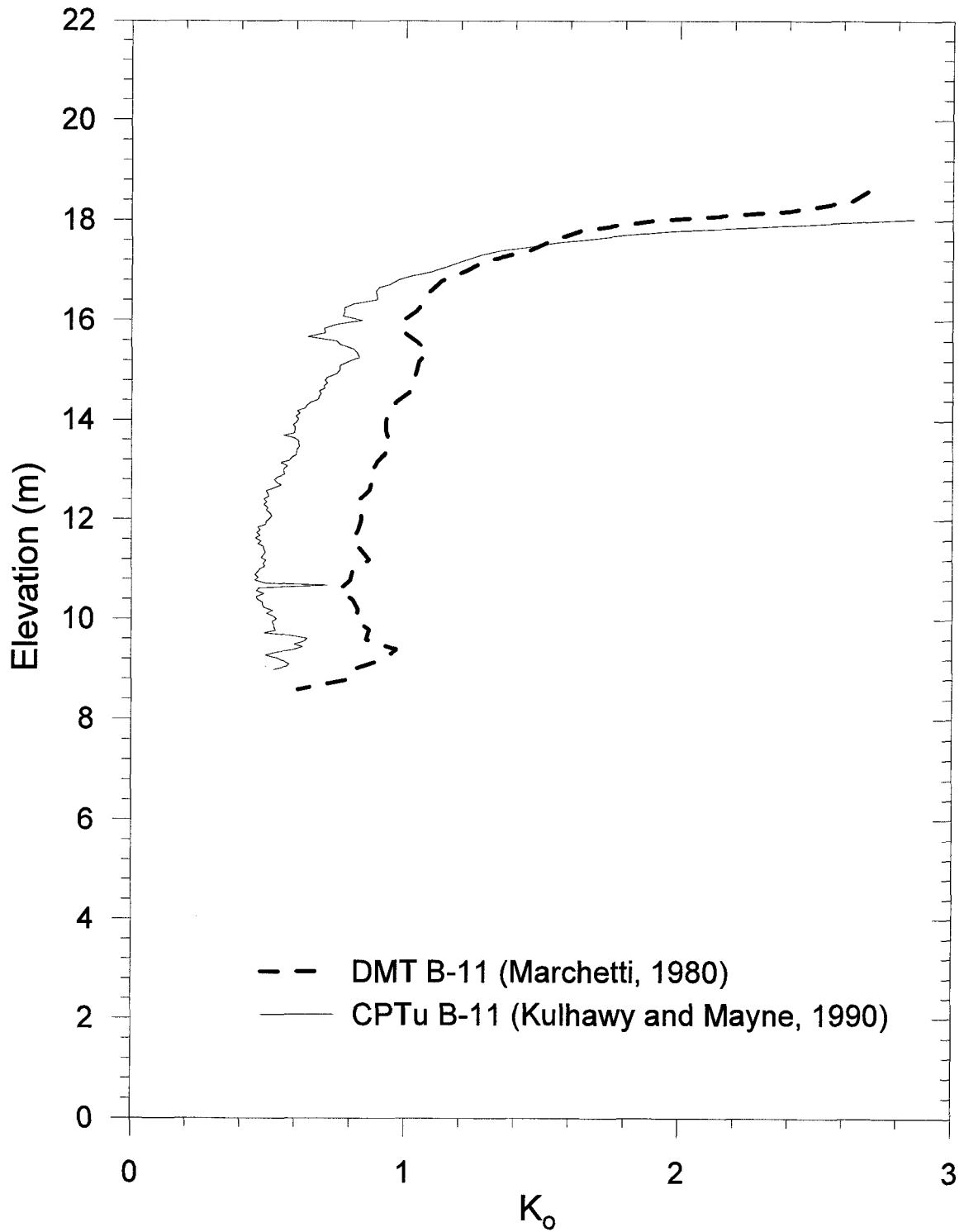


Figure 4.38 - Estimates of K_o based on CPTu and DMT Data at CPTu B-11 and DMT B-11 Respectively

4.2.9 - Coefficient of Horizontal Consolidation (c_h)

An estimate of the horizontal coefficient of consolidation (c_h) can be made in fine grained soils by monitoring the dissipation of excess pore pressures following stoppage of steady piezocone penetration. Torstensson (1975, 1977) provided the initial framework for computing the dissipation of pore pressures using cavity expansion theory and linear uncoupled one-dimensional consolidation theory. Using this model Torstensson suggested that the coefficient is best determined at 50% dissipation of excess pore pressures using the following formula:

$$c = \frac{T_{50}}{t_{50}} \cdot r_o^2 \quad [4-35]$$

Where t_{50} is the measured time for 50% excess pore pressure dissipation, r_o is the penetrometer radius and T_{50} is the time factor found using the theoretical models. The appropriate time factor for this model is dependent on the location of the pore pressure filter element.

Further research conducted by Baligh and Levadoux (1980, 1985, 1986) analyzed the dissipation of pore pressures in normally consolidated Boston Blue Clay using the strain path method to predict the initial pore pressure distribution. Among the findings of the research conducted by Baligh and Levadoux (1985) is that the consolidation taking place past 50% dissipation is primarily secondary compression, and that the dissipation is primarily in the horizontal plane.

Houlsby and Teh (1988) developed a formula to determine the horizontal coefficient of consolidation using a large strain finite element analysis that is similar to the

Baligh and Levadoux derived theory. The Houlsby and Teh method is based on an elastic plastic soil model, and therefore incorporates the rigidity index (I_r) as well. Robertson et. al. (1992) predicted the coefficient of consolidation from multiple piezocone tests using the method of Houlsby and Teh (1988) and found that it provided reasonable estimates of c_h when compared to reference data from field observations and laboratory tests. This research also found that the u_2 filter location provided pore pressure data with considerably less scatter than other filter element locations.

The dissipation tests conducted at the RWS site were interpreted at 50% decay of excess pore pressure using the method of Houlsby and Teh (1988) and the following formula:

$$T^* = \frac{c_h \cdot t}{r^2 \cdot \sqrt{I_r}} \quad [4-36]$$

Where r is the radius of the piezocone, t is the time to 50% decay of excess pore pressure and the modified time factor (T^*) as determined using Terzaghi-Rendulic theory is given in Table 4.4. The rigidity index (I_r) has been taken as 500, which is the value for normally consolidated Boston Blue Clay.

Table 4.4 - Modified Time Factors (T^*) from Houlsby and Teh (1988)

Degree of Consolidation	Location			
	Cone (u_1)	Above Cone Base (u_2)	Five radii above cone base	Ten radii above cone base
20%	0.014	0.038	0.294	0.378
30%	0.032	0.078	0.503	0.662
40%	0.063	0.142	0.756	0.995
50%	0.118	0.245	1.110	1.458
60%	0.226	0.439	1.650	2.139
70%	0.463	0.804	2.430	3.238
80%	1.040	1.600	4.100	5.240

The two piezocone dissipation tests were performed in a borehole adjacent to CPTu B-11 at depths of 3.68 meters and 7.96 meters respectively. Plots of the pore pressure dissipation with time are presented in Figure 4.39 for the first test depth and Figure 4.40 for the second test depth. The results of the two tests, including time to 50% decay of excess pore pressure and estimated horizontal coefficient of consolidation are presented in Table 4.5. At the first test depth a c_h of 0.215 m²/day (2.319 ft²/day) was found using the method of Teh and Houlsby (1988), while at the second deeper test location a c_h of 0.242 m²/day (2.603 ft²/day) was estimated.

Table 4.5 - Results of CPTu Dissipation Tests;
 c_h estimated using method of Teh and Houlsby (1991)

Horizontal Coefficient of Consolidation at CPTu B-11				
$i_p = 500; T^* = 0.245$				
Test	Depth (m)	EI (m)	t_{50} (sec)	c_h (m ² /day)
1	3.68	17.5	2803.5	0.215
2	7.96	13.2	2493.0	0.242

While no estimate of the horizontal coefficient of consolidation is available for the RWS test site for comparison, a similar marine clay deposit in Portsmouth, New Hampshire has been examined by Murray (1995). These analyses used the same rigidity index value of 500; however the dissipation tests were conducted using a Wissa piezocone, with the filter element in the u_1 location. Though much of this data appears to be influenced by silty lenses within the clay stratum, there are two distinct ranges of c_h for locations outside the influence of lenses of $0.182 \text{ m}^2/\text{day}$ ($1.956 \text{ ft}^2/\text{day}$) and $0.057 \text{ m}^2/\text{day}$ ($0.609 \text{ ft}^2/\text{day}$). Though these values are lower than those found at the RWS test site, they provide a good indication that the results are reasonable; with differences accounted for by the filter location and the soil itself.

Further observation of the dissipation test data reveals a small spike in pore pressure within a few seconds after the test has begun. This spike is likely attributed to a minimal increase in downward pressure on the cone tip caused by clamping the drill rods at the surface to prevent slippage as the test is being conducted. This increase highlights the importance of stopping and immediately securing the cone. Should further penetration occur, even to the small degree observed in these tests, the pore pressures may be significantly changed and the test results affected.

Normalized Data - Dissipation Test 1

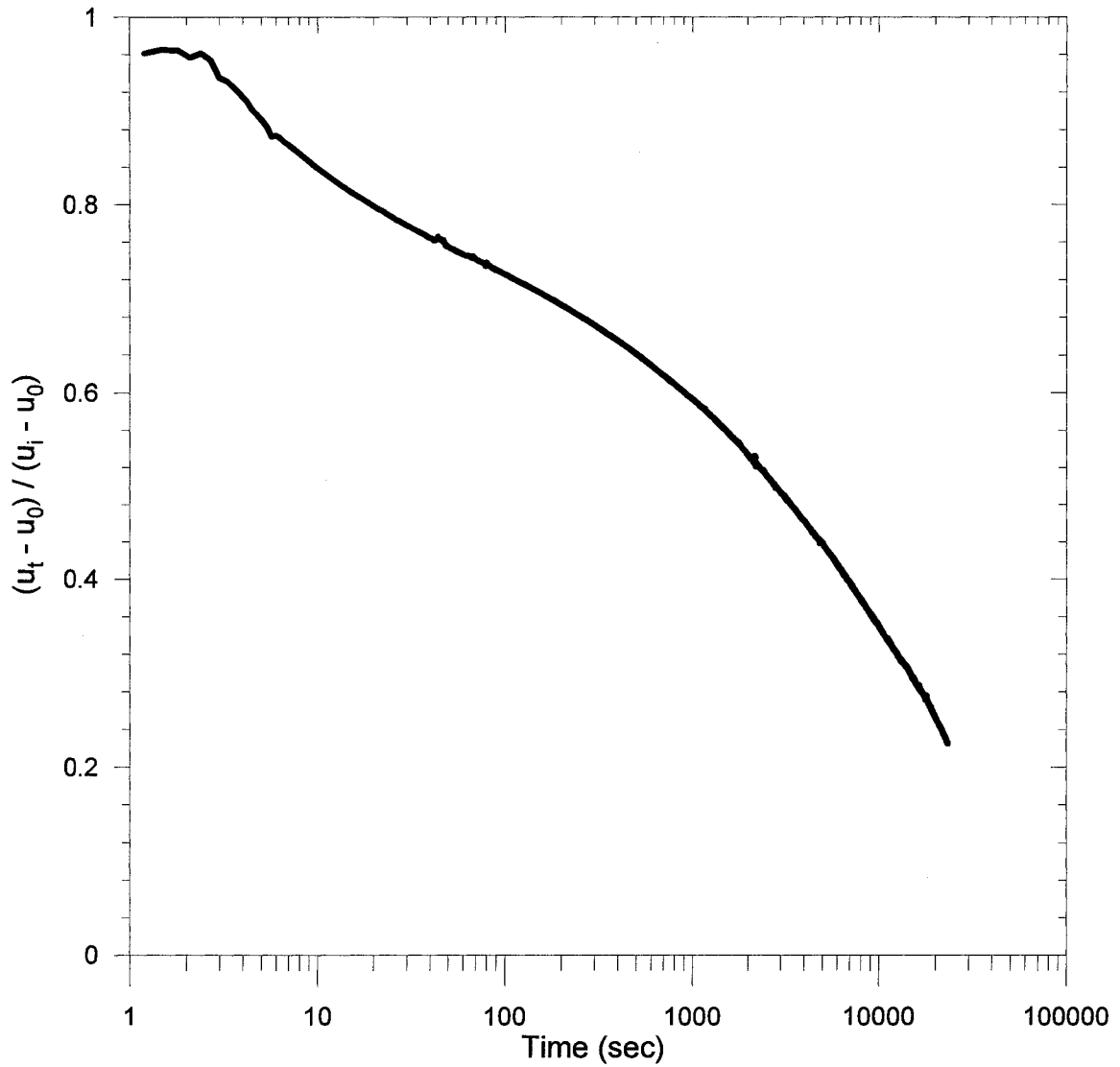


Figure 4.39 – Dissipation of Excess Pore Pressure at 3.68 m (12.07 ft) Depth

Normalized Data - Dissipation Test 2

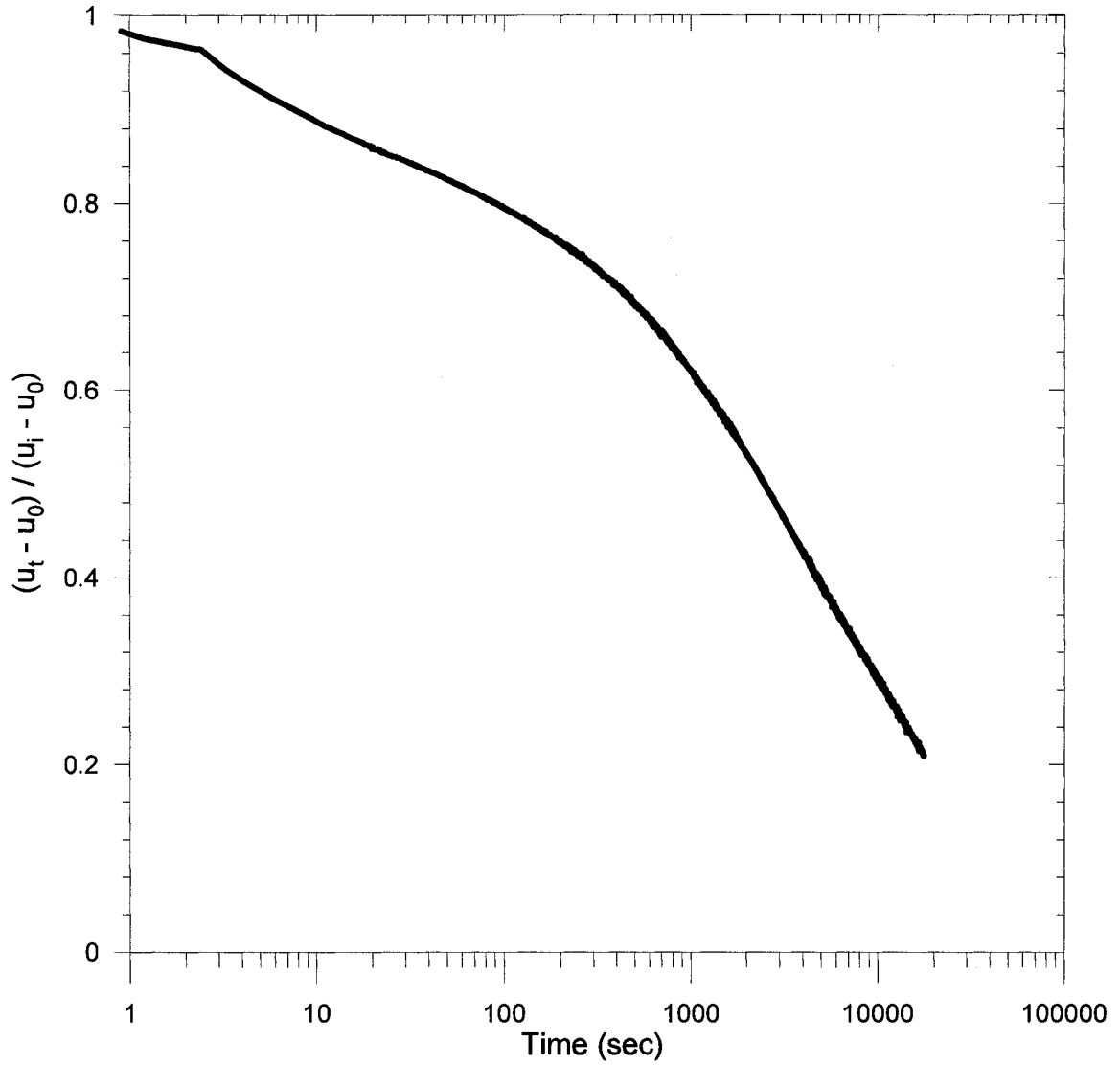


Figure 4.40 - Dissipation of Excess Pore Pressure at 7.96 m (26.11 ft) Depth

CHAPTER V

FINITE ELEMENT MODELING

5.1 - Introduction

For the proposed Phase IV cell, planned to be constructed 15 to 25 years in the future, a computer model of the RWS site was created to determine the strength characteristics of the soft gray silty clay. Finite element computer models of the virgin conditions at the RWS landfill were developed incorporating data from the current field and laboratory testing programs as well as data from previous site investigations. Loading of the landfill was simulated using survey data to approximate actual loading rates and, historical data from site instrumentation in terms of pore pressures and settlement were then compared to initial model outputs. To simulate actual in situ conditions, parameters within the model were adjusted to match the historical data as closely as possible. The completed models allow for a prediction of soil strengths across the site in preparation for the proposed Phase IV "piggy-back" layers. The change in the strength of the gray silty clay stratum at various future dates will aid in the design of Phase IV with regards to when loading may begin, the acceptable rate of waste loading and, geometry of the landfill cells to maintain a minimum factor of safety.

5.2 - Plaxis Finite Element Software

5.2.1 - Introduction

The finite element models of the RWS landfill were created using Plaxis 2D Professional Version, which is a finite element code specifically created for geotechnical applications. The Plaxis software package has four programs, each of which performs a different role in the analysis. The Input program allows users to define the geometry and material properties of a model, and automatically generates the finite element mesh and the initial pore water pressures. Prescribed loads or displacements are then applied in the Calculation program. Finally the post-processing of the Plaxis models is performed using the Output and Curves programs, which allow the user to generate data sets of several model parameters.

The level of functionality, as well as previous modeling experience at UNH using Plaxis were factors in the selection of this software for use at the RWS site. Plaxis incorporates many features which allow for the modeling of complex geotechnical problems, such as the availability of multiple soil behavior models and control over groundwater conditions, including the ability to model steady-state flow when creating models. Additional functionality is added with automatic mesh generation, staged construction inputs and updated Lagrangian analysis, which continually updates mesh geometry during calculation phases to account for large deformations.

The initial modeling of the RWS site was performed using release 8.2.7 of the 2D Professional package. An update, version 8.4, was released in July of 2006 to fix known errors in the previous software codes, and final modeling was performed using this latest release.

5.2.2 - Plaxis Soil Models

5.2.2.1 - Introduction

The Plaxis finite element software package requires that the user define specific regions, called clusters in which the soil properties are similar enough that the cluster can be modeled as a continuum despite the fact that soil is inherently heterogeneous. The degree to which the model replicates the true in situ conditions is then in part limited by the amount of individual clusters that the user creates, which is typically limited by the users knowledge of the material properties for the site in question.

The numerical models used to define the response of the soil clusters due to changes in stress states vary with regard to how closely the model can simulate in situ conditions. Multiple soil models are made available for use in the Plaxis software package, and the user may use multiple soil models throughout the finite element model in order to best fit the in situ conditions. The Mohr-Coulomb Model, the Soft Soil and Soft Soil Creep Models and the Hardening Soil Model are included in the Plaxis software package and are the most commonly used models. Plaxis also allows the user to create a soil model using FORTRAN programming language, and makes select user-defined models available for online downloads. Specific soil models may provide a more rigorous calculation than others, or be better suited to specific soil types and loading conditions. The material properties required for each soil model vary, and therefore the user must also determine if the soil model can be used with the available laboratory or field data.

Certain material properties are common to all of the soil models, and are defined using the same input as the model specific properties. These common material properties include the wet and saturated unit weights, the horizontal and vertical permeability, the overconsolidation ratio, and the at-rest lateral earth pressure coefficient. In addition the user must designate that the material behaves as a drained or undrained material.

5.2.2.2 - The Soft Soil Model (SSM)

The soft soil model was selected to model the behavior of both the stiff weathered clay crust as well as the soft silty clay at the RWS site. This model is well suited for modeling primary compression during embankment loading of near normally-consolidated clayey soils. It combines both the traditional Cam-Clay and Mohr-Coulomb type models to define the behavior of the soil. An advantage of the SS model when compared to the more advanced soil models available is that the model uses material properties which are available from common laboratory tests and the in situ test methods already performed at the RWS site.

The material properties required for the Soft Soil model are:

λ^*	Modified Compression Index	[-]
κ^*	Modified Swelling Index	[-]
c	Cohesion	[kN/m ² or psf]
ϕ	Friction Angle	[°]
ψ	Dilatancy Angle	[°]

The compression and swelling indices are modified versions of the Cam-Clay parameters λ and κ as they are defined by the volumetric strain (ϵ_v) as opposed to the void ratio (e). The modified indices were obtained by one-dimensional consolidation tests performed on undisturbed samples recovered from the RWS site, The relationships presented in Equations 5.1 and 5.2 display the relationship between the values of C_c and C_r obtained the laboratory tests and the values of λ^* and κ^* .

$$\lambda^* = \frac{C_c}{2.3(1+e_0)} \quad [5-1]$$

$$\kappa^* = \frac{2C_r}{2.3(1+e_0)} \quad [5-2]$$

Plaxis requires a value greater than zero to be input for the friction angle and for the cohesion in order to properly complete the calculation phases. At the RWS site the friction angle of the clays was input as 5 degrees to fulfill this requirement. The value of 5 degrees was chosen to ensure that the friction angle was large enough to avoid calculation errors, while remaining relatively small such that excessive additional strength was not added to the soil. The soils typically modeled by the SS model would have a dilatancy angle of zero, and therefore the software can accept a value of zero when required.

The response of the soil due to changes in stress in the SS model is handled using the assumption that a logarithmic relationship exists between the volumetric strain (ϵ_v) and the mean effective stress (p') as shown in Figure 5.1. This relationship is

expressed in Equation 5.3 for virgin compression and in Equation 5.4 for unloading and reloading.

$$\varepsilon_v - \varepsilon_v^0 = -\lambda^* \ln\left(\frac{p'}{p^0}\right) \quad [5-3]$$

$$\varepsilon_v^e - \varepsilon_v^{e0} = -\kappa^* \ln\left(\frac{p'}{p^0}\right) \quad [5-4]$$

Where p' is the current mean effective stress and p^0 is the initial mean effective stress. The mean effective stress is often used to describe the stress state in numerical modeling and is based on the three principal effective stresses, σ_1 , σ_2 and σ_3 . The mean effective stress is defined in Equation 5.5.

$$p' = \frac{1}{3}(\sigma'_1 + \sigma'_2 + \sigma'_3) \quad [5-5]$$

In addition to the mean effective stress, the equivalent shear stress, q is used to define the stress state. In conditions where $\sigma'_2 = \sigma'_3$, the value of q can be expressed as:

$$q = |\sigma'_1 - \sigma'_2| \quad [5-6]$$

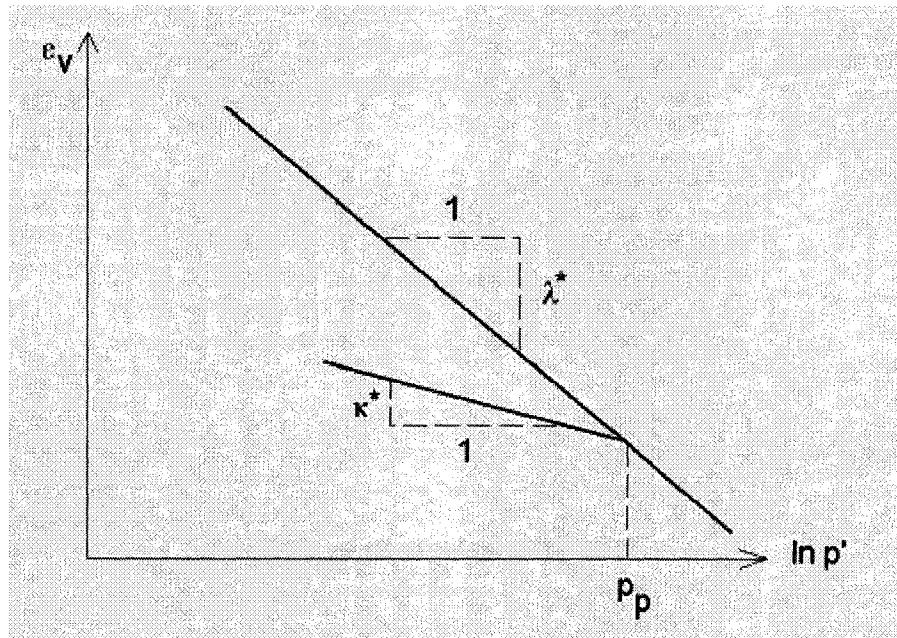


Figure 5.1- Logarithmic Relationship between Volumetric Strain and Mean Effective Stress (Plaxis Material Models Manual)

The yield function used in the SS model describes the boundary of the region in which elastic strains occur. Plastic strains, which are irreversible, occur due to changes in stress outside of this region. The SS model assumes that the soil response during unloading and reloading is completely elastic, and that plastic strains only develop once the stresses during primary compression reach the yield surface.

In the case where $\sigma'_2 = \sigma'_3$ Plaxis describes the yield function (f) using Equation 5.7.

$$f = \bar{f} - p_p \quad [5-7]$$

Where \bar{f} is a function of p' and q , and p_p is the preconsolidation pressure, which is a function of the plastic strain. These values are expressed using Equations 5.8 and 5.9

$$\bar{f} = \frac{q^2}{M^2(p' + c \cot \phi)} + p' \quad [5-8]$$

$$p_p = p_p^0 \exp\left(\frac{-\varepsilon_v^p}{\lambda^* - \kappa^*}\right) \quad [5-9]$$

The yield function in the Soft Soil model creates an ellipse, as seen in Figure 5.2 in when plotted on the p', q plane, and forms the cap of the yield contours. This cap increases during primary compression. The peak of the ellipse is located on a line in the p', q plane which has a slope of M . The parameter M is found in Equation 5.8, and is a function of the user defined value of K_0 . The line which has the slope of M in p', q space is referred to as the critical state line (CSL) in the Cam-Clay model. The CSL defines the stresses within a particular soil at failure. In the soft soil model the critical state line does not indicate failure of the soil; instead the failure state is defined by the Mohr-Coulomb failure envelope. The Mohr-Coulomb failure envelope is a function of the soils friction angle and cohesion. The slope of the CSL is greater than or equal to the angle of the Mohr-Coulomb failure envelope; therefore the failure state is reached before stresses within the soil reach the CSL.

The threshold ellipse defined in Figure 5.2, defines a minimum value of $c \cot \phi$ to ensure that the cap of the yield contours exists only in compression ($p' > 0$).

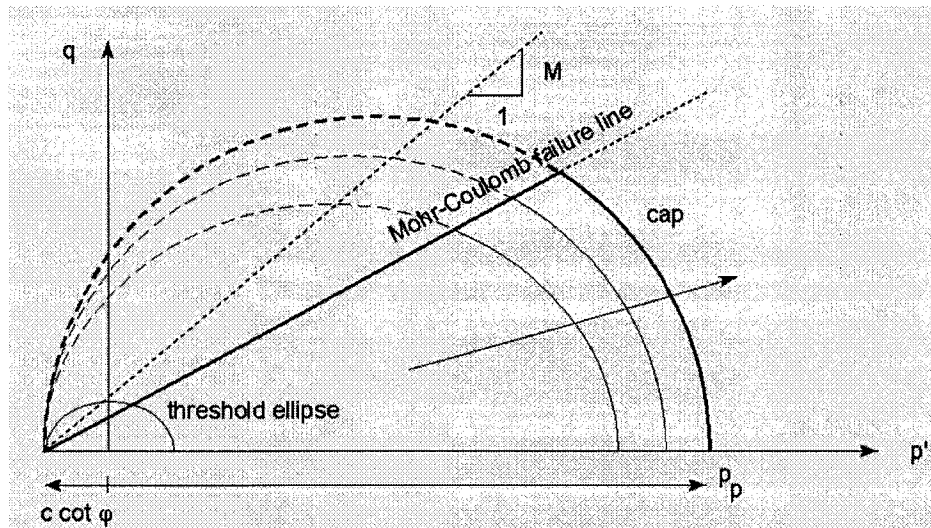


Figure 5.2 - Schematic of Soft Soil Model Yield Function (Plaxis, 2002)

In the principal effective stress space the SS model yield contour is expressed using a combination of three Mohr-Coulomb functions and three yield functions, as shown in Figure 5.3. The three dimensional object defined by these functions encompasses all of the stress states which may exist for a particular soil. Combinations of the principal effective stresses which fall along the boundary of this object occur when the soil is at failure, while stress states outside of the bounds of this object are not possible.

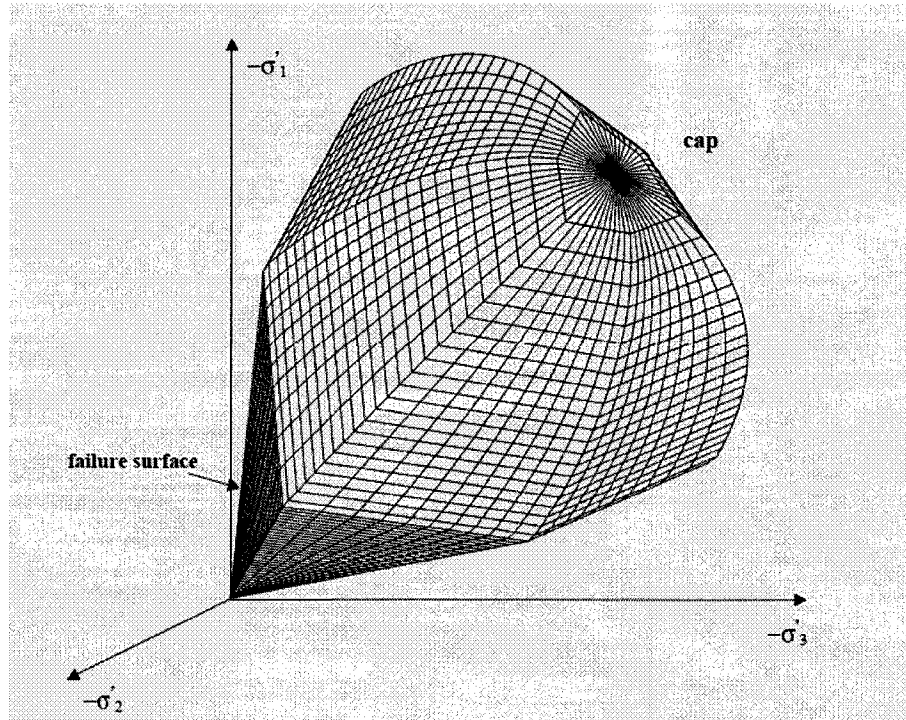


Figure 5.3 - Soft Soil Model Yield Contour in Principal Effective Stress Space (Plaxis, 2002)

5.2.2.3 - The Mohr-Coulomb Model (MC Model)

The Mohr-Coulomb model was used to model the ash, the drainage sand, the glacial sands and the glacial till in the finite element model of the RWS site. The Mohr-Coulomb model is the least rigorous soil model available in the Plaxis software package; however these materials do not require an advanced soil model in this analysis. The Mohr-Coulomb model describes elastic perfectly-plastic behavior in the material, which is accounted for using five parameters. An example of elastic perfectly-plastic behavior is displayed in Figure 5.4.

E	Young's Modulus	[kN/m ² or psf]
v	Poisson's Ratio	[-]
c	Cohesion	[kN/m ² or psf]

φ	Friction Angle	[°]
ψ	Dilatancy Angle	[°]

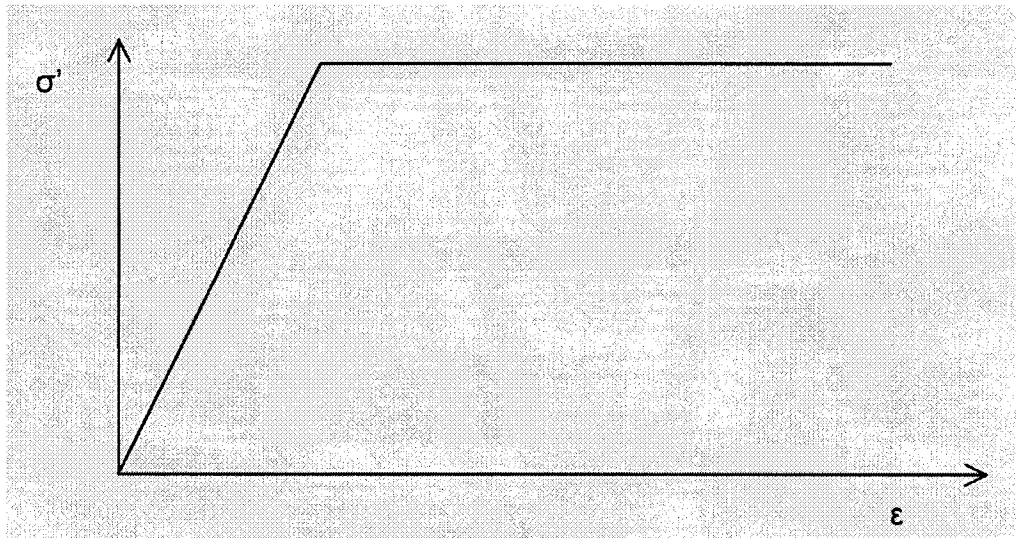


Figure 5.4 - Elastic Perfectly Plastic Behavior

The Young's modulus and the Poisson's ratio govern the material behavior within the yield surface, during which the material acts as a linear elastic material. The remaining three material properties govern the plastic behavior of the soil. The friction angle and the cohesion value also govern the Mohr-Coulomb failure envelope as depicted in Figure 5.5.

The material properties of the MC model are used in six yield functions and six plastic potential functions to describe the soils behavior with a change in stress. Figure 5.6 displays the Mohr-Coulomb yield envelope, which is a hexagonal cone when the cohesion is equal to zero. Stress states within this cone behave elastically, and as the stresses extend past the boundary, the failure state has been reached and the soil behaves plastically.

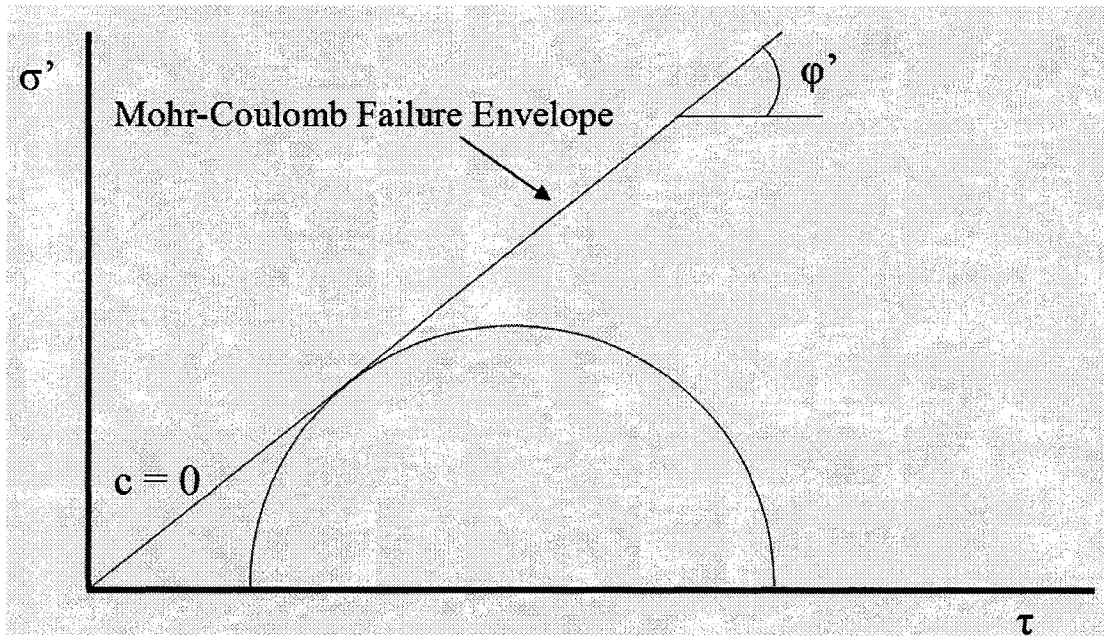


Figure 5.5 - Mohr-Coulomb Failure Envelope

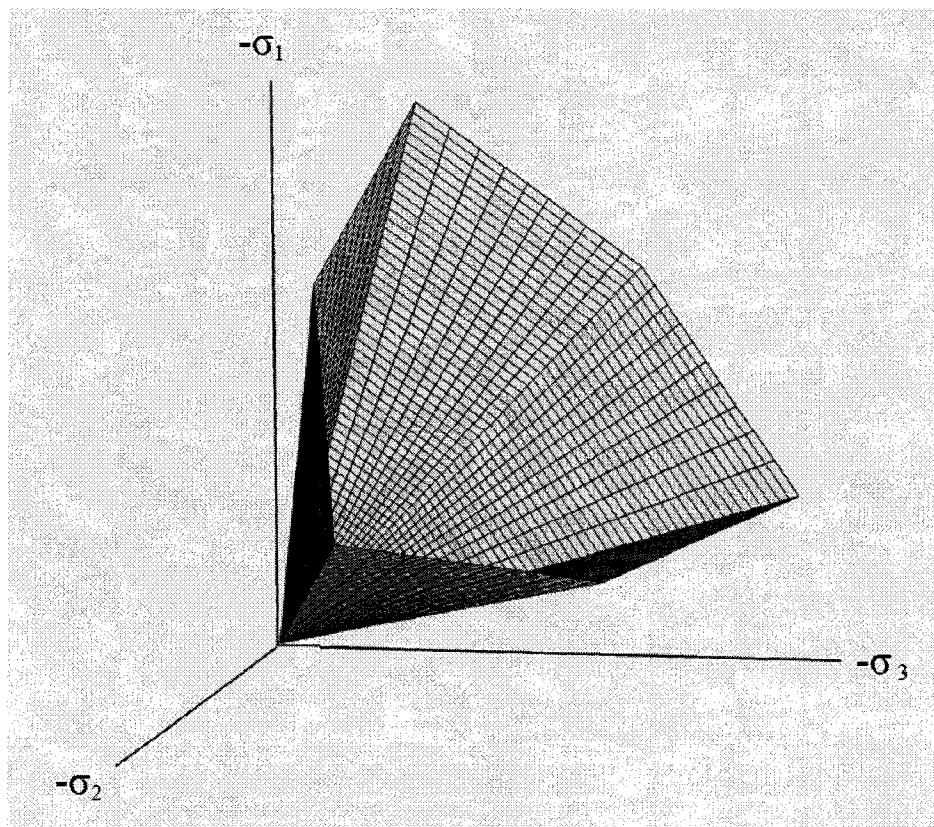


Figure 5.6 - Mohr-Coulomb Yield Envelope

5.3 - Finite Element Model

5.3.1 - Introduction

The RWS site was modeled using two profiles, one running across the site in a North/South direction and the other in an East/West direction as shown in Figure 5.7. The two profiles capture a larger portion of this site, which will provide multiple locations to be analyzed for strength changes with time. The predominant direction of horizontal displacement and zones of apparent shear softening are captured in the East/West profile as well.

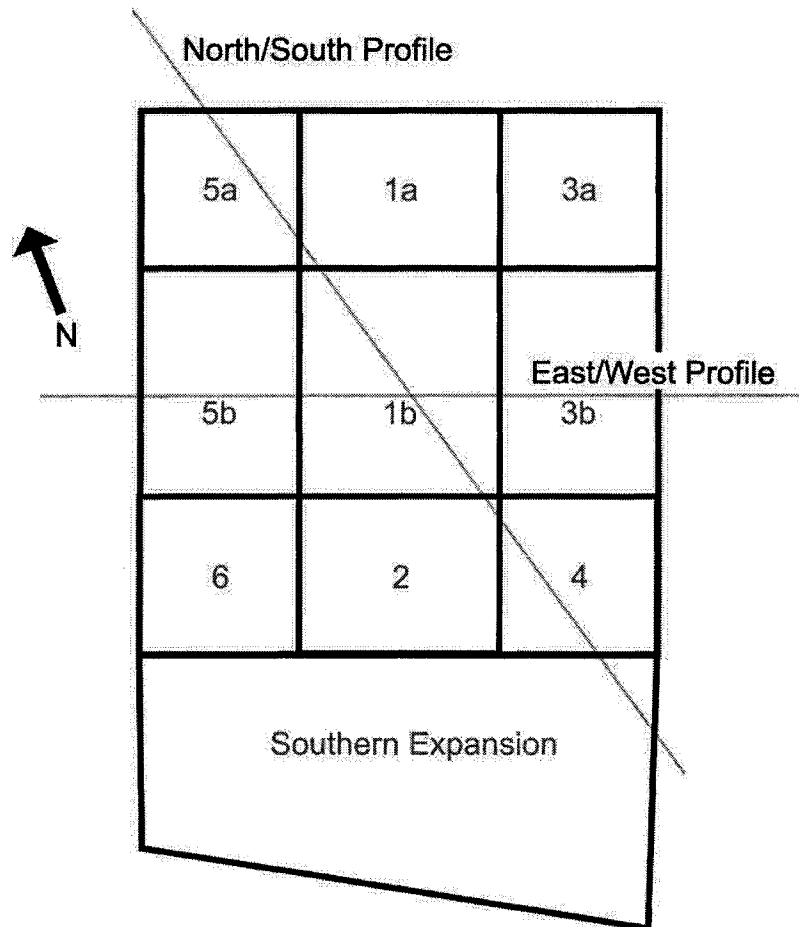


Figure 5.7 - RWS Landfill Schematic

The plane strain model was used in each of the profiles at the RWS site. In a plane strain problem, the geometry and loading conditions in the perpendicular plane (z-axis) to the cross-sectional profile must be fairly uniform and extend for a large distance.

The RWS profiles were modeled using 15-Node triangular elements. A 15-Node element provides a fourth order analysis of displacement due to the increased number of nodes when compared to the 6-Node triangular elements which are available as well. This results in a more accurate model with regards to displacements and stresses. A diagram of the node positions for a 15-Node element is presented in Figure 5.8.

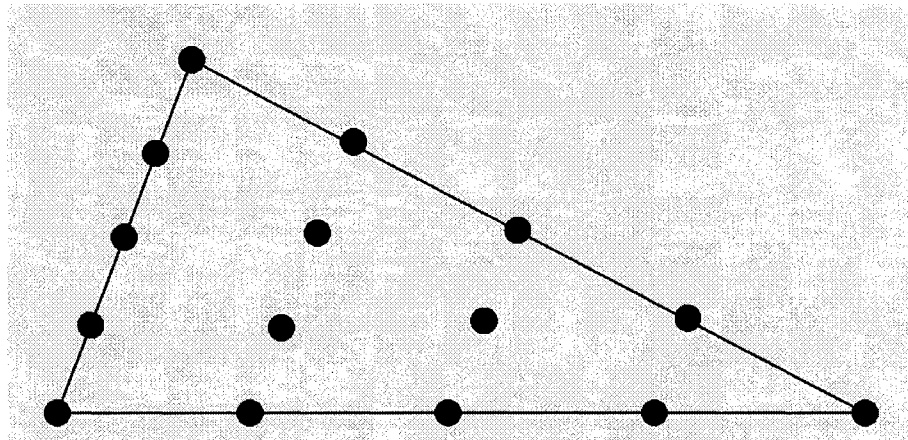


Figure 5.8 - 15-Node Triangular Element

5.3.2 - Model Geometry

The geometry of the Plaxis models was based upon data from boring logs available in site design reports (E.C. Jordan, Co., 1985; Rabasca, 1995) as well as the logs from the 2006 in situ testing program. Features identified in these logs include the original ground surface elevation, the elevation at which transitions in material type occur and in some log the elevation of the surface of the upper groundwater unit.

Linear interpolations of these elevations between the boring locations were then made to create a basic model.

To further refine the model geometry, the soft gray silty clay was divided into multiple sub-layers based on the undrained shear strength of the soil. This allows for a more accurate model, as the material properties are averaged within thin layers. In both East/West and North/South models the undrained shear strength profiles appear to vary slightly from one side of the model to the other. For the East/West model a division was made through the soft gray silty clay at the center of the site, allowing each side to be discretized more thoroughly. The surface of the bedrock slopes upwards towards the North at the RWS site, and in situ tests indicate that in the North where the bedrock is shallowest the strength of the soft gray silty clay is greater than that at equivalent depths in the rest of the profile. Therefore the North/South model was divided into a Northern section, and a section covering the Southern and central portion of the profile. Figure 5.9 displays the East/West profile created in Plaxis. High resolution versions of this figure, as well as the North/South profile are available on the accompanying CD as Figures D.1 and D.2 to allow for a detailed view of the model geometry.

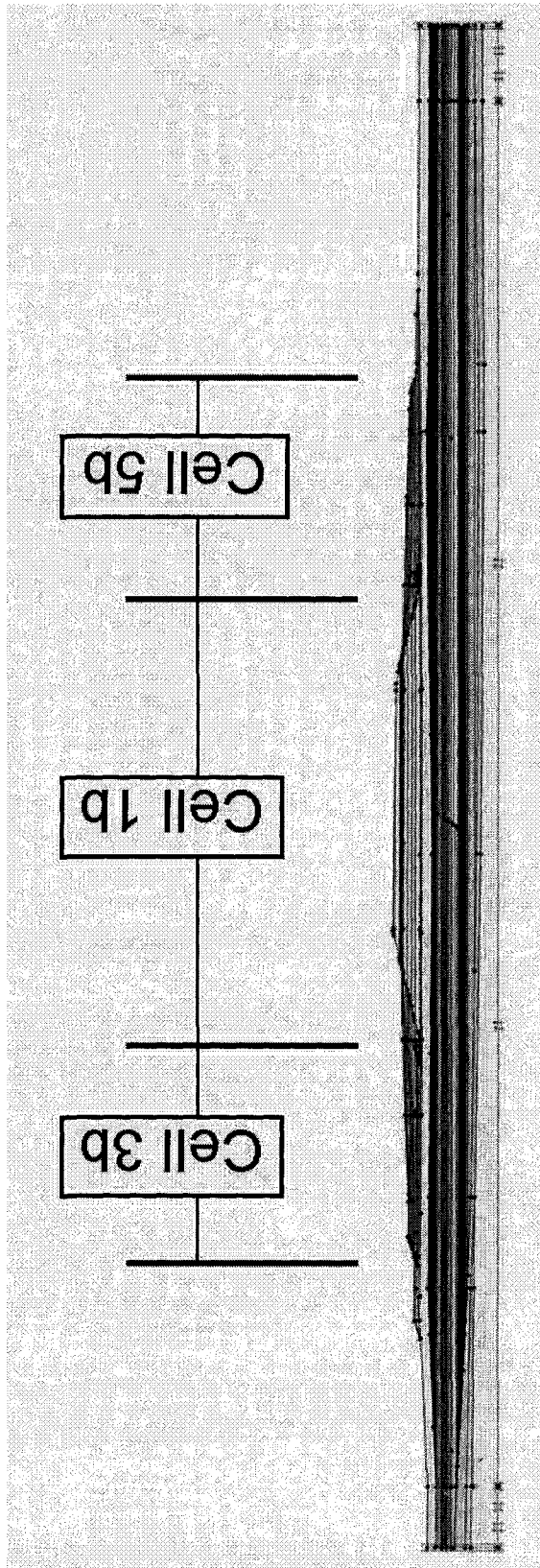


Figure 5.9 – East/West Plaxis Profile

During the construction of the landfill a layer of drainage sand, approximately 0.6 meters (2 ft), thick was placed at the surface of the stiff brown weathered clay. This layer was also placed in the models, in order to provide a drainage path for vertical flow of groundwater from the clay.

In order to replicate the actual conditions of the site within the model, boundary conditions were assigned in the form of fixities. A fixity assigns a prescribed displacement of zero to a geometry line in the Plaxis model. The bottom plane in the model runs horizontally through bedrock and both horizontal and vertical fixities ($u_x=u_y=0$) were assigned to this plane, as it is assumed that no displacements occur within the bedrock. Horizontal fixities ($u_x=0$) were assigned to the vertical planes along the sides of the model, as it was assumed that the conditions on each side of the plane are the same, and therefore no horizontal displacement should occur. This assumption required that the edges of the RWS models extend a sufficient distance from the landfill so as to not be affected by any loading. The default boundary condition for groundwater flow in Plaxis assigns a value of zero to the excess pore pressures at the edges of the model, which once again requires the edges of the model to extend sufficiently far past the landfill.

Plaxis automatically generates the finite element mesh based on the global coarseness selected by the user. Five degrees of coarseness are available, ranging from very coarse to very fine. The element sizes in the mesh are a function of the global coarseness and the overall dimensions of the model. A very fine mesh will provide a greater number of nodes and result in a more accurate calculation than a very coarse mesh, however the very fine mesh requires a greater calculation time.

For the RWS profiles a medium mesh was used to reduce the calculation time while still providing a high degree of accuracy. A complete analysis of either profile using the medium mesh required less than 50 minutes to perform, increasing to over 2 hours when using a very fine mesh. The East/West and North/South profile meshes are presented in Figures 5.10 and 5.11, and are found in the CD which accompanies the text.

5.3.3 - Material Properties

As discussed in Section 5.3.2 the soft gray silty clay was divided into multiple layers, each based on undrained shear strength. Figures 5.12 and 5.13 present the undrained shear strength used in each model along with reference uncorrected field vane strength values for the East/West and North/South profiles respectively. The soil properties in each layer were then finalized within the range of reported values during the model validation.

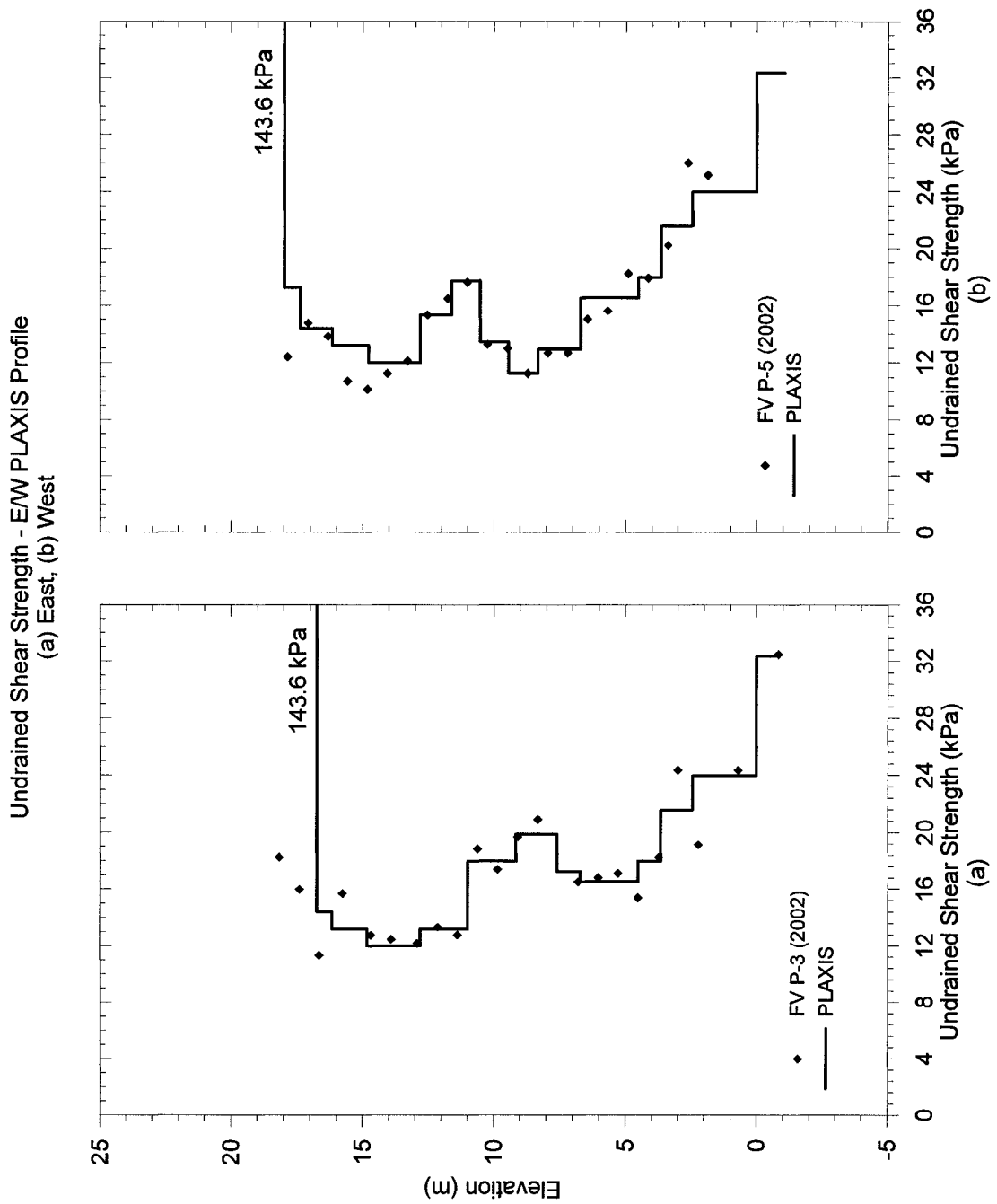


Figure 5.12 - Undrained Shear Strength Profiles for Modeling, East/West Profile

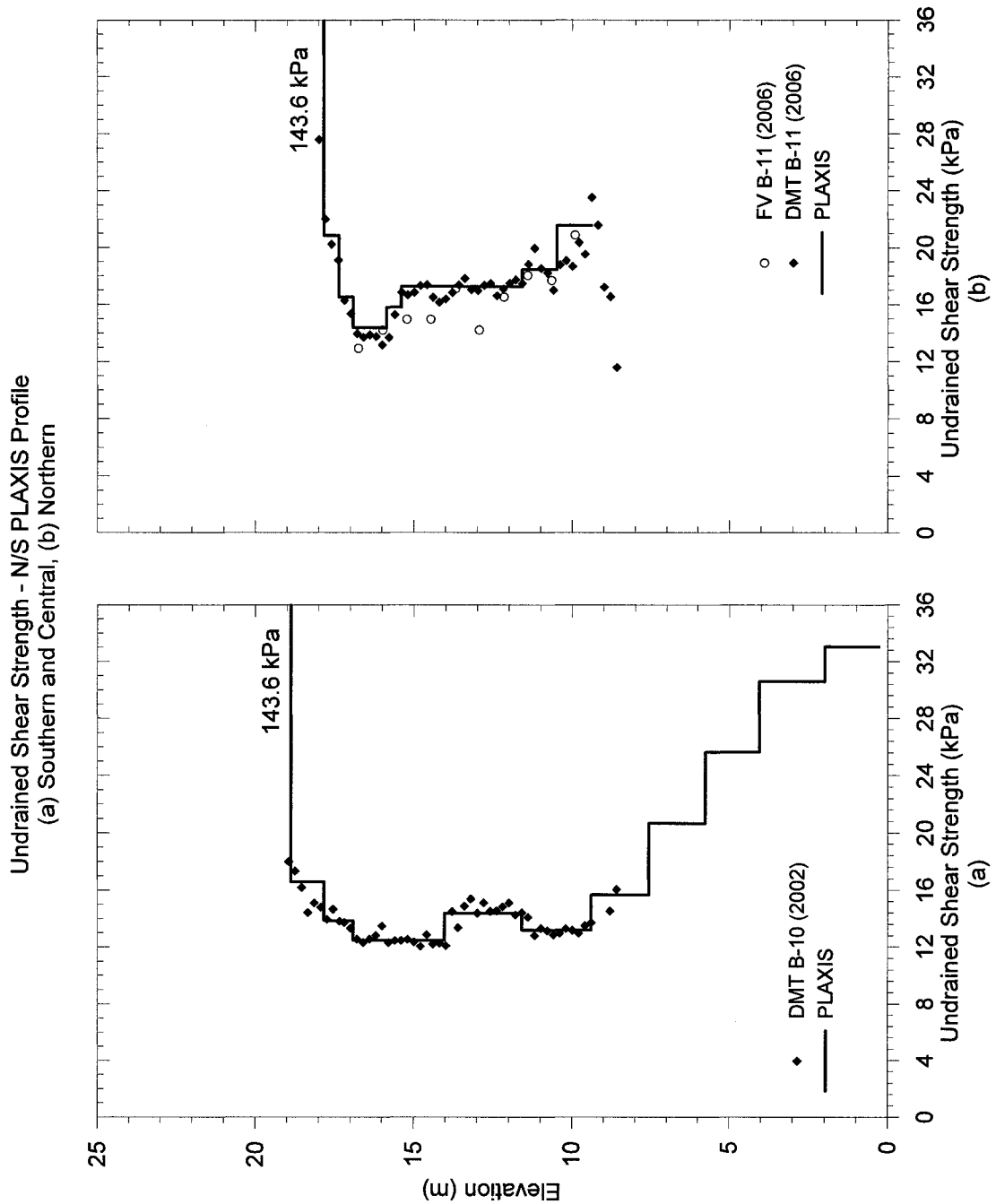


Figure 5.13 - Undrained Shear Strength Profiles for Modeling, North/South Profile

The initial void ratio and the overconsolidation ratio were not adjusted in the validation stages as these values are fairly well defined through one dimensional consolidation laboratory tests and cone penetration tests. The overconsolidation

ratio used in the East/West profile is presented in Figure 5.14, while the values used in the North/South profile are presented in Figure 5.15. A complete summary of the layers used in the Plaxis models and the material properties for each layer is presented in Appendix D.

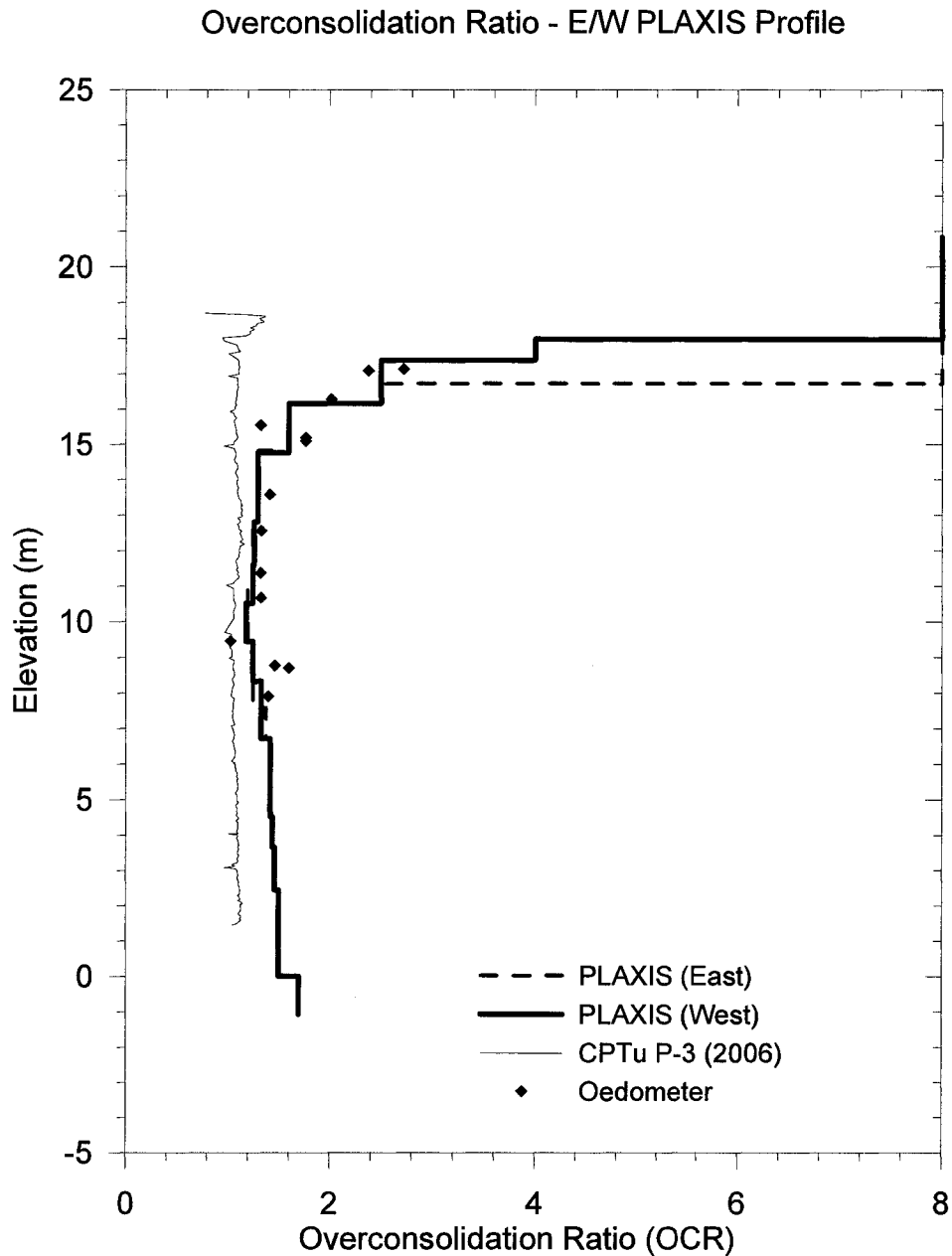


Figure 5.14 - Overconsolidation Ratio Profile for Modeling, East/West Profile

Overconsolidation Ratio - N/S PLAXIS Profile

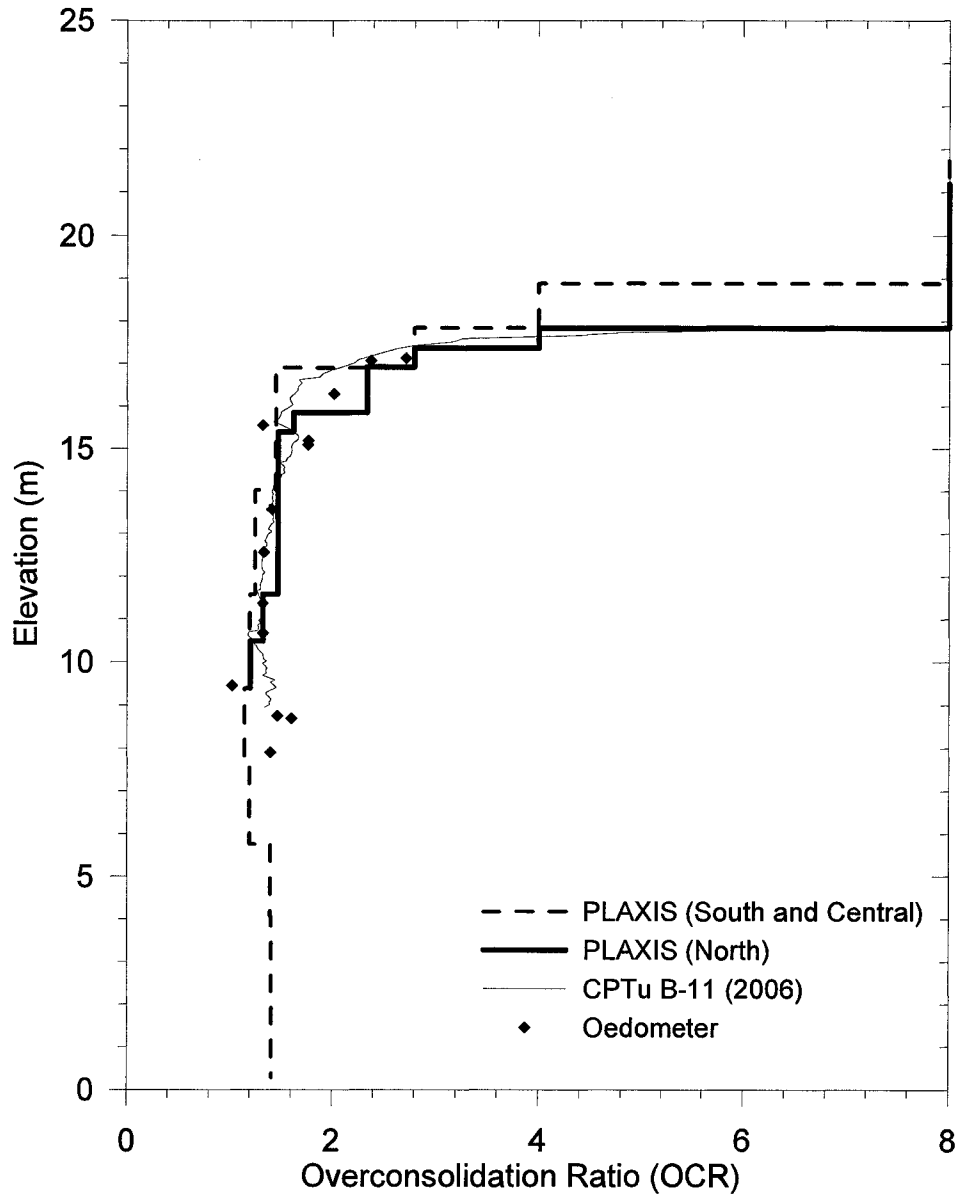


Figure 5.15 - Overconsolidation Ratio Profile for Modeling, North/South Profile

The permeability and the elastic properties of the ash at the RWS site were estimated using the assumption that the material behaved similar to poorly graded silty sand based on results of grain size analyses and Atterberg limits tests of municipal solid-waste incinerator fly ash as reported by Goh and Tay (1993) and

Poran and Ahtchi-Ali (1989). Goh and Tay (1993) report that direct shear tests performed on unsaturated incinerator fly ash compacted to maximum dry density indicate a drained friction angle of 43 degrees and no apparent cohesion, while Poran and Ahtchi (1989) report a friction angle of 45 degrees with an apparent cohesion of 65 kPa based on UU triaxial tests. Based on these results the value of the friction angle and cohesive strength were selected for the RWS site. The unit weight of the ash is the most important property however, as this value will determine the amount that the soft gray silty clay is loaded. The compacted ash unit weight has been determined based upon survey data and the weight of ash hauled to the RWS site, and is presented on a cell by cell basis in Table 5.1.

Table 5.1 - Compacted Ash Unit Weight by Cell

Cell	Ash Unit Weight	
	kN/m ³	pcf
1a	11.8	75
1b	16.7	125
2 Upper	16.5	104.9
2 Lower	18.4	117.2
3b	17.2	109.6
4	15.2	96.8
5a	16.1	102.7
5b	17.3	110

5.3.4 - Initial Conditions

The initial conditions must be input into the Plaxis model after the model geometry is defined, material properties assigned to clusters and a mesh is generated. Material clusters which represent the waste in the landfill were inactivated as this material does not exist at the beginning of the calculation phases. The initial vertical

overburden stresses were then generated using the Calculation program in the Plaxis software package.

The two groundwater units at the site were then defined in the model. The upper unit, encountered within the stiff brown weathered clay, was manually input into the model using a line to define the phreatic level, which varied between 0.15 and 1 meter below the ground surface. The second groundwater unit was assigned as a total piezometric head to the boundary between the glacial sands and the soft gray silty clay. The piezometric head at this boundary was interpolated from the equipotential lines of vertical groundwater flow nets created by E.C. Jordan Co. for initial design at the RWS facility. The pore water pressures were then generated by the Plaxis software based on the piezometric head as defined by these two input sources.

5.3.5 - Model Calculation Phases

The Calculation program is used to define the loading phases of the landfill once the Input program had been completed. Each phase requires the user to define the calculation type, and the manner of loading input. Two calculation types were used for the RWS models: a Plastic analysis for the first stage and Consolidation analysis for all subsequent phases.

A Plastic analysis performs an elasto-plastic deformation calculation and does not consider the effect of the decay of excess pore pressures. The consolidation analysis allows the model to generate pore pressures with loading, and models the decay of excess pore pressures with time. This type of analysis was used for the construction of the landfill in phases after the initial phase, as the consolidation

behavior of the clays at the RWS facility was an important factor to consider when determining the future soil properties. The option to update the mesh and the water pressure during calculation phases was selected during the Consolidation analyses. Updating the mesh and water pressures during calculation phases accounts for changes in the mesh geometry or phreatic levels due to large deformations which lead to computational difficulties.

Unlike the initial pore pressures, which were generated in the Input program, the initial vertical overburden stresses were generated by gravity loading during the first calculation phase. To generate the vertical overburden stresses the weight of the soil is applied to the model by using a Plastic calculation during which undrained behavior is ignored. Displacements occur during the gravity loading phase which must be reset to zero in the first phase to follow the procedure. The beginning of this second calculation phase represents the initial unloaded conditions at the site.

The landfill was constructed in the Calculation program by activating ash layers and using an updated Consolidation analysis with a staged construction loading input. Activating a layer applies the self weight of the material to the model, and the staged construction input allows the load to be incrementally activated over a user defined time period. The loading rate of the landfill, which was determined by periodic surveys of the RWS site, was matched by activating ash layers at specific times. The stage construction input was also used in phases where no additional loads were activated to simulate the decay of excess pore pressures with time.

The calculation phases for the East/West and North/South models are summarized in Tables 5.2 and 5.3 respectively.

Table 5.2 - East/West Profile Calculation Phases

Phase	Clusters Activated	Calculation Type	Load Input	Length (Days)	Start Date
1	Gravity Loading	Plastic	Total Multipliers	-	-
2	Cell 1b, Layer 1	Consolidation	Staged	214	6/1/1988
3	No Additional Loading	Consolidation	Staged	211	1/2/1989
4	Cell 1b, Layer 2	Consolidation	Staged	286	8/2/1989
5	Berm at SPL 5	Consolidation	Staged	261	5/16/1990
6	Cell 1b, Layer 3	Consolidation	Staged	241	2/2/1991
7	No Additional Loading	Consolidation	Staged	243	10/2/1991
8	Cell 1b, Layer 4	Consolidation	Staged	238	6/2/1992
9	No Additional Loading	Consolidation	Staged	119	1/27/1993
10	Cell 1b, Layer 5	Consolidation	Staged	26	5/27/1993
11	No Additional Loading	Consolidation	Staged	284	6/22/1993
12	Berm at SPL 6	Consolidation	Staged	29	4/3/1994
13	No Additional Loading	Consolidation	Staged	117	5/3/1994
14	Cell 3b, Layer 1	Consolidation	Staged	425	8/28/1994
15	Cell 1b, Layer 6; Cell 3b, Layer 2; Cell 5b, Layer 1	Consolidation	Staged	230	10/29/1995
16	Cell 1b, Layer 7; Cell 3b, Layer 3; Cell 5b, Layer 2	Consolidation	Staged	517	6/17/1996
17	Cell 1b, Layer 8; Cell 3b, Layer 4; Cell 5b, Layer 3	Consolidation	Staged	326	5/1/1997
18	Cell 3b, Layer 5; Cell 5b, Layer 4	Consolidation	Staged	310	6/18/1999
19	Cell 1b, Layer 9; Cell 3b, Layer 6; Cell 5b, Layer 5	Consolidation	Staged	418	10/7/1999
20	Cell 1b, Layer 10; Cell 3b, Layer 7; Cell 5b, Layer 6	Consolidation	Staged	266	11/30/2000
21	Cell 3b, Layer 8; Cell 5b, Layers 7 and 8	Consolidation	Staged	282	7/6/2001
22	Cell 3b, Layers 9 and 10; Cell 5b, Layer 9	Consolidation	Staged	545	4/16/2002
23	Cell 1b, Layer 11; Cell 3b, Layer 11; Cell 5b, Layer 10	Consolidation	Staged	175	10/14/2003
24	Cell 1b, Layer 12; Cell 3b, Layers 12 and 13; Cell 5b, Layer 11	Consolidation	Staged	542	4/7/2004
25	No Additional Loading	Consolidation	Staged	105	10/3/2005
26	No Additional Loading	Consolidation	Staged	5098	1/17/2006
27	No Additional Loading	Consolidation	Staged	1826	1/3/2020
28	No Additional Loading	Consolidation	Staged	1826	1/2/2025

Table 5.3 - North/South Profile Calculation Phases

Phase	Clusters Activated	Calculation Type	Load Input	Length (Days)	Start Date
1	Gravity Loading	Plastic	Total Multipliers	-	-
2	Cell 1b, Layer 1	Consolidation	Staged	214	6/1/1988
3	No Additional Loading	Consolidation	Staged	211	1/2/1989
4	Cell 1b, Layer 2	Consolidation	Staged	286	8/2/1989
5	No Additional Loading	Consolidation	Staged	261	5/16/1990
6	Cell 1b, Layer 3	Consolidation	Staged	241	2/2/1991
7	No Additional Loading	Consolidation	Staged	243	10/2/1991
8	Cell 1b, Layer 4	Consolidation	Staged	238	6/2/1992
9	No Additional Loading	Consolidation	Staged	119	1/27/1993
10	Cell 1b, Layer 5	Consolidation	Staged	26	5/27/1993
11	Cell 2, Layer 1	Consolidation	Staged	79	6/24/1993
12	No Additional Loading	Consolidation	Staged	40	9/12/1993
13	Cell 2, Layer 2	Consolidation	Staged	106	10/23/1993
14	Cell 1b, Layer 6; Cell 2, Layer 3	Consolidation	Staged	168	2/7/1994
15	Cell 2, Layer 4	Consolidation	Staged	189	7/27/1994
16	Cell 2, Layer 5	Consolidation	Staged	279	2/2/1995
17	Cell 1b, Layer 7	Consolidation	Staged	233	11/9/1995
18	Cell 2, Layer 6	Consolidation	Staged	133	6/30/1996
19	No Additional Loading	Consolidation	Staged	263	11/11/1996
20	Cell 4, Layer 1	Consolidation	Staged	355	8/2/1997
21	Cell 4, Layer 2	Consolidation	Staged	355	7/24/1998
22	No Additional Loading	Consolidation	Staged	355	7/15/1999
23	Cell 5a, Layer 1	Consolidation	Staged	234	7/5/2000
24	Cell 5a Layer 2; Cell 4, Layer 3	Consolidation	Staged	235	2/25/2001
25	Cell 5a Layer 3	Consolidation	Staged	202	10/19/2001
26	Cell 5a, Layer 4; Cell 4, Layer 4	Consolidation	Staged	267	5/10/2002
27	Cell 2, Layer 7; Cell 4, Layer 5	Consolidation	Staged	106	2/2/2003
28	Cell 2, Layer 8; Cell 4, Layer 6	Consolidation	Staged	110	5/20/2003
29	No Additional Loading	Consolidation	Staged	64	9/8/2003
30	Cell 1b, Layer 8	Consolidation	Staged	91	11/12/2003
31	Cell 1b, Layer 9	Consolidation	Staged	86	2/12/2004
32	No Additional Loading	Consolidation	Staged	113	5/9/2004
33	Cell 1b, Layer 10	Consolidation	Staged	75	8/31/2004
34	No Additional Loading	Consolidation	Staged	357	11/15/2004
35	No Additional Loading	Consolidation	Staged	69	11/8/2005
36	No Additional Loading	Consolidation	Staged	5098	1/17/2006
37	No Additional Loading	Consolidation	Staged	1826	1/3/2020
38	No Additional Loading	Consolidation	Staged	1826	1/3/2025

5.4 - Finite Element Model Validation

To increase the reliability of the forecasted soil behavior for Phase IV waste placement it was necessary that the Plaxis finite element models could accurately predict the behavior of the soil during the initial construction and filling phases at the RWS landfill.

In order to validate the Plaxis models, the historical data available from settlement platforms, piezometers and inclinometers was compared to the model outputs. Based on these comparisons the model was then adjusted to correct the discrepancies between the historical data and the model output. The East/West model was adjusted first, as a greater number of settlement platforms and piezometers were available for comparison than in the North/South model. Figures 5.16 and 5.17 provide schematics of the locations of the available historical data for the East/West and North/South profiles respectively. Settlement data is available at locations marked "SPL", piezometer data is indicated by "P", and inclinometer data is indicated by "I".

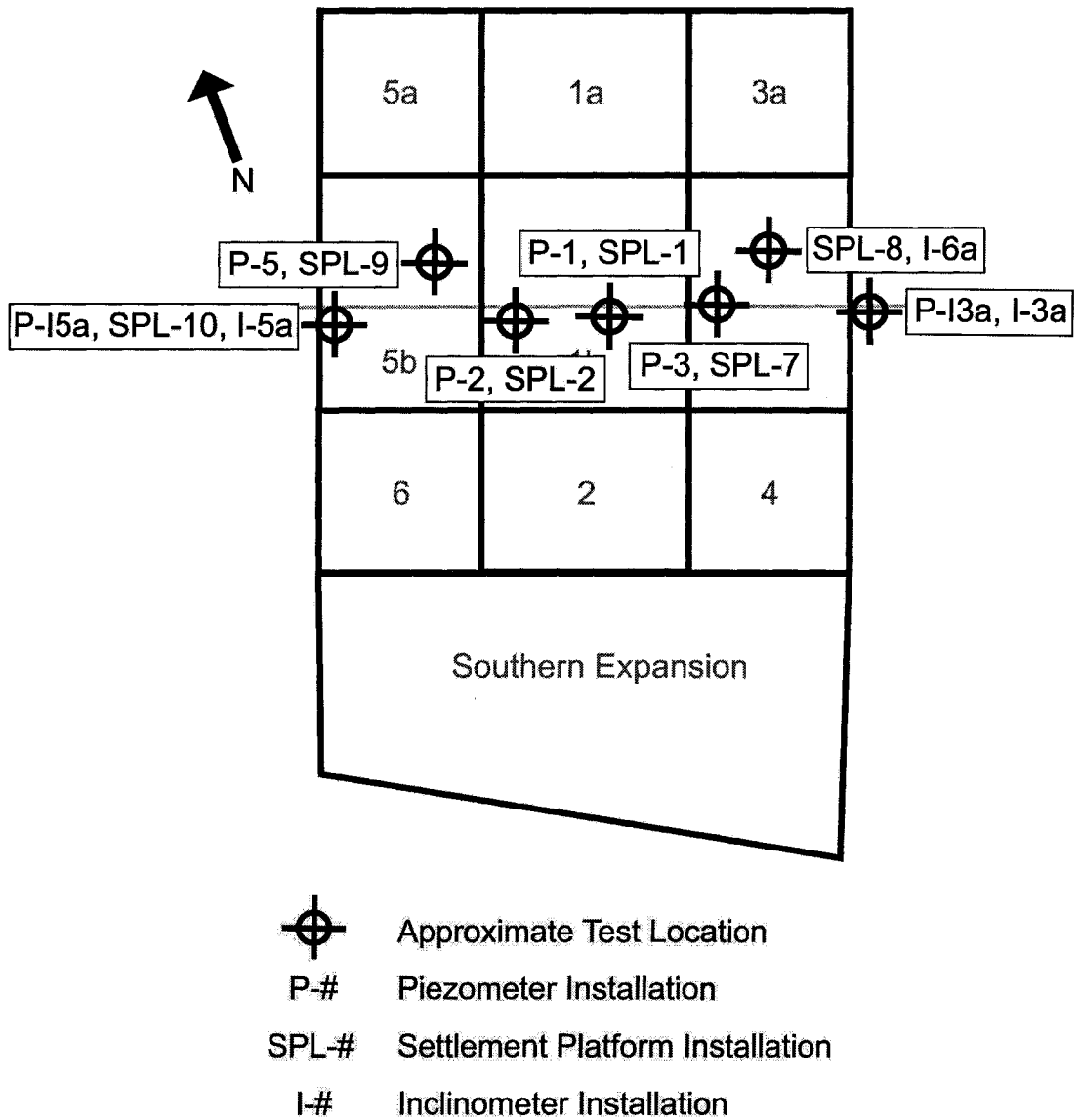


Figure 5.16 - East/West Profile with Historic Monitoring Installations

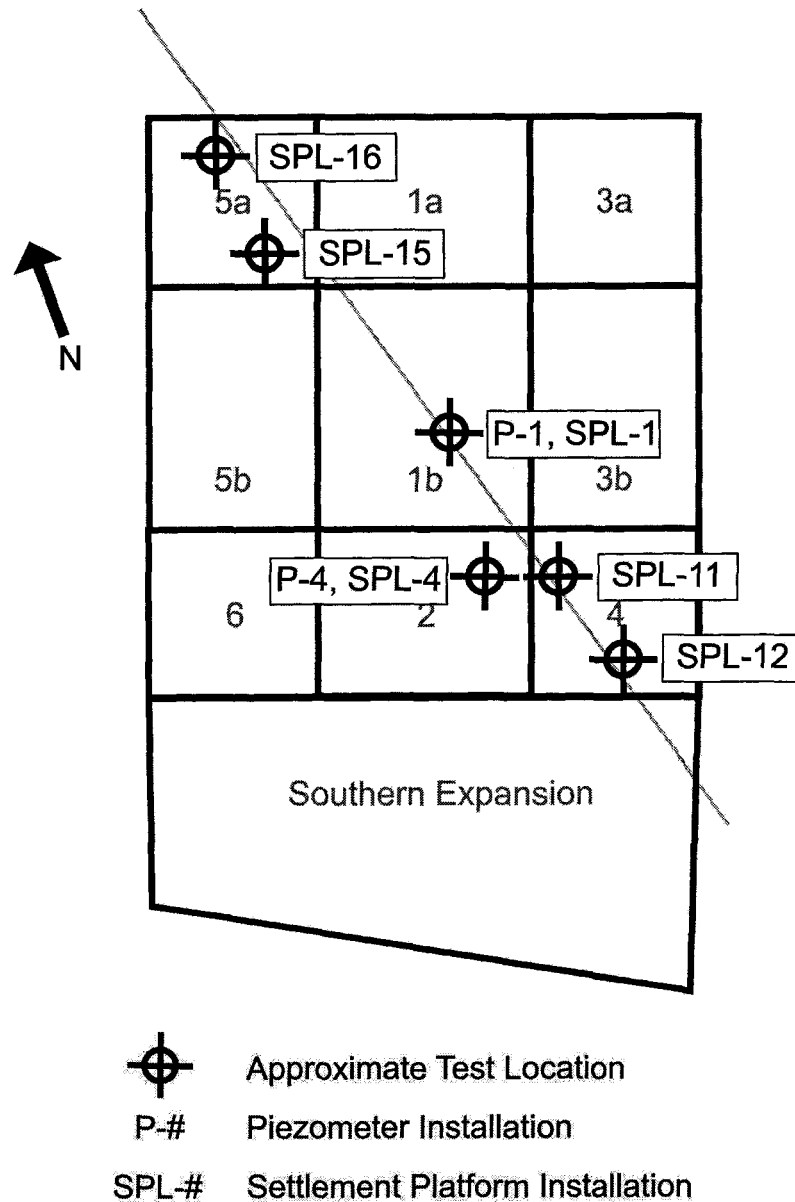


Figure 5.17 - North/South Profile with Historic Monitoring Installations

The initial optimization of the E/W model was based on the data available from the piezometers. Adjustment of the horizontal and vertical permeability values in the soft gray silty clay was required to match as closely as possible the rate of decay of excess pore pressures during periods without loading. The model was then optimized with regards to settlements by adjusting the compression indices of the

foundation soils and by small adjustments to the waste loading rates. The adjustments were made on only one parameter at a time to determine the effect which the change would make on the model outputs. The soil parameters from the final optimized East/West model were used in the North/South model without any changes. Optimization of the North/South model consisted of adjustments in the waste loading rates to match as closely as possible the predicted settlement and pore pressures to the historical data. Adjustments of the waste loading rates were made by increasing or decreasing the length of individual calculation phases, which were initially based on the time between changes in ash elevation at survey points across the site.

The final optimized East/West profile settlements and pore pressures matched very closely with the historical data however some variance is expected as the models cannot completely replicate the complexity of the site conditions and waste loading sequence. Figure 5.18 provides an example of the settlements predicted by Plaxis and the settlement platform data at the SPL-1 location in Cell 1-b. The historical settlement and pore pressure data is unavailable prior to 1992; however the Plaxis predictions are presented from the initial time of waste loading in this figure, as well as others in Section 5.4. The Plaxis results typically vary from the actual settlement data by less than 7% at all locations with the exception of SPL-10, which over predicts the settlement by up to 210%. The over prediction may be a result of erroneous interpolation of ash thicknesses between survey points, which resulted in a greater ash thickness than is actually present. In addition the error may be a result of incorrect ash loading rates within the area near SPL-10.

The East/West model was generally able to accurately predict the pore pressures at all depths towards the center of the model as presented in Figure 5.19 at the location of the P-2 piezometer in Cell 1b. Towards the edges of the landfill footprint the model overpredicted the pore pressures after 2001. The pore pressures at the P-5 location in Cell 5b at the western edge of the landfill are presented in Figure 5.20. Plaxis both over predicts and under predicts the pore pressures at the P-5 location, which is in part due to minor differences in the rate of waste loading used in the model when compared to reality. The model does not perform well deeper within the soft silty clay stratum. This error may be a result of a lower than expected permeability in the glacial sands, resulting in a reduced capacity for drainage from the clay. No test data is available from these sands to confirm this theory.

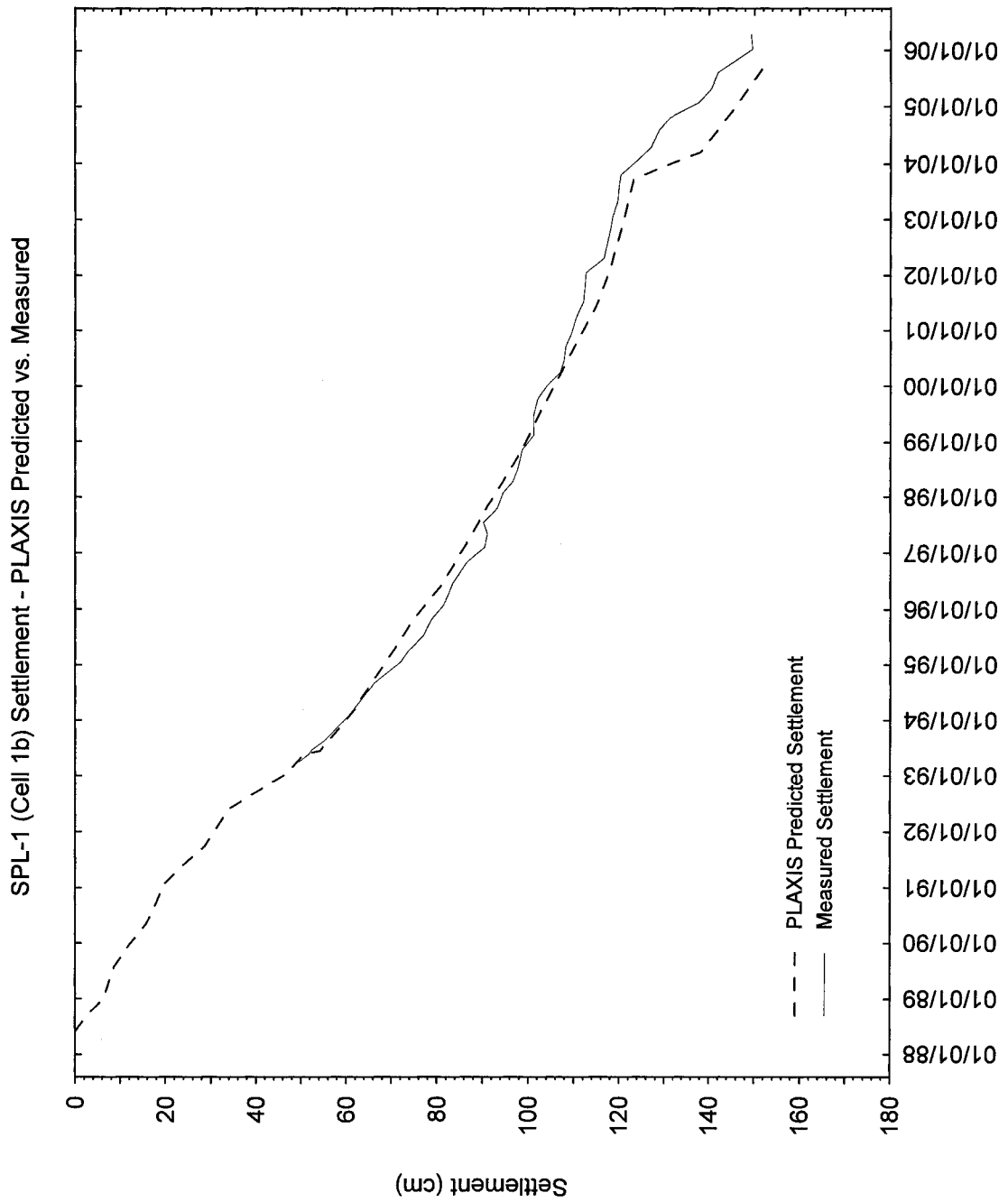
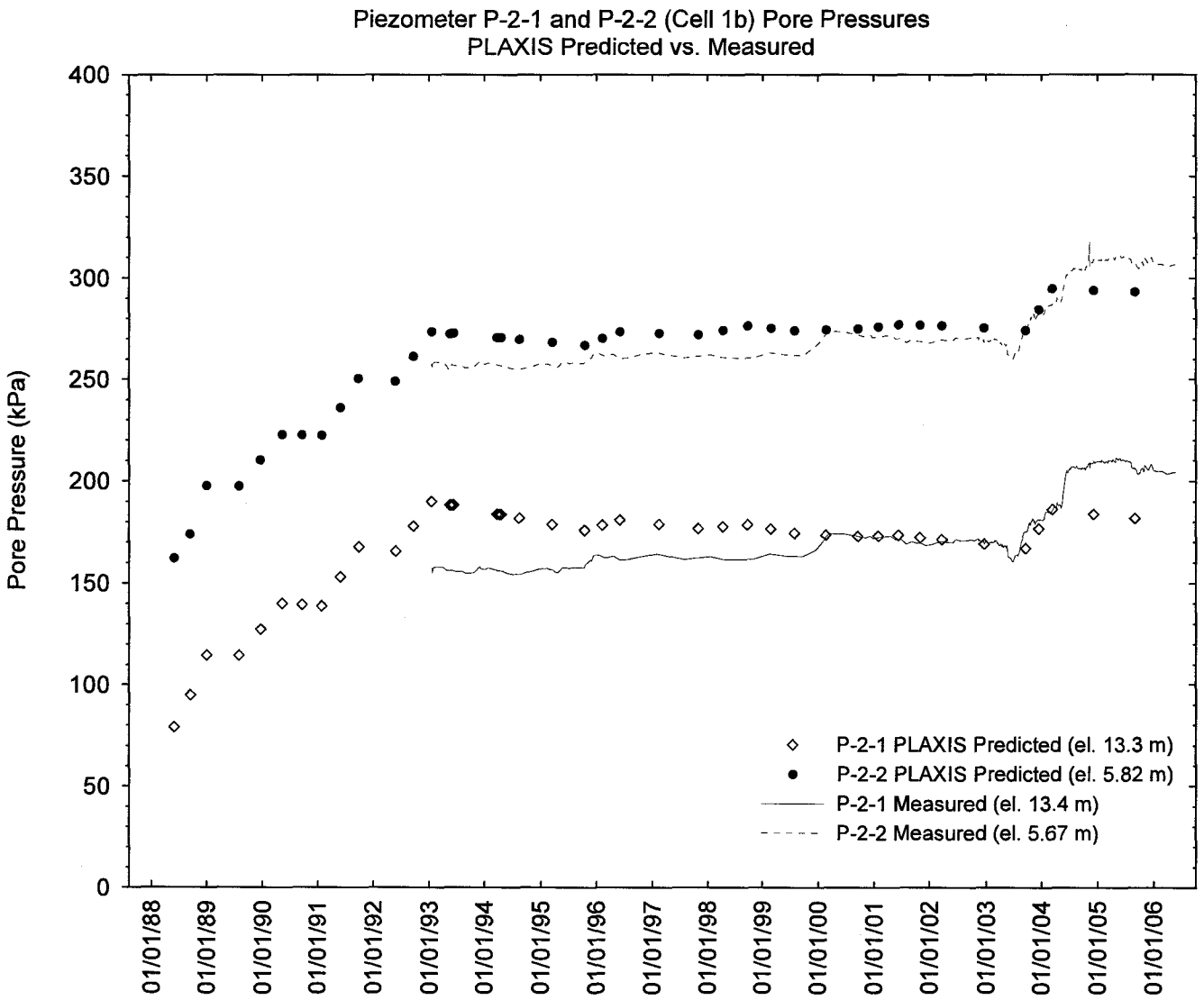


Figure 5.18 - SPL-1 (Cell 1b) - Plaxis Predicted vs. Measured Settlements

Figure 5.19 - Piezometer P-2 (Cell 1b) - Plaxis Predicted vs. Measured Pore Pressures



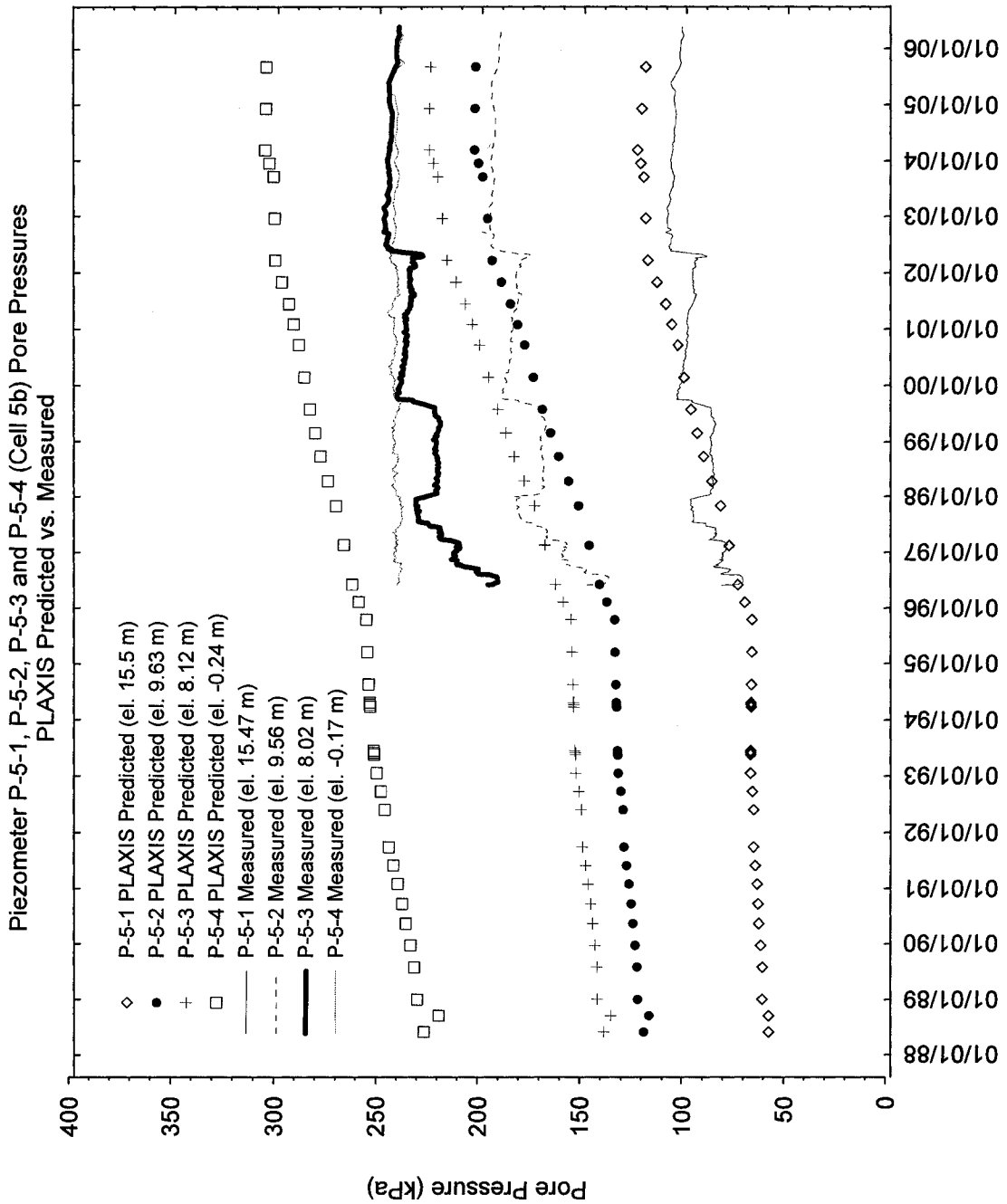


Figure 5.20 - Piezometer P-5 (Cell 5b) - Plaxis Predicted vs. Measured Pore Pressures

Historical data from inclinometers was available for the East/West Profile, though adjustments to the soil properties or waste loading rates were not performed based on this data. The Plaxis model over predicted the horizontal displacement by over

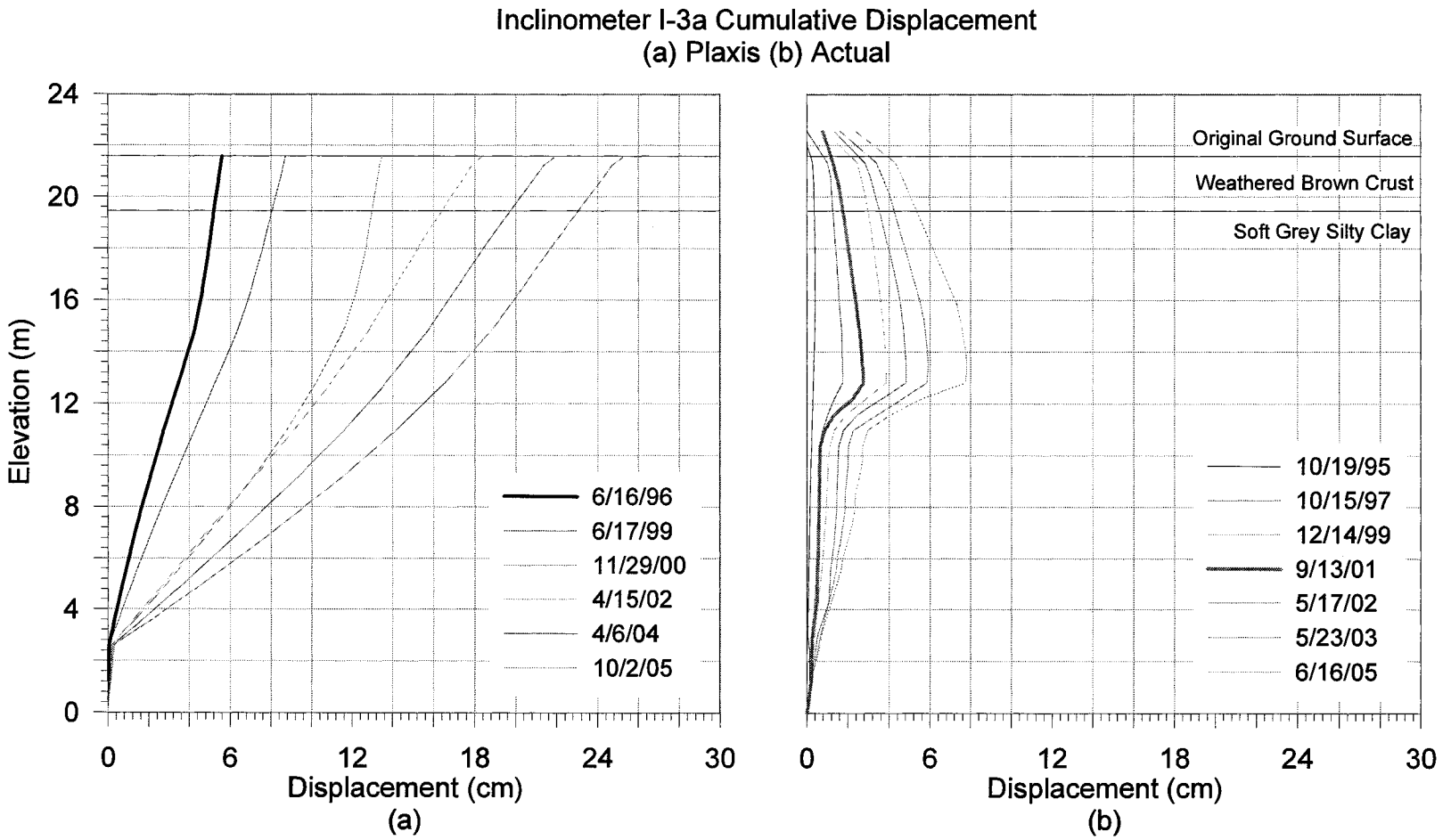
500% (over 21 cm) in some locations, as presented in Figure 5.21. One concern for future expansion of the RWS facility are the zones of higher than expected horizontal displacement observed in inclinometer data. Despite the large displacements which were predicted in the model, especially near the original ground surface, these zones were not present.

The settlements predicted by Plaxis for the North/South model did not match the historical data as well as those in the East/West Model. As observed in the East/West profile the settlements predicted by Plaxis matched the historical data well towards the center of the site at SPL-1, with an average variance of approximately 8%. Plaxis increasingly over predicts the settlements as the location moves further away from the center of the landfill. Figure 5.22 presents the settlement at SPL-4, which is located in Cell 2 at approximately the mid-point from the center to the edge of the landfill. While Plaxis significantly over predicts the magnitude of the settlement at this location, the general trend of the predicted settlements matches the historical data.

The North/South profile predicts the pore pressures equally as well as the East/West profile in the center of the landfill at the P-1 location (Figure 5.23). The data available for the P-4 location indicates that Plaxis also models the pore pressure well at this location.

The final optimized models for both the North/South and East/West profiles performed well during the initial phases of operation at the RWS landfill. Though some variation from historical data exists in each profile, this can be expected as the site is relatively large and difficult to accurately model.

Figure 5.21 - Inclinerometer I-3a Cumulative Displacement - Plaxis Predicted vs. Measured Displacement



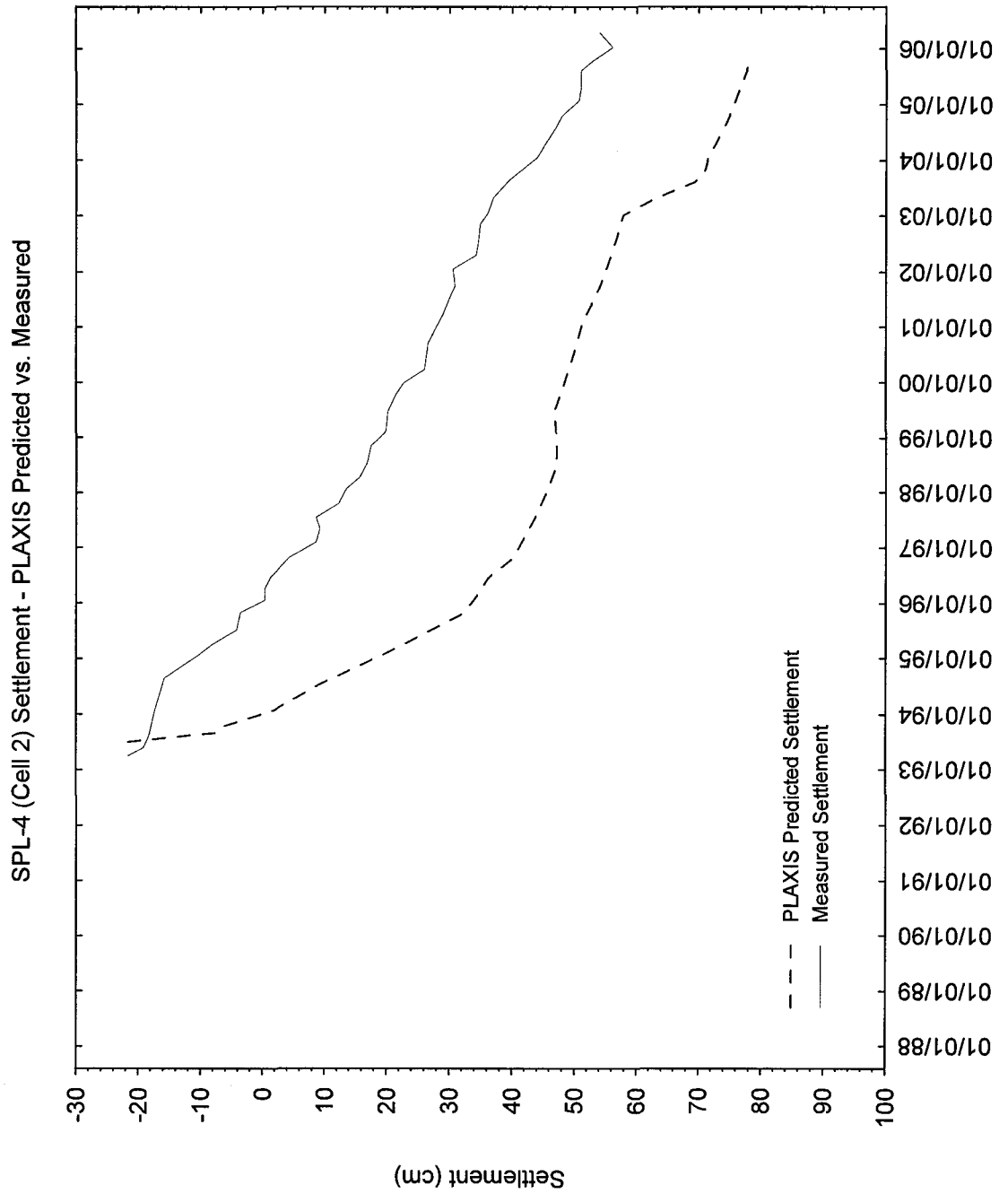
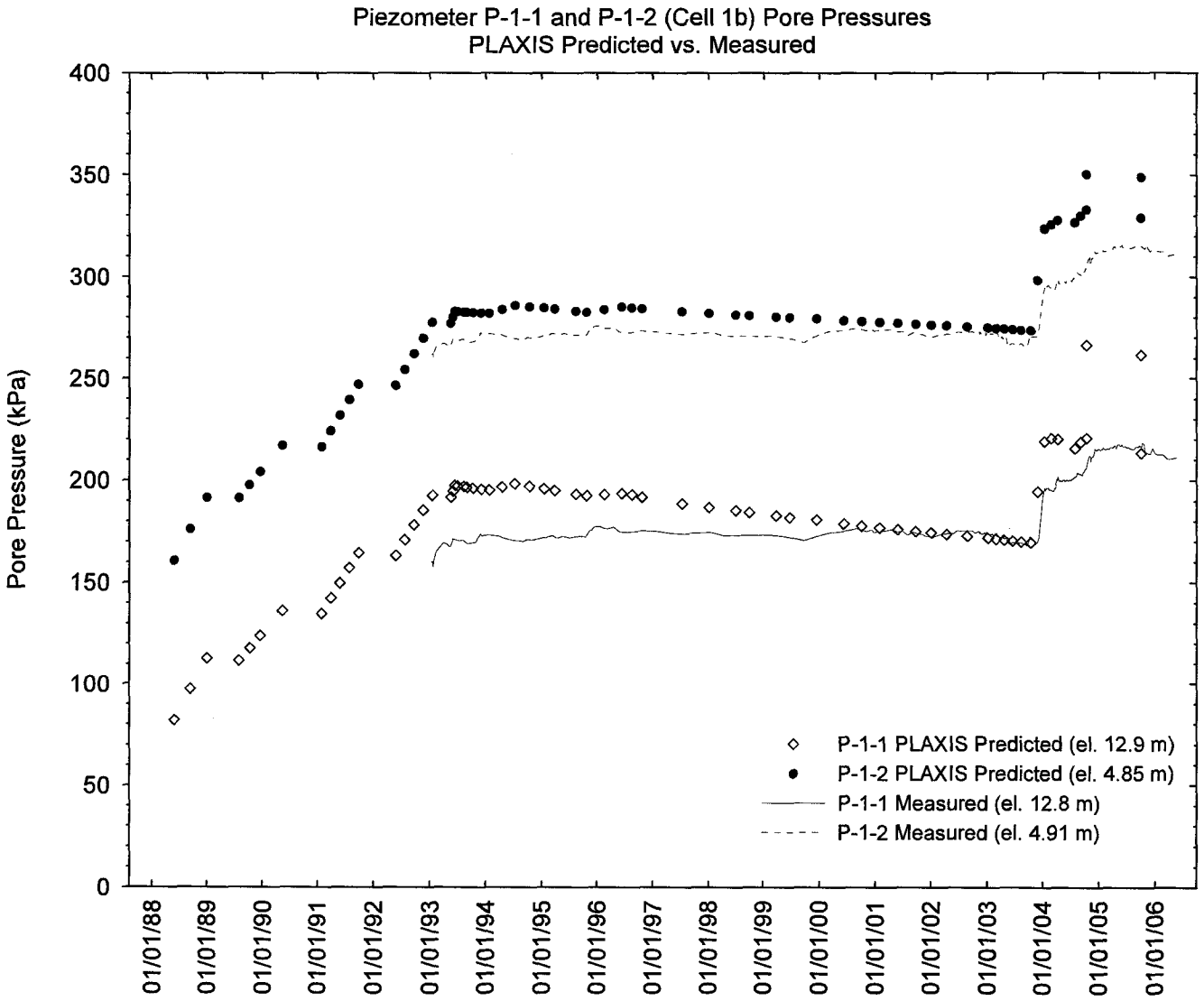


Figure 5.22 - SPL-4 (Cell 2) - Plaxis Predicted vs. Measured Settlements

Figure 5.23 - Piezometer P-1 (Cell 1b) - Plaxis Predicted vs. Measured Pore Pressures



5.5 - Prediction of Future Soil Strengths

A previous comparison of the actual and theoretical strength change in the soft gray silty clay stratum at the RWS site had been performed at the B-1, P-3 and P-5 locations (Figure 5.24) for the period of 1994 to 2002 (Rabasca, 2003). During this period the test locations were loaded with up to 7 meters of ash. At each location the change in undrained shear strength measured using the field shear vane agreed well with the theoretical change, as determined using the TCON analysis discussed in Section 2.2.3. The tests generally observed strength gains varying between 1.2 and 3.6 kPa (25 and 75 psf) with the exception of an approximately 1.5 meter thick zone between 7.6 and 12.2 meters elevation, where a strength loss of 1.2 to 3.6 kPa was noted. The zone of strength loss was not attributed to any one specific factor, though it was noted by Rabasca (2003) that both strain softening and normal variations in test procedures were likely contributors.

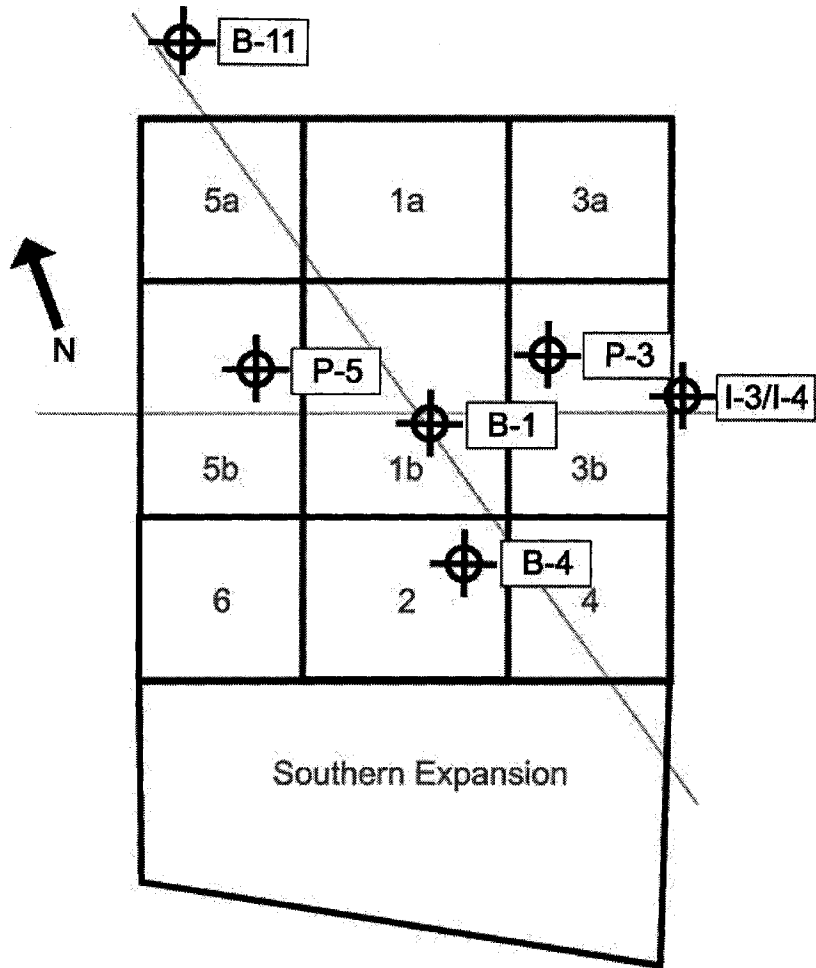


Figure 5.24 - Locations of Strength Change Analysis

To analyze the change in strength at specific locations for the Plaxis analysis as well as the previous analysis in 2003, the change in vertical effective overburden stress ($\Delta\sigma'_v$) due to consolidation was used in conjunction with the known ratio of field shear vane strength to effective stress $S_{u(fv)}/\sigma'_{vo}$. At the RWS site this ratio has been reported as varying between 0.10 and 0.15 (Rabasca, 2003) and the Plaxis analysis assumed a ratio of 0.125. The change in effective stress measured in the Plaxis analysis was then multiplied by the strength ratio to determine the change in undrained shear strength from the baseline values.

The effective stress at each location was recorded using Plaxis at the time of any previous field shear vane investigation, as well as during January of 2006, 2020, 2025 and 2030. Figure 5.25 provides an example of the increase in effective overburden pressure at the B-4 location. In order to forecast the theoretical undrained shear strength the Plaxis model assumes that no additional loading will occur at the site after October of 2005. Three initial analyses were performed using Plaxis data at the B-1, P-3 and P-5 locations from the period of 1994 to 2002 in order to determine the ability of the model to predict strength changes. The comparison of actual and calculated strengths at the B-1 location is presented in Figure 5.26. The calculated strength determined by Plaxis appears to agree fairly well with the actual change in strength below 8.8 meters (29 feet) elevation, though above 11 meters (36 feet) elevation the Plaxis model tends to over predict the change in strength by approximately 14%. The over prediction may be the result of the combination of a shorter drainage path and high excess pore pressures, resulting in a greater degree of consolidation than that experienced in lower depths. In zones where an apparent strength loss occurs, such as that between 8.8 and 11 meters in the B-1 profile, Plaxis does not predict such strength loss. This is likely due to the inability of the Soft Soil Model to account for strain softening.

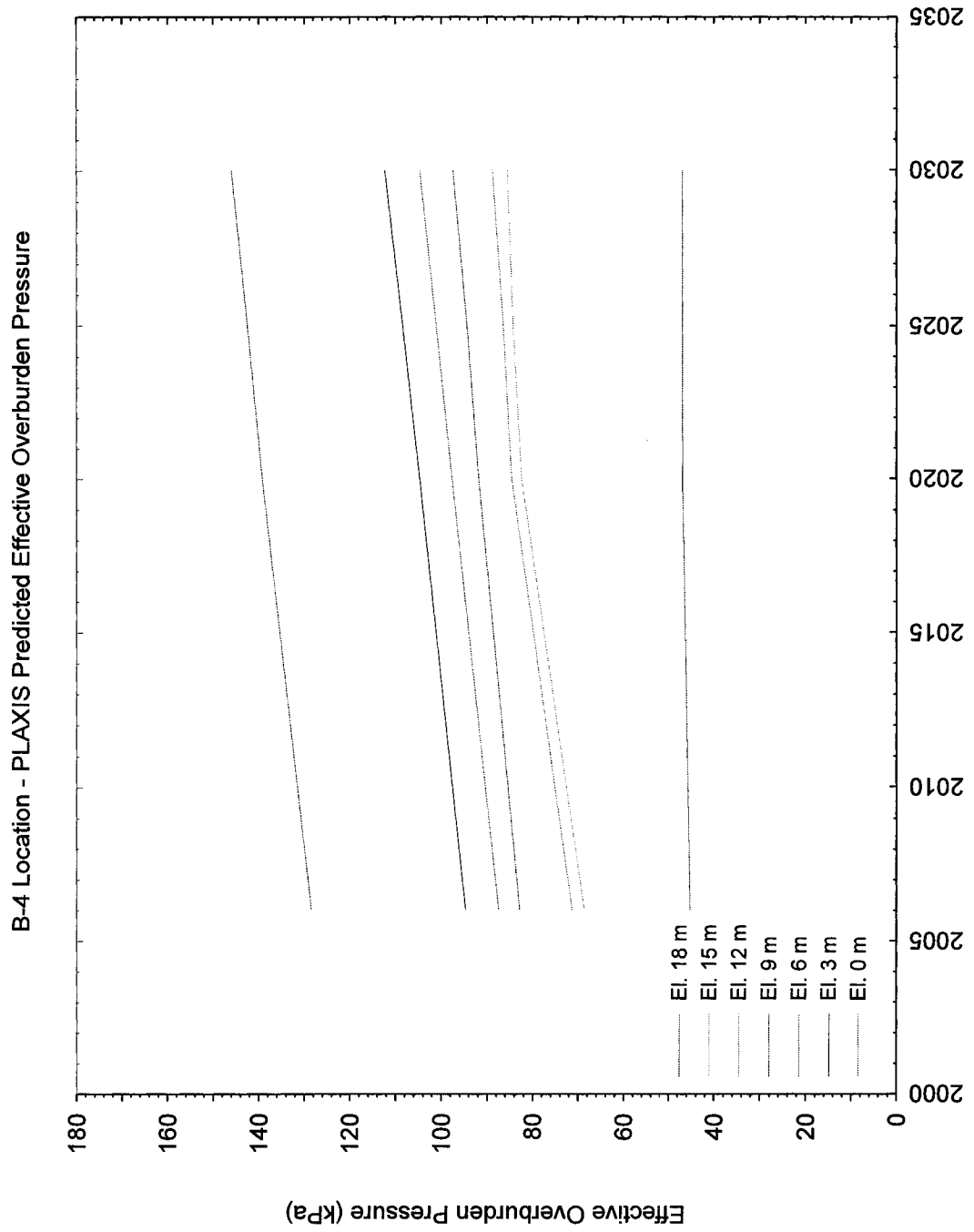


Figure 5.25 - Plaxis Predicted Change in Effective Overburden Pressure with Time (B-4 Location)

Undrained Shear Strength Profile at B-1

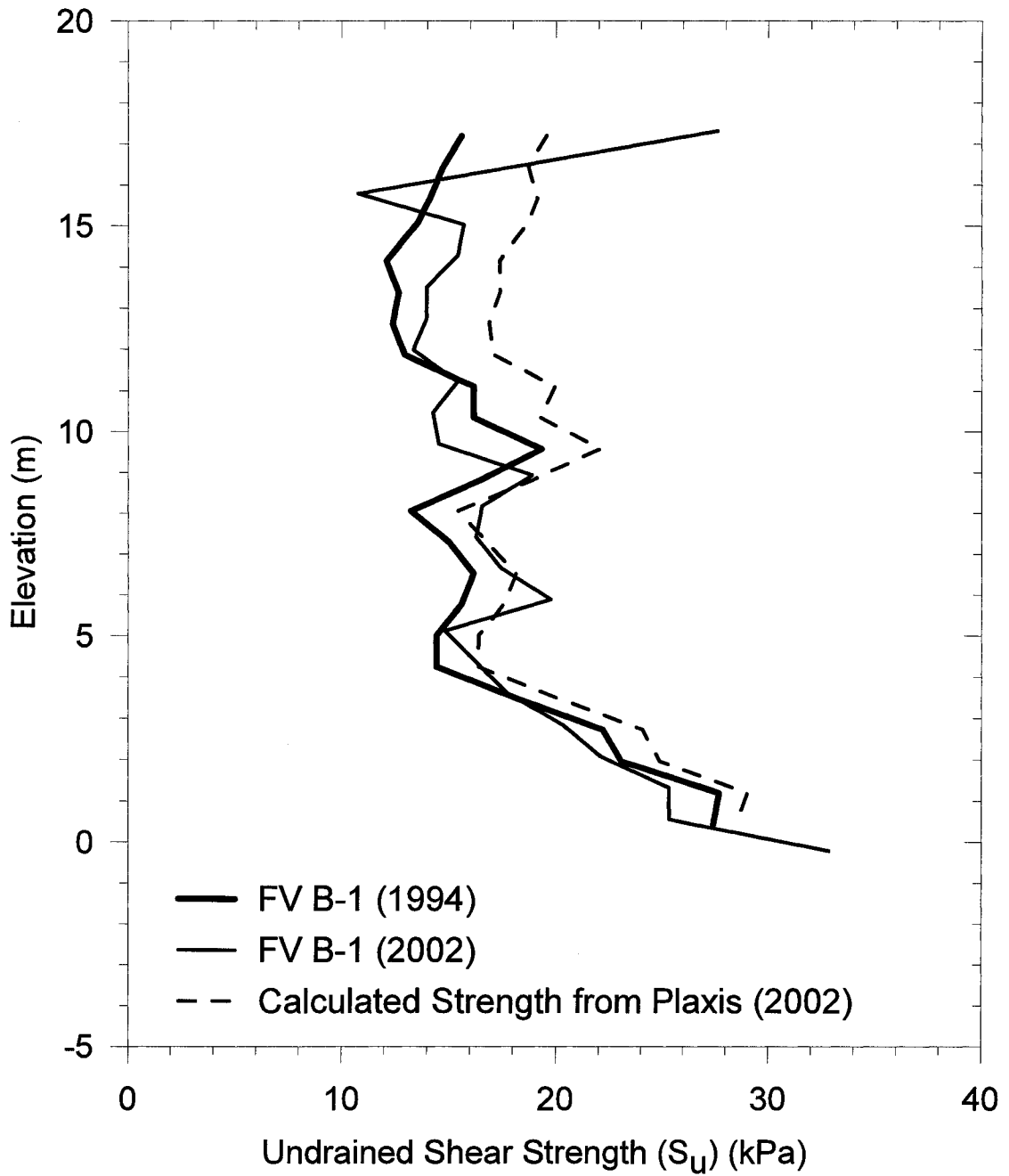


Figure 5.26 - Change in Undrained Shear Strength at B-1 (1994-2002)

The 2002 field shear vane strength profile was used as the baseline value for strength estimation to 2006, 2020, 2025 and 2030 at the B-1, B-4, P-3, P-5, and I-3/I-4 locations. An additional analysis was performed at the B-11 location using the 2006 field shear vane strength profile as a baseline.

Figures 5.27 and 5.28 present the theoretical strength gains at the I-3/I-4 location and the B-1 location respectively and are indicative of the theoretical strength gains observed at the RWS site. The theoretical strength gain in the B-1 profile is approximately 40% over the 2002 strength at the top of the profile (approximately 15 meters elevation), which is the interface between the soft gray silty clay and the stiff brown weathered crust clays. The theoretical strength increase gradually reduces to approximately 21% in the lower regions of the B-1 profile. This distribution agrees with anticipated results, as the excess pore pressures developed due to additional loading is less, as the change in vertical overburden pressure is reduced with depth. The minimal strength gain within the weathered crust may be due the high OCR and lower initial void ratio, resulting in a lower overall amount of consolidation in this layer.

While it was expected that the greatest theoretical strength gain would correlate with the locations of the greatest amount of ash loading, the degree to which the loading would extend horizontally was overestimated both in terms of horizontal and vertical stresses. This may be due to the very shallow slopes of the landfill. The strength increase at the I-3/I-4, which is located along the eastern edge of the landfill, is presented in Figure 5.28. The strength increase predicted for 2020 in the upper portions of this profile is only 4% greater than the 2002 baseline strength. In the

lower portions of the profile the increase is approximately 2% greater than the 2002 strength. Allowing an additional 10 years of consolidation, to 2030 has little effect on the theoretical strength gain.

Undrained Shear Strength Profile at B-1

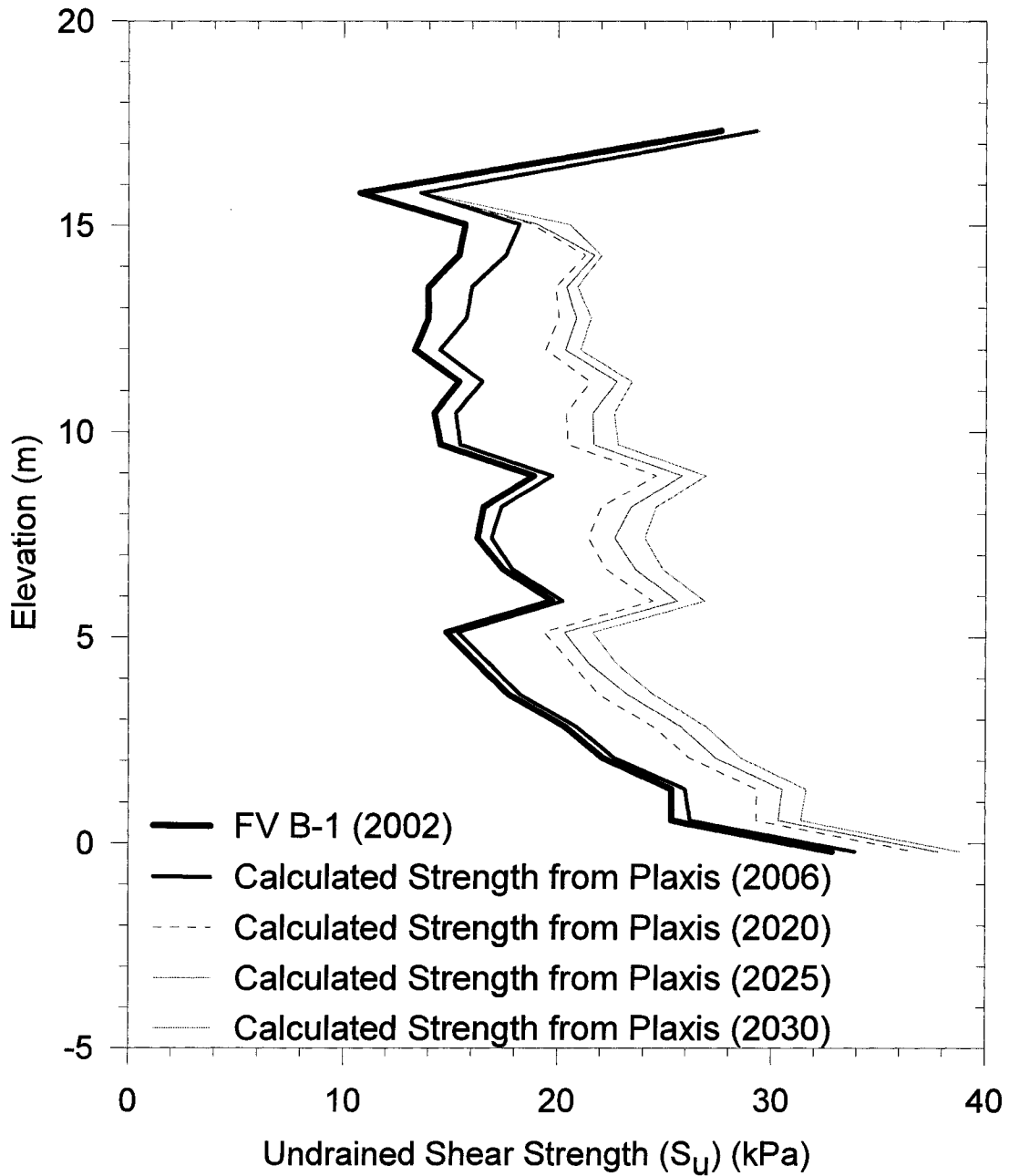


Figure 5.27 - Change in Undrained Shear Strength at B-1 (2002-2030)

Undrained Shear Strength Profile at I-3/I-4

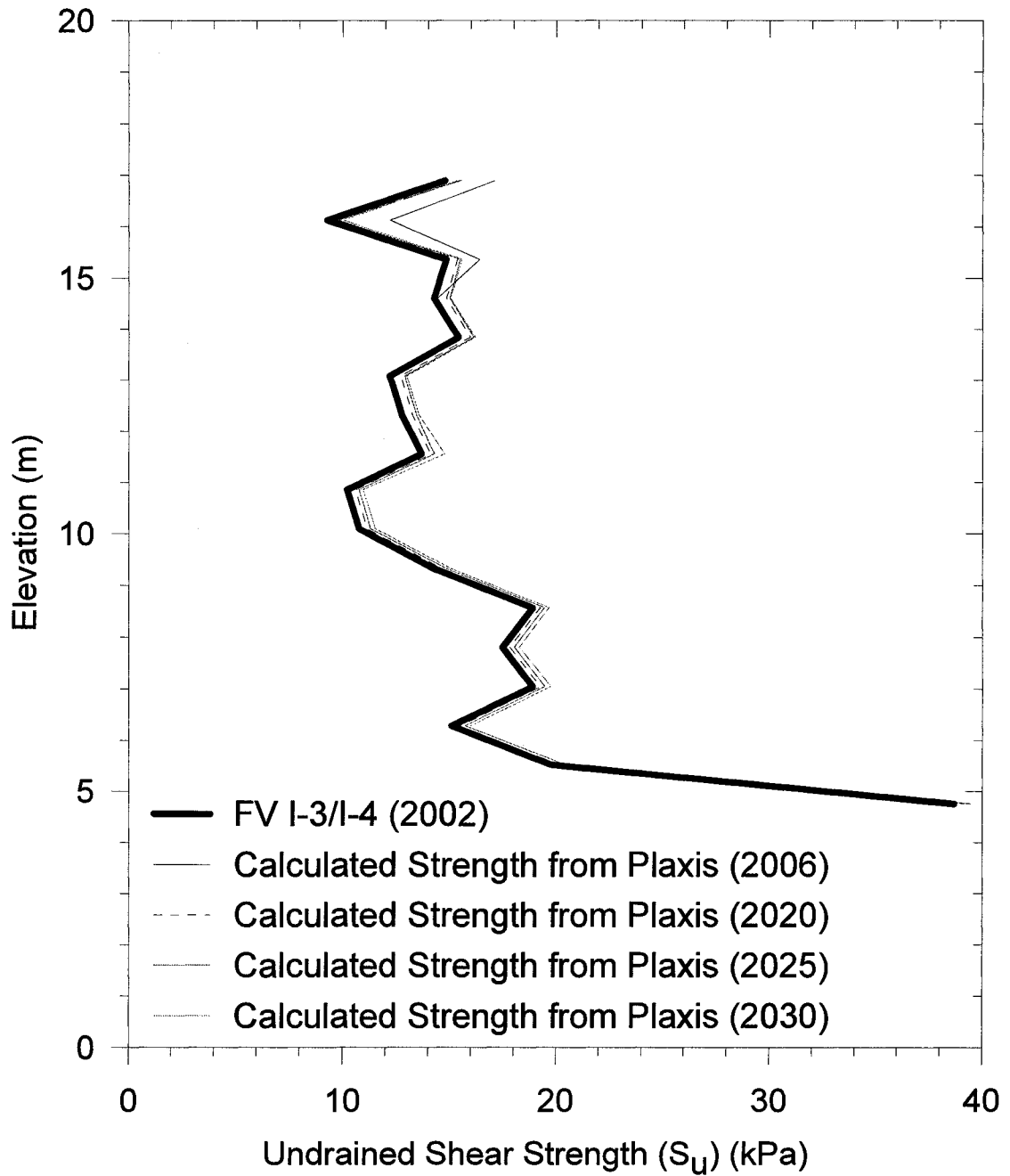


Figure 5.28 - Change in Undrained Shear Strength at I-3/I-4 (2002-2030)

While the Plaxis models appear capable of modeling the theoretical strength gain at the RWS site, shear softening of the soils cannot be accounted for in these analyses as the Soft Soil model is not capable of simulating this behavior. The 2002 field shear vane investigation revealed localized regions, typically no more than 1.5 meters thick, of apparent strength loss within multiple profiles. These losses ranged from 7 to 16% of the baseline 1994 strength. These regions of apparent strength loss do correlate with regions of high shear strain, which indicates the likely occurrence of post-peak shear softening. Therefore the Plaxis output may overestimate the theoretical strength gain in these locations.

CHAPTER VI

SUMMARY AND CONCLUSIONS

6.1 - Summary

In preparation for a proposed vertical expansion of the RWS Ashfill/Balefill facility in South Portland, Maine, a prediction of the long term strength gain in the underlying soft, sensitive marine silty clays was required to evaluate the overall stability of the landfill. To facilitate this requirement, a finite element analysis was used to replicate the phased construction of the landfill site. North/South and East/West profiles were created using both survey data and boring logs to determine model geometry, with the survey data also used to determine waste loading rates on a cell by cell basis. The material properties for the modeling study were primarily gathered during an in situ testing program consisting of piezocone, field shear vane and dilatometer profiles and laboratory testing. Additional information was provided from previous site investigations in 1985, 1994 and 2002. Historical data from settlement platforms and piezometers installed at the site was used to tune the models to more accurately represent the in situ conditions.

Strength gain within the soft grey silty clay stratum was calculated based on the ratio of vertical effective stress to undrained shear strength. The strength gain was first calculated between 1994 and 2002 and compared to measured strength gain during the same period to validate the model. Calculations were then performed to

determine the strength gain to 2020, 2025 and 2030 for the landfill expansion analysis.

6.2 - Conclusions

The following conclusions can be drawn from the field work performed at the RWS landfill, and using the Plaxis finite element software to model the site.

The Plaxis finite element modeling generally provided a good indication of the behavior at the RWS landfill in terms of settlement and excess pore pressures from initial waste loading in 1988 to 2006. The models successfully estimated the settlement towards the center of the site with less than 8% error, though overestimation of settlement was observed towards the edges of the landfill by more than 200%. Consideration of both the development of excess pore pressures from loading and the dissipation of pore pressures under no-load conditions was necessary for accurate modeling at the site. The pore pressures estimated from the finite element model generally agreed with the historical data, varying only by approximately 10% on average. However, deeper within the soft gray silty clay stratum the model estimated the pore pressure to within +/- 30%. Though both settlement and pore pressures vary from historical data at some locations or depths, the general trend of the predicted behavior closely follows the recorded

The long term behavior of the site may not be as accurately depicted in the finite element modeling a result of the computational limitations of the Soft Soil Model used to describe soil behavior. The strength changes predicted to the years 2020, 2025 and 2030, using 2002 field shear vane profiles as baseline strengths, indicate

that a strength gain of up to 40% may be realized within the center of the site by the year 2020 due to the consolidation of the soft gray silty clay stratum. Extending outward from the perimeter of the landfill the calculated strength gain is significantly less, on the order of 2 to 4% above the 2002 strengths. No strength losses, similar to those observed in the field, were noted based on the change in effective stresses from Plaxis. This model does not account for strain softening of the soil, a behavior which has previously been observed within localized depths of the soft gray silty clay stratum. Under no-load conditions the rate of strain throughout the soft gray silty clay profile is expected to decrease during the period from 2006 to 2020 from the current rate of 0.02 to 0.03% per month. Therefore, while strength loss may not be significant within the zones of large displacement within the stratum, the change in strength calculated from the results of the Plaxis finite element models may be slightly overestimated.

Where comparisons were made between horizontal displacement within the Plaxis models and inclinometer data, the finite element model significantly overestimated the displacement throughout the site. The displacement in the stiff silty clay crust was overestimated by over 600% at some locations, while displacements within the upper portions of the soft gray silty clay were overestimated by nearly 500%. Additionally the 1 to 2 meter thick locations of large horizontal displacement observed in the inclinometers, at elevations varying between 11 and 15 meters, were not observed in the finite element model. The zones of greatest horizontal displacement at the site occur at the depths where a discontinuity was observed in virgin field shear vane strength profiles at the site. The sudden drop in undrained shear strength was accounted for in the finite element models. While the cause for

this error is not readily apparent, the over prediction of the horizontal displacement in the clays at the site does not appear to affect the models ability to estimate settlement and development of excess pore pressures. This lends to the conclusion that the Soft Soil model is not well suited for accurate analysis of horizontal displacements.

6.3 - Future Work

To account for the Soft Soil Models limitations with regards to strain softening behavior, it is recommended that the Hardening Soil Model be used in further analyses of the site. This model is capable of handling the effects of strain softening. For the Hardening Soil Model, further laboratory and in situ testing would be required to obtain the necessary input material properties. It is also recommended that the material properties of the glacial sands be confirmed through in situ or laboratory testing to supplement the material properties reported by E.C. Jordan, Co. (1985). These properties may impact the dissipation of excess pore pressures in the soft gray silty clay.

Strength profiles from field shear vane tests, and the large horizontal displacements observed at the site seem to suggest the presence of a historic slip surface which may have been re-activated due to waste placement. Further investigation at the site using the dilatometer may be warranted to ascertain the extent of a slip surface, if one exists. A sudden change in the dilatometer horizontal stress index, K_D , has been reported by Totani et al. (1997) as an indicator of slip surfaces. Dilatometer profiles adjacent to inclinometer installations where the large displacements have been observed may confirm the presence of the slip surface.

Unlike the field shear vane, the piezocone profiles completed at the site did not indicate a change in the undrained shear strength, overconsolidation ratio and preconsolidation pressure at the depths where large horizontal displacements are observed in the P-3 and I-3/I-4 locations. Likewise the soil behavior classifications by the methods of Larsson and Mulabdic (1991) and Robertson (1990) do not indicate a zone of material which behaves differently than the remainder of the soft gray silty clay stratum. Therefore additional piezocone profiles may be beneficial at the site to help determine why the piezocone does not indicate changes.

LIST OF REFERENCES

Aas, G., Lacasse, S., Lunne, T., and Hoeg, K. (1986), "Use of in situ tests for foundation design in clay," ASCE Specialty Conference IN SITU 86. Blacksburg, Virginia, pp. 1-30.

Ahnberg, H., Larsson, R., Berglund, C. (2004), "Influence of vane size and equipment on the results of field vane tests", Proceedings ISC-2 on Geotechnical and Geophysical site characterization, Viana da Fonseca and Mayne, Ed., Rotterdam.

Annual Book of ASTM Standards v.4.08, 2001. "Standard Test Method for Field Shear Vane Test in Cohesive Soil" American Society of Testing and Materials Standard D 2573-01, ASTM, Philadelphia, PA.

Annual Book of ASTM Standards v.4.09, 2001. "Standard Test Method for Performing Electronic Friction Cone and Piezocone Penetration Testing of Soils", American Society of Testing and Materials Standard D 5778-95(2000), ASTM, Philadelphia, PA.

Annual Book of ASTM Standards v.4.09, 2001. "Standard Test Method for Performing the Flat Plate Dilatometer" American Society of Testing and Materials Standard D 6635-01, ASTM, Philadelphia, PA.

Baligh, M.M., (1975), "Theory of Deep Site Static Cone Penetration Resistance", Massachusetts Institute of Technology, Department of Civil Engineering, Cambridge, Mass., Publication No. R75-56.

Baligh, M.M., Vivatrat, V., and Ladd, C.C. (1980), "Cone penetration in soil profiling", Journal of the Geotechnical Engineering Division, ASCE, 106 (GT4), pp. 447-461.

Baligh, M.M., and Levadoux, J.N., (1980), "Pre Pressure dissipation after cone penetration", Massachusetts Institute of Technology, Department of Civil Engineering, Cambridge, Mass., Report R80-11

Baligh, M.M., Azzouz, A.S., Wissa, A.Z.E., Matyin, R.T., and Morrison, M.H. (1981), "The Piezocone penetrometer, Cone Penetration Testing and Experience", Proceedings of the Session ASCE National Convention, St. Louis, pp. 247-263, American Society of Civil Engineers (ASCE).

Baligh, M.M., and Levadoux, J.N., (1986), "Consolidation after undrained piezocone penetration, II: Interpretation", *Journal of Geotechnical Engineering, ASCE*, 112(7), pp.727-745.

Baligh, M.M., (1985), "Strain Path Method", *Journal of the Geotechnical Engineering Division, ASCE*, 111(GT9), pp. 1108-1136.

Battaglio, M., Bruzzi, D., Jamiolkowski, M., Lancellotta, R., (1986), "Interpretation of CPTs and CPTus", *Proceedings of the 4th International Geotechnical Seminar, Singapore*, pp. 129-143, Nanyang Technical Institute, Singapore.

Beem, L.H, "Mineralogy of Fine-Grained Glaciomarine Sediments, Coastal Maine", *Geological Society of America Abstracts with Programs*, Vol. 36, No. 2, March 2004.

Benoît, J., "In Situ Vane Shear Testing", Final Report Submitted to Soil Metrics LLC, and Regional Waste Systems, February 2003.

Bjerrum, L., (1972), "Problems of Soil Mechanics and Construction on Soft Clays", *Proceedings of the 8th International Conference on Soil Mechanics and Foundation Engineering*, Vol. 3., pp. 111-159.

Brinkgreve, R.B.J., P.A. Vermeer (1998) "Plaxis Manual (Version8)" University of Stuttgart, Germany A.A.Balkema/Rotterdam/Brookfield-D

Broms, B.B., Flodin, N. (1988), "History of Soil Penetration Testing", *Proceedings of the First International Symposium on Penetration Testing, ISOPT-1, Orlando, FL*, Vol. 1, pp 157-220.

Brooker, E.W., and Ireland, H.O., (1965), "Earth Pressure at rest related to stress history", *Canadian Geotechnical Journal*, 2(1), pp. 1-15.

Bruzzi, D., Battaglio, M. (1989), "Pore Pressure Measurements During Cone Penetration Test", ISMES Research Report No. 229, Italy.

Buisman, A.S.K. (1935), "De weerstnad van pallpunten in zand", *De Ingenieur*, 50(14), pp. 28-35.

Burghignoli, A., Cavalera, L., Chieppa, V., Jamiolkowski, M., Mancuso, C., Marchetti, S., Pane, V., Paoliani, P., Silvestri, F., Vinale, F. & Vittori, E. (1991). "Geotechnical characterization of Fucino clay". Proc. X ECSMFE, Florence, Vol. 1, pp. 27-40.

Calding, L., and Odenstad, S. (1950), "The Vane Borer", Royal Swedish Geotechnical Institute, Proceedings No. 2.

Campanella, R.G., and Robertson, P.K. (1981), "Applied cone research. Cone Penetration Testing and Experience", Proceedings of the ASCE National Convention, St. Louis, pp. 343-362.

Campanella, R.G., Gillespie, D., Robertson, P.K., (1982), "Pore Pressure during cone penetration testing" Proceedings of the 2nd European Symposium on Penetration Testin, ESOPT-II, Amsterdam, pp. 507-512, Balkema Pub., Rotterdam.

Campanella, R.G., Robertson, P.K., Gillespie, D., and Greig, J., (1985), "Recent developments in in-situ testing of soils", Proceedings of the 11th International Conference on Soil Mechanics and Foundation Engineering, San Francisco, 2, pp. 849-854, Balkema Pub., Rotterdam.

Campanella, R.G and Robertson, P.K. (1988), "Current Status of the Piezocone Test", Proceedings of the First International Symposium on Penetration Testing, ISOPT-1, Orlando, FL, Vol. 1, pp 93-116.

Campanella, R.G., Sully, J.P., Greig, J.W., and Jolly, G., (1990), "Research and development of a lateral stress piezocone", Transportation Research Record, No. 1278, pp. 215-224.

Carlson, L., (1948), "Determination In Situ of the Shear Strength of Undisturbed Clay by Means of a Rotating Auger", Proceedings of the 2nd International Conference on Soil Mechanics and Foundation Engineering, Vol. 1, pp. 265-270.

Chandler, R.J. (1988), "The in-situ measurement of the undrained shear strength of clays using the field vane," Vane Shear Strength Testing in Soils: Field and Laboratory Studies, ASTM STP 1014, A.F. Richards, Ed., American Society for Testing and Materials, Philadelphia, pp. 13-44

Chen, B.S., and Mayne, P.W. (1994), "Profiling the Overconsolidation Ratio of Clays by Piezocone Test", National Science Foundation, Report No. GIT-CEECEO-94-1, August.

de Ruiter, J. (1981), "Current penetrometer practice: Cone Penetration Testing and Experience", Proceedings of the ASCE National Convention, St. Louis, pp. 1-48.

Donals, I.B., Jordan, D.O., Parker, R.J., and Toh, C.T., (1977) "The Vane Test – A Critical Appraisal", Proceedings of the 9th International Conference on Soil Mechanics and Foundation Engineering, Vol. 1., pp. 81-88.

EC Jordan & Co., "Regional Waste Systems, Inc. Ashfill/Balefill, Exhibit 7, Design Report", 1985.

Gillespie, D.G., (1990), "Evaluating velocity and pore pressure data from cone penetration test", Ph.D. thesis, Department of Civil Engineering, University of British Columbia, Vancouver, BC.

Goh, T., Tay, Joo-Hwa, (1993), "Municipal Solid-Waste Incinerator Fly Ash for Geotechnical Applications", Journal of the Geotechnical Engineering Division, ASCE, 119 (GT 5), pp. 811-825.

Hirshfield, T., Deaton, T., Milanovich, F., Klainer, S.M., and Fitzsimmons, C. (1984), "The feasibility of using fiber optics for monitoring groundwater contaminants", Project Summary, Environmental Monitoring Systems Laboratory, USEPA, January.

Holtz, R.D., Kovacs, W.D., "An Introduction to Geotechnical Engineering", Prentice-Hall, Inc., Englewood Cliffs, NJ, 1981.

Houlsby, G.T., (1988), "Piezocone penetration test", Proceedings of the Geotechnology Conference: Penetration Testing in the UK, Birmingham, pp. 141-146, Thomas Telford, London.

Houlsby, G.T., and Teh, C.I., (1988), "Analysis of the piezocone on clay", Proceedings of the International Symposium on Penetration Testing, ISOPT-1, 2, pp. 777-783, Balkema Pub., Rotterdam.

Huizinga, T.K. (1942), Grundmechanica, Amsterdam, Arend and Son, pp. 79.

Jaky, J., (1944), "The coefficient of earth pressure at rest", Journal of the Society of Hungarian Architects and Engineers, pp. 355-358.

Jamiolkowski, M., Ghionna, V.N., and Lancellotta, R., (1988), "New correlations of penetration tests for design practice", Proceedings of the International Symposium on Penetration Testing, ISOPT-1, Orlando, 1, pp. 263-296, Balkema Pub., Rotterdam.

Janbu, N., and Senneset, K. (1974), "Effective stress interpretation of in situ static penetration tests", Proceedings of the European Symposium on Penetration Testing, ESOPT, Stockholm, 2.2, pp. 181-193.

Jefferies, M.G., Jonsson, L., and Been, K., (1987), "Experience with measurement of horizontal geostatic stress in sand during cone penetration test profiling", Geotechnique, 37(4), pp. 483-498.

Kamei, T. & Iwasaki, K. (1995). "Evaluation of undrained shear strength of cohesive soils using a Flat Dilatometer". Soils and Foundations, Vol. 35, No. 2, June, pp. 111-116.

Kjekstad, O., Lunne, T., and Clausen, C.J.F., (1978), "Comparison between in situ cone resistance and laboratory strength for overconsolidated North Sea clays", Marine Geotechnology, 3(1), pp. 23-36.

Konrad, J.M., and Law, K., (1987), "Undrained shear strength from piezocone tests", Canadian Geotechnical Journal, 24(3), pp. 392-405, Balkema Pub., Rotterdam.

Kulhawy, F.H., and Mayne, P.H., (1990), "Manual on estimating soil properties for foundation design", Electric Power Research Institute, EPRI.

Lacasse, S., and Lunne, T., (1982) "Penetration tests in two Norwegian clays", Proceedings of the 2nd European Symposium on Penetration Testing, ESOPT-II, Amsterdam 1982, 2, pp. 661-669, Balkema Pub., Rotterdam.

Lacasse S., and Lunne, T., (1988), "Calibration of dilatometer correlations", Proceedings of the International Symposium of Penetration Testing, ISOPT-1, Orlando, 1, pp. 539-548, Balkema Pub., Rotterdam.

Ladanyi, B., (1963), "Expansion of a cavity in a saturated clay medium", Journal of the Soil Mechanics and Foundations Division, ASCE, 89, No. SM4, pp. 127-161.

Ladd, C.C. (1972), "Test Embankment On Sensitive Clay" ASCE, SMFD Specialty Conference on Performance of Earth and Earth-Supported Structures", Purdue University, Vol 1, Part 1, June 1972, pp. 101-128.

Ladd, C.C., Rixner, J.J., Gifford, D.G. (1972), "Performance of Embankment With Sand Drains On Sensitive Clay" ASCE, SMFD Specialty Conference on Performance of Earth and Earth-Supported Structures", Purdue University, Vol 1, Part 1, June 1972, pp. 211-242.

Larsson, R., Mulabdic, M. (1991), "Piezocone Tests in Clay", Swedish Geotechnical Institute, Report No. 42, 240 p.

Lunne, T., and Kleven, A., (1981), "Role of CPT in North Sea foundation engineering", Session at the ASCE National Convention: Cone Penetration Testing and Materials, St. Louis, pp. 76-107, American Society of Engineers (ASCE).

Lunne, T., Robertson, P.K., Powell, J. (1997), "Cone Penetration Testing in Geotechnical Practice", Blackie Academic and Professional.

Lunne, T., Eidsmoen, T., Gillespie, D. and Howland, J.D. (1986), "Laboratory and field evaluation of cone penetrometers", Proceedings of the ASCE Specialty Conference In Situ '86: Use of In Situ Tests in Geotechnical Engineering, Blacksburg, pp. 714-729, American Society of Civil Engineers (ASCE).

Lutenegger, A.J. (1988), "Current Status of the Marchetti Dilatometer Test", Proceedings of the First International Symposium on Penetration Testing, ISOPT-1, Orlando, FL, Vol. 1, pp 137-155.

Marchetti, S., (1980), "In Situ Tests by Flat Dilatometer", Journal of the Geotechnical Engineering Division, ASCE, 106 (GT3), pp. 299-321.

Marchetti, S., Monaco, P., Totani, G., and Calabrese, M. (2001), "The Flat Dilatometer Test in Soil Investigations" A Report by the ISSMGE Committee TC 16, Proceedings, IN SITU 2001, International Conference on In Situ Measurement of Soil Properties, Bali, Indonesia. 41 pp.

Masood, T., Mitchell, J.K., Vaslestad, J., Lunne, T., and Makkelbost, K.H., (1990), "Testing with lateral stress cone, special dilatometer, and stepped blade at three sites in Drammen", Joint Research Project, Norwegian Road Research Laboratory, Norwegian Geotechnical Institute and University of California, Berkeley, Norwegian Geotechnical Institute, Oslo, Report 521600-1.

Massarch, K.R., and Broms, B.B., (1981), "Pile driving in clay slopes", Proceedings of the 10th International Conference on Soil Mechanics and Foundation Engineering, Stockholm, 3, pp. 469-474, Balkema Pub., Rotterdam.

Mayne, P.W., and Holtz, R.D., (1988), "Profiling stress history from piezocone soundings", *Soils and Foundations*, 28(1), pp. 16-28.

Murray, R.F. (1995), "Piezocone Exploration of the Marine Clay Deposit at Pease Air Force Base, New Hampshire", Thesis Presented in Partial Fulfillment of the Requirements for the Masters Degree, University of New Hampshire, Durham, NH, 254 p.

Nash, D.F.Y., Powell, J.J.M. & Lloyd, I.M. (1992). "Initial investigations of the soft clay test site at Bothkennar". *Geotéchnique*, 42, No. 2, pp. 163-181.

Ollie, J.J., Van Ree, C.C.D.F., and Bremner, C. (1992), "In situ measurement by chemoprobe of groundwater from in situ sanitation of versatic acid spill", *Geotechnique*, 42(1), pp. 13-21.

Poran, C., Ahtchi-Ali, F., (1989), "Properties of Solid Waste Incinerator Fly Ash", *Journal of the Geotechnical Engineering Division, ASCE*, 115 (GT 8), pp. 1118-1133.

Powell, J.J.M., and Quarterman, R.S.T., (1988) "The interpretation of cone penetration tests in clays, with particular reference to rate effects", Proceedings of the International Symposium on Penetration Testing, ISOPT-1, Orlando, 2, pp. 903-910, Balkema Pub., Rotterdam.

Powell, J.J.M., and Quarterman, R.S.T., (1991) "The effect of filter position on the measurement of pore water pressures in piezocone tests", BRE Report

Rabasca, S.J., "Phase Ila Supplemental Geotechnical Evaluation for Ashfill/Balefill Facility", Final Report Submitted to Regional Waste Systems, Inc., July 1995.

Rabasca, S.J., "Report of 2002 In Situ Vane Shear Testing", Final Report Submitted to L.R. Higgins, Inc., May 2003.

Rabasca, S.J., "Annual Geotechnical Monitoring Report for 2004", Final Report Submitted to Regional Waste Systems, Inc., June 2005.

Robertson, P.K., Campanella, R.G., Gillespie, D., Greig, J. (1986), "Use of Piezometer Cone Data", Use of In Situ Tests in Geotechnical Engineering (GSP 6), ASCE Specialty Conference In-Situ 86, Blacksburg, Va, pp. 1263-1280.

Robertston, P.K. (1990), "Soil Classification Using the Cone Penetration Test", Canadian Geotechnical Journal, Vol. 27 (1), pp. 151-158.

Robertson, P.K., Sully, J.P., Woeller, D.J., Lunne, T., Powell, J.J.M., and Gillespie, D.G., (1992), "Estimating coefficient of consolidation from piezocone tests", Canadian Geotechnical Journal, 29(4), pp. 551-557.

Roy, M., Tremblay, M., Tavenas, F., and La Rochelle, P. (1980), "Induced pore pressures in static penetration tests in sensitive clay", Proceedings of the 33rd Canadian Geotechnical Conference, Calgary, Preprint Volume, 11.3.1 to 11.3.13.

Roy, M., and LeBlanc, A. (1988), "Factors Affecting the Measurements and Interpretation of the Vane Strength in Soft Sensitive Clays", Vane Shear Strength Testing in Soils: Field and Laboratory Studies, ASTM STP 1014, A.F. Richards, Ed., American Society for Testing and Materials, Philadelphia, pp. 117-128.

Sanglerat, G. (1972), "The penetrometer and soil exploration", Elsevier, Amsterdam, 464 pp.

Schapp, L.J.H and Zuidberg, H.M. (1982), "Mechanical and electrical aspects of the electric cone penetrometer tip", Proceedings of the 2nd European Symposium on Penetration Testing, ESOPT-II, Amsterdam, 2, pp. 841-851, Balkema Pub., Rotterdam.

Schmertmann, J.H. (1974), "Penetration pore pressure effects on quasi-static cone bearing, q_c ", Proceedings of the European Symposium on Penetration Testing, ESOPT, Stockholm, 2.2, pp. 345-351.

Senneset, K., Janbu, N., and Svano, G., (1982), "Strength and deformation parameters from cone penetration tests", Proceedings of the 2nd European Symposium on Penetration Testing, ESOPT-II, Amsterdam, 2, pp. 863-870, Balkema Pub., Rotterdam.

Skempton, A.W., (1948) "Vane Test in the Alluvial Plains of River Firth near Grangemouth", Geotechnique, Vol. 1., No. 2, pp.111-125.

Smits, F.P., (1982) "Penetration pore pressure measured with piezometer cones", Proceedings of the 2nd European Symposium on Penetration Testing, ESOPT-II, Amsterdam, 2, pp.871-876, Balkema Pub., Rotterdam.

Sully, J.P., and Campanella, R.G., (1991), "Effect of lateral stress on CPT penetration pore pressure", Journal of Geotechnical Engineering, ASCE, 117(7), pp. 1082-1088.

Tavenas, F., and Leroueil, S., (1987), "State-of-the-art on laboratory and in situ stress-strain-time behavior of soft clays", Proceedings of the International Symposium on Geotechnical Engineering of Soft Soils, Mexico City, pp. 1-46.

Teh, C.I., and Houlsby, G.T., (1991), "An analytical study of the cone penetration test in clay", Geotechnique, 41(1), pp. 17-34.

Torstensson, B.A. (1975), "Pore Pressure Sounding Instrument", Proceedings of the ASCE Specialty Conference on In Situ Measurement of Soil Properties, Raleigh, North Carolina, 2, pp. 48-54, American Society of Civil Engineers, (ASCE).

Torstensson, B.A., (1977), "Time Dependent Effects in the Field Vane Test", Proceedings of the International Symposium on Soft Clays, Bangkok, 1977, pp. 387-397.

Torstensson, B.A., (1982), "A Combined Pore Pressure and Point Resistance Probe", Proceedings of the 2nd European Symposium on Penetration Testing, ESOPT II, Amsterdam, Vol II, pp. 903-908.

Totani, G., Calabrese, M., Marchetti, S. & Monaco, P. (1997). "Use of in situ flat dilatometer (DMT) for ground characterization in the stability analysis of slopes". Proc. XIV ICSMFE, Hamburg, Vol. 1, pp. 607-610.

Totani, G., Marchetti, S., Monaco, P., and Calabrese, M., (2001), "Use of the Flat Dilatometer Test (DMT) in geotechnical design", IN SITU 2001, International Conference on In Situ Measurement of Soil Properties, Bali, Indonesia.

U.S. Department of Transportation, Federal Highway Administration, "In-Situ Geotechnical Tests", Subsurface Investigations Course: FHWA-NHI-132031, October 2001.

Vermeiden, J. (1948), "Improved sounding apparatus as developed in Holland since 1936", Proceedings of the 2nd International Conference on Soil Mechanics and Foundation Engineering, Rotterdam, 1, pp. 280-287.

Vesic, A.S., (1972), "Expansion of Cavities in Infinite Soil Masses", Journal of Soil Mechanics and Foundation Division, ASCE, Vol. 98, SM3, pp. 265-290.

Vesic, A.S., (1975), "Principles of Pile Foundation Design", Soil Mechanics Series No. 38, Duke University, Durham, NC.

Weddle, T.K., "A General Introduction to the Presumpscot Formation – Maine's 'Blue Clay'", Maine Department of Conservation, Maine Geological Survey, October 2005.

Weisel, C.E., (1973), "Some Factors Influencing In Situ Vane Test Results", Proceedings of the 8th International Conference on Soil Mechanics and Foundation Engineering, Moscow, Vol. 1.2, pp. 475-479.

Wissa, A.E.Z., Martin, R.T., and Garlanger, J.E. (1975), "The piezometer probe", Proceedings of the ASCE Specialty Conference on In Situ Measurement of Soil Properties, Raleigh, North Carolina, 1, pp. 536-545, American Society of Civil Engineers, (ASCE).

Wroth, C.P., (1984), "The interpretation of in situ soil test", 24th Rankine Lecture, Geotechnique, 34(4), pp. 449-489.

Wroth, C.P. (1988), "Penetration Testing – A More Rigorous Approach to Interpretation", Proceedings of the First International Symposium on Penetration Testing, ISOPT-1, Orlando, FL, Vol. 1, pp 303-311.

APPENDICES

APPENDIX A

FIELD SHEAR VANE TEST DATA

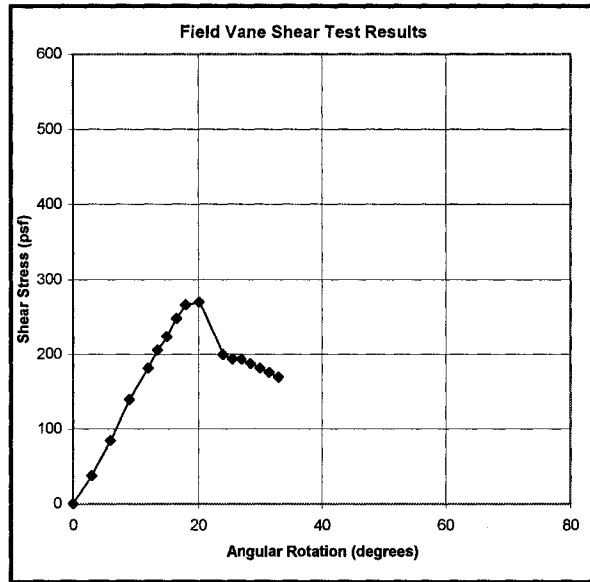
**Regional Waste Systems
Ash/Bale Fill Facility
South Portland, Maine**

University of New Hampshire
Geonor H-10 Vane Borer Testing

Boring No.: B-11
Ground surface elev. (ft): 68.9
Test date: 1/18/2006
Calibr. factor (psf/reading): 12.114

Test No.: 1
Depth to center of vane (ft): 14.0
Elev. to center of vane (ft): 54.9

Time (min)	Instrument Reading	Rotation (degrees)	Shear Stress (psf)
0.0	0.0	0	0.0
0.5	3.1	3	37.6
1.0	7.0	6	84.8
1.5	11.5	9	139.3
2.0	15.0	12	181.7
2.3	17.0	14	205.9
2.5	18.5	15	224.1
2.8	20.5	17	248.3
3.0	22.0	18	266.5
3.4	22.3	20	270.1
4.0	16.5	24	199.9
4.3	16.0	26	193.8
4.5	16.0	27	193.8
4.8	15.5	29	187.8
5.0	15.0	30	181.7
5.3	14.5	32	175.7
5.5	14.0	33	169.6



Elapsed time from insertion to rotation for undisturbed test (min): 5:22
 Calculated undrained shear strength (psf): 270
 Instrument reading for remolded: 2
 Calculated remolded shear strength (psf): 24
 Sensitivity: 11

Vane shape: Rectangular
 Vane height (mm): 130
 Vane diameter (mm): 65
 Vane blade thickness (mm): 2
 Vane rotation rate (degree/sec): 0.1
 Number of revolutions for remolded test: 10

Comments:

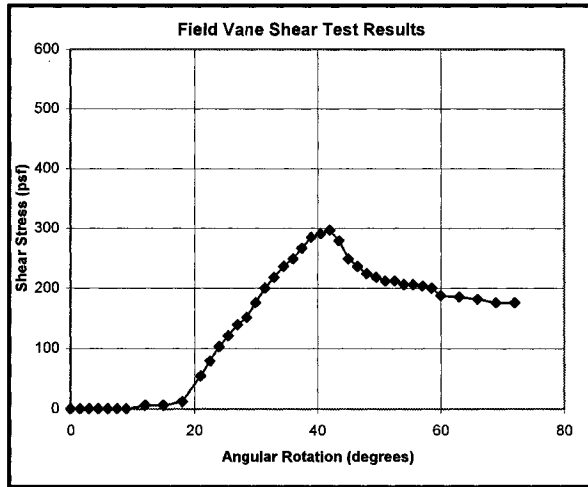
**Regional Waste Systems
Ash/Bale Fill Facility
South Portland, Maine**

University of New Hampshire
Geonor H-10 Vane Borer Testing

Boring No.: B-11
Ground surface elev. (ft): 68.9
Test date: 1/18/2006
Calibr. factor (psf/reading): 12.114

Test No.: 2
Depth to center of vane (ft): 16.5
Elev. to center of vane (ft): 52.4

Time (min)	Instrument Reading	Rotation (degrees)	Shear Stress (psf)
0.0	0.0	0	0.0
0.3	0.0	2	0.0
0.5	0.0	3	0.0
0.8	0.0	5	0.0
1.0	0.0	6	0.0
1.3	0.0	8	0.0
1.5	0.0	9	0.0
2.0	0.5	12	6.1
2.5	0.5	15	6.1
3.0	1.0	18	12.1
3.5	4.5	21	54.5
3.8	6.5	23	78.7
4.0	8.5	24	103.0
4.25	10.0	26	121.1
4.5	11.5	27	139.3
4.8	12.5	29	151.4
5.0	14.5	30	175.7
5.3	16.5	32	199.9
5.5	18.0	33	218.1
5.8	19.5	35	236.2
6.0	20.5	36	248.3
6.3	22.0	38	266.5
6.5	23.5	39	284.7
6.8	24.0	41	290.7
7.0	24.5	42	296.8
7.3	23.0	44	278.6
7.5	20.5	45	248.3
7.8	19.5	47	236.2
8.0	18.5	48	224.1
8.3	18.0	50	218.1
8.5	17.5	51	212.0
8.8	17.5	53	212.0
9.0	17.0	54	205.9
9.3	17.0	56	205.9
9.5	16.8	57	203.5
9.8	16.5	59	199.9
10.0	15.5	60	187.8
10.5	15.3	63	185.3
11.0	15	66	181.7
11.5	14.5	69	175.7
12.0	14.5	72	175.7



Elapsed time from insertion to rotation for undisturbed test (min): 3:00
 Calculated undrained shear strength (psf): 297
 Instrument reading for remolded: 2.25
 Calculated remolded shear strength (psf): 27
 Sensitivity: 11

Vane shape: Rectangular
 Vane height (mm): 130
 Vane diameter (mm): 65
 Vane blade thickness (mm): 2
 Vane rotation rate (degree/sec): 0.1
 Number of revolutions for remolded test: 10

Comments:

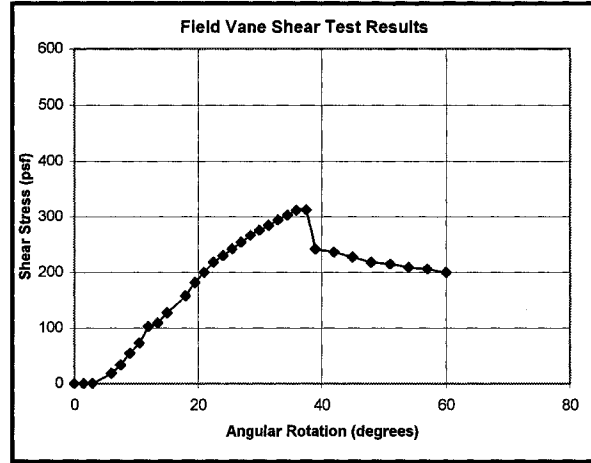
**Regional Waste Systems
Ash/Bale Fill Facility
South Portland, Maine**

University of New Hampshire
Geonor H-10 Vane Borer Testing

Boring No.: B-11
Ground surface elev. (ft): 68.9
Test date: 1/18/2006
Calibr. factor (psf/reading): 12.114

Test No.: 3
Depth to center of vane (ft): 19.0
Elev. to center of vane (ft): 49.9

Time (min)	Instrument Reading	Rotation (degrees)	Shear Stress (psf)
0.0	0.0	0	0.0
0.3	0.0	2	0.0
0.5	0.0	3	0.0
1.0	1.5	6	18.2
1.3	2.8	8	33.3
1.5	4.5	9	54.5
1.8	6.0	11	72.7
2.0	8.5	12	103.0
2.3	9.0	14	109.0
2.5	10.5	15	127.2
3.0	13.0	18	157.5
3.3	15.0	20	181.7
3.50	16.5	21	199.9
3.8	18.0	23	218.1
4.0	19.0	24	230.2
4.3	20.0	26	242.3
4.5	21.0	27	254.4
4.8	22.0	29	266.5
5.0	22.8	30	275.6
5.3	23.5	32	284.7
5.5	24.3	33	293.8
5.8	25.0	35	302.9
6.0	25.8	36	311.9
6.3	25.8	38	312.5
6.5	20.0	39	242.3
7.0	19.5	42	236.2
7.5	18.8	45	227.1
8.0	18.0	48	218.1
8.5	17.8	51	215.0
9.0	17.3	54	209.0
9.5	17.0	57	205.9
10.0	16.5	60	199.9



Elapsed time from insertion to rotation for undisturbed test (min): 3:00
 Calculated undrained shear strength (psf): 313
 Instrument reading for remolded: 3
 Calculated remolded shear strength (psf): 36
 Sensitivity: 9

Vane shape: Rectangular
 Vane height (mm): 130
 Vane diameter (mm): 65
 Vane blade thickness (mm): 2
 Vane rotation rate (degree/sec): 0.1
 Number of revolutions for remolded test: 10

Comments:

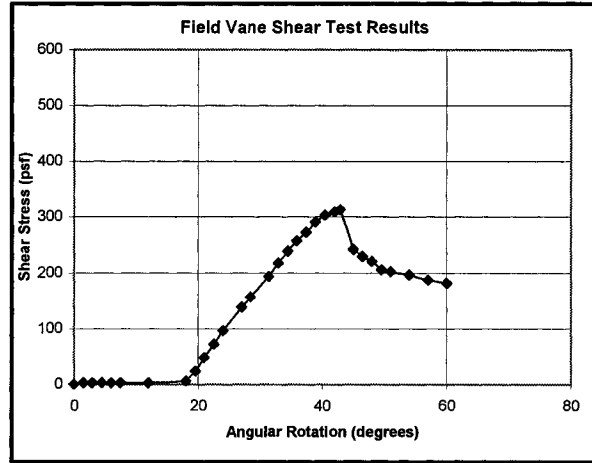
**Regional Waste Systems
Ash/Bale Fill Facility
South Portland, Maine**

University of New Hampshire
Geonor H-10 Vane Borer Testing

Boring No.: B-11
Ground surface elev. (ft): 68.9
Test date: 1/18/2006
Calibr. factor (psf/reading): 12.114

Test No.: 4
Depth to center of vane (ft): 21.5
Elev. to center of vane (ft): 47.4

Time (min)	Instrument Reading	Rotation (degrees)	Shear Stress (psf)
0.0	0.0	0	0.0
0.3	0.3	2	3.0
0.5	0.3	3	3.0
0.8	0.3	5	3.0
1.0	0.3	6	3.0
1.3	0.3	8	3.0
2.0	0.3	12	3.0
3.0	0.5	18	6.1
3.3	2.0	20	24.2
3.5	4.0	21	48.5
3.8	6.0	23	72.7
4.0	8.0	24	96.9
4.50	11.5	27	139.3
4.8	13.0	29	157.5
5.3	16.0	32	193.8
5.5	18.0	33	218.1
5.8	19.8	35	239.3
6.0	21.3	36	257.4
6.3	22.5	38	272.6
6.5	24.0	39	290.7
6.8	25.0	41	302.9
7.0	25.5	42	308.9
7.2	25.8	43	312.5
7.5	20.0	45	242.3
7.8	19.0	47	230.2
8.0	18.3	48	221.1
8.3	17.0	50	205.9
8.5	16.8	51	202.9
9.0	16.3	54	196.9
9.5	15.5	57	187.8
10.0	15.0	60	181.7



Elapsed time from insertion to rotation for undisturbed test (min): 3:00
 Calculated undrained shear strength (psf): 313
 Instrument reading for remolded: 2.8
 Calculated remolded shear strength (psf): 34
 Sensitivity: 9

Vane shape: Rectangular
 Vane height (mm): 130
 Vane diameter (mm): 65
 Vane blade thickness (mm): 2
 Vane rotation rate (degree/sec): 0.1
 Number of revolutions for remolded test: 10

Comments:

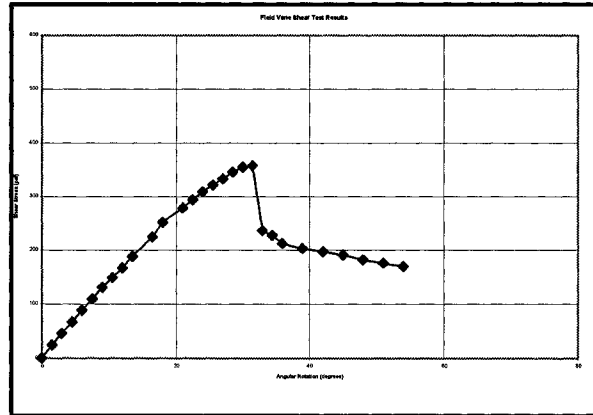
**Regional Waste Systems
Ash/Bale Fill Facility
South Portland, Maine**

University of New Hampshire
Geonor H-10 Vane Borer Testing

Boring No.: B-11
Ground surface elev. (ft): 68.9
Test date: 1/18/2006
Calibr. factor (psf/reading): 12.114

Test No.: 5
Depth to center of vane (ft): 24.0
Elev. to center of vane (ft): 44.9

Time (min)	Instrument Reading	Rotation (degrees)	Shear Stress (psf)
0.0	0.0	0	0.0
0.3	2.0	2	24.2
0.5	3.8	3	45.4
0.8	5.5	5	66.6
1.0	7.3	6	87.8
1.3	9.0	8	109.0
1.5	10.8	9	130.2
1.8	12.3	11	148.4
2.0	13.8	12	166.6
2.3	15.5	14	187.8
2.8	18.5	17	224.1
3.00	20.8	18	251.4
3.5	23.0	21	278.6
3.8	24.3	23	293.8
4.0	25.5	24	308.9
4.3	26.5	26	321.0
4.5	27.5	27	333.1
4.8	28.5	29	345.2
5.0	29.3	30	354.3
5.3	29.5	32	357.4
5.5	19.5	33	236.2
5.8	18.8	35	227.1
6.0	17.5	36	212.0
6.5	16.8	39	202.9
7.0	16.3	42	196.9
7.5	15.8	45	190.8
8.0	15.0	48	181.7
8.5	14.5	51	175.7
9.0	14.0	54	169.6



Elapsed time from insertion to rotation for undisturbed test (min): 5:30
 Calculated undrained shear strength (psf): 357
 Instrument reading for remolded: 2.5
 Calculated remolded shear strength (psf): 30
 Sensitivity: 12

Vane shape: Rectangular
 Vane height (mm): 130
 Vane diameter (mm): 65
 Vane blade thickness (mm): 2
 Vane rotation rate (degree/sec): 0.1
 Number of revolutions for remolded test: 10

Comments:

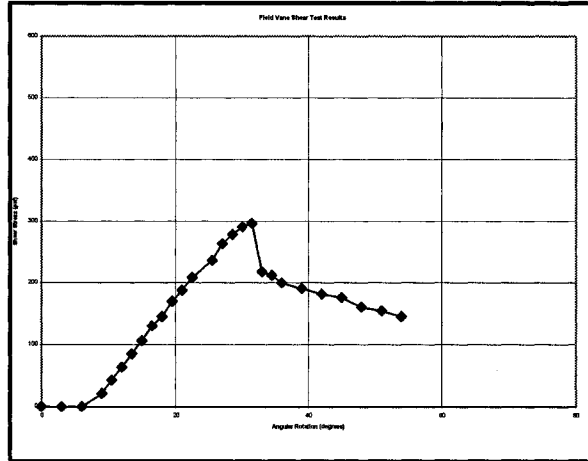
**Regional Waste Systems
Ash/Bale Fill Facility
South Portland, Maine**

University of New Hampshire
Geonor H-10 Vane Borer Testing

Boring No.: B-11
Ground surface elev. (ft): 68.9
Test date: 1/18/2006
Calibr. factor (psf/reading): 12.114

Test No.: 6
Depth to center of vane (ft): 26.5
Elev. to center of vane (ft): 42.4

Time (min)	Instrument Reading	Rotation (degrees)	Shear Stress (psf)
0.0	0.0	0	0.0
0.5	0.0	3	0.0
1.0	0.0	6	0.0
1.5	1.8	9	21.2
1.8	3.5	11	42.4
2.0	5.3	12	63.6
2.3	7.0	14	84.8
2.5	8.8	15	106.0
2.8	10.8	17	130.2
3.0	12.0	18	145.4
3.3	14.0	20	169.6
3.5	15.5	21	187.8
3.8	17.3	23	209.0
4.25	19.5	26	236.2
4.5	21.8	27	263.5
4.8	23.0	29	278.6
5.0	24.0	30	290.7
5.3	24.5	32	296.8
5.5	18.0	33	218.1
5.8	17.5	35	212.0
6.0	16.5	36	199.9
6.5	15.8	39	190.8
7.0	15.0	42	181.7
7.5	14.5	45	175.7
8.0	13.3	48	160.5
8.5	12.8	51	154.5
9.0	12.0	54	145.4



Elapsed time from insertion to rotation for undisturbed test (min): 1:45
 Calculated undrained shear strength (psf): 297
 Instrument reading for remolded: 2.75
 Calculated remolded shear strength (psf): 33
 Sensitivity: 9

Vane shape: Rectangular
 Vane height (mm): 130
 Vane diameter (mm): 65
 Vane blade thickness (mm): 2
 Vane rotation rate (degree/sec): 0.1
 Number of revolutions for remolded test: 10

Comments:

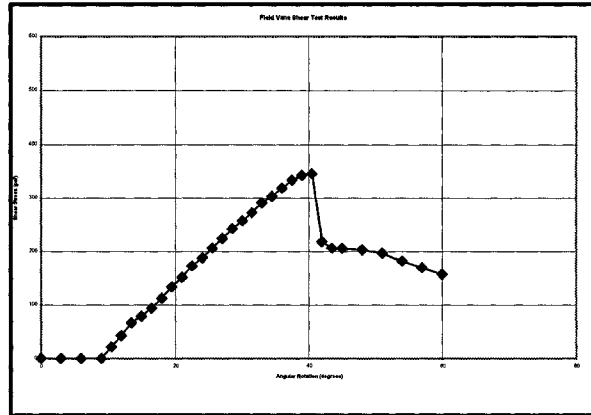
**Regional Waste Systems
Ash/Bale Fill Facility
South Portland, Maine**

University of New Hampshire
Geonor H-10 Vane Borer Testing

Boring No.: B-11
Ground surface elev. (ft): 68.9
Test date: 1/18/2006
Calibr. factor (psf/reading): 12.114

Test No.: 7
Depth to center of vane (ft): 29.0
Elev. to center of vane (ft): 39.9

Time (min)	Instrument Reading	Rotation (degrees)	Shear Stress (psf)
0.0	0.0	0	0.0
0.5	0.0	3	0.0
1.0	0.0	6	0.0
1.5	0.0	9	0.0
1.8	1.8	11	21.2
2.0	3.5	12	42.4
2.3	5.5	14	66.6
2.5	6.5	15	78.7
2.8	7.8	17	93.9
3.0	9.3	18	112.1
3.3	11.0	20	133.3
3.50	12.5	21	151.4
3.8	14.3	23	172.6
4.0	15.5	24	187.8
4.3	17.0	26	205.9
4.5	18.5	27	224.1
4.8	20.0	29	242.3
5.0	21.3	30	257.4
5.3	22.5	32	272.6
5.5	24.0	33	290.7
5.8	25.0	35	302.9
6.0	26.3	36	318.0
6.3	27.5	38	333.1
6.5	28.3	39	342.2
6.8	28.5	41	345.2
7.0	18.0	42	218.1
7.3	17.0	44	205.9
7.5	17.0	45	205.9
8.0	16.8	48	202.9
8.5	16.3	51	196.9
9.0	15.0	54	181.7
9.5	14.0	57	169.6
10.0	13.0	60	157.5



Elapsed time from insertion to rotation for undisturbed test (min): 2:00
 Calculated undrained shear strength (psf): 345
 Instrument reading for remolded: 2
 Calculated remolded shear strength (psf): 24
 Sensitivity: 14

Vane shape: Rectangular
 Vane height (mm): 130
 Vane diameter (mm): 65
 Vane blade thickness (mm): 2
 Vane rotation rate (degree/sec): 0.1
 Number of revolutions for remolded test: 10

Comments:

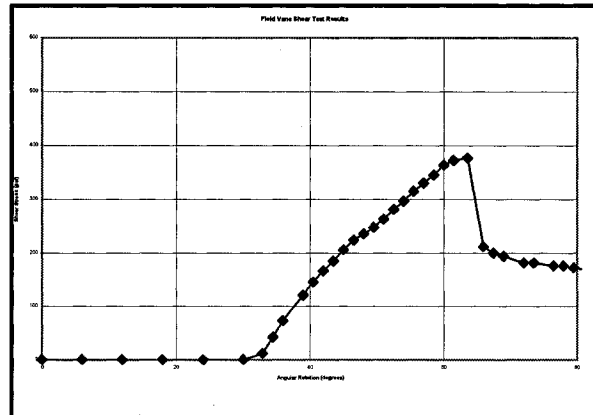
**Regional Waste Systems
Ash/Bale Fill Facility
South Portland, Maine**

University of New Hampshire
Geonor H-10 Vane Borer Testing

Boring No.: B-11
Ground surface elev. (ft): 68.9
Test date: 1/18/2006
Calibr. factor (psf/reading): 12.114

Test No.: 8
Depth to center of vane (ft): 31.5
Elev. to center of vane (ft): 37.4

Time (min)	Instrument Reading	Rotation (degrees)	Shear Stress (psf)
0.0	0.0	0	0.0
1.0	0.0	6	0.0
2.0	0.0	12	0.0
3.0	0.0	18	0.0
4.0	0.0	24	0.0
5.0	0.0	30	0.0
5.5	1.0	33	12.1
5.8	3.5	35	42.4
6.0	6.0	36	72.7
6.5	10.0	39	121.1
6.8	12.0	41	145.4
7.0	13.8	42	166.6
7.3	15.3	44	184.7
7.5	17.0	45	205.9
7.8	18.5	47	224.1
8.0	19.5	48	236.2
8.3	20.5	50	248.3
8.5	21.8	51	263.5
8.8	23.3	53	281.7
9.0	24.5	54	296.8
9.3	26.0	56	315.0
9.5	27.3	57	330.1
9.8	28.5	59	345.2
10.0	30.0	60	363.4
10.3	30.8	62	372.5
10.6	31.1	64	376.7
11.0	17.5	66	212.0
11.3	16.5	68	199.9
11.5	16.0	69	193.8
12.0	15.0	72	181.7
12.3	15.0	74	181.7
12.8	14.5	77	175.7
13.0	14.5	78	175.7
13.3	14.3	80	172.6
13.5	14	81	169.6



Elapsed time from insertion to rotation for undisturbed test (min): 5:00
 Calculated undrained shear strength (psf): 377
 Instrument reading for remolded: 3.1
 Calculated remolded shear strength (psf): 38
 Sensitivity: 10

Vane shape: Rectangular
 Vane height (mm): 130
 Vane diameter (mm): 65
 Vane blade thickness (mm): 2
 Vane rotation rate (degree/sec): 0.1
 Number of revolutions for remolded test: 10

Comments: Gritty feeling when cranking

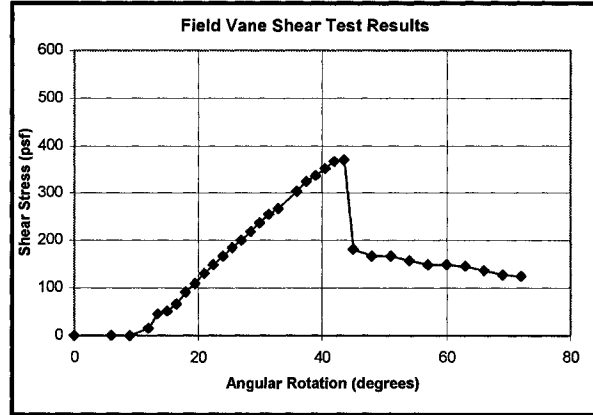
**Regional Waste Systems
Ash/Bale Fill Facility
South Portland, Maine**

University of New Hampshire
Geonor H-10 Vane Borer Testing

Boring No.: B-11
Ground surface elev. (ft): 68.9
Test date: 1/18/2006
Calibr. factor (psf/reading): 12.114

Test No.: 9
Depth to center of vane (ft): 33.9
Elev. to center of vane (ft): 35.0

Time (min)	Instrument Reading	Rotation (degrees)	Shear Stress (psf)
0.0	0.0	0	0.0
1.0	0.0	6	0.0
1.5	0.0	9	0.0
2.0	1.3	12	15.1
2.3	3.8	14	45.4
2.5	4.3	15	51.5
2.8	5.5	17	66.6
3.0	7.5	18	90.9
3.3	9.0	20	109.0
3.5	10.8	21	130.2
3.8	12.3	23	148.4
4.0	13.8	24	166.6
4.3	15.3	26	184.7
4.5	16.5	27	199.9
4.8	18.0	29	218.1
5.0	19.5	30	236.2
5.3	21.0	32	254.4
5.5	22.0	33	266.5
6.0	25.0	36	302.9
6.3	26.8	38	324.0
6.5	27.8	39	336.2
6.8	29.0	41	351.3
7.0	30.3	42	366.4
7.3	30.5	44	369.5
7.5	15.0	45	181.7
8.0	13.8	48	166.6
8.5	13.8	51	166.6
9.0	13.0	54	157.5
9.5	12.3	57	148.4
10.0	12.3	60	148.4
10.5	12.0	63	145.4
11.0	11.3	66	136.3
11.5	10.5	69	127.2
12.0	10.3	72	124.2



Elapsed time from insertion to rotation for undisturbed test (min): 3:00
 Calculated undrained shear strength (psf): 369
 Instrument reading for remolded: 2.5
 Calculated remolded shear strength (psf): 30
 Sensitivity: 12

Vane shape: Rectangular
 Vane height (mm): 130
 Vane diameter (mm): 65
 Vane blade thickness (mm): 2
 Vane rotation rate (degree/sec): 0.1
 Number of revolutions for remolded test: 10

Comments: Hard layer encountered approx. 6-12" after start of vane push.
 Pushed through to soft clay.

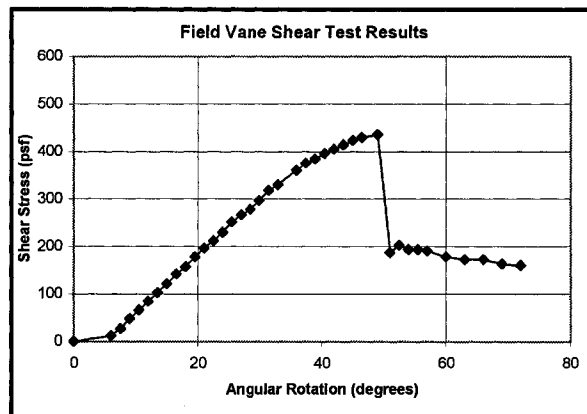
**Regional Waste Systems
Ash/Bale Fill Facility
South Portland, Maine**

University of New Hampshire
Geonor H-10 Vane Borer Testing

Boring No.: B-11
Ground surface elev. (ft): 68.9
Test date: 1/18/2006
Calibr. factor (psf/reading): 12.114

Test No.: 10
Depth to center of vane (ft): 36.4
Elev. to center of vane (ft): 32.5

Time (min)	Instrument Reading	Rotation (degrees)	Shear Stress (psf)
0.0	0.0	0	0.0
1.0	1.0	6	12.1
1.3	2.3	8	27.3
1.5	4.0	9	48.5
1.8	5.5	11	66.6
2.0	7.0	12	84.8
2.3	8.5	14	103.0
2.5	10.0	15	121.1
2.8	11.8	17	142.3
3.0	13.0	18	157.5
3.3	14.8	20	178.7
3.5	16.3	21	196.9
3.8	17.5	23	212.0
4.0	19.0	24	230.2
4.3	20.8	26	251.4
4.5	22.0	27	266.5
4.8	23.0	29	278.6
5.0	24.5	30	296.8
5.3	26.3	32	318.0
5.5	27.3	33	330.1
6.0	29.8	36	360.4
6.3	31.0	38	375.5
6.5	31.8	39	384.6
6.8	32.8	41	396.7
7.0	33.5	42	405.8
7.3	34.3	44	414.9
7.5	35.0	45	424.0
7.8	35.5	47	430.0
8.2	36.0	49	436.1
8.5	15.5	51	187.8
8.8	16.8	53	202.9
9.0	16.0	54	193.8
9.3	16.0	56	193.8
9.5	15.8	57	190.8
10.0	14.8	60	178.7
10.5	14.3	63	172.6
11.0	14.3	66	172.6
11.5	13.5	69	163.5
12.0	13.3	72	160.5



Elapsed time from insertion to rotation for undisturbed test (min): 4:00
 Calculated undrained shear strength (psf): 436
 Instrument reading for remolded: 4.75
 Calculated remolded shear strength (psf): 58
 Sensitivity: 8

Vane shape: Rectangular
 Vane height (mm): 130
 Vane diameter (mm): 65
 Vane blade thickness (mm): 2
 Vane rotation rate (degree/sec): 0.1
 Number of revolutions for remolded test: 10

Comments: Probable sand lense 15-18" from bottom of vane borer

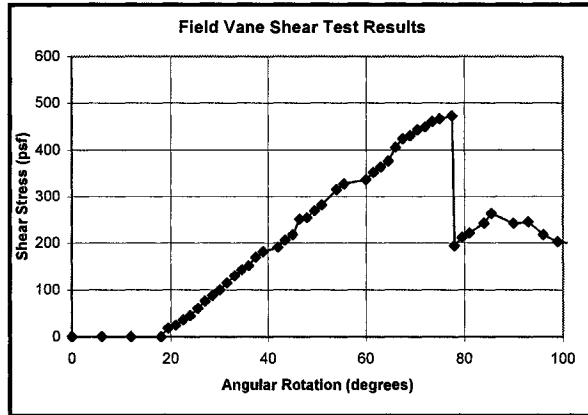
**Regional Waste Systems
Ash/Bale Fill Facility
South Portland, Maine**

University of New Hampshire
Geonor H-10 Vane Borer Testing

Boring No.: B-11
Ground surface elev. (ft): 68.9
Test date: 1/18/2006
Calibr. factor (psf/reading): 12.114

Test No.: 11
Depth to center of vane (ft): 38.8
Elev. to center of vane (ft): 30.1

Time (min)	Instrument Reading	Rotation (degrees)	Shear Stress (psf)
0.0	0.0	0	0.0
1.0	0.0	6	0.0
2.0	0.0	12	0.0
3.0	0.0	18	0.0
3.3	1.5	20	18.2
3.5	2.0	21	24.2
3.8	3.0	23	36.3
4.0	3.8	24	45.4
4.3	5.0	26	60.6
4.5	6.3	27	75.7
4.8	7.3	29	87.8
5.0	8.3	30	99.9
5.3	9.5	32	115.1
5.5	10.8	33	130.2
5.8	11.8	35	142.3
6.0	12.5	36	151.4
6.3	14.0	38	169.6
6.5	15.0	39	181.7
7.0	15.8	42	190.8
7.3	17.0	44	205.9
7.5	18.0	45	218.1
7.8	20.8	47	251.4
8.0	21.0	48	254.4
8.3	22.3	50	269.5
8.5	23.3	51	281.7
9.0	26.0	54	315.0
9.3	27.0	56	327.1
10.0	27.8	60	336.2
10.3	29.0	62	351.3
10.5	30.0	63	363.4
10.8	31.0	65	375.5
11.0	33.5	66	405.8
11.3	35.0	68	424.0
11.5	35.5	69	430.0
11.8	36.5	71	442.2
12.0	37.0	72	448.2
12.3	38.0	74	460.3
12.5	38.5	75	466.4
12.9	39.0	78	472.4
13.0	16.0	78	193.8
13.3	17.5	80	212.0
13.5	18.3	81	221.1
14.0	20.0	84	242.3
14.3	21.8	86	263.5
15.0	20.0	90	242.3
15.5	20.3	93	245.3
16.0	18.0	96	218.1
16.5	16.8	99	202.9
17.0	16.5	102	199.9



Elapsed time from insertion to rotation for undisturbed test (min): 2:00
 Calculated undrained shear strength (psf): 472
 Instrument reading for remolded: 4.25
 Calculated remolded shear strength (psf): 51
 Sensitivity: 9

Vane shape: Rectangular
 Vane height (mm): 130
 Vane diameter (mm): 65
 Vane blade thickness (mm): 2
 Vane rotation rate (degree/sec): 0.1
 Number of revolutions for remolded test: 10

Comments: Probable sand lense 15-18" from bottom of vane borer

APPENDIX B

CALIBRATION OF THE VANE APPARATUS

A check of previous calibrations of the torque measuring head of the vane shear apparatus was most recently conducted in the fall of 2005 in the laboratory using a device similar to that shown in Figure B.1. Use of the apparatus was minimal in the period between the calibration and use at the RWS facility, and a check of the calibration was deemed unnecessary for this testing program.

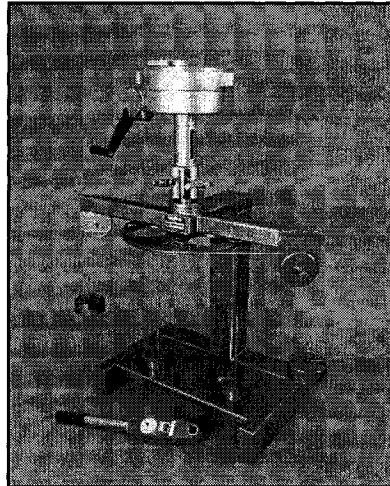


Figure B.1 - Geonor H-10 Calibration Equipment (Geonor, Inc.)

The calibration is performed by attaching the torque measuring head to an aluminum disc with a known diameter that is supported by the frame of the calibration equipment. A thin wire is attached at opposite ends of the disc, and is threaded through a pulley system. Weight is then suspended from the wire and the reading on the torque head is noted along with the calculated torque applied. Several measurements are made through the range of the Geonor H-10 equipment and plotted with a linear trend line. Based on this trend line the calibration factor used for the vane shear apparatus during this testing program was 0.580 kPa per dial increment on the torque measuring head. This value is based on a best fit line applied to the instrument readings less than 40. Over the full range of the equipment

the calibration factor was found to be 0.603 kPa per dial increment; however the calibration factor for the lower range of the instrument was used due to the soft nature of the clays at the RWS site. Previous calibrations of the equipment in 1994 and 2002 resulted in factors varying between 0.575 and 0.591 kPa per increment for the instrument range of 0 to 100.

APPENDIX C

CALIBRATION OF THE PIEZOCONE

In order to convert the piezocone sensor outputs into load and pressure values the probe was calibrated in the laboratory. Although the manufacturer supplied a calibration report correlating the sensor output voltages to engineering units, a check on this calibration was performed on the new cone penetrometer using an Instron Model 1350 loading machine with a 90 kN capacity. In addition a Geotest Strain Controlled Load Frame, Model S5710 with a 4.5kN capacity load cell (Figure C.1) was used to test the lower range output from the friction sleeve. The pore pressure transducer was spot checked against the manufacturer calibration report using a water column 1.22 meters in height.

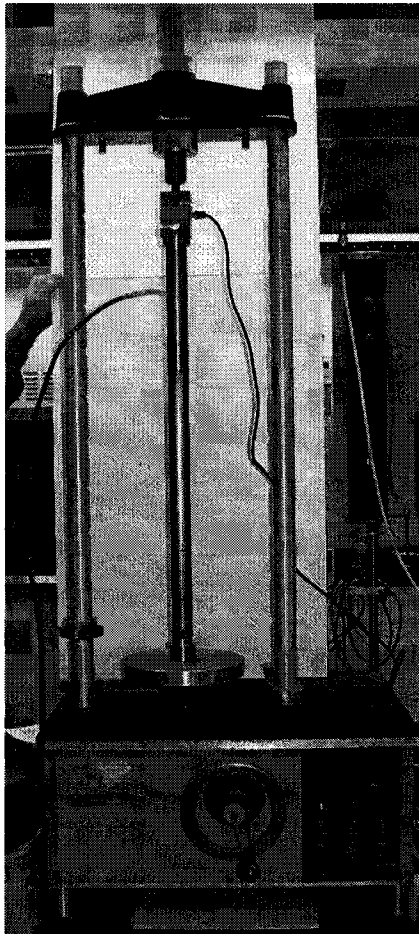


Figure C.1 - Geotest S5710 Load Frame with Piezocone

To check the calibration of the point and sleeve load cells the probe was fully assembled, less the saturation fluid and was powered for 20 minutes to allow sensors to stabilize. The complete data acquisition system was used during the testing. A stainless steel adaptor, as seen in Figure C.2, was machined to support the cone and apply loads through the tip only. Loads were then applied at approximately 5.34 kN increments up to the maximum test load, and then back to zero in similar increments. The check of the friction sleeve load cell is performed in a similar manner. The cone tip and filter element are removed during this test while a second stainless steel adaptor, as seen in Figure C.3 supports and loads the friction sleeve. Loads were applied in 2.22 kN increments to 90 percent of the maximum friction sleeve load cell capacity. The probe was then unloaded in similar increments back to zero load.

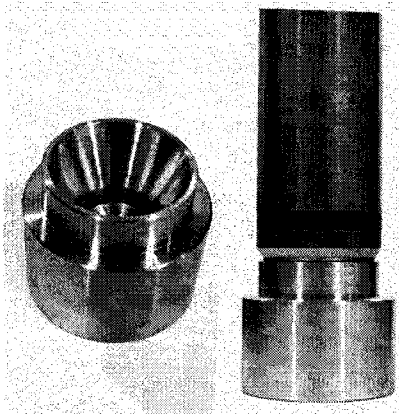


Figure C.2 - Cone Tip Support for Laboratory Loading

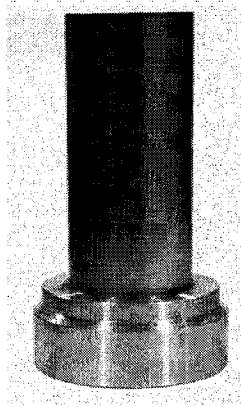


Figure C.3 - Friction Sleeve Support for Laboratory Loading

Results from each of the load cell calibration checks are plotted alongside the manufacturer calibration data in Figures C.4 and C.5. A linear best fit curve was applied to both data sets, which reveal that the calibration data supplied by the manufacturer is accurate. In addition the manufacturers' crosstalk data is presented in Figure C.6. Crosstalk is defined as the effect of the tip pressure on the friction sleeve output. While the crosstalk was not checked in the lab, it was accounted for during data reduction.

The pore pressure transducer did not receive a full check of the calibration data provided by the manufacturer. Instead the system was checked in a 1.22 meter column of water for a good response to the change in pore pressure, indicating saturation of the hydraulic circuit between the pressure transducer and the filter element. The probe was held at mid-depth and full depth of the column repeatedly, and the calculated water pressure was compared to the output from the cone, incorporating the manufacturers' calibration equation. Though this method does not test the full range of the pressure transducer, the piezocone output closely matched

the calculated pressure. The manufacturers' calibration data, with a linear best fit curve is presented in Figure C.7.

Piezocone Point Load Cell Calibration

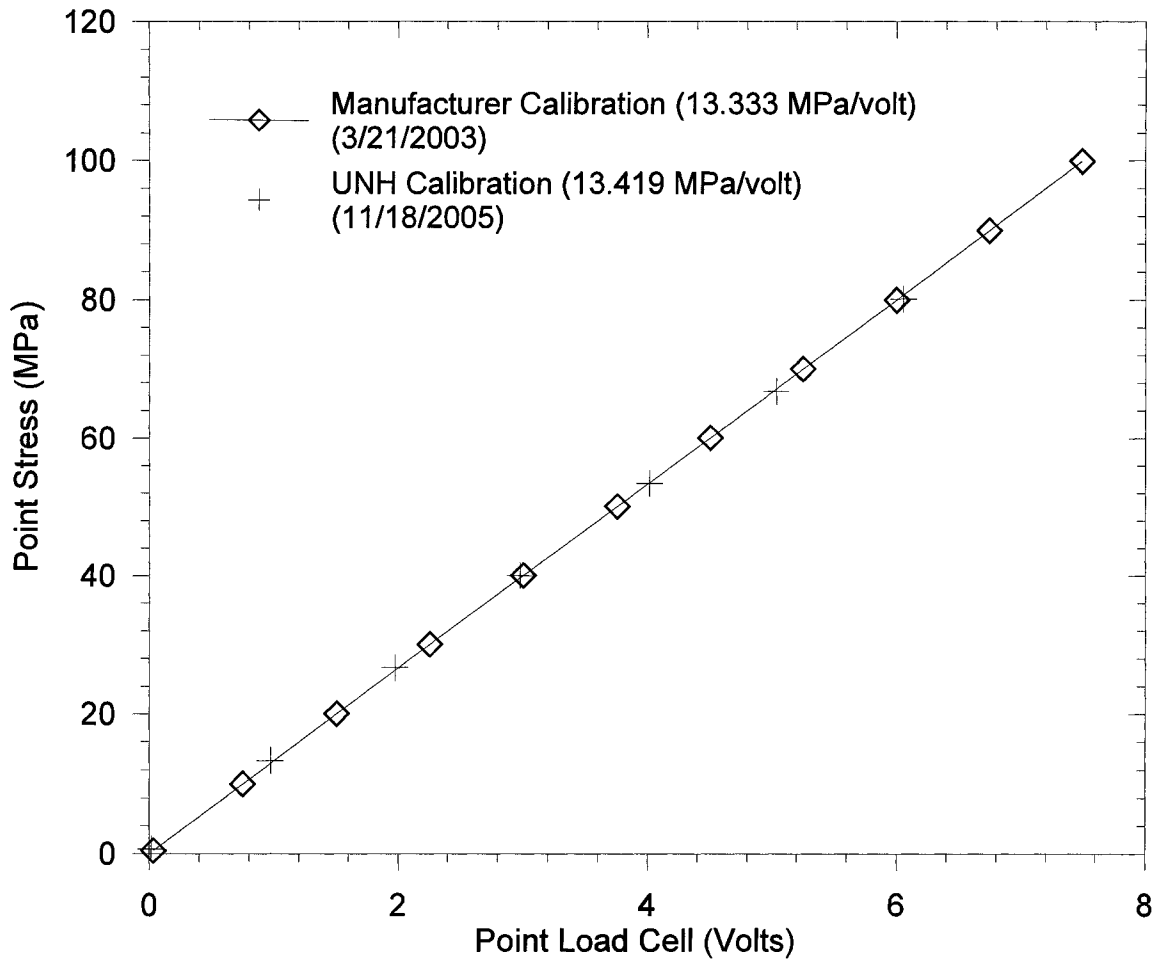


Figure C.4 – Point Load Cell Calibration

Piezocone Sleeve Load Cell Calibration

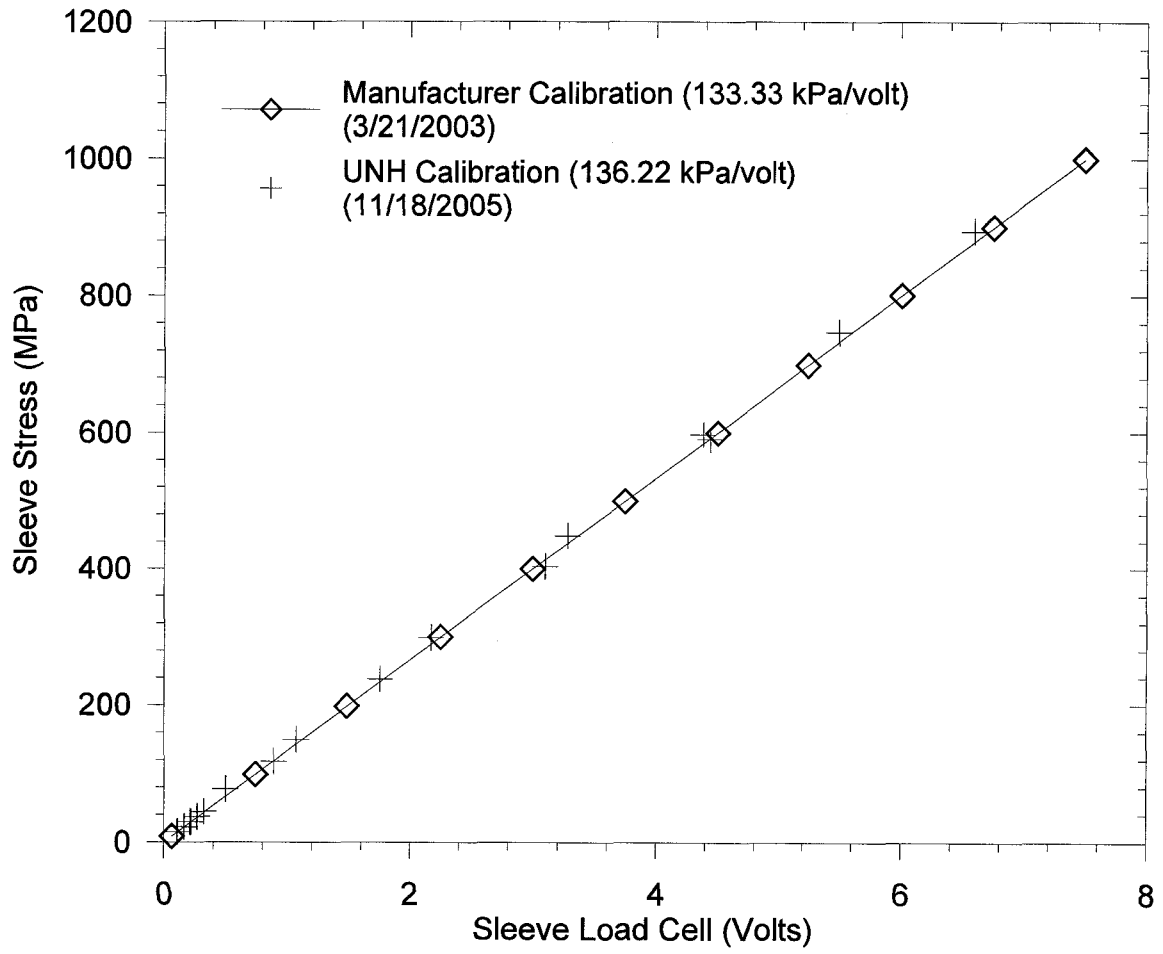


Figure C.5 – Friction Sleeve Load Cell Calibration

Crosstalk (Effect of Tip Load on Friction Measurements)

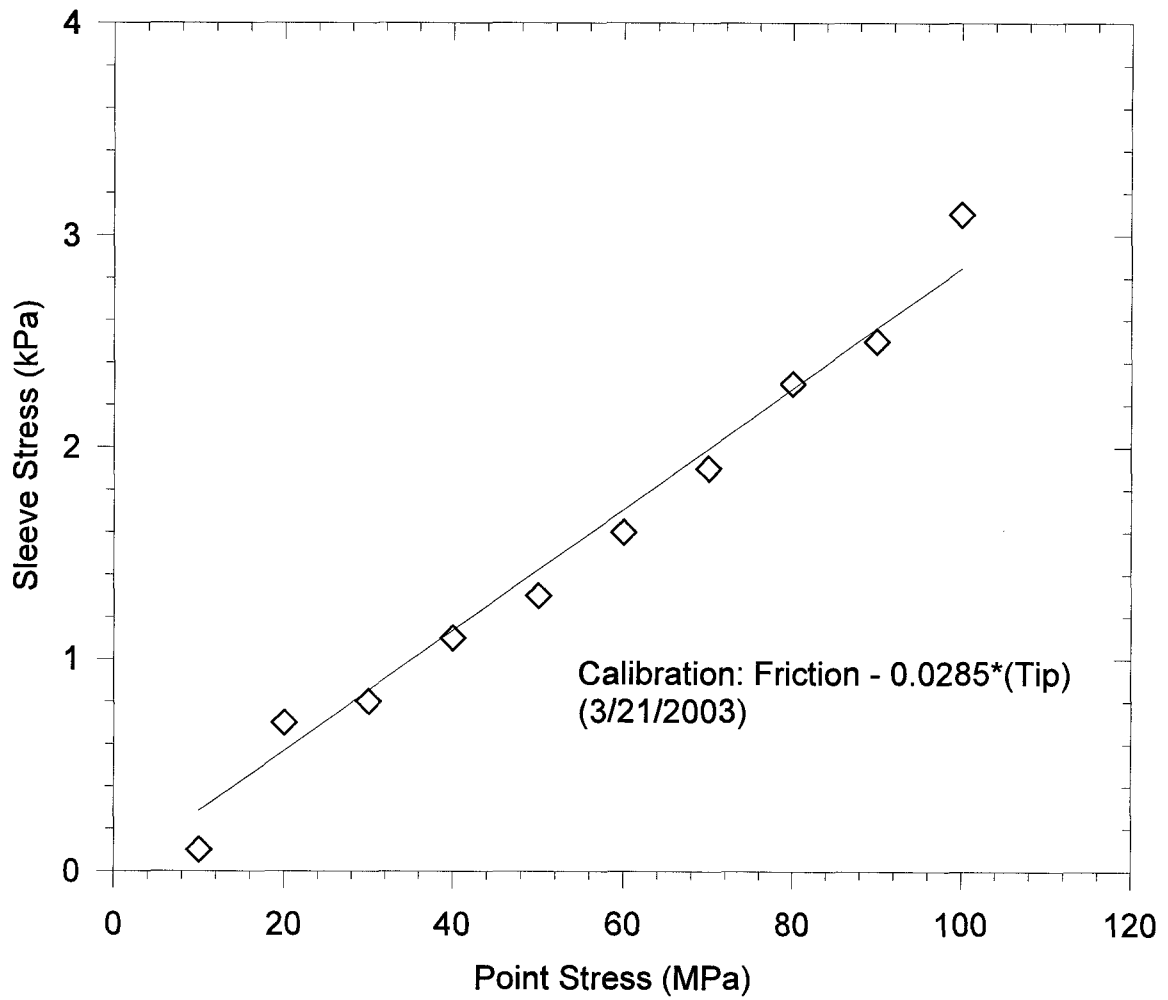


Figure C.6 – Effect of Tip Resistance on Friction Sleeve Load Cell

Piezocone Pore Pressure Transducer Calibration

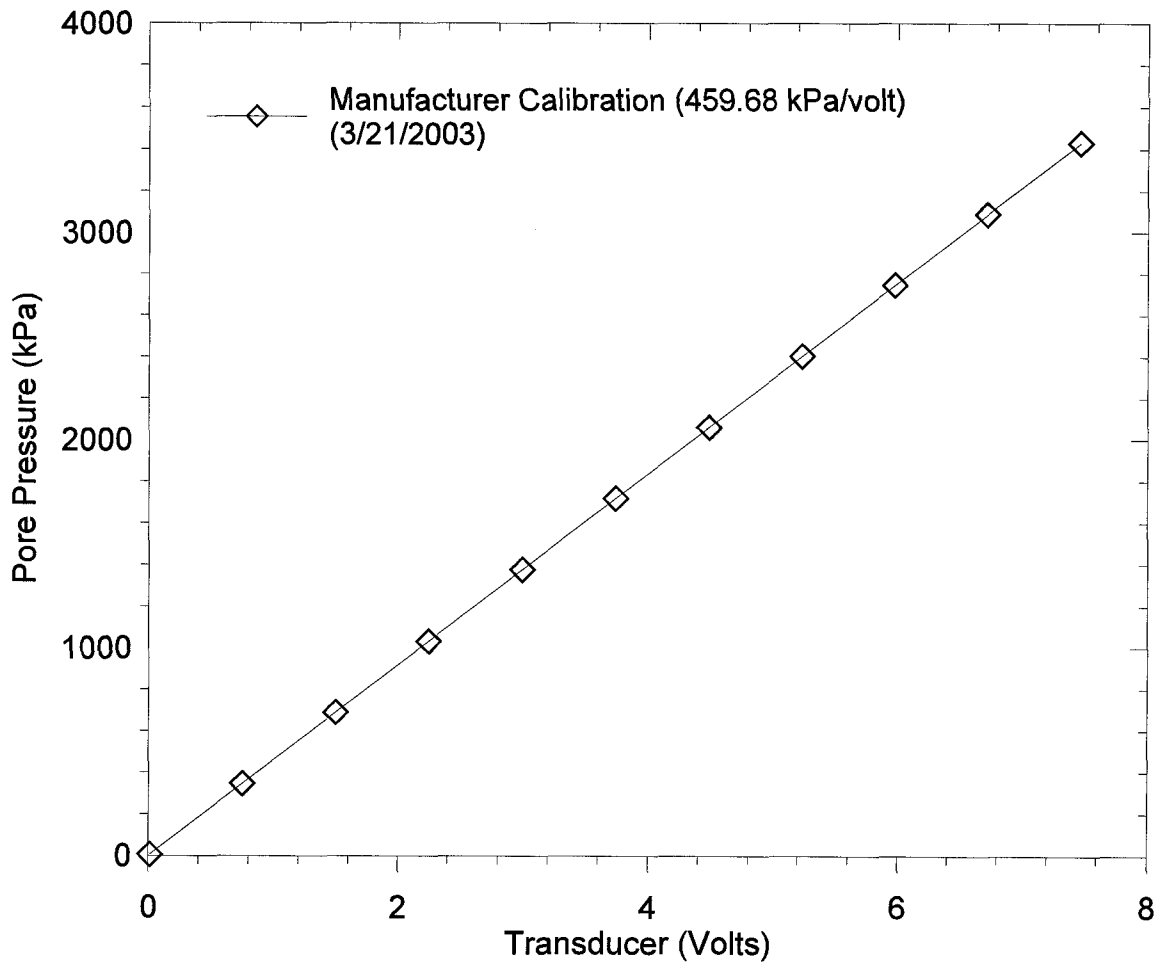


Figure C.7 – Pore Pressure Transducer Calibration

APPENDIX D

PLAXIS MATERIAL PROPERTIES

Table D.1 – Plaxis Material Cluster Properties

Layer Name ⁽¹⁾	Soil Model ⁽¹⁾	Drained or Undrained Behavior	OCR	k_s	Unsaturated Unit Weight (kN/m ³)	Saturated Unit Weight (kN/m ³)	Horizontal Permeability [k _v] (cm/sec)	Vertical Permeability [k _v] (cm/sec)	Compression Index [C _c]	Recompression Index [C _r]	Initial Void Ratio [e]	Undrained Shear Strength (kPa)	Friction Angle [φ]	Dilatancy Angle [ψ]	Young's Modulus [E] (kPa)	Poisson's Ratio [ν]
Stiff Clay Crust	Soft Soil Model	Undrained	8	2	17.3	17.3	3.39E-07	1.04E-07	0.59	0.015	0.85	143.6	10	2	-	-
Glacial Till	Mohr-Coulomb	Undrained	-	-	18.9	19.7	1.41E-06	1.41E-06	-	-	-	21.5	35	0	22408	0.35
Glacial Sand	Mohr-Coulomb	Drained	-	-	18.1	18.1	3.00E-05	3.00E-05	-	-	-	0.5	35	0	22408	0.4
Drainage Sand	Mohr-Coulomb	Drained	-	-	18.1	18.1	1.76E-02	1.76E-02	-	-	-	0.5	35	0	22408	0.4
Ash	Mohr-Coulomb	Drained	-	-	Varies	Varies	1.50E-04	1.50E-04	-	-	-	0.5	43	0	12410	0.35
NS-1(B-10)	SSM	Undrained	4	1.8	17.2	17.2	8.01E-07	6.39E-08	0.845	0.03	1.60	16.6	5	0	-	-
NS-2(B-10)	SSM	Undrained	2.5	1.2	17.2	17.2	8.01E-07	6.39E-08	0.845	0.03	1.60	13.8	5	0	-	-
NS-3(B-10)	SSM	Undrained	1.45	0.92	17.2	17.2	8.01E-07	6.39E-08	0.845	0.03	1.48	12.4	5	0	-	-
NS-4(B-10)	SSM	Undrained	1.3	0.65	17.2	17.2	8.01E-07	6.39E-08	0.845	0.03	1.37	14.4	5	0	-	-
NS-5(B-10)	SSM	Undrained	1.326	0.5	17.2	17.2	8.01E-07	6.39E-08	0.845	0.03	1.32	13.2	5	0	-	-
NS-A	SSM	Undrained	1.23	0.55	17.2	17.2	8.01E-07	6.39E-08	0.845	0.03	1.34	15.7	5	0	-	-
NS-B	SSM	Undrained	1.2	0.55	17.2	17.2	8.01E-07	6.39E-08	0.845	0.03	1.33	20.6	5	0	-	-
NS-C	SSM	Undrained	1.35	0.55	17.2	17.2	8.01E-07	6.39E-08	0.845	0.03	1.34	25.6	5	0	-	-
NS-D	SSM	Undrained	1.41	0.55	17.2	17.2	8.01E-07	6.39E-08	0.845	0.03	1.35	30.6	5	0	-	-
NS-E	SSM	Undrained	1.55	0.55	17.2	17.2	8.01E-07	6.39E-08	0.845	0.03	1.36	33.0	5	0	-	-
NS-1(B-11)	SSM	Undrained	4	1.3	17.2	17.2	8.01E-07	6.39E-08	0.845	0.03	1.30	20.8	5	0	-	-
NS-2(B-11)	SSM	Undrained	2.5	1.12	17.2	17.2	8.01E-07	6.39E-08	0.845	0.03	1.58	16.5	5	0	-	-
NS-3(B-11)	SSM	Undrained	2	0.88	17.2	17.2	8.01E-07	6.39E-08	0.845	0.03	1.55	14.4	5	0	-	-
NS-4(B-11)	SSM	Undrained	1.5	0.7	17.2	17.2	8.01E-07	6.39E-08	0.845	0.03	1.47	15.8	5	0	-	-
NS-5(B-11)	SSM	Undrained	1.23	0.6	17.2	17.2	8.01E-07	6.39E-08	0.845	0.03	1.45	17.2	5	0	-	-
NS-6(B-11)	SSM	Undrained	1.326	0.55	17.2	17.2	8.01E-07	6.39E-08	0.845	0.03	1.43	18.4	5	0	-	-
NS-7(B-11)	SSM	Undrained	1.38	0.55	17.2	17.2	8.01E-07	6.39E-08	0.845	0.03	1.32	21.5	5	0	-	-
EW-Top-1	SSM	Undrained	4	1.8	17.2	17.2	8.01E-07	6.39E-08	0.845	0.03	1.34	17.2	5	0	-	-
EW-Top-2	SSM	Undrained	2.5	1.1	17.2	17.2	8.01E-07	6.39E-08	0.845	0.03	1.55	14.4	5	0	-	-
EW-Top-3	SSM	Undrained	1.6	0.85	17.2	17.2	8.01E-07	6.39E-08	0.845	0.03	1.394	13.2	5	0	-	-
EW-Top-4	SSM	Undrained	1.3	0.68	17.2	17.2	8.01E-07	6.39E-08	0.845	0.03	1.37	12.0	5	0	-	-
EW-Bot-1	SSM	Undrained	1.42	0.55	17.2	17.2	8.01E-07	6.39E-08	0.845	0.03	1.33	16.5	5	0	-	-
EW-Bot-2	SSM	Undrained	1.44	0.55	17.2	17.2	8.01E-07	6.39E-08	0.845	0.03	1.357	18.0	5	0	-	-
EW-Bot-3	SSM	Undrained	1.46	0.55	17.2	17.2	8.01E-07	6.39E-08	0.845	0.03	1.36	21.5	5	0	-	-
EW-Bot-4	SSM	Undrained	1.5	0.55	17.2	17.2	8.01E-07	6.39E-08	0.845	0.03	1.37	23.9	5	0	-	-
EW-Bot-5	SSM	Undrained	1.7	0.55	17.2	17.2	8.01E-07	6.39E-08	0.845	0.03	1.38	32.3	5	0	-	-
EW-P3-1	SSM	Undrained	1.25	0.55	17.2	17.2	8.01E-07	6.39E-08	0.845	0.03	1.4	13.2	5	0	-	-
EW-P3-2	SSM	Undrained	1.2	0.55	17.2	17.2	8.01E-07	6.39E-08	0.845	0.03	1.325	18.0	5	0	-	-
EW-P3-3	SSM	Undrained	1.25	0.55	17.2	17.2	8.01E-07	6.39E-08	0.845	0.03	1.352	19.9	5	0	-	-
EW-P3-4	SSM	Undrained	1.38	0.55	17.2	17.2	8.01E-07	6.39E-08	0.845	0.03	1.33	17.2	5	0	-	-
EW-P5-1	SSM	Undrained	1.26	0.55	17.2	17.2	8.01E-07	6.39E-08	0.845	0.03	1.4	15.3	5	0	-	-
EW-P5-2	SSM	Undrained	1.25	0.55	17.2	17.2	8.01E-07	6.39E-08	0.845	0.03	1.506	17.7	5	0	-	-
EW-P5-3	SSM	Undrained	1.18	0.55	17.2	17.2	8.01E-07	6.39E-08	0.845	0.03	1.325	13.4	5	0	-	-
EW-P5-4	SSM	Undrained	1.25	0.55	17.2	17.2	8.01E-07	6.39E-08	0.845	0.03	1.36	11.3	5	0	-	-
EW-P5-5	SSM	Undrained	1.33	0.55	17.2	17.2	8.01E-07	6.39E-08	0.845	0.03	1.346	12.9	5	0	-	-

Notes:

- 1) SSM denotes the Soft Soil Model
- 2) Figures D.1 and D.2 are provided on the attached CD, and provide the East/West and North/South Plaxis profiles with labeled layers.

APPENDIX E

PLAXIS MODEL VALIDATION FIGURES

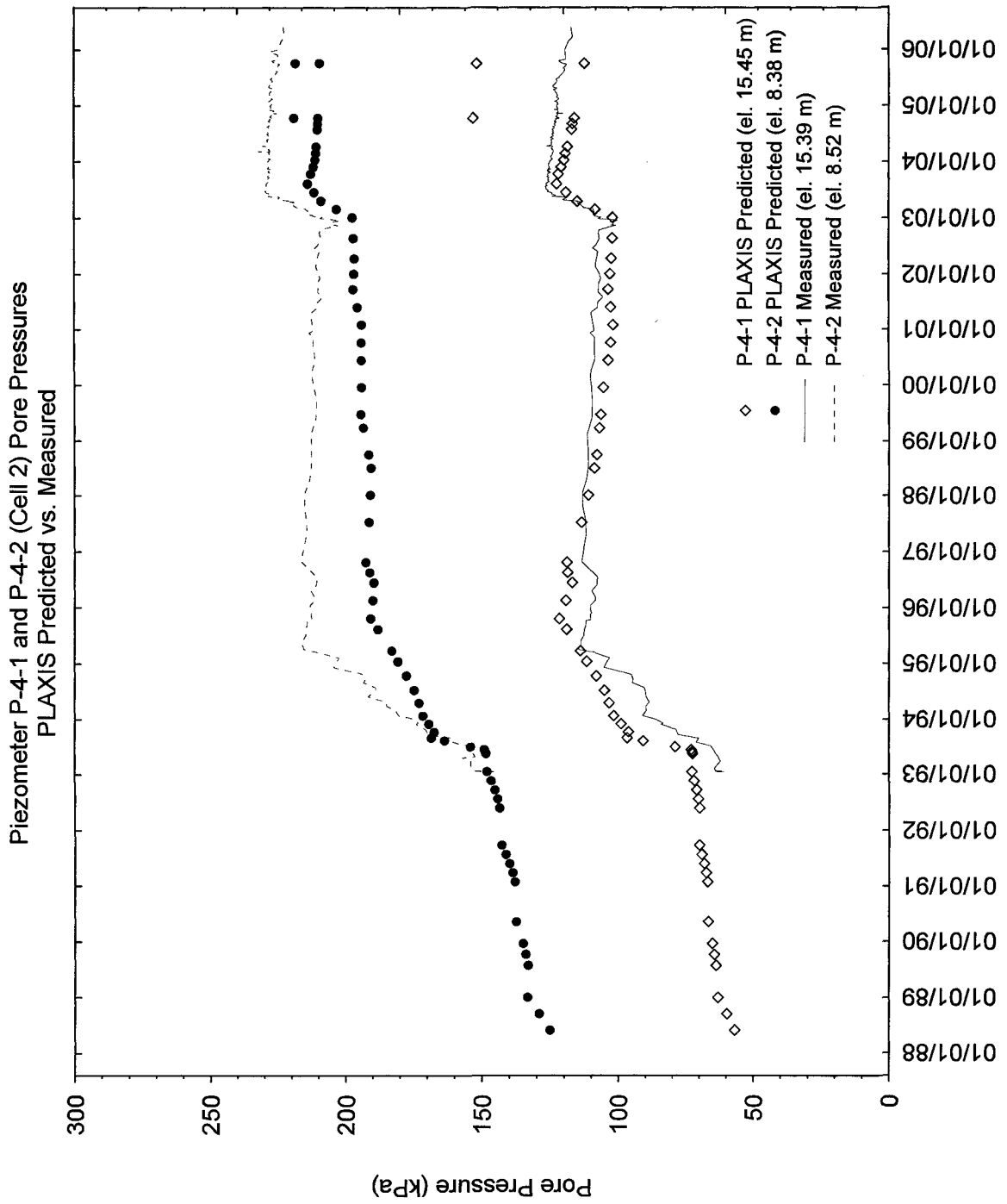


Figure E.1 - Piezometer P-4 (Cell 2)
 Plaxis Predicted vs. Measured Pore Pressures
 North/South Model

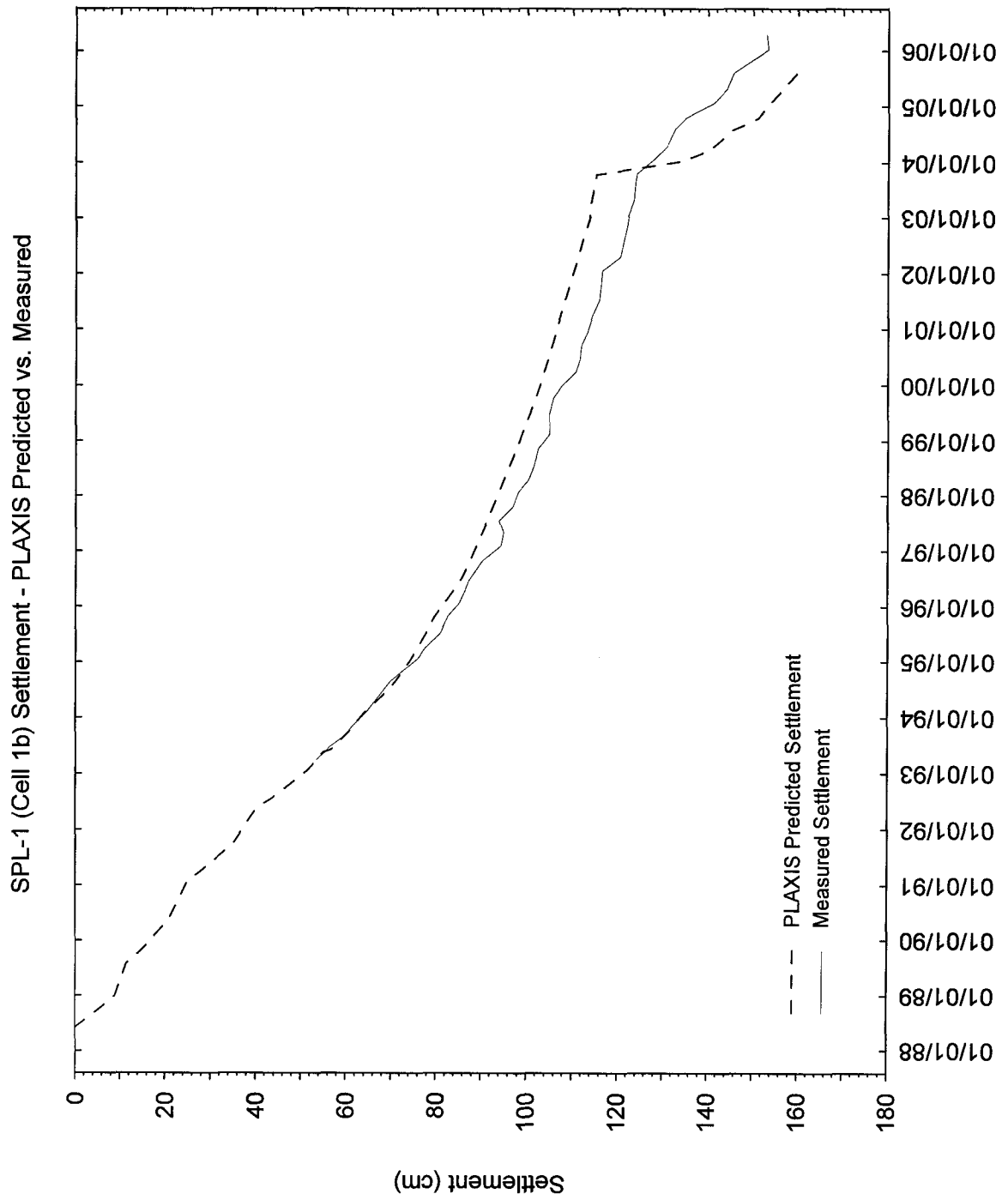


Figure E.2 - SPL-1 (Cell 1b)
 Plaxis Predicted vs. Measured Settlement
 North/South Model

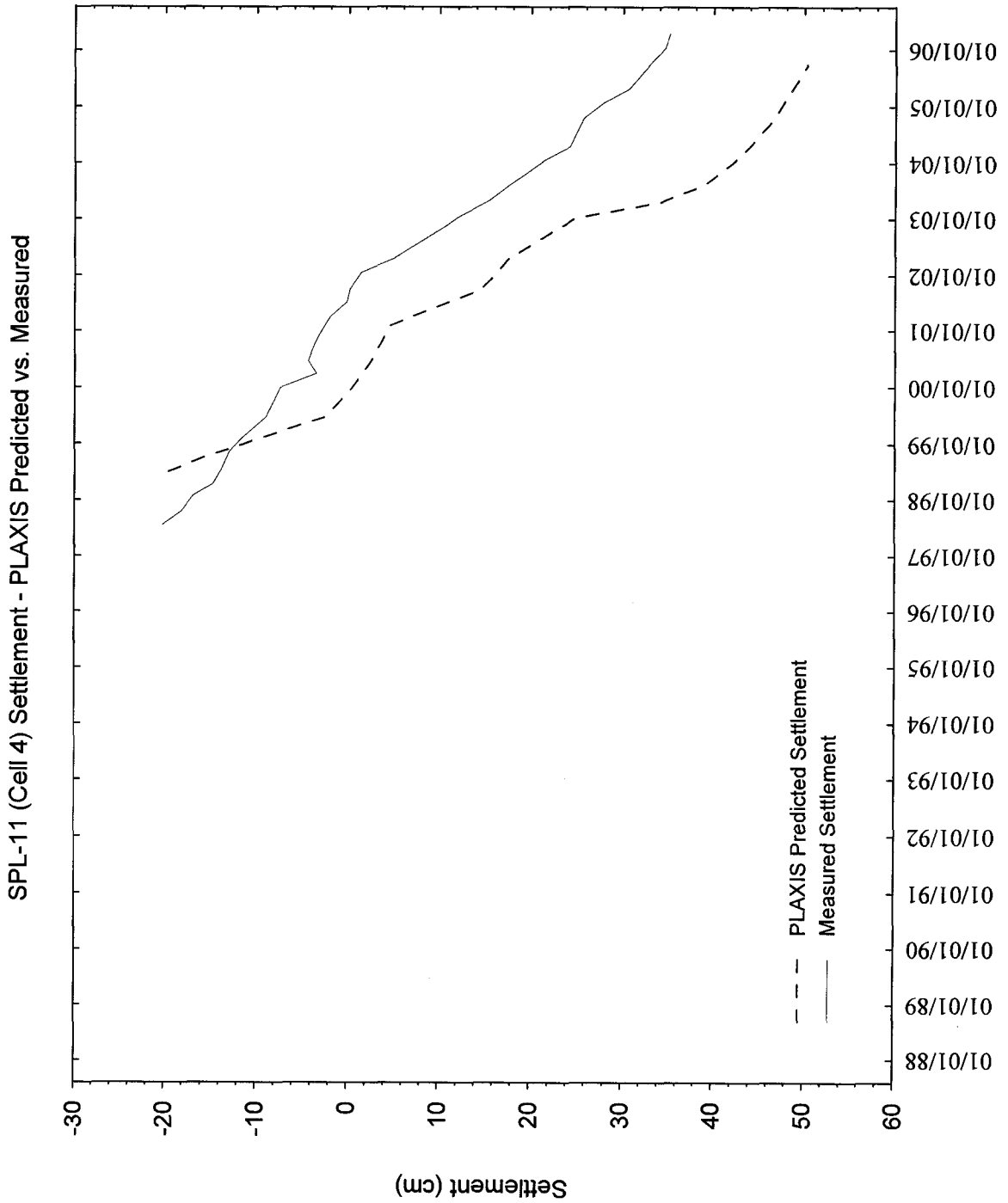


Figure E.3 - SPL-11 (Cell 4)
Plaxis Predicted vs. Measured Settlement
North/South Model

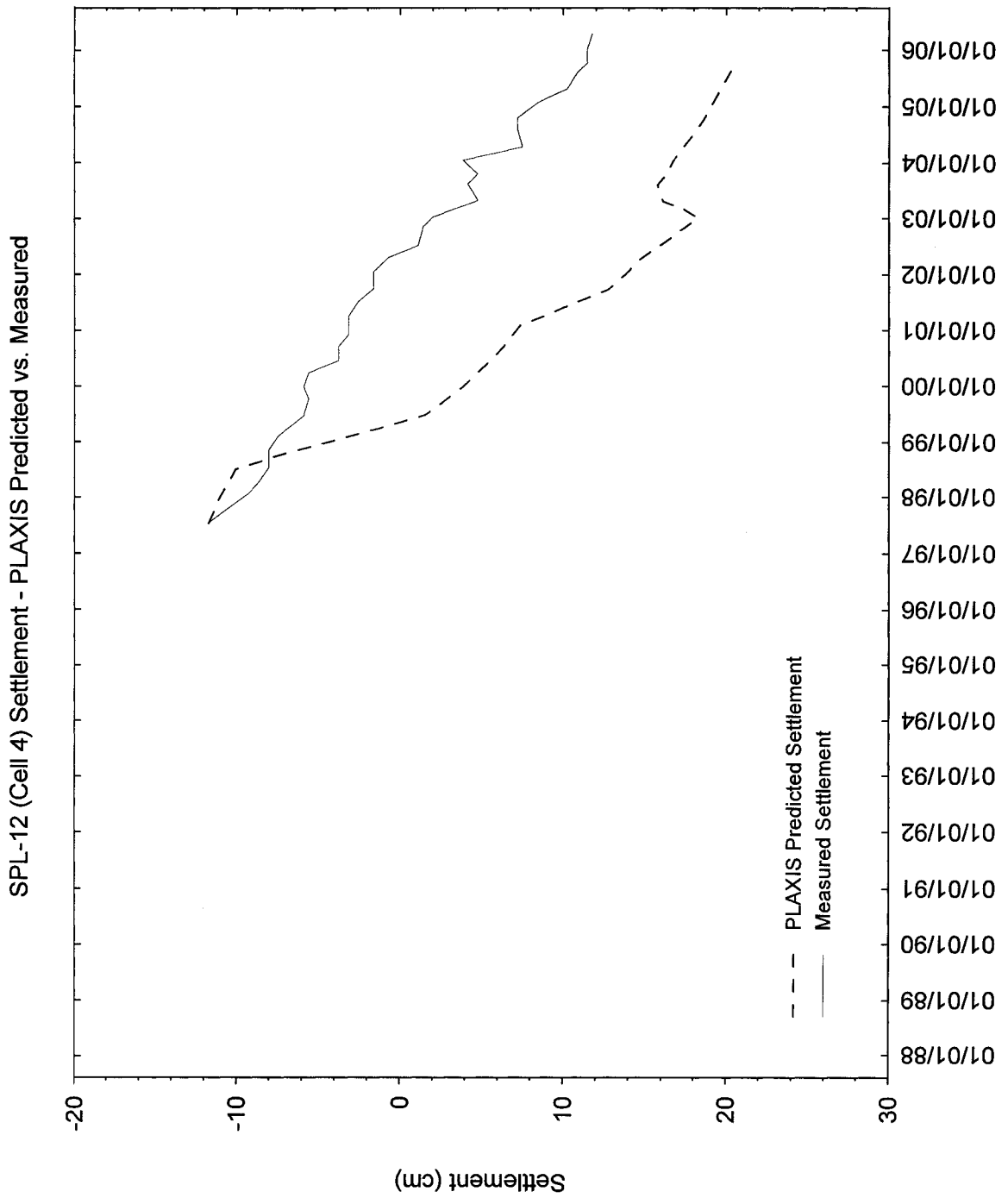


Figure E.4 - SPL-12 (Cell 4)
Plaxis Predicted vs. Measured Settlement
North/South Model

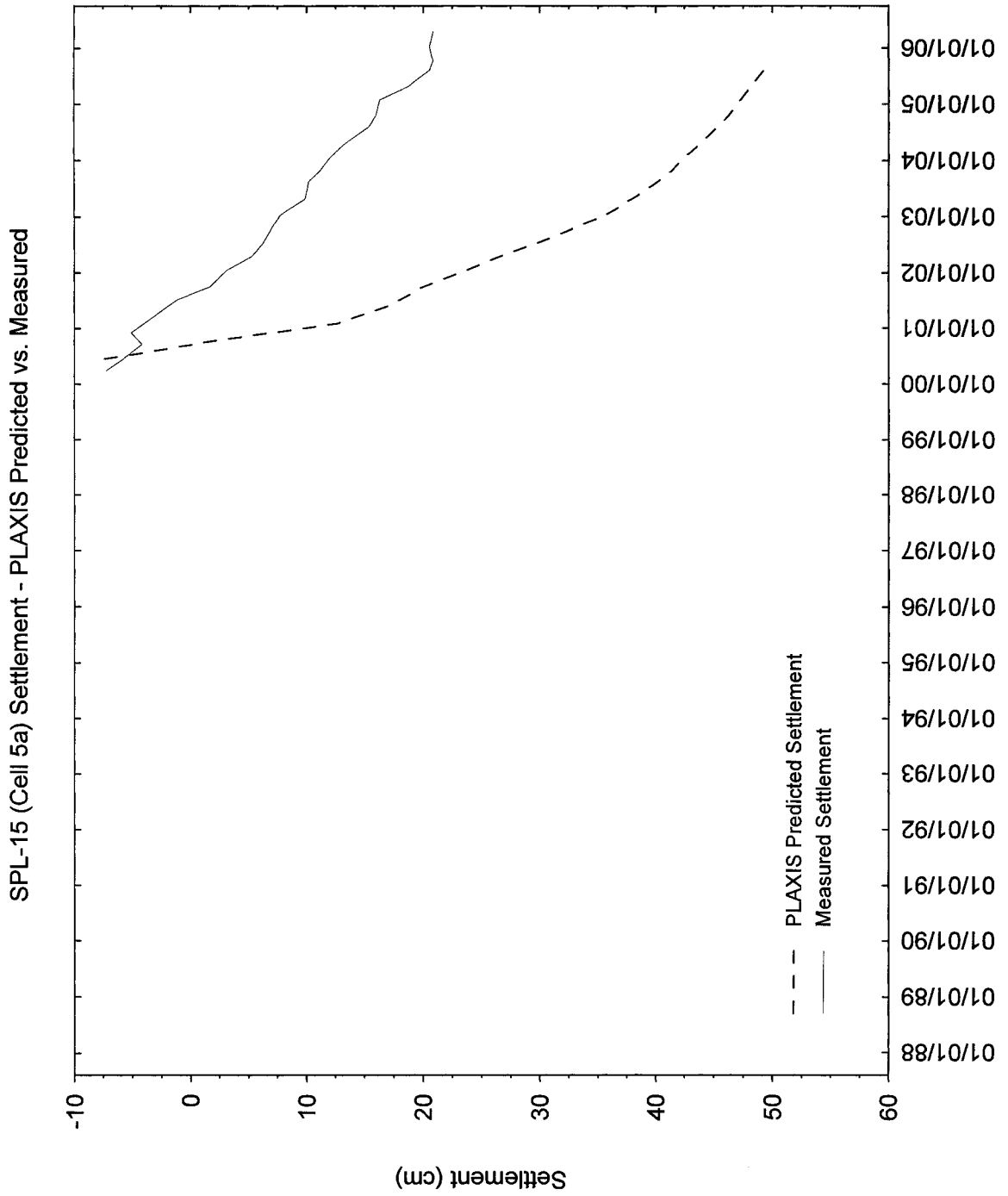


Figure E.5 - SPL-15 (Cell 5a)
 Plaxis Predicted vs. Measured Settlement
 North/South Model

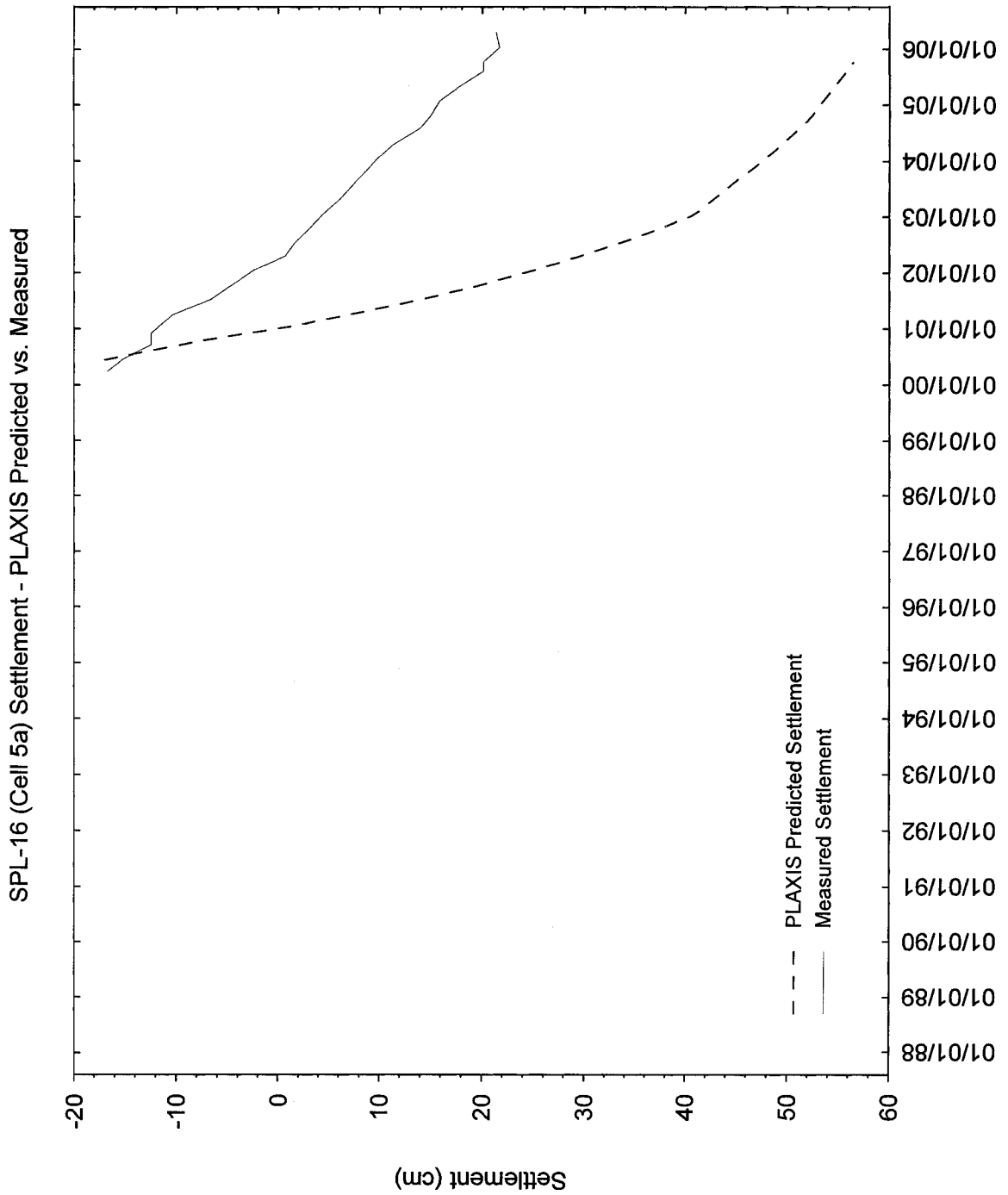


Figure E.6 - SPL-16 (Cell 5a)
 Plaxis Predicted vs. Measured Settlement
 North/South Model

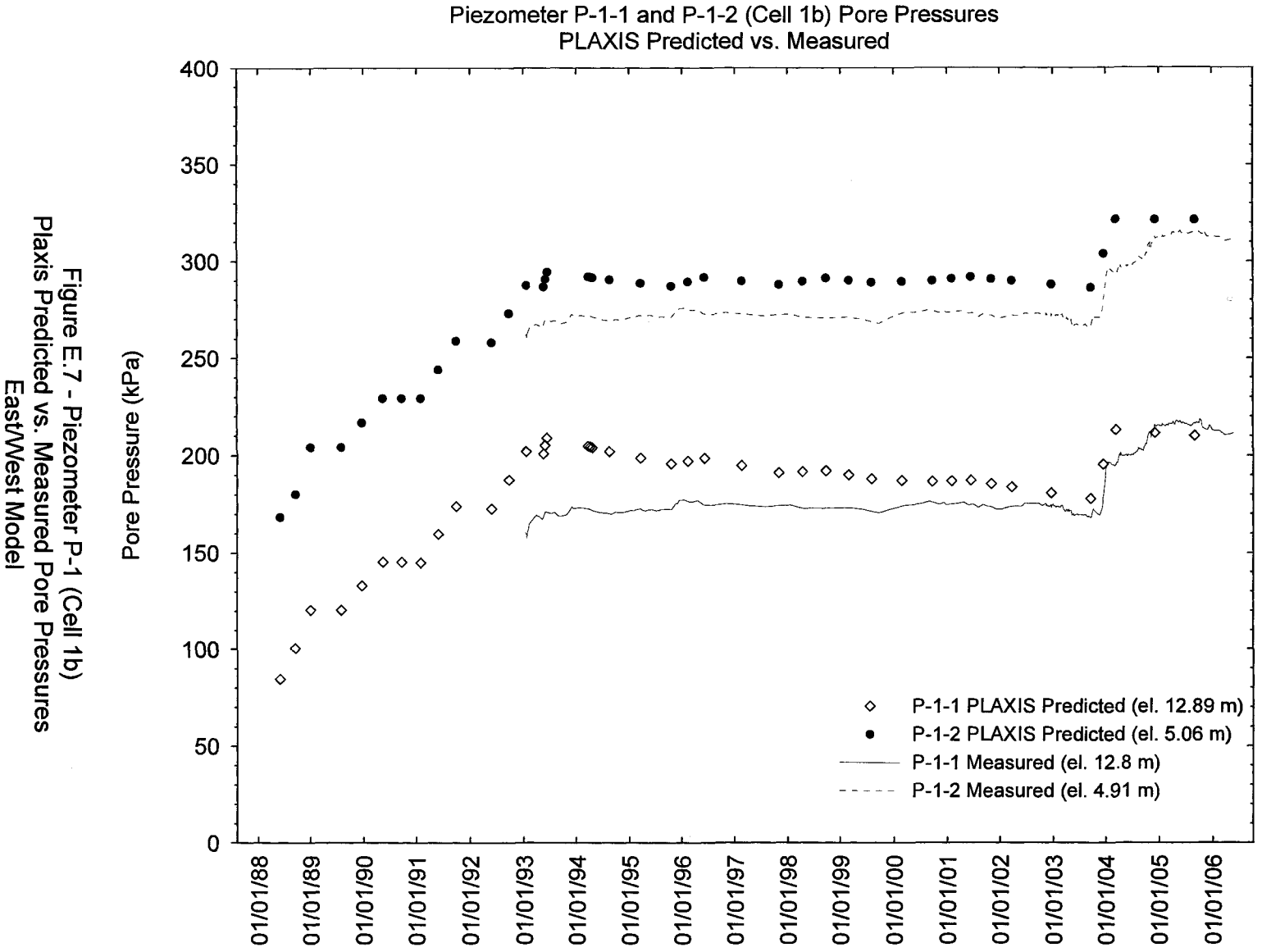
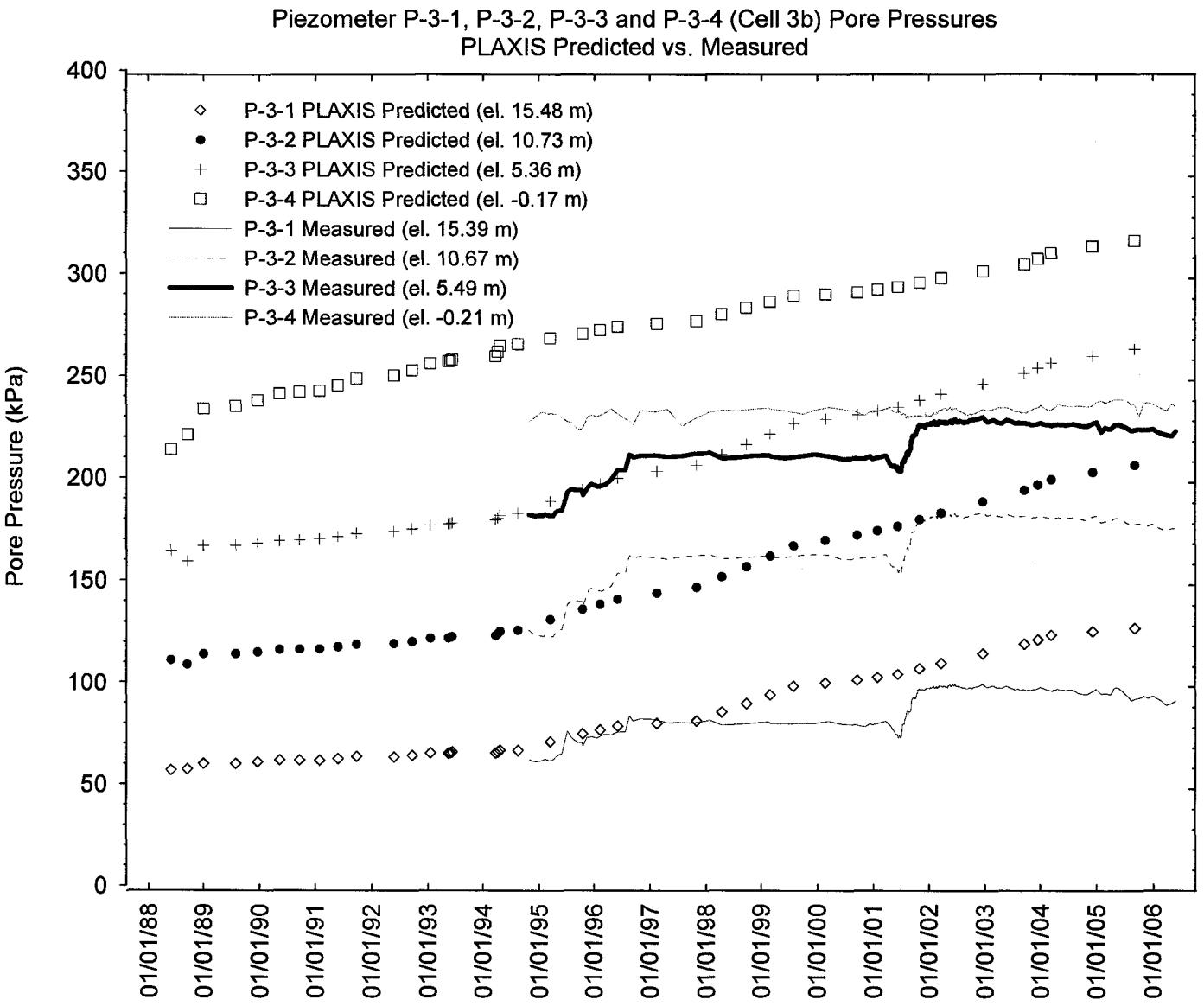


Figure E.8 - Piezometer P-3 (Cell 3b)
Plaxis Predicted vs. Measured Pore Pressures
EastWest Model



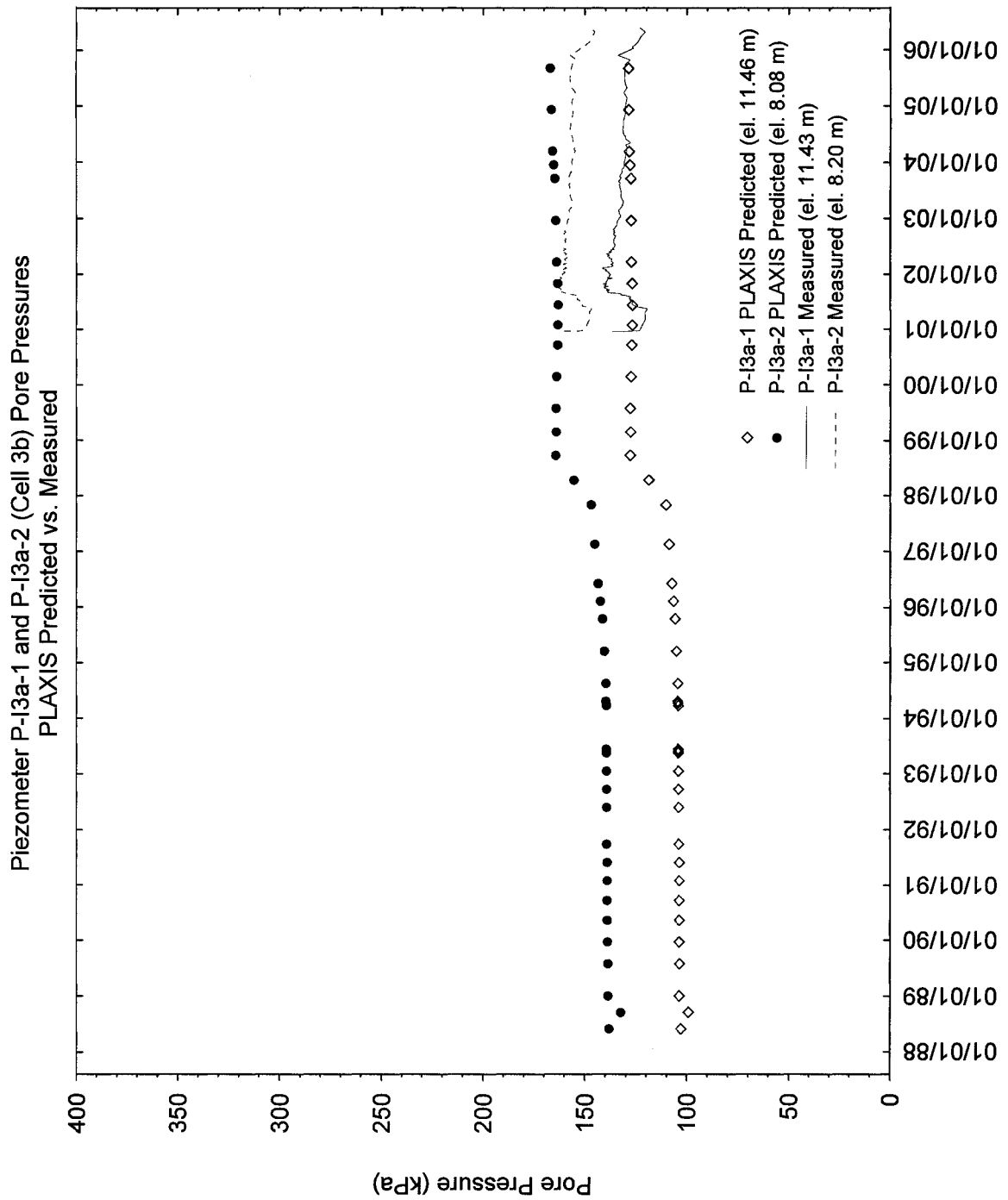


Figure E.9 - Piezometer P-13a (Cell 3b)
 Plaxis Predicted vs. Measured Pore Pressures
 East/West Model

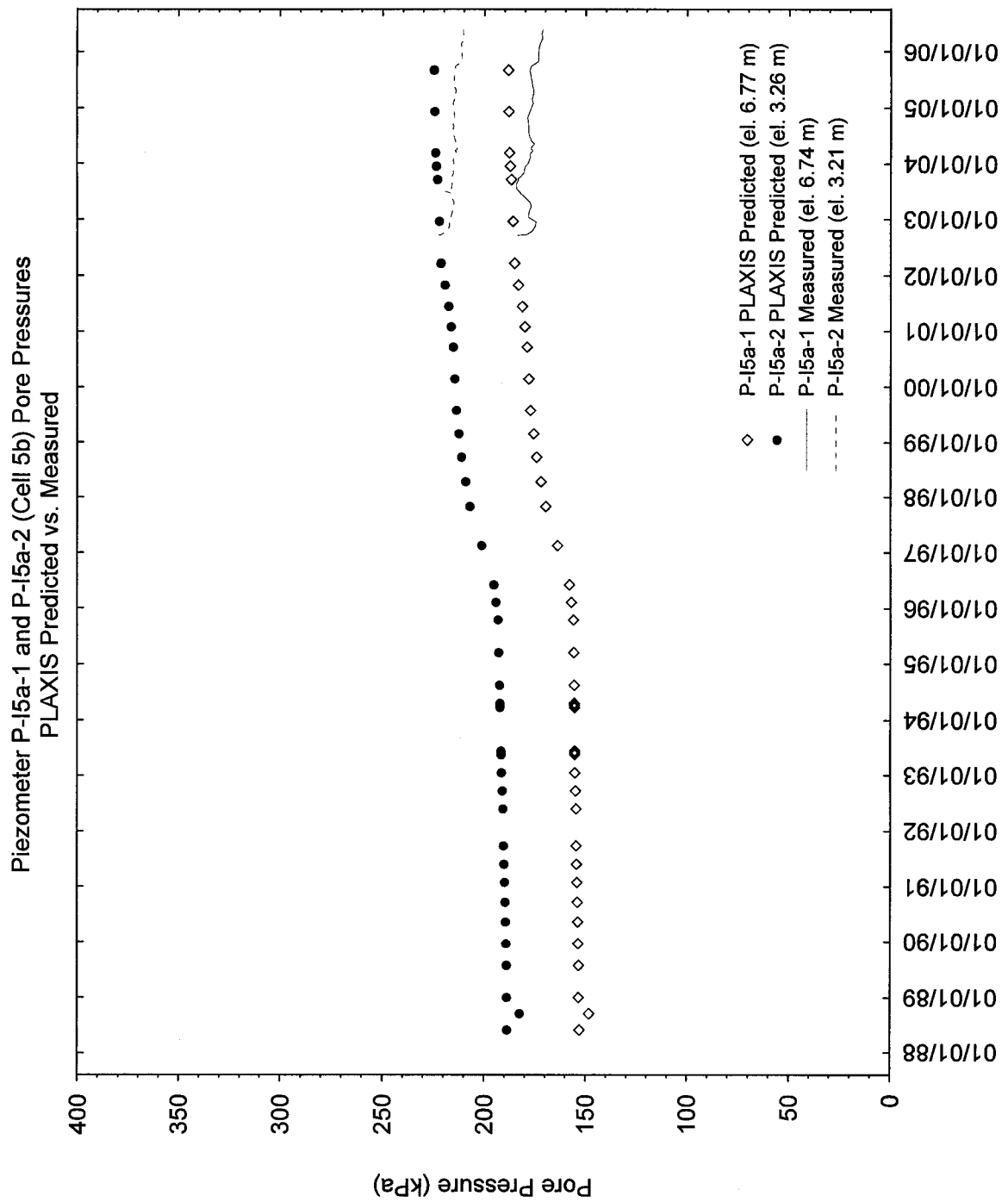


Figure E.10 - Piezometer P-15a (Cell 5b)
Plaxis Predicted vs. Measured Pore Pressures
East/West Model

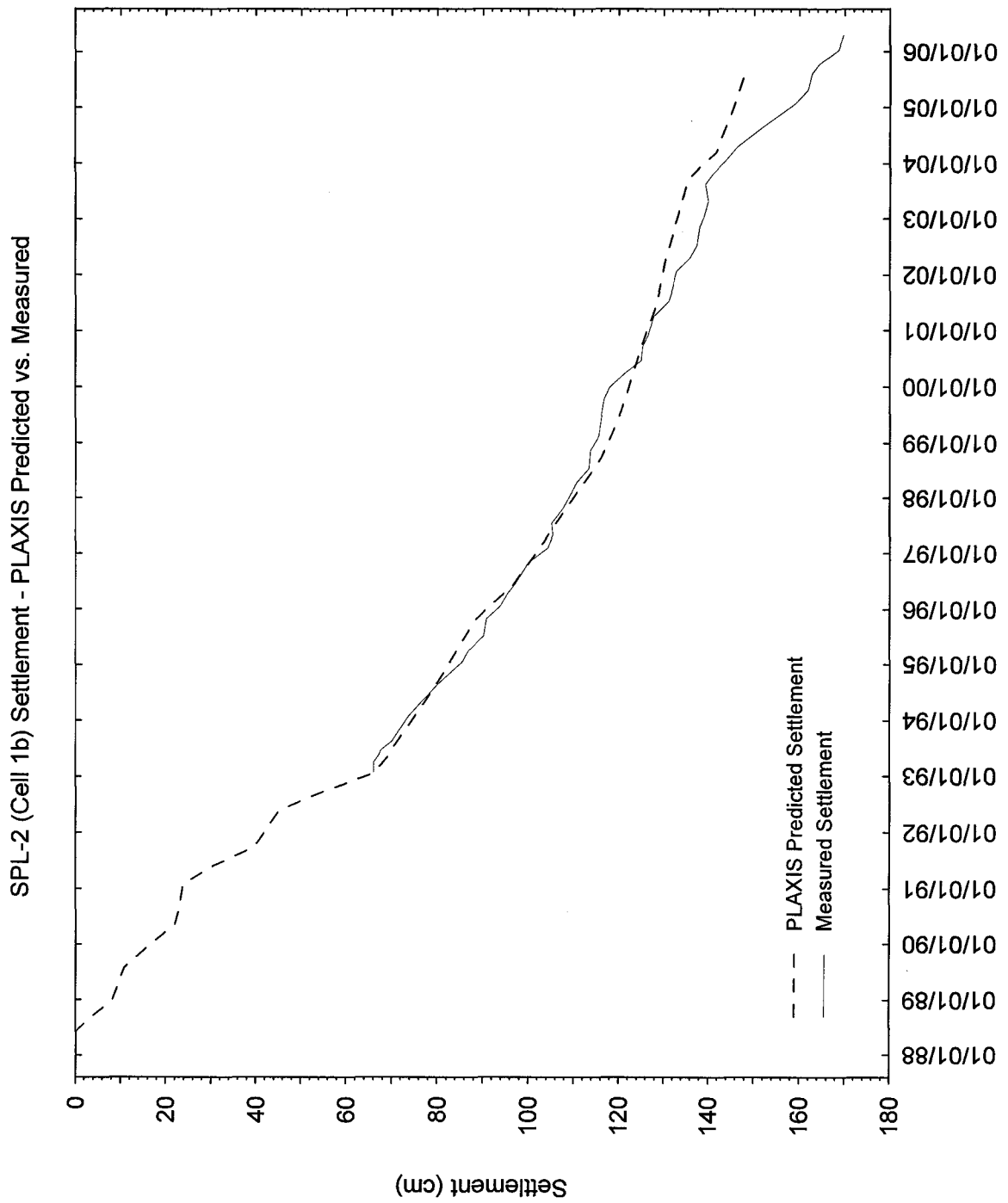


Figure E.11 - SPL-2 (Cell 1b)
 Plaxis Predicted vs. Measured Settlement
 North/South Model

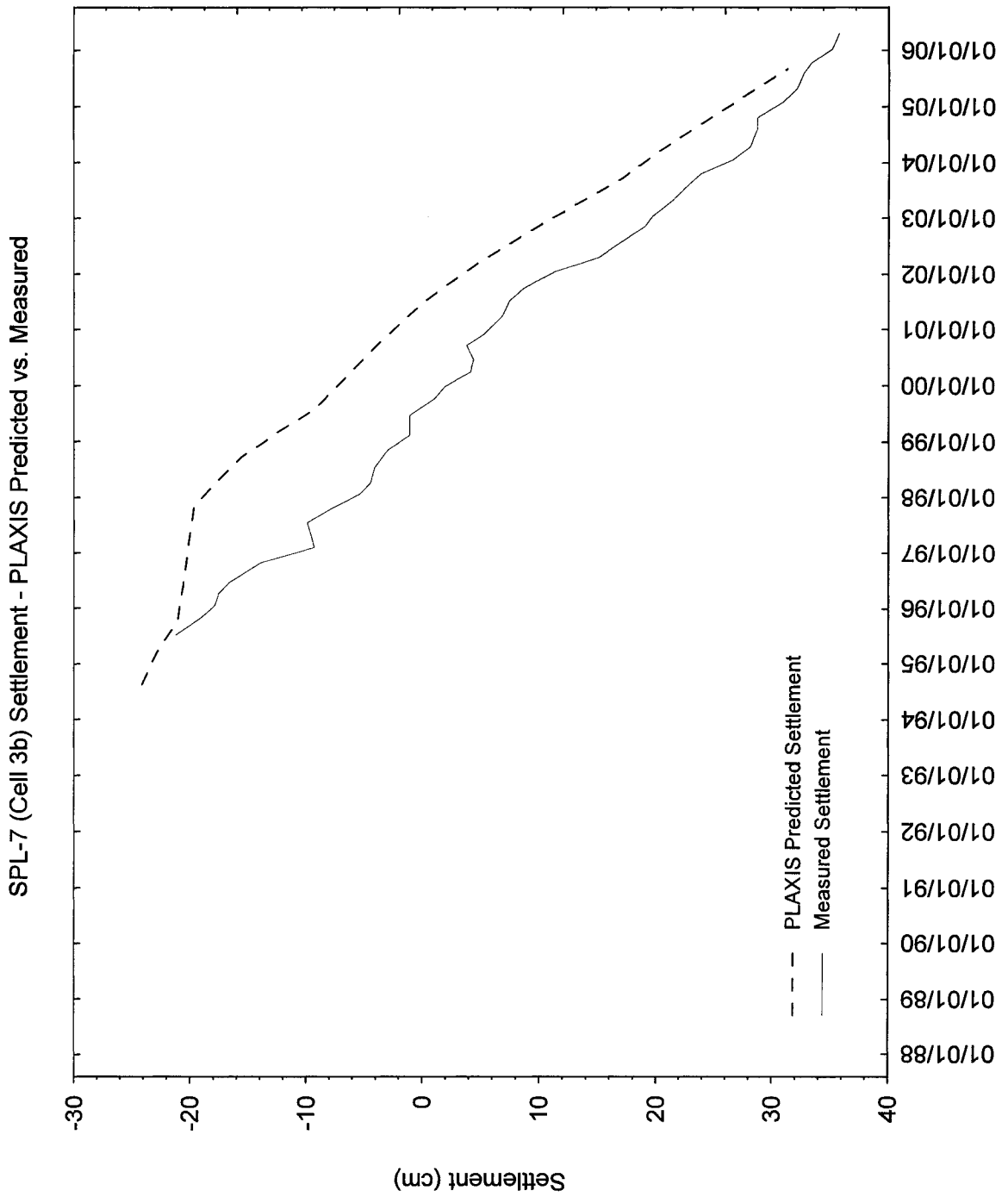


Figure E.12 - SPL-7 (Cell 3b)
 Plaxis Predicted vs. Measured Settlement
 North/South Model

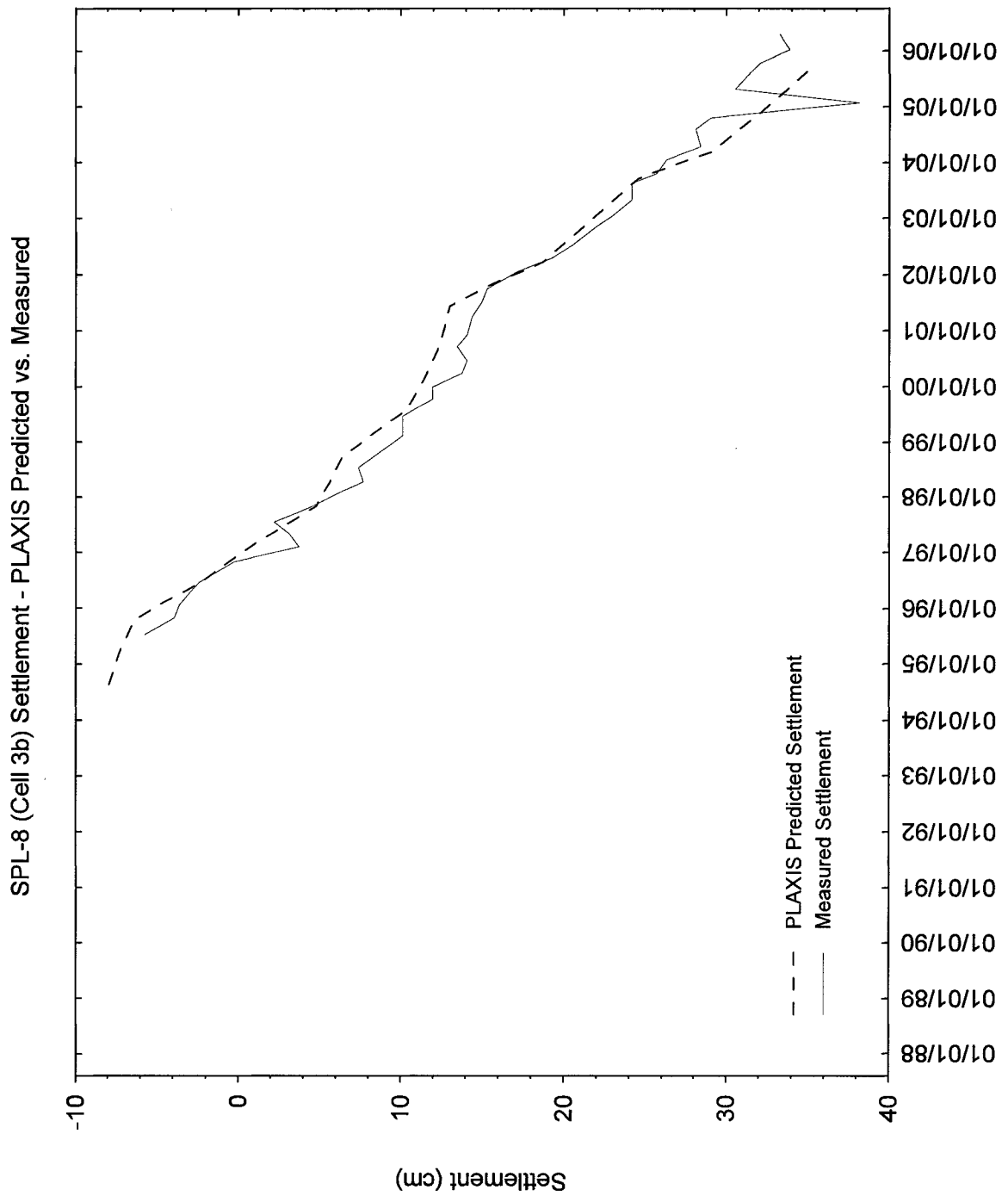


Figure E.13 - SPL-8 (Cell 3b)
Plaxis Predicted vs. Measured Settlement
North/South Model

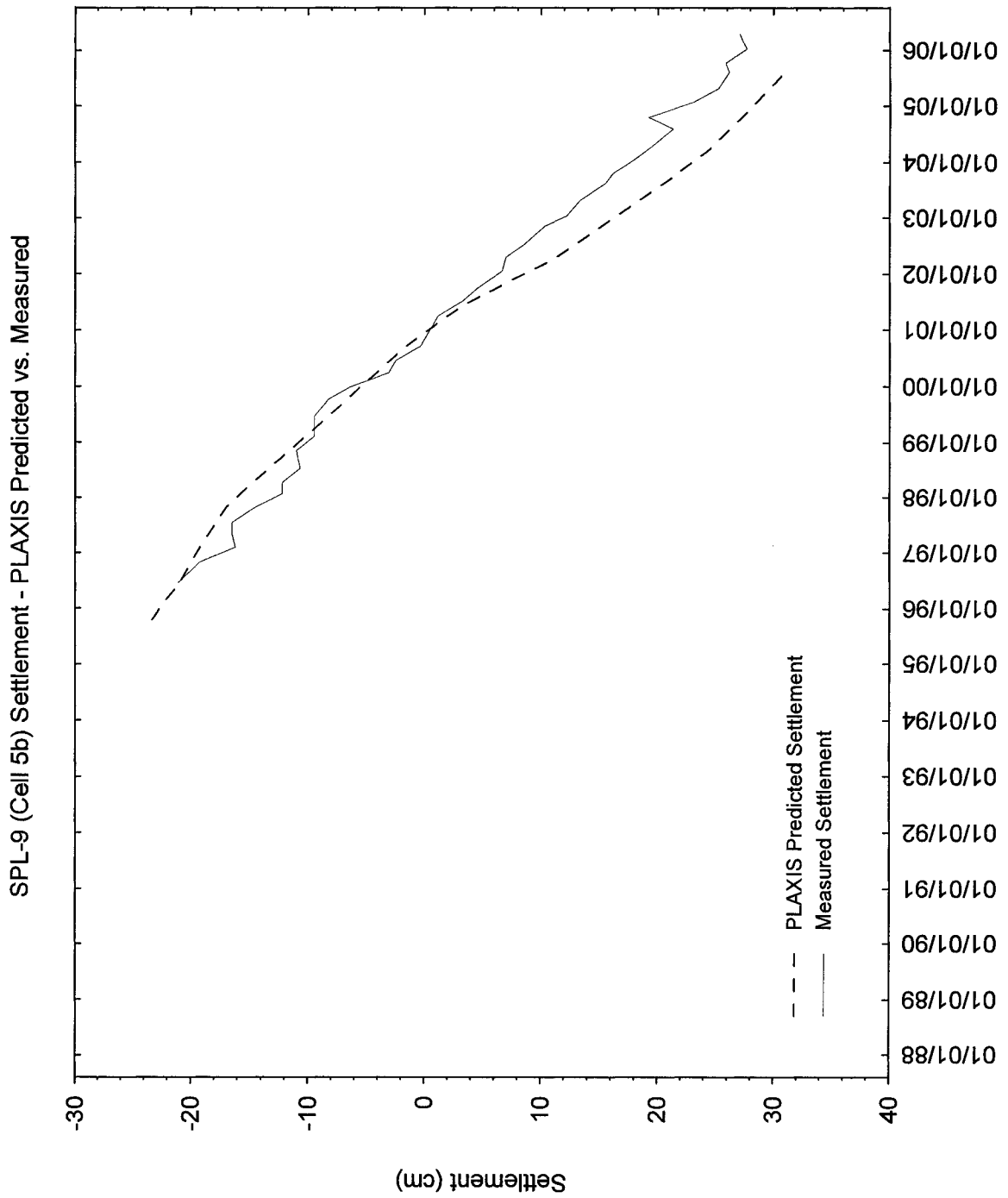


Figure E.14 - SPL-9 (Cell 5b)
 Plaxis Predicted vs. Measured Settlement
 North/South Model

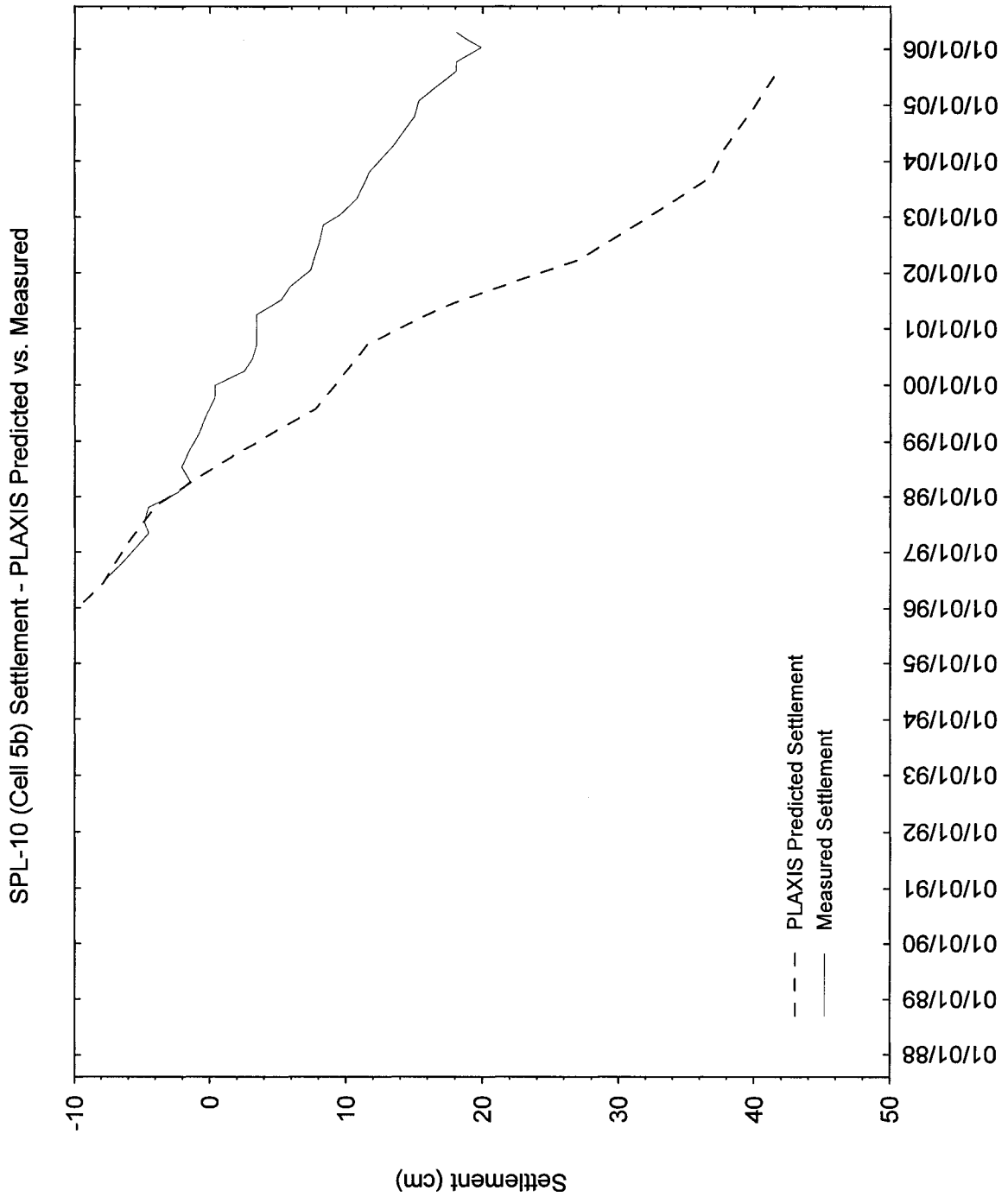


Figure E.15 - SPL-10 (Cell 5b)
 Plaxis Predicted vs. Measured Settlement
 North/South Model

Inclinometer I-5a Cumulative Displacement (a) Plaxis (b) Actual

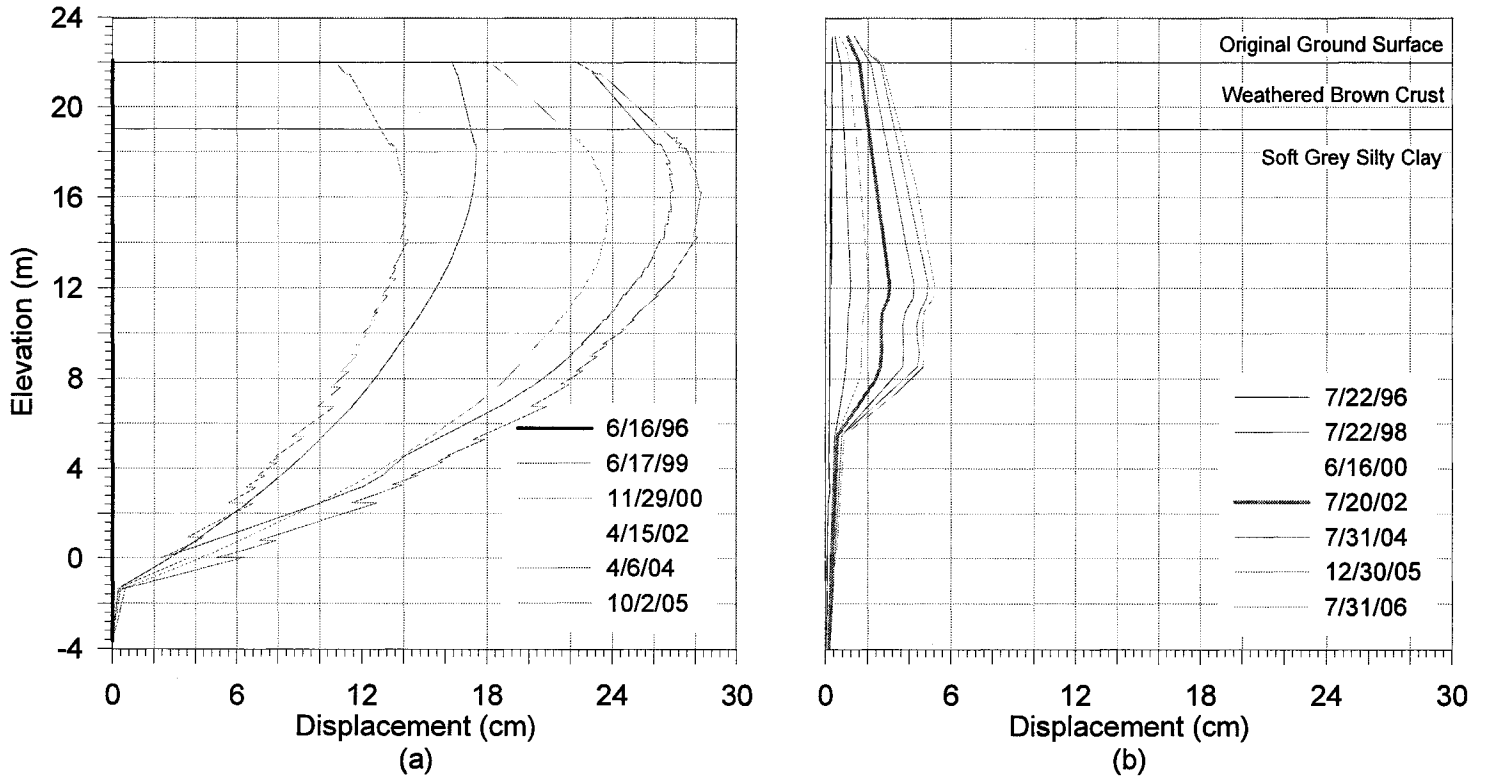


Figure E.16 – Inclinometer I-5a
Plaxis Predicted vs. Measured Displacement
North/South Model

Inclinometer I-6a Cumulative Displacement (a) Plaxis (b) Actual

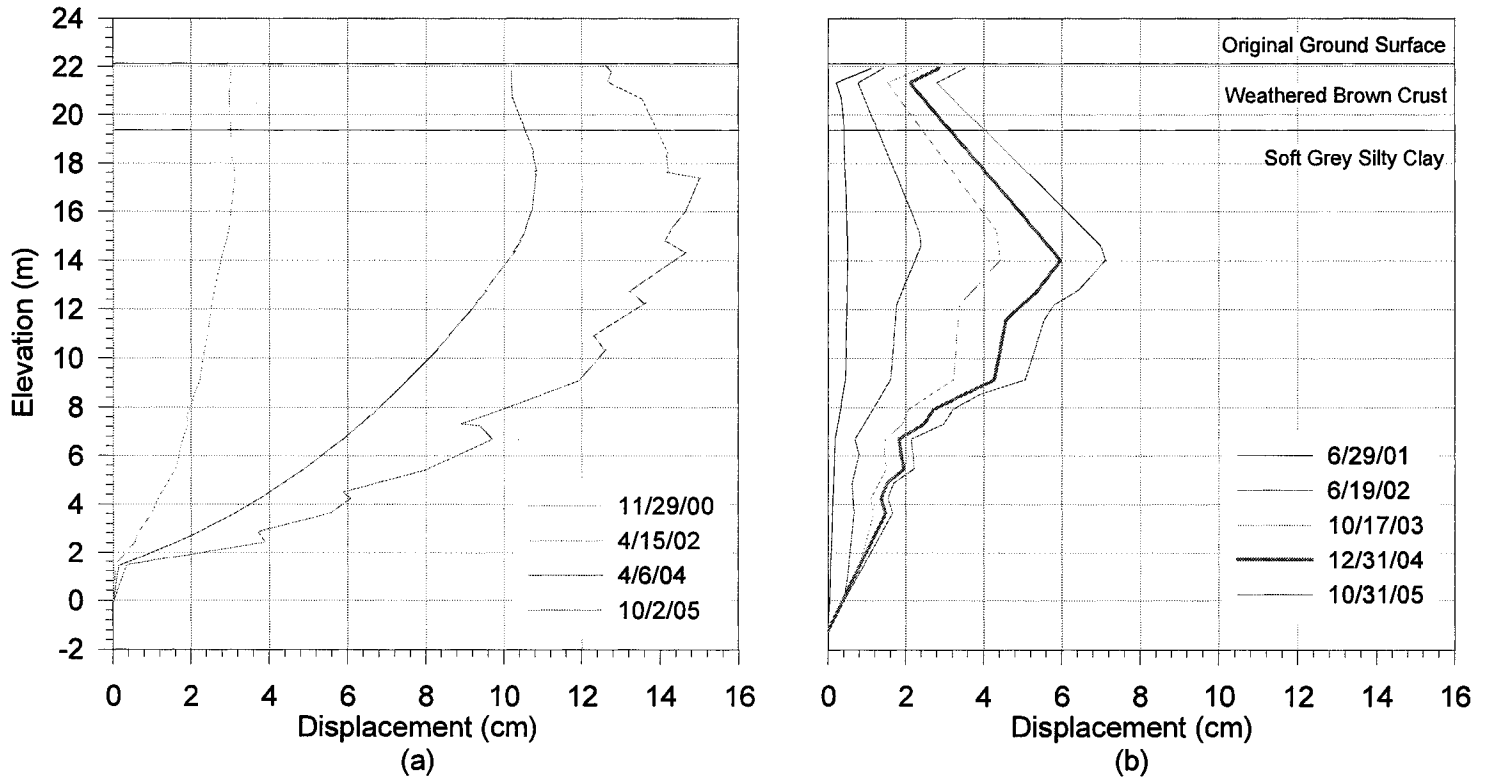


Figure E.17 – Inclinometer I-6a
Plaxis Predicted vs. Measured Displacement
North/South Model

APPENDIX F

UNDRAINED SHEAR STRENGTH GAIN FIGURES

Undrained Shear Strength Profile at I-3/I-4

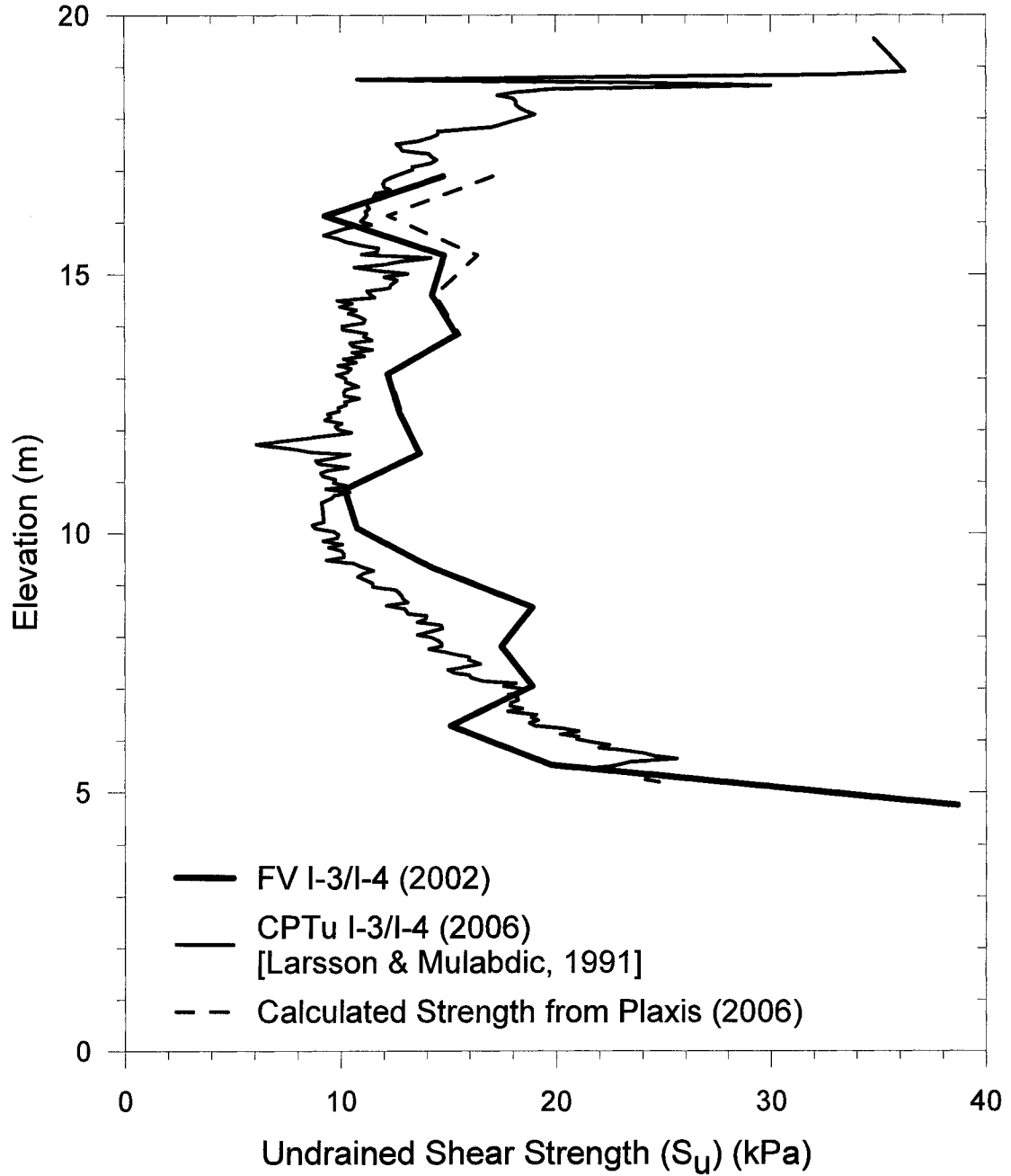


Figure F.1 - Change in Undrained Shear Strength at I-3/I-4 (2002-2006)

Undrained Shear Strength Profile at B-4

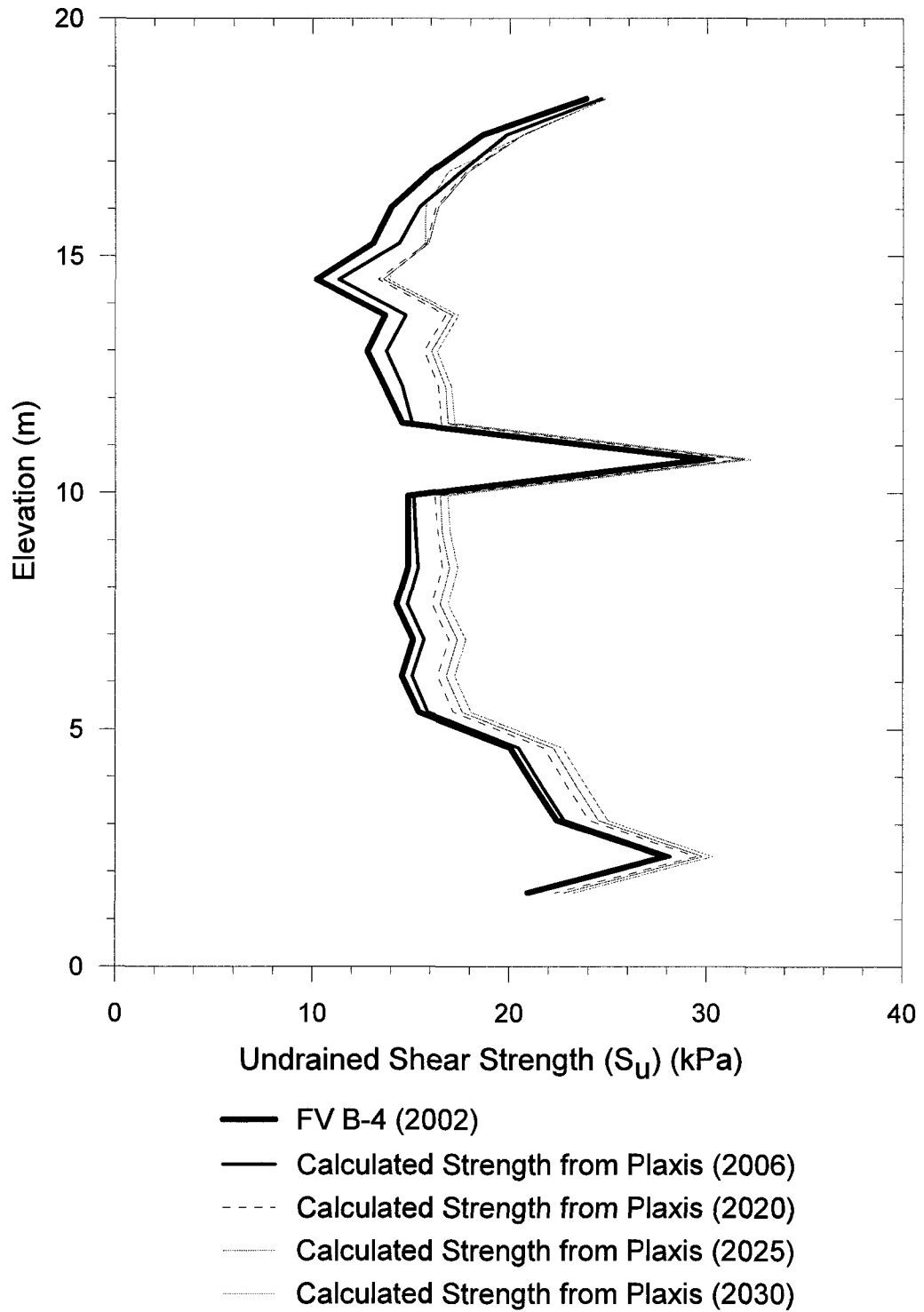


Figure F.2 - Change in Undrained Shear Strength at B-4 (2002-2030)

Undrained Shear Strength Profile at B-11

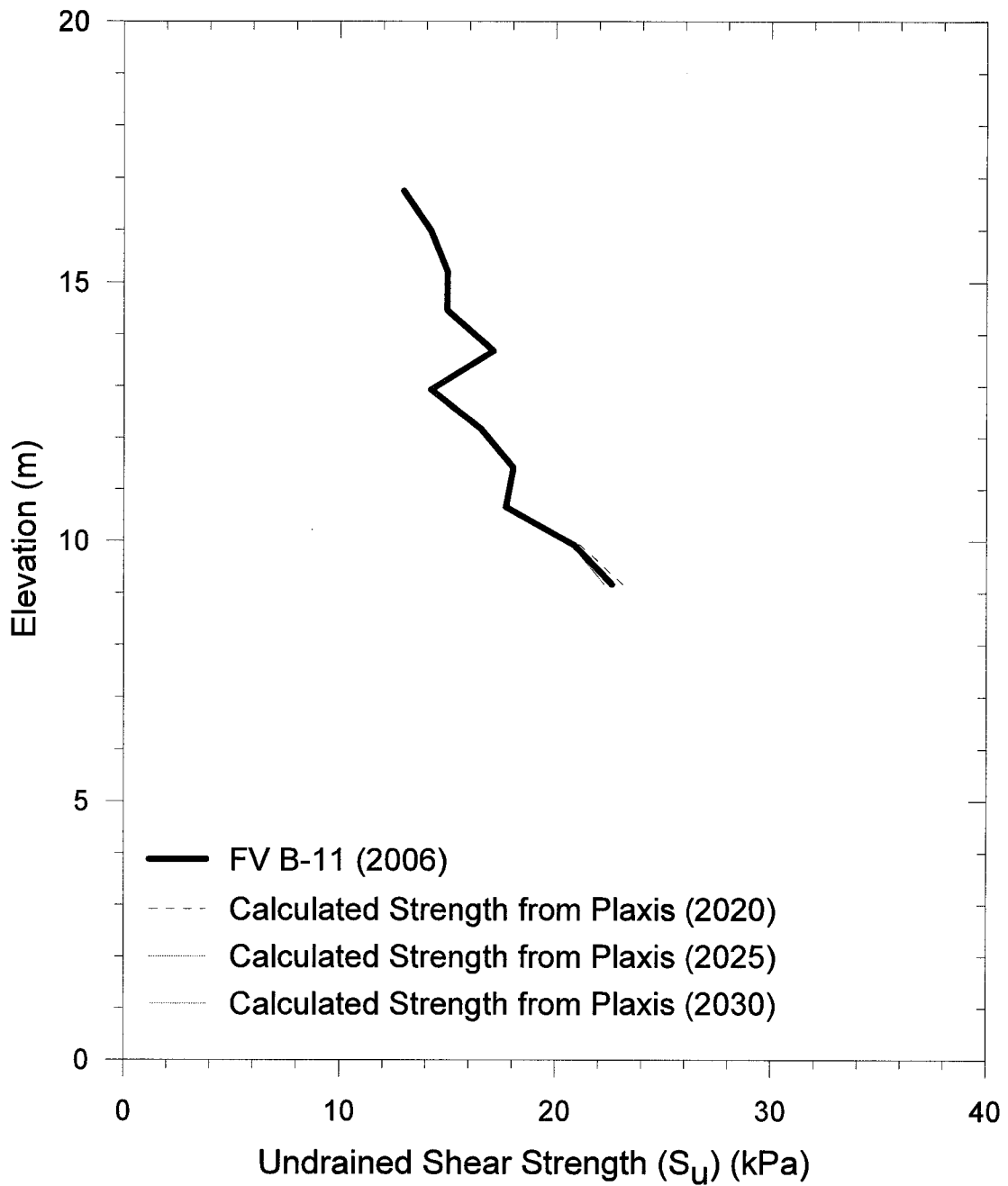


Figure F.3 - Change in Undrained Shear Strength at B-11 (2006-2030)

Undrained Shear Strength Profile at P-3

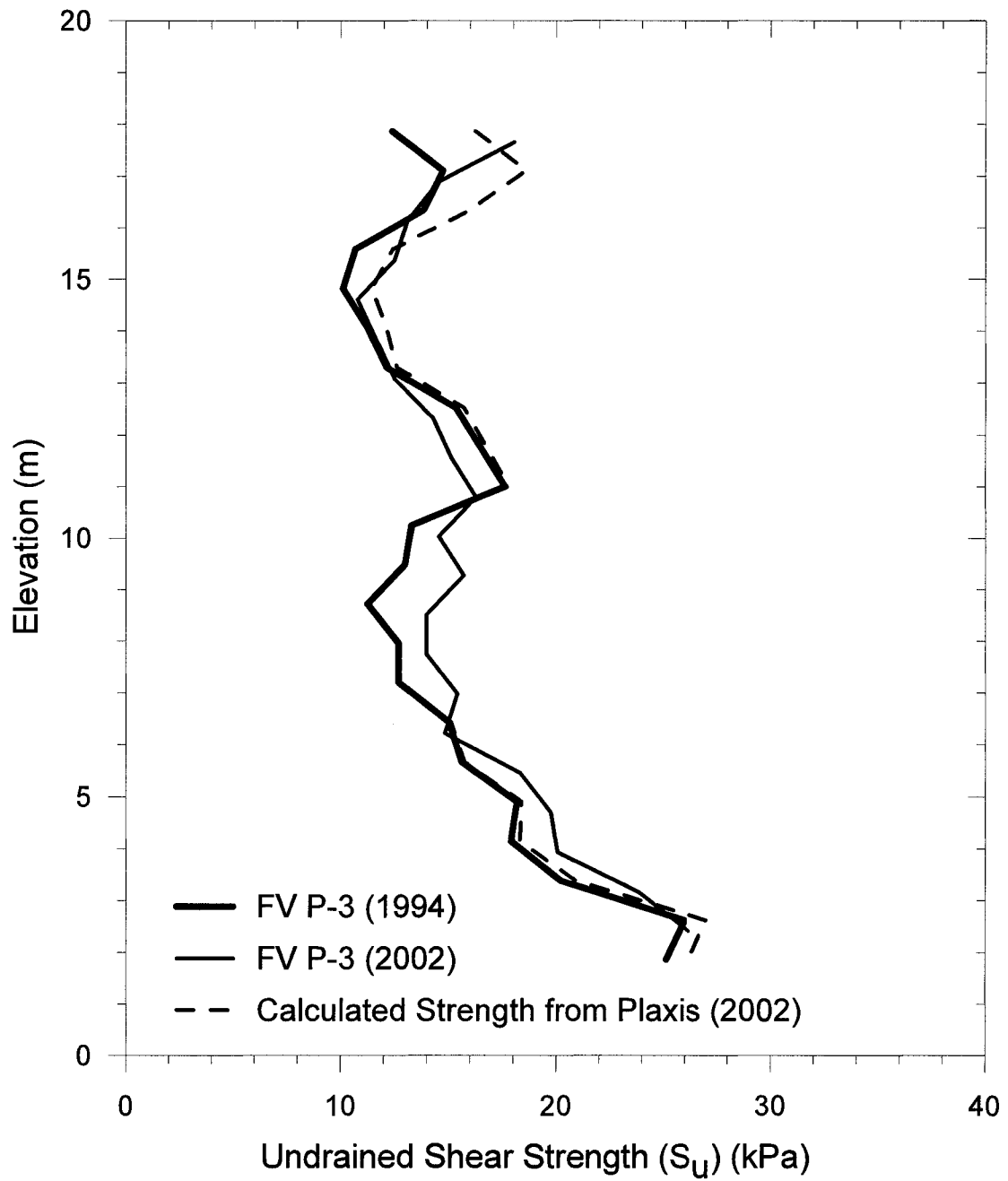


Figure F.4 - Change in Undrained Shear Strength at P-3 (1994-2002)

Undrained Shear Strength Profile at P-3

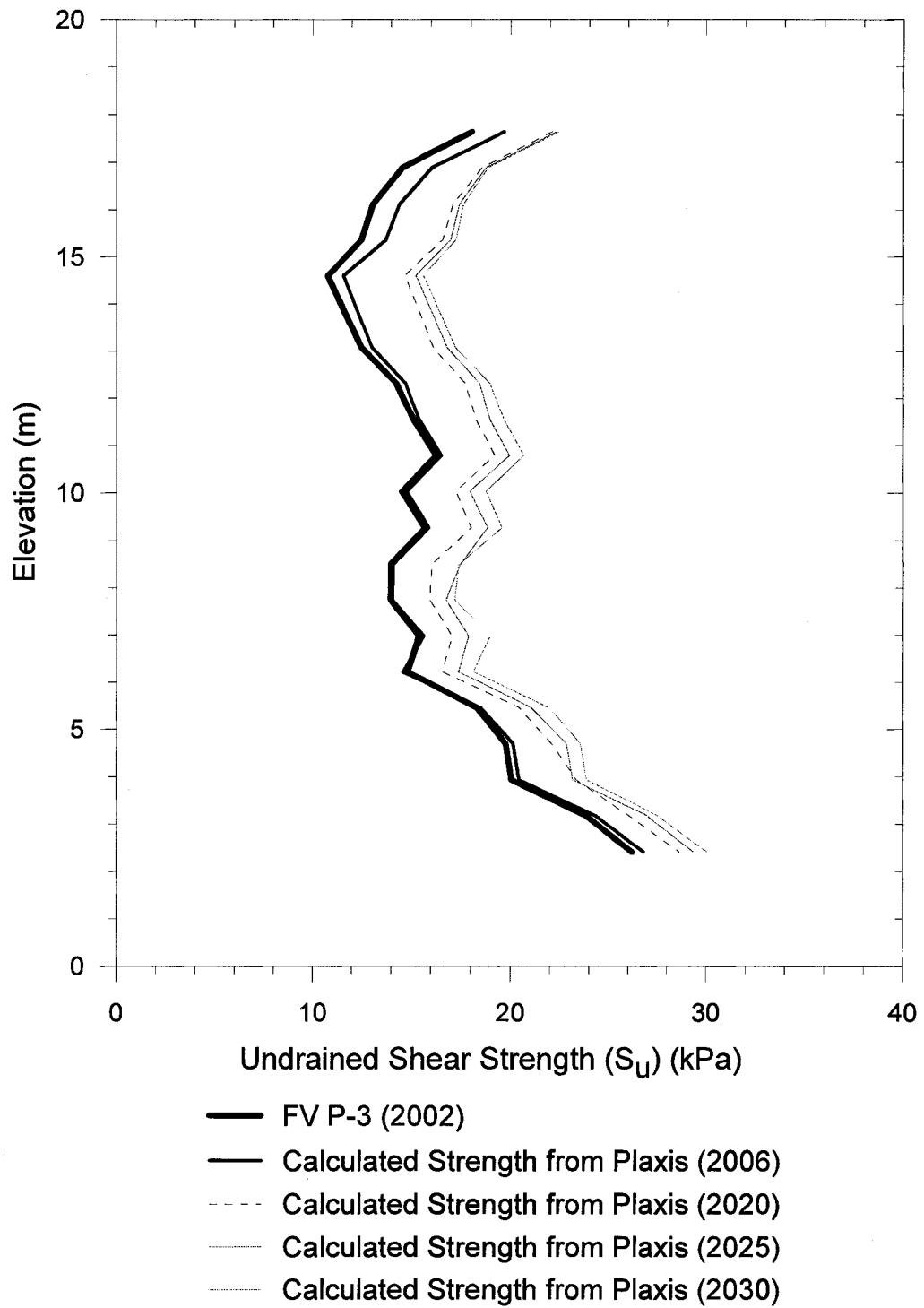


Figure F.5 - Change in Undrained Shear Strength at P-3 (2002-2030)

Undrained Shear Strength Profile at P-5

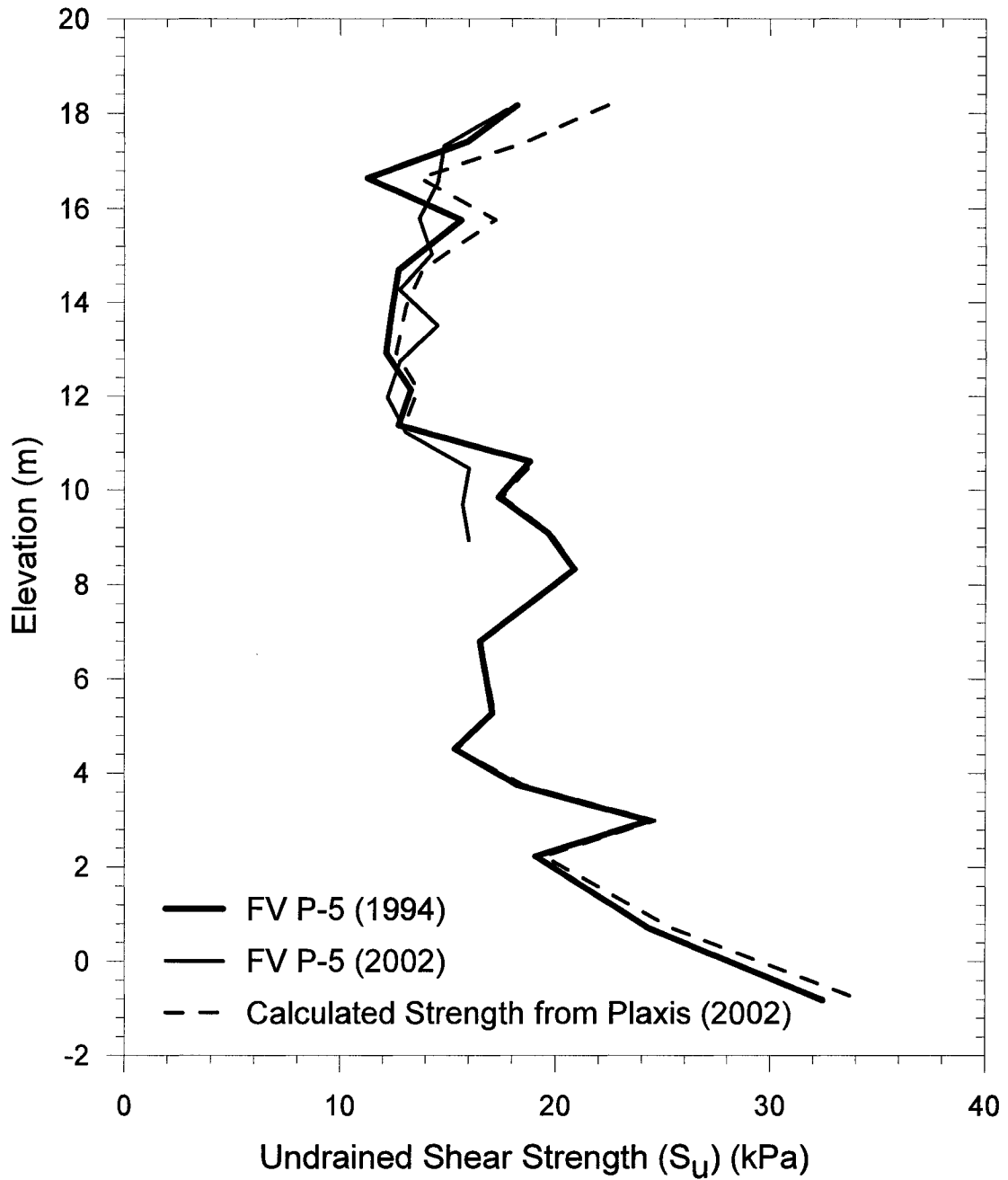


Figure F.6 - Change in Undrained Shear Strength at P-5 (1994-2002)

Undrained Shear Strength Profile at P-5

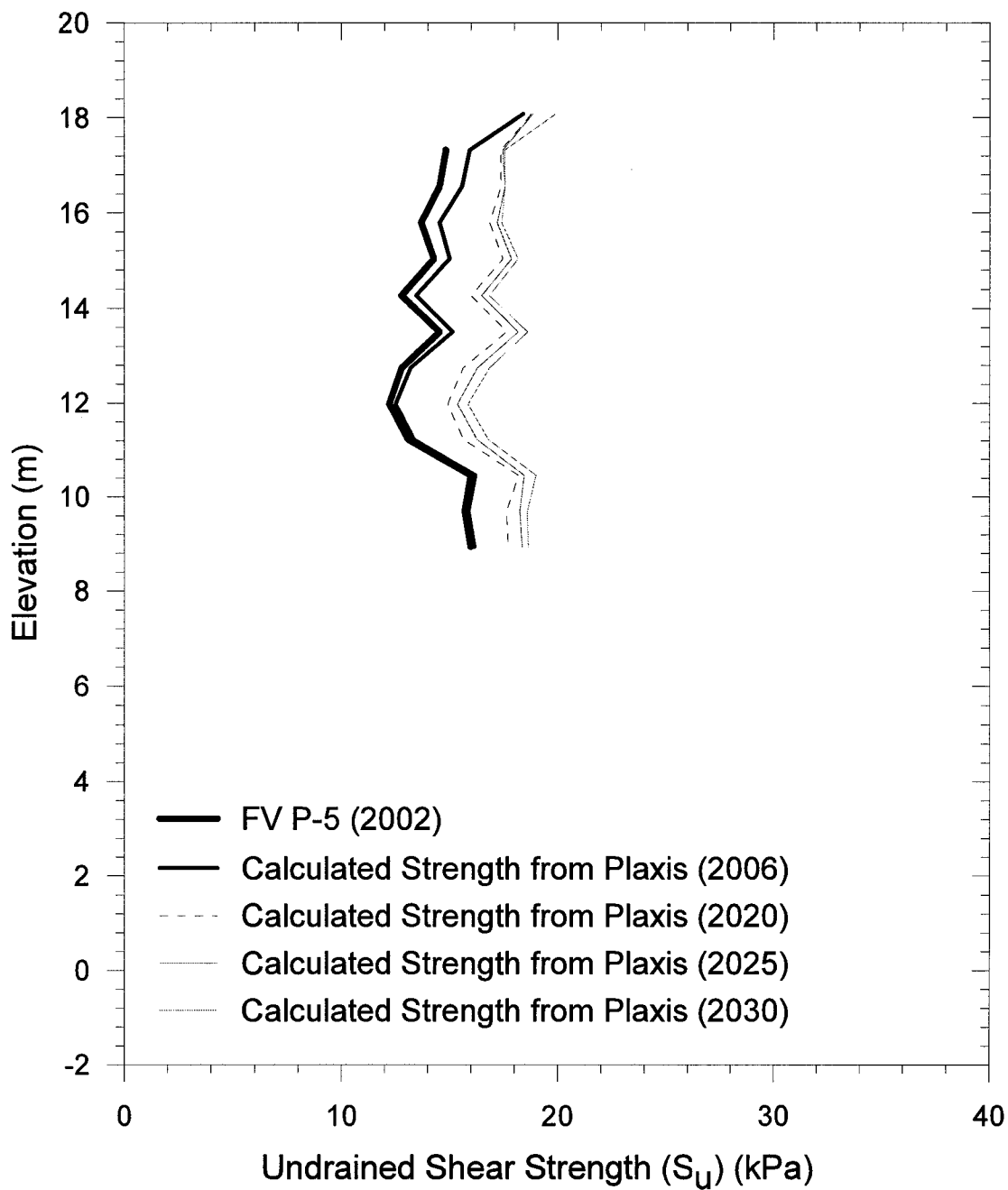


Figure F.7 - Change in Undrained Shear Strength at P-5 (2002-2030)

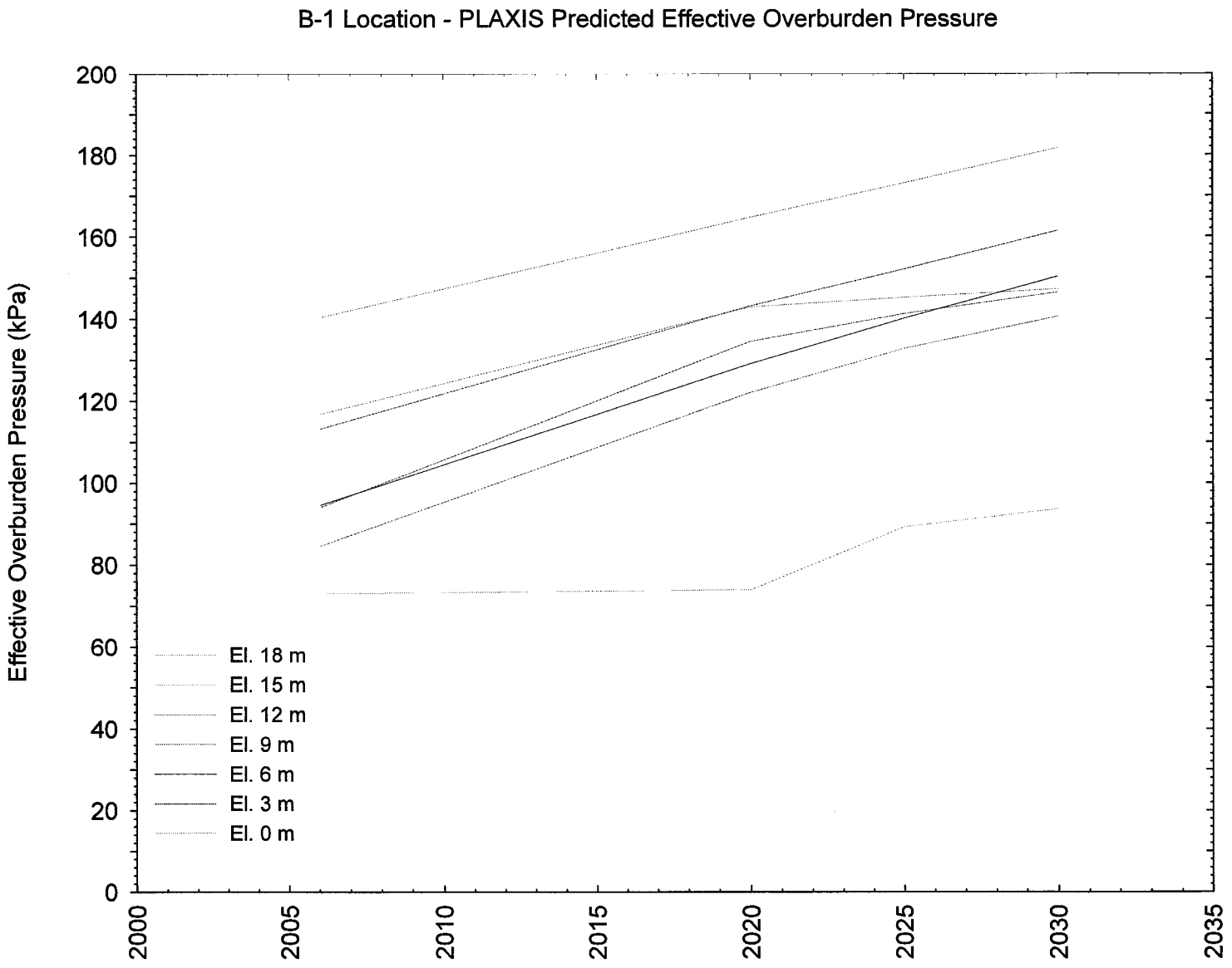


Figure F.8 - Plaxis Predicted Change in Effective Overburden Pressure with Time (B-1 Location)

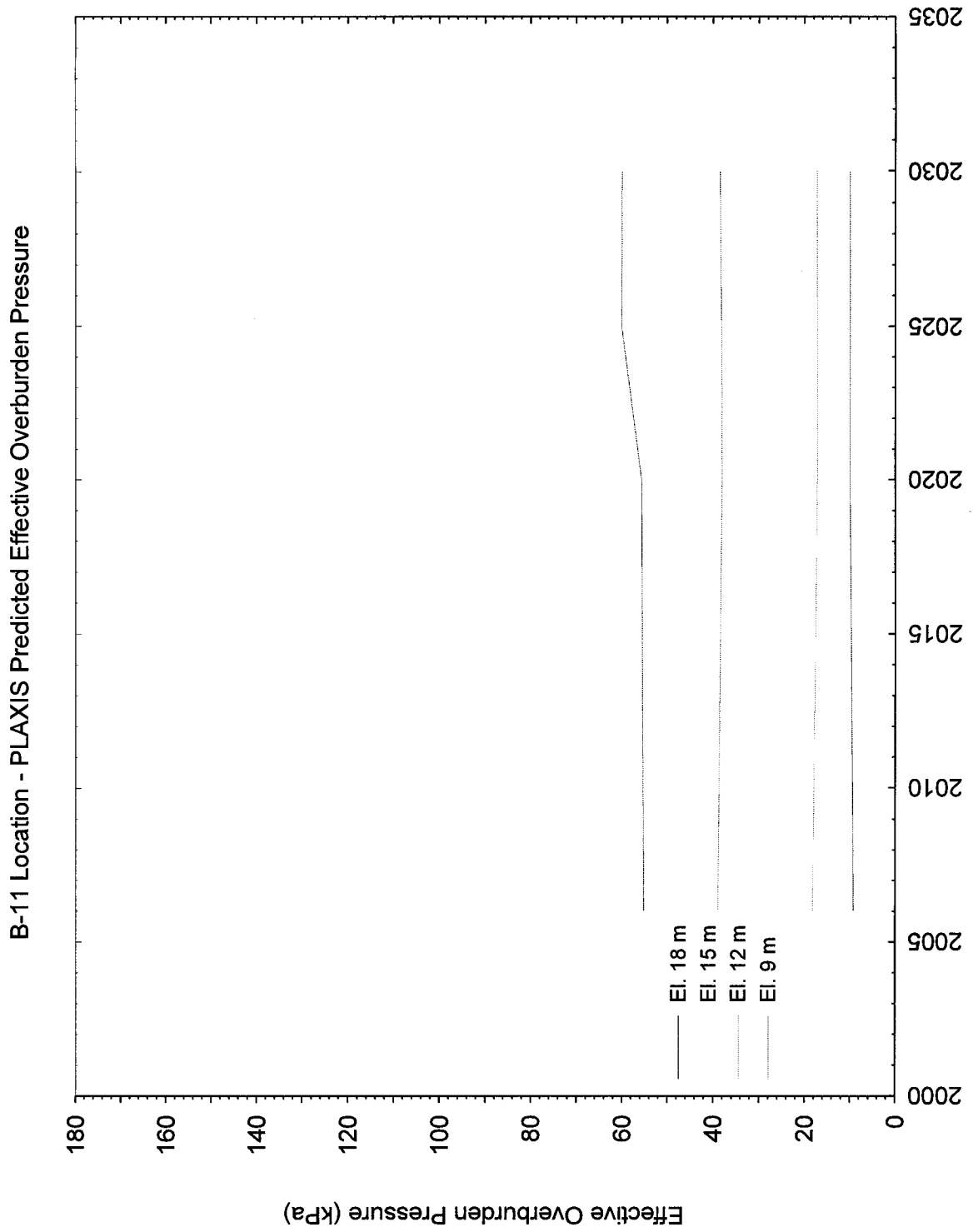


Figure F.9 - Plaxis Predicted Change in Effective Overburden Pressure with Time (B-11 Location)

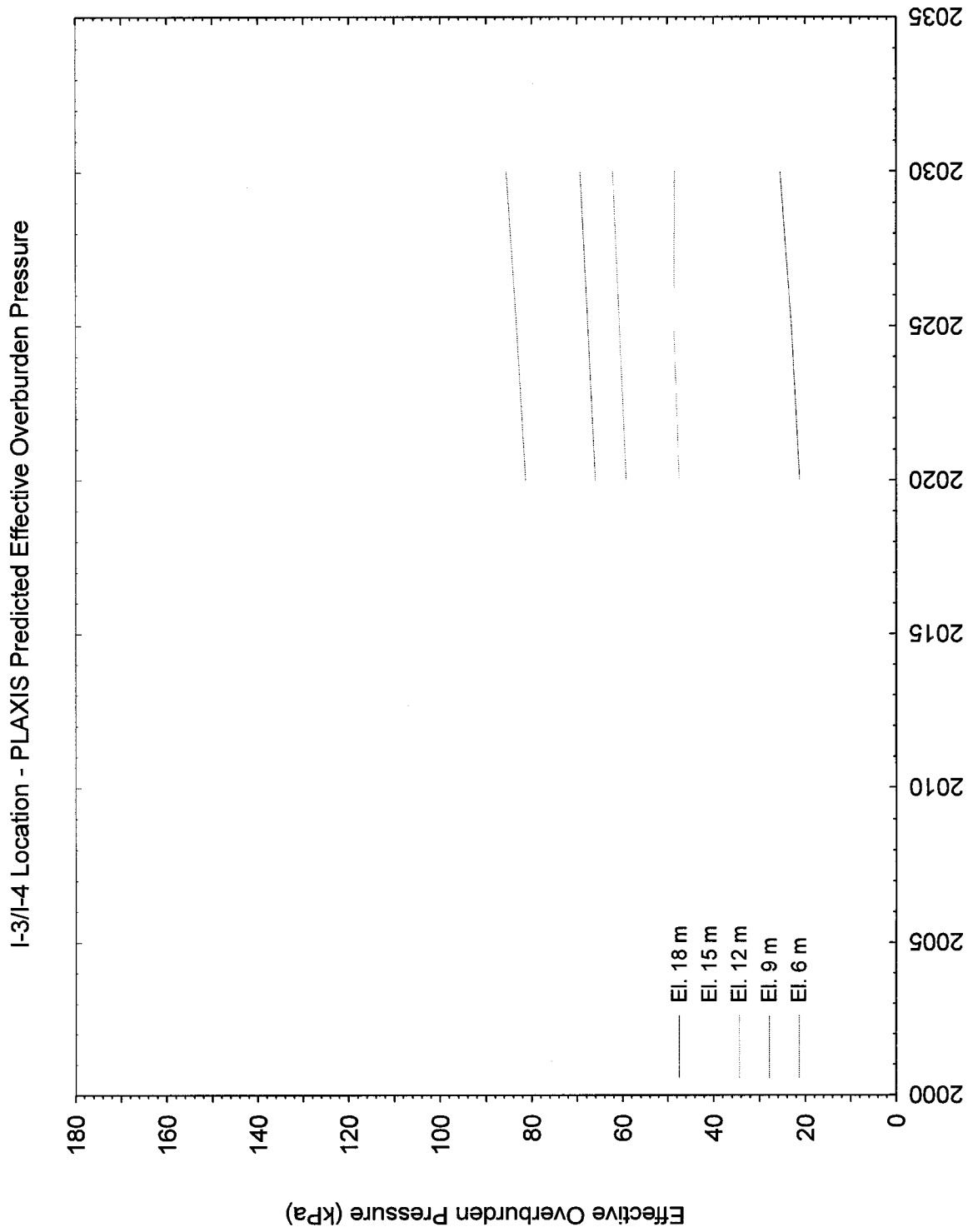


Figure F.10 - Plaxis Predicted Change in Effective Overburden Pressure with Time (I-3/I-4 Location)

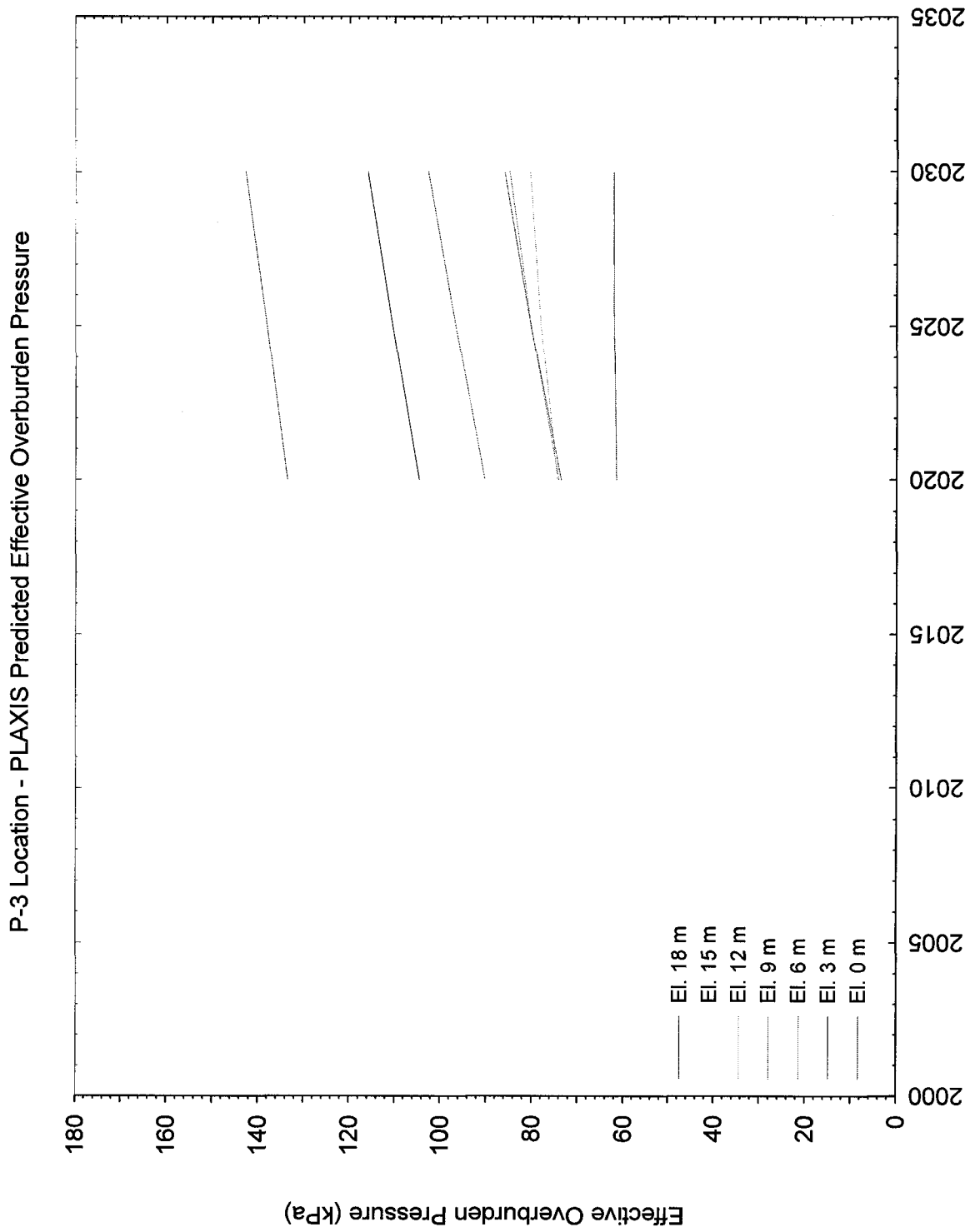


Figure F.11 - Plaxis Predicted Change in Effective Overburden Pressure with Time (P-3 Location)

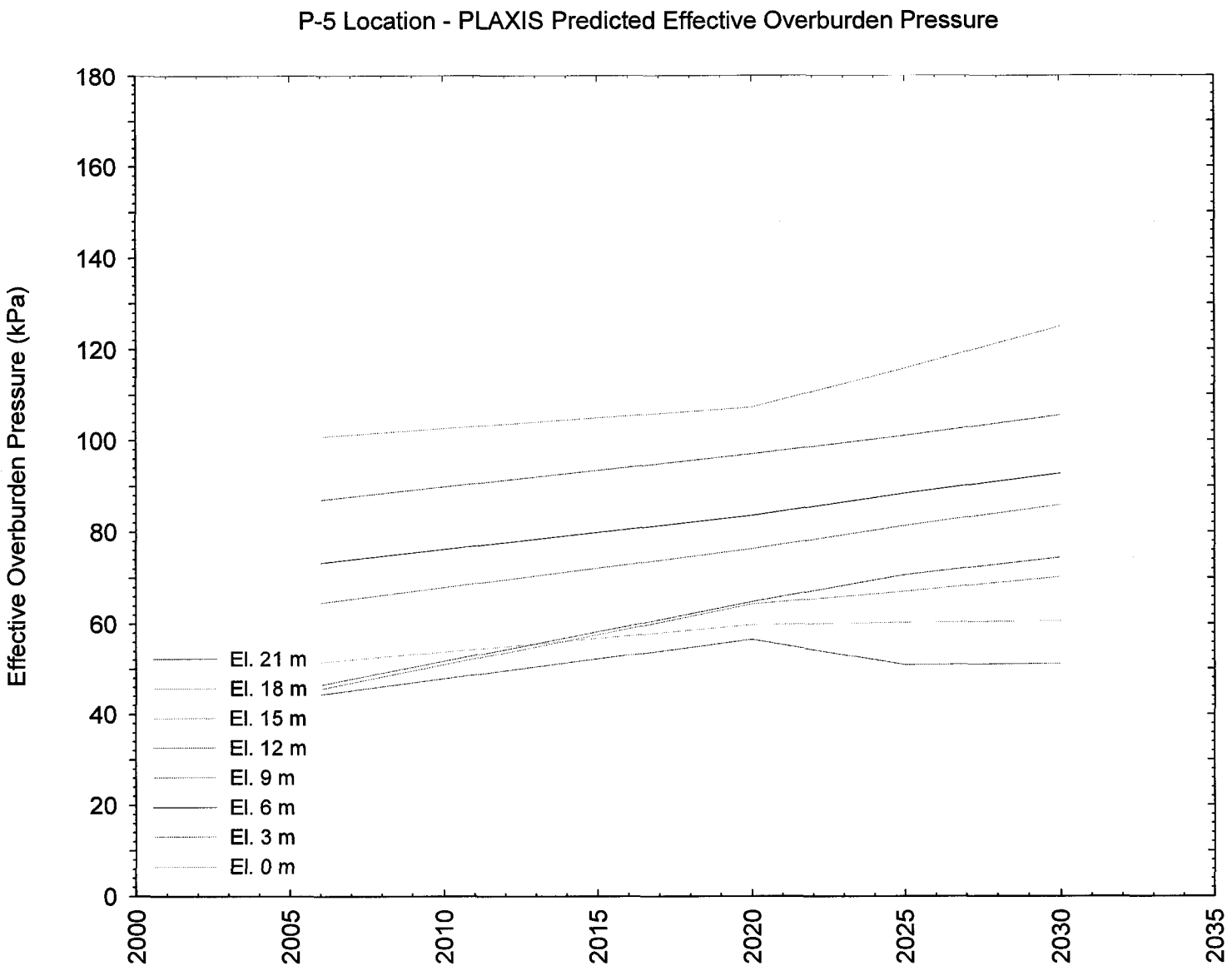


Figure F.12 - Plaxis Predicted Change in Effective Overburden Pressure with Time (P-5 Location)

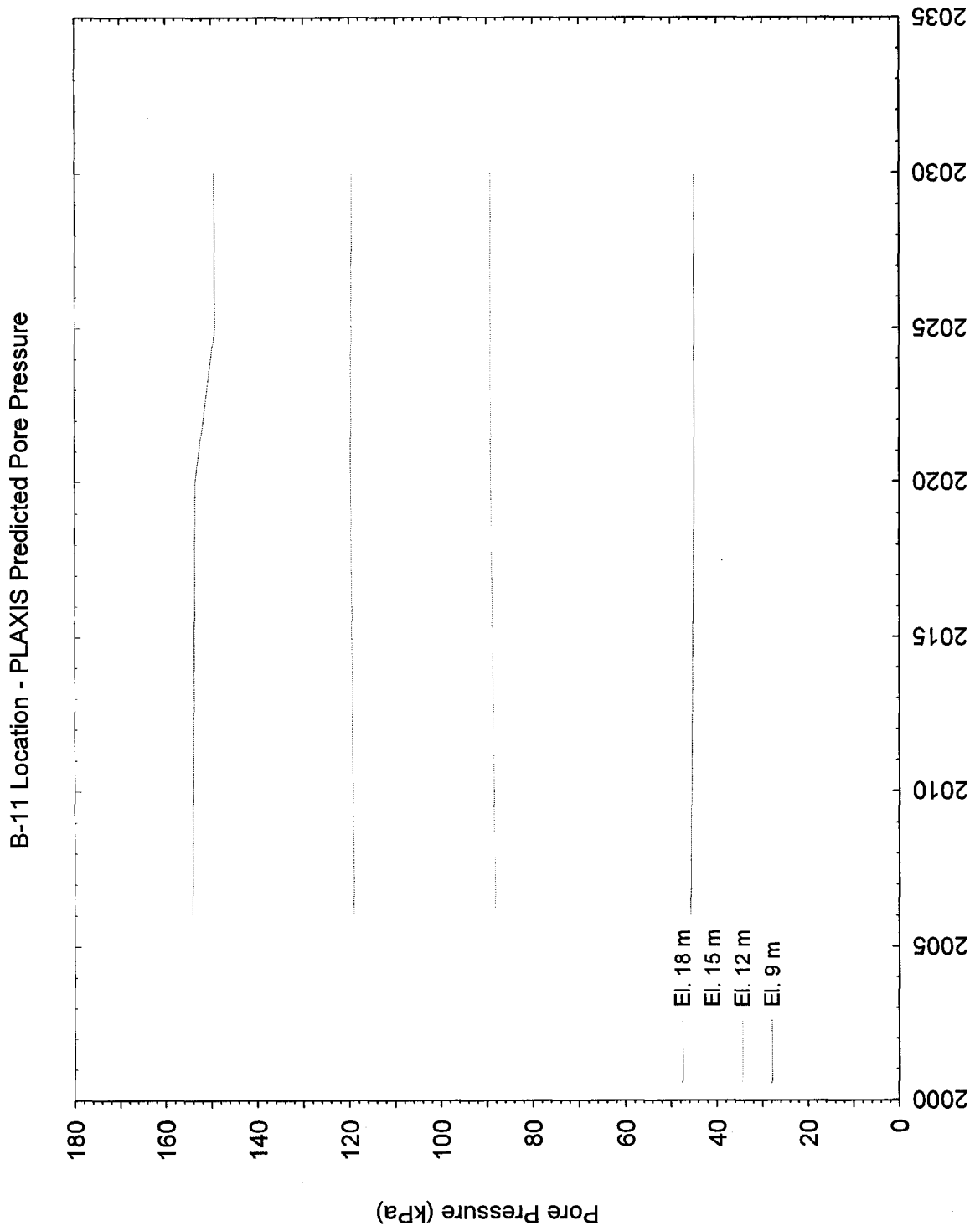


Figure F.13 - Plaxis Predicted Change in Pore Pressure with Time (B-11 Location)

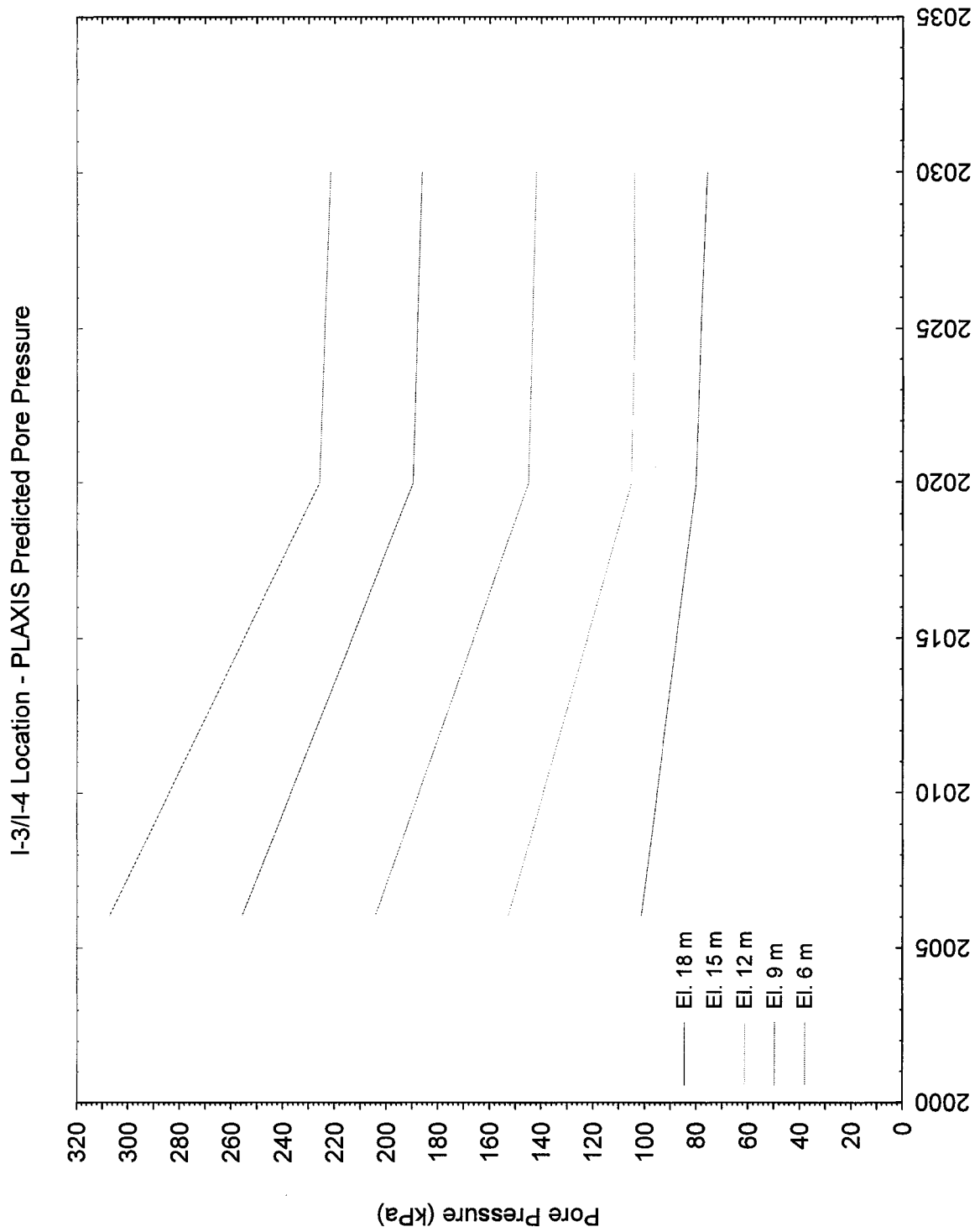


Figure F.14 - Plaxis Predicted Change in Pore Pressure with Time (I-3/I-4 Location)

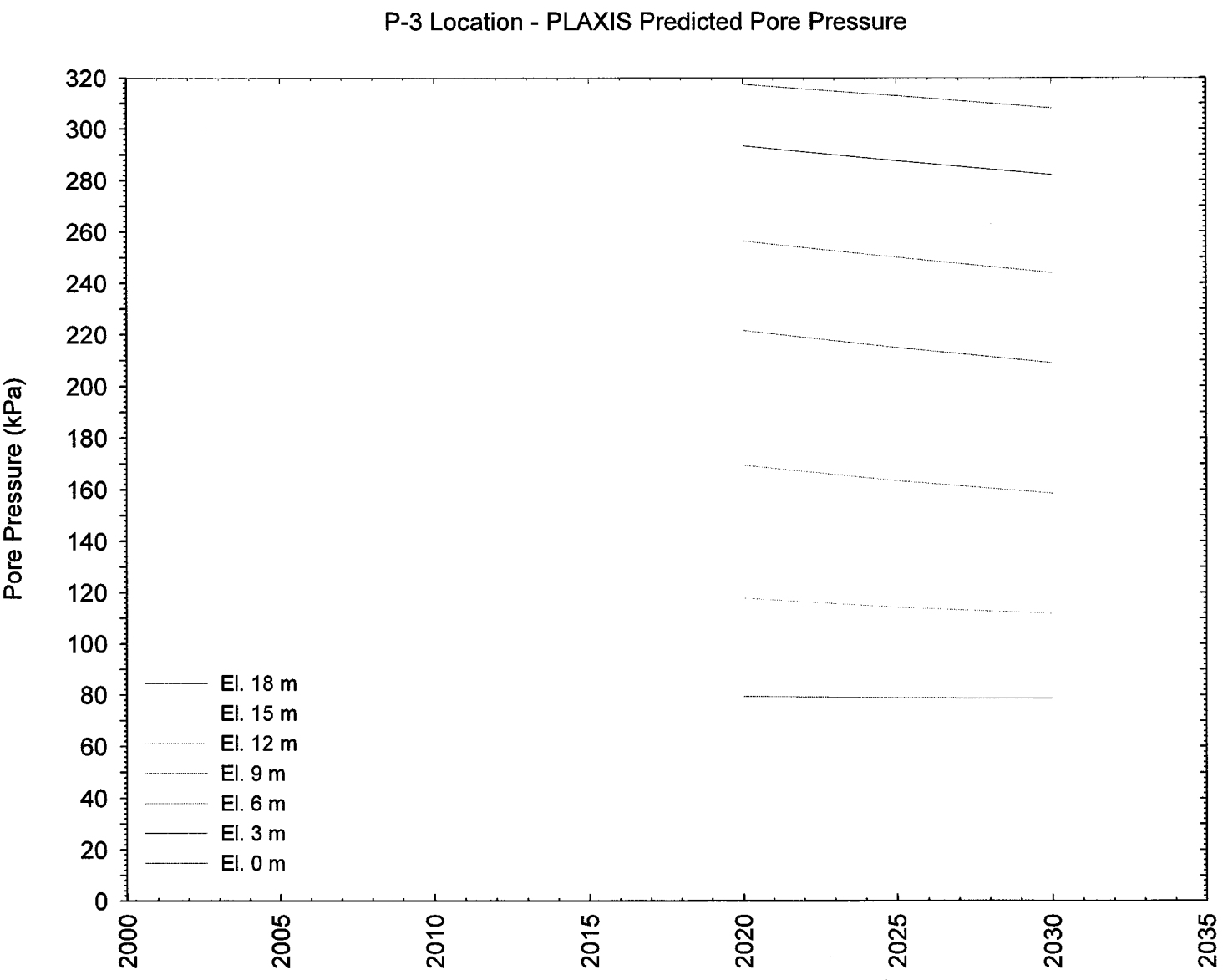


Figure F.15 - Plaxis Predicted Change in Pore Pressure with Time
(P-3 Location)

APPENDIX G

LABORATORY CONSOLIDATION CURVES

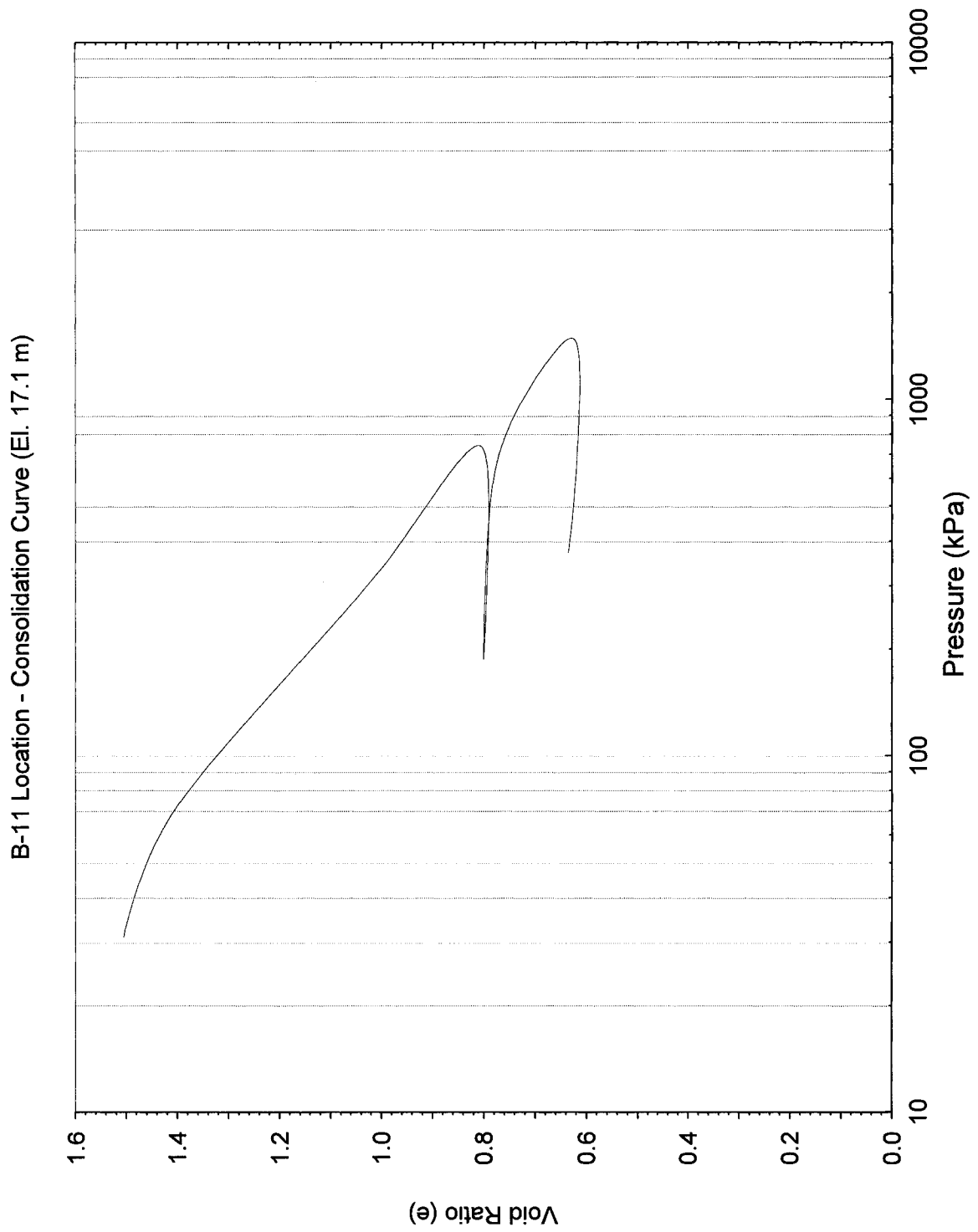


Figure G.1 - Results of One-dimensional Consolidation Test
(B-11 Location, El. 17.1 m)

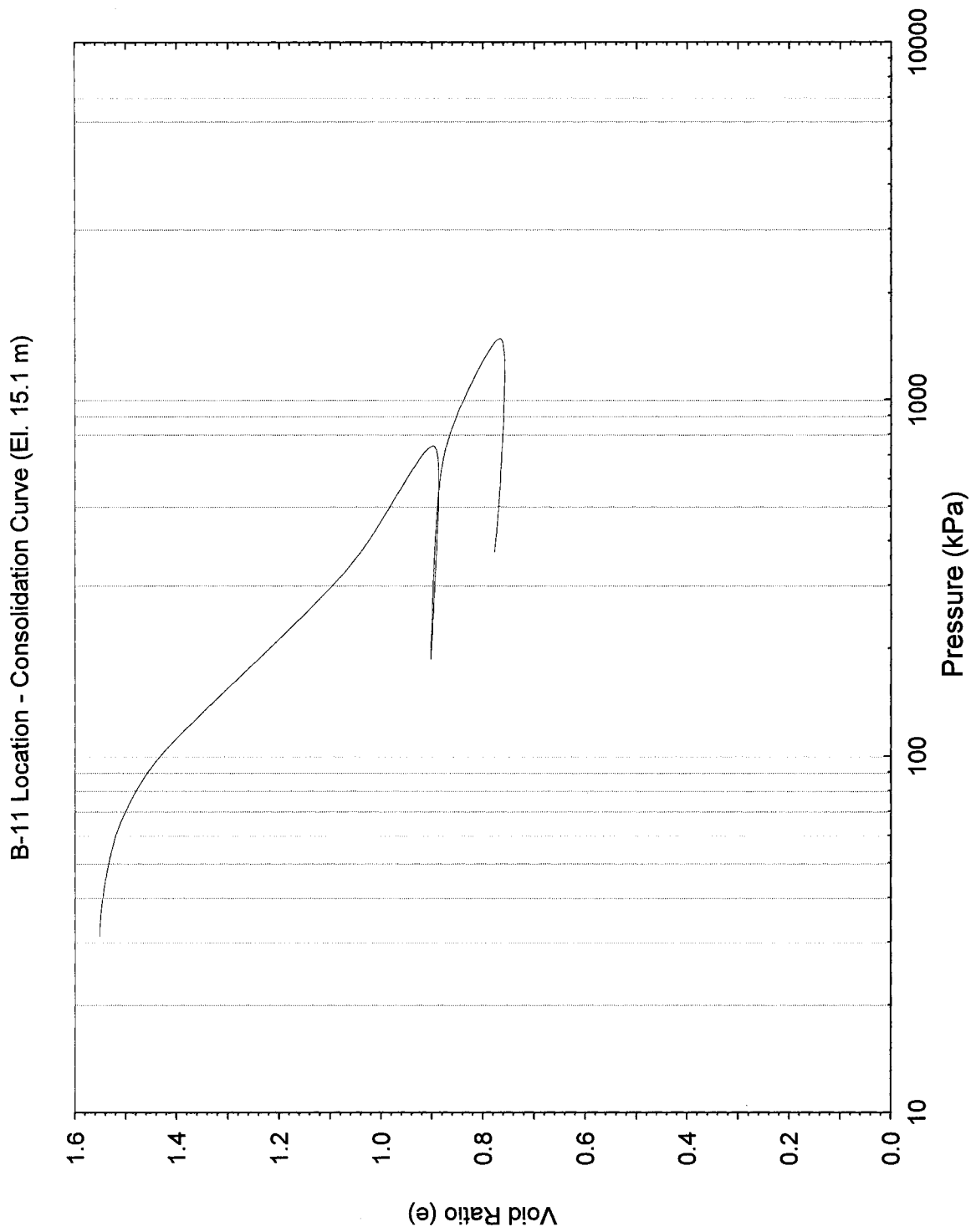
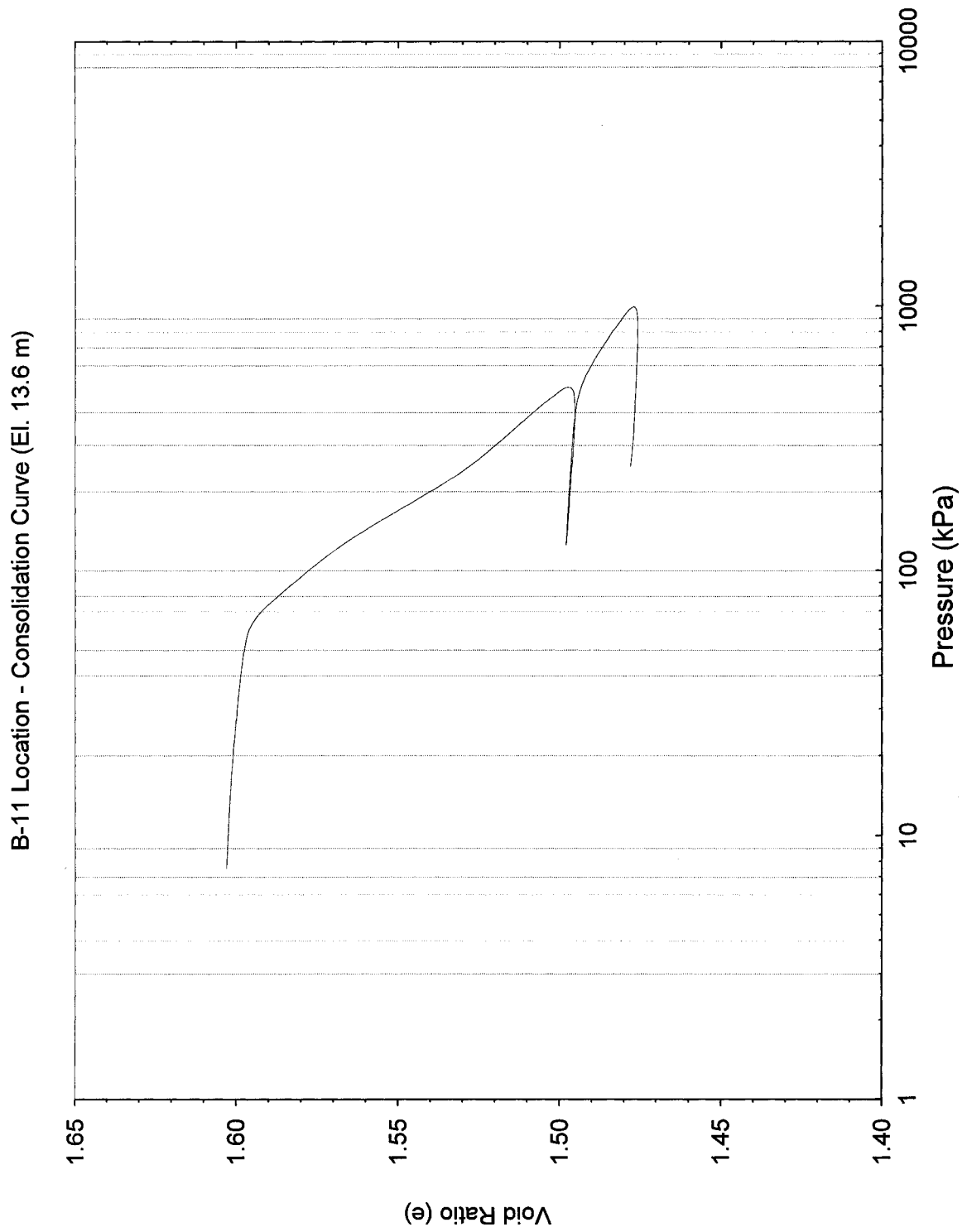


Figure G.2 – Results of One-dimensional Consolidation Test
(B-11 Location, El. 15.1 m)



**Figure G.3 - Results of One-dimensional Consolidation Test
(B-11 Location, El. 13.6 m)**

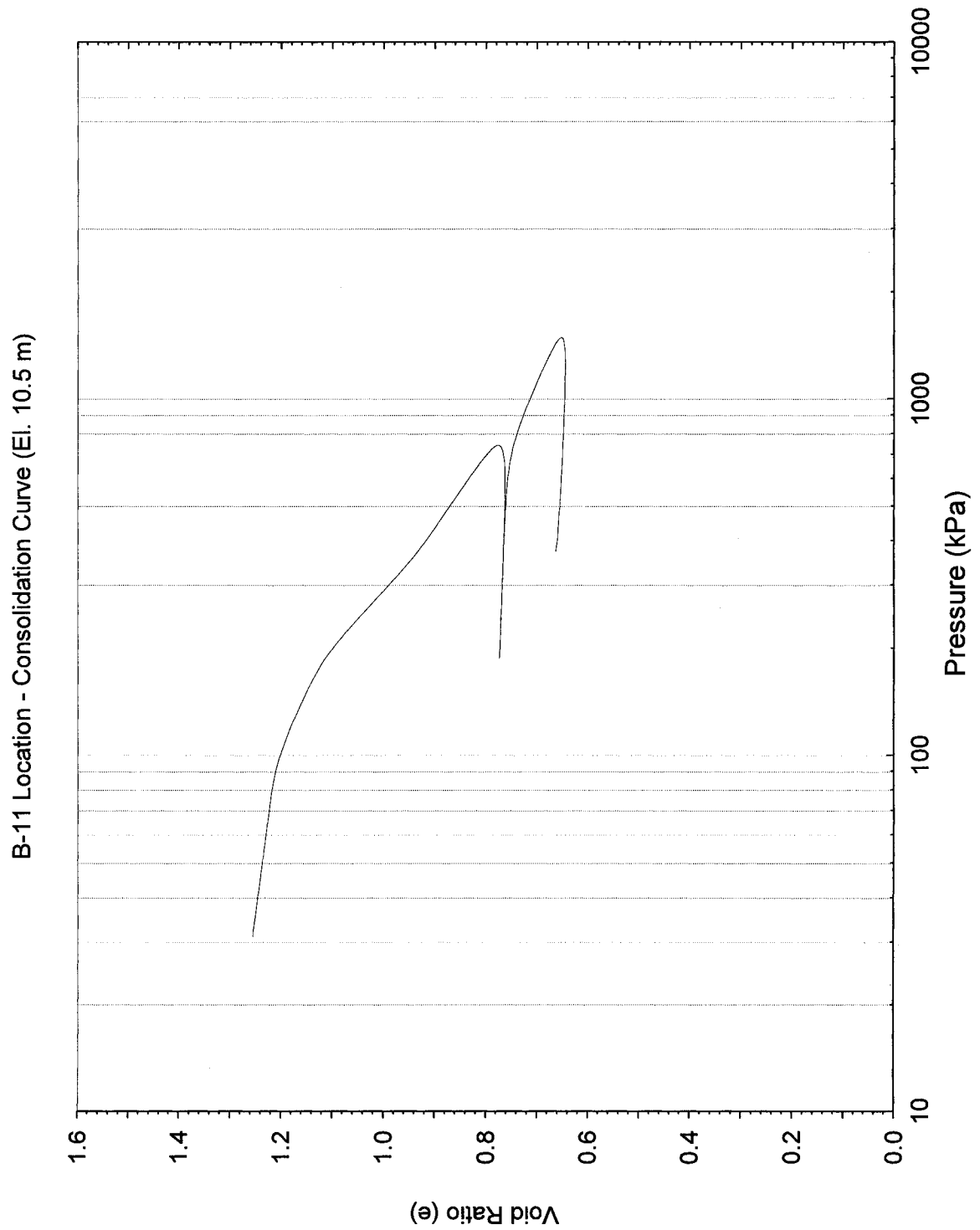


Figure G.4 - Results of One-dimensional Consolidation Test
(B-11 Location, El. 10.5 m)